GRUPPO NAZIONALE DI GEOFISICA
DELLA TERRA SOLIDA

# Atti del 34° Convegno Nazionale

Trieste, 17-19 novembre 2015
Palazzo dei Congressi
della Stazione Marittima

## Tema 1: Geodinamica

ISTITUTO NAZIONALE DI
OCEANOGRAFIA E DI
GEOFISICA SPERIMENTALE

GRUPPO NAZIONALE DI GEOFISICA DELLA TERRA SOLIDA

# 34° convegno nazionale

# Trieste

17-19 novembre 2015

Stazione Marittima

## ATTI

## Tema 1: Geodinamica

ISTITUTO NAZIONALE DI OCEANOGRAFIA E DI GEOFISICA SPERIMENTALE

GRUPPO NAZIONALE DI GEOFISICA DELLA TERRA SOLIDA

# 34° Convegno Nazionale
## Atti - Tema 1: Geodinamica

**Comitato organizzatore**

D. Slejko
D. Albarello
A. Argnani
F. Bianco
G. Caielli
G. Cassiani
A. Del Ben
D. Di Bucci
M. Dolce
E. Eva
G. Florio
P. Galli
L. Martelli
P. Mazzucchelli
G. Naso
R. Nicolich
F. Pacor
R. Petrini
L. Sambuelli

ISBN: 978-88-940442-5-6 questo volume
ISBN: 978-88-940442-4-9 collezione completa

A cura di: D. Slejko, A. Riggio,
A. Rebez, A. Argnani, F. Bianco,
A. Del Ben, E. Eva,
P. Galli, R. Petrini

Con la collaborazione di:
M. Bobbio e P. Giurco

Copertina: M. Sedmach

Impaginazione e stampa:
Luglioprint, Trieste

Finito di stampare nel mese di novembre 2015

*Ancora a Trieste. Perché l'OGS è di casa, perché la città ospita un palazzo dei congressi bello e adeguato alle necessità, ma anche, o soprattutto, perché Trieste è risultata gradita nel passato ai partecipanti.*

*Come ben si sa il Gruppo Nazionale di Geofisica della Terra Solida (GNGTS) ufficialmente non esiste dal 2000, anno in cui il Consiglio Nazionale delle Ricerche (CNR) ha deciso di chiudere i suoi Organi. Da allora il GNGTS esiste nella misura in cui i ricercatori hanno creduto, e credono, che esista: si potrebbe dire che il GNGTS è la materializzazione del desiderio dei ricercatori di incontrarsi una volta all'anno e raccontarsi cosa hanno fatto e soprattutto cosa stanno sviluppando. Niente "messa cantata", dunque, ma snella presentazione dei "lavori in corso". Nelle intenzioni di chi coordina il GNGTS, per dar spazio soprattutto ai giovani di "presentarsi in società" e fare il "battesimo del fuoco". Recentemente la partecipazione dei giovani sembra un po' diminuita, probabilmente perché sempre meno giovani trovano posto negli atenei e negli istituti di ricerca e anche perché i fondi sono sempre più risicati e pure trasferte vicine gravano sui bilanci. Oppure, come qualcuno mi ha segnalato recentemente, perché il convegno si è spostato anche su temi di carattere normativo e applicativo coinvolgendo professionisti ed amministratori e perdendo, forse, un po' della sua verginità scientifica.*

*Il GNGTS, dicevo, non esiste ufficialmente e, dopo esser sopravvissuto 15 anni in questa "terra di mezzo" è giunta l'ora di strutturarlo. Per questo è in fase di realizzazione un accordo fra enti per garantire in futuro l'esistenza di questa realtà, finchè se ne sentirà l'utilità.*

*L'ubicazione relativamente decentrata di Trieste e il ripetersi per la quinta volta del convegno in questa sede non dovrebbero favorire l'affluenza dei ricercatori, considerando anche i fondi sempre limitati destinati alla ricerca che condizionano da anni la partecipazione, specialmente dei più giovani. I presupposti per una buona riuscita del convegno, comunque, ci sono, visto l'alto numero di note ricevute per la presentazione e il numero di pre-iscritti che un mese prima del convegno sfiora le 200 unità.*

*La strutturazione del convegno su 3 temi, proposta negli ultimi anni, é stata mantenuta: ci sembra rispecchi le principali discipline geofisiche e risulta di semplice organizzazione. Pertanto anche quest'anno le presentazioni sono state suddivise nei tre temi generali: Geodinamica, Caratterizzazione Sismica del Territorio e Geofisica Applicata, che sintetizzano i grandi filoni lungo i quali si articola la ricerca geofisica italiana. Ogni tema, poi, si sviluppa in tre sessioni specifiche con apertura sia alla componente geologica che a quella ingegneristica. È doveroso segnalare l'interesse che l'argomento sismologico riveste da alcuni anni e che si manifesta in maniera decisa con l'elevato numero di relative presentazioni che spaziano dall'individuazione di faglie potenzialmente attive e lo studio di particolari terremoti alle stime di pericolosità sismica e di risposta locale per giungere alle ricadute in termini normativi atti a salvaguardare la sicurezza di persone e cose nel caso di terremoto.*

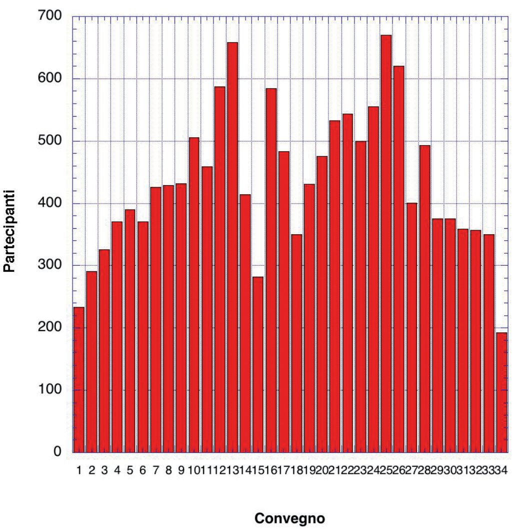


Fig. 1 – Numero di partecipanti ai convegni GNGTS. Il primo convegno si è tenuto nel 1981 e, in seguito, ha avuto cadenza annuale con l'eccezione del 1982. Il numero dei partecipanti all'ultimo convegno è aggiornato ad un mese prima dell'inizio del convegno stesso.

*Anche quest'anno è stata fatta la scelta di raccogliere note estese (ma non troppo) a*

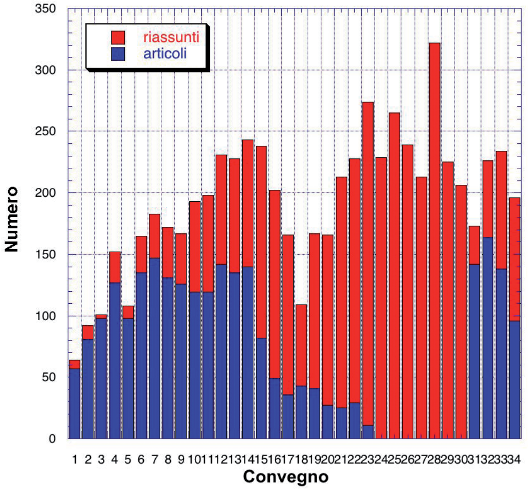


Fig. 2 – Numero di note presentate nei convegni GNGTS. Fino al 2004 è stato pubblicato il volume (dal 1997 sotto forma di CD-Rom) degli atti del convegno contenente in forma estesa le note presentate (barre rosse). In seguito, si è deciso di pubblicare soltanto il volume dei riassunti estesi (barre blu).

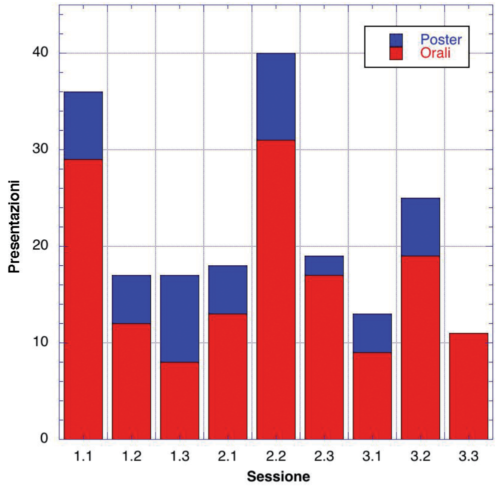


Fig. 3 – Numero di note presentate nelle varie sessioni del 34° convegno. Vengono indicate le comunicazioni orali con il colore rosso e quelle in forma di poster con il colore blu.

*formare gli atti del convegno. Ricordiamo che questa scelta è stata dettata dalla necessità di produrre un volume utilizzabile per la valutazione ufficiale dell'attività scientifica dei ricercatori e degli enti. Il presente volume raccoglie ben 96 note, delle 195 che verranno presentate al convegno. Si tratta di una percentuale (49%) decisamente più bassa di quella degli anni passati, che deve far riflettere. La produzione di atti di rilevanza scientifica ha determinato la necessità di avviare un processo di referaggio di tutti i testi. I convenor se ne sono fatti carico e, pertanto, risultano responsabili della qualità del materiale presentato. La notevole mole di materiale da stampare ha fatto confermare la scelta di suddividere gli atti in tre volumi, ciascuno dei quali raccoglie le note relative ad uno dei tre temi. Molte note (64) sono in lingua inglese: ciò permette una diffusione del presente volume anche all'estero. Delle 196 note in programma, ben 149 sono destinate alla presentazione orale.*

*Anche quest'anno alcune sessioni del convegno GNGTS (quelle di Geofisica Applicata) sono state organizzate in collaborazione con la Sezione Italiana EAGE-SEG, che realizza così il suo 15° Convegno Nazionale.*

*Una segnalazione degna di nota va all'Associazione Geofisica Licio Cernobori, che ha scelto anche quest'anno il convegno GNGTS quale sede per l'attribuzione del premio in memoria di un caro collega ed amico prematuramente scomparso anni or sono.*

*Un ringraziamento particolare va ai convenor (Dario Albarello, Andrea Argnani, Francesca Bianco, Grazia Caielli, Giorgio Cassiani, Anna Del Ben, Daniela Di Bucci, Mauro Dolce, Elena Eva, Giovanni Florio, Paolo Galli, Luca Martelli, Paolo Mazzucchelli, Giuseppe Naso, Rinaldo Nicolich, Francesca Pacor, Riccardo Petrini e Luigi Sambuelli), che hanno proposto e organizzato le varie sessioni e hanno curato il referaggio dei testi, ed alla Segreteria Organizzativa (Anna Riggio, Alessandro Rebez, Paolo Giurco e Muzio Bobbio), che ha raccolto e preparato tutto il materiale qui stampato. Desideriamo ringraziare, infine e soprattutto, il Presidente dell'OGS, che ha accolto ancora una volta con entusiasmo e con generosità l'idea di finanziare il convegno GNGTS, nonostante le difficoltà economiche con cui tutti gli enti di ricerca devono scontrarsi, e Codevintec Italiana S.r.l. e Misure Meccaniche S.r.l., nostri sponsor i questo convegno.*

*Dario Slejko*

*"...cerco qualcosa: un briciolo di conoscenza in questo nostro piccolo grande pianeta.*
*E in me stesso..." L. C. 1989.*

## PREMIO DELL'ASSOCIAZIONE PER LA GEOFISICA "LICIO CERNOBORI" - 2015

L'Associazione per la Geofisica Licio Cernobori - AGLC, nata il 30 ottobre del 2000 per ricordare Licio Cernobori, geofisico prematuramente scomparso, ed il suo entusiasmo contagioso, ha come fine la promozione degli studi geofisici, e soprattutto la formazione scientifica e la crescita dei più giovani.

Tale fine è stato perseguito attraverso l'elargizione di un premio di studio presso l'Università di Trieste, aperto anche a laureandi/laureati in Geofisica Applicata di altre università o strutture scientifiche coinvolte in progetti comuni con l'Ateneo di Trieste. Si ricordano i vincitori degli anni passati Giulio Paoli (2001), Sara Cisilin (2002), Marica Calabrese (2003), Manfredi Scozzi (2004), Ivan Gladich (2006), Manuela Zuliani (2006), Andreika Starec (2008), Sara Ferrante (2009).

Oltre all'attività didattica/divulgativa che i componenti dell'Associazione svolgono in diverse occasioni, sono stati finanziati negli anni diversi convegni, scuole, progetti, iniziative, in Italia e all'estero:

- Copie degli Atti del Convegno TRANSALP (Trieste, febbraio 2003) per le biblioteche universitarie;
- Agevolazioni per gli studenti al Congresso: STRUCTURES IN THE CONTINENTAL CRUST AND GEOTHERMAL RESOURCES (Siena, 24-27 September 2003);
- Sovvenzione di uno studente, Alberto Gaudio dell'università di Urbino, per la Scuola di Processing dati sismici marini (Trieste, ottobre 2004);
- Agevolazioni per studenti del terzo mondo alla partecipazione del Workshop IRIS-Orfeus "Understanding and managing information from seismological networks" (Palmanova (UD) 28 febbraio – 6 marzo 2005);
- Finanziamento di € 400 Euro ad Andrejka Starec (2006), allora studentessa, per garantirle un altro mese presso il TNO (Paesi Bassi) a conclusione della sua borsa e consentirle la conclusione della tesi sullo stoccaggio geologico della $CO_2$, con la guida di Pascal Winthaegen e del chiar.mo Prof. Rinaldo Nicolich dell'Università di Trieste.
- Finanziamento annuale di € 400 per la partecipazione di un insegnante ai seminari GIFT per gli insegnanti delle scuole elementari e secondarie nell'ambito del convegno dell'European Geosciences Union - Geophysical Information for Teachers (GIFT): Giovanni Banchelli (2007), Pier Paolo Caputo (2008), Giovanni Aglialoro (2009), Francesco Gobbo (2010), Giulia Realdon (2011), Eva Godini (2012), Maria Barbera (2013).

Nell'occasione del decennale (2010) si è istituito un premio per i giovani relatori al Congresso annuale GNGTS, ripetuto nel 2011. Nel 2010 il premio di 2000,00 € è andato alla dottoressa Marina Pastori, per il lavoro *"Crustal fracturing field and presence of fluid as revealed by seismic anisotropy: case-histories from seismogenic areas in the Apennines"*, selezionato tra 40 lavori e 8 finalisti, nel 2011 al dott. Edoardo Peronace, per il lavoro *"Shallow geophysical imaging of the mt. Marzano fault zone; a kaleidoscopic view through ERT, GPR and HVSR analyses"*, selezionato tra 38 lavori e 13 finalisti.

Dal 2012 il premio è stato suddiviso tre premi di 700,00 €, uno per ciascuno dei Temi del convegno: *Geodinamica, Caratterizzazione sismica del territorio e Geofisica applicata*. I vincitori sono stati: Lorenzo Bonini, per il lavoro: *"Comprendere la gerarchia delle faglie attive per migliorare la caratterizzazione sismica del territorio: l'esempio del terremoto di L'Aquila del 2009 (Mw 6.3)"*, Rocco Ditommaso, per il lavoro *"Risposta sismica delle strutture: dalla non stazionarietà alla non linearità apparente"*, Gianluca Fiandaca, per il lavoro *"Time domain induced polarization: 2D inversion for spectral information"*, selezionati tra 31 lavori presentati.

Nel 2013 i vincitori sono stati: Giuseppe Pezzo, per il lavoro *"Fault activity measurements from InSAR space geodesy: the fundamental role of geological constraints for correct data interpretation and analytical fault modeling"*, Giovanni Rinaldin, per il lavoro *"Effectiveness of the N2 Method for the seismic analysis of structures with different hysteretic behaviour"* e Daniele Sampietro, per il lavoro *"Il modello GEMMA: realizzazione, validazione e distribuzione"*, selezionati su 28 candidati.

Nel 2014 i vincitori sono stati: Daniele Cheloni, per il lavoro *"Interseismic coupling along the southern front of the Eastern Alps and implications for seismic hazard assessment in N-E Italy"*, Chiara Bedon, per il lavoro *"Structural monitoring and seismic analysis of a base-isolated bridge in Dogna"* e Jacopo Boaga per il lavoro *"L-shaped array refractions microtremors (LeMi)"*, selezionati su 18 candidati.

Quest'anno i lavori presentati sono 11. Purtroppo si è registrato un generale calo nelle domande, in particolare per il tema 1 che per il tema 2, sulle cui cause ci stiamo interrogando ed invitiamo tutta la comunità scientifica a riflettere ed a suggerire possibili rimedi e strategie. I riassunti e le presentazioni preliminari sono attualmente all'esame delle tre commissioni, che stanno lavorando per scegliere i vincitori, che verranno annunciati e premiati nel corso dell'Assemblea del Convegno (18 novembre 2015).

Per altre informazioni, per diventare socio e contribuire a continuare e migliorare le iniziative dell'Associazione per la Geofisica Licio Cernobori –AGLC, scrivere a cernobor@units.it.

## Roberto Cassinis (31/10/1921-22/8/2015)

Lo scorso agosto è mancato Roberto Cassinis, classe 1921, insigne scienziato della Geofisica italiana. La sua carriera è stata contrassegnata dalla partecipazione ad importanti progetti e decisioni che hanno trasformato la Geofisica, soprattutto quella di prospezione, attribuendole lustro anche a livello internazionale.

Roberto, professore di Geofisica Mineraria all'Università di Palermo (1964-1968), poi ordinario di Fisica Terrestre all'Università degli Studi di Milano (dal 1968 al pensionamento, nel 1997), è stato direttore dell'Istituto di Geofisica della Litosfera del C.N.R. e direttore della Scuola Internazionale di Geofisica di Erice. Ha effettuato numerose campagne di prospezione geofisica finalizzate sia alla ricerca di giacimenti di idrocarburi, sia di giacimenti di minerali solidi. Ha anche svolto studi geofisici per accertare la fattibilità di grandi opere civili, fra cui il ponte sullo Stretto di Messina. È stato autore di numerose pubblicazioni scientifiche, libri e dispense su cui molti studenti e colleghi hanno avuto modo di imparare ed apprezzare le tecniche di studio dell'interno del nostro pianeta.

Anche dopo il pensionamento si è occupato, in maniera discreta come nel suo carattere, del tutorato di giovani laureandi o laureati che si avvicinavano al mondo del lavoro. Ha altresì continuato a collaborare alla stesura di pubblicazioni scientifiche con colleghi a cui raccontava dei "bei tempi" in cui i progetti erano degni di tale nome e di quante difficoltà vi fossero nel trattare ingenti quantità di dati con i limitati mezzi informatici dell'epoca. Uno dei suoi grandi rammarichi era proprio la convinzione che "se fosse nato dopo", come diceva lui, gli stessi dati avrebbero rappresentato una fonte inesauribile di informazioni grazie alla possibilità di acquisirli e sfruttarli in maniera adeguata. Per questo usava ogni mezzo a sua disposizione, dalla disponibilità a collaborare in progetti fino alla condivisione di testi ed informazioni personali, per conservare la memoria di quei *database* e divulgarli per consentire anche ad altri di poterne usufruire.

Sulla scorta di una carriera brillante, sarebbe dunque semplice descrivere lo scienziato Roberto Cassinis elencando i titoli, le conquiste di carriera e le responsabilità scientifiche per inquadrarne la capacità, l'importanza ed il ruolo di rilievo nel suo campo di studio. Ma chi lo ha conosciuto sa anche che era un uomo molto aperto, affatto presuntuoso, sempre disponibile alla discussione, un fine osservatore della società in generale e non solo di quella scientifica, un grande appassionato della Scienza, una persona sempre alla ricerca di risposte nello stile proprio di un vero ricercatore. Ed è così che lo vogliamo ricordare, quando a più di ottanta anni, ancora lucidissimo, apriva con cura il suo computer e snocciolava dati e teorie chiedendo scusa di averci dovuto meditare un po' su, giustificando con l'età avanzata l'onestà intellettuale di chi vuole capire prima di esporre una idea; accettando critiche e commenti come chi sa che la Scienza è confronto; insomma come uno della "vecchia scuola", quella in cui le persone contavano più delle cariche o delle pubblicazioni.

**Claudio Eva e Stefano Solarino**

## Fabio Meloni (18/11/1957-29/8/2015)

Quest'estate, sul mare d'agosto, ancora più tragica e inaspettata ci ha raggiunto la notizia che Fabio se n'era andato. Inaspettata perché chi a conoscenza della sua malattia ne era stato da lui stesso rassicurato sugli sviluppi e sulle prospettive.

Fabio era nato a Sant'Angelo Romano nel 1957, laureandosi alla Sapienza di Roma nel 1983 con uno "Studio di macrosismica e sismotettonica nell'alto Lazio e nell'Abruzzo settentrionale". E gli studi sulla sismicità storica sono sempre rimasti il suo maggiore interesse scientifico e una passione che ha perseguito anche quando, entrato in Regione Lazio, di tutt'altre incombenze ha dovuto occuparsi.

I suoi primi lavori su questo argomento datano dalla metà degli anni Ottanta fino a tutti gli anni Novanta quando, con l'ENEA e l'ISMES prima e col CNR-GNDT poi, ha compiuto numerose ricerche sulla sismicità storica non solo del Lazio, ma di numerose parti d'Italia, ivi comprese quelle sugli indizi delle liquefazioni avvenute in occasione dei terremoti storici, producendo decine e decine di rapporti tecnici. Già a partire dal 1985 Fabio ha presentato in anteprima le sue ricerche proprio qui, al GNGTS, che lo ha visto partecipe per oltre 25 anni, sino al Convegno del 2011.

Dopo essere stato responsabile della segreteria tecnica del GNDT fino a tutto il 1998, Fabio transitò in Regione Lazio, nell'ex Ufficio Geologico, dove i colleghi lo ricordano per la sua impostazione rigorosamente scientifica anche nei confronti del disbrigo delle pratiche di carattere più amministrativo o burocratico.

Di fatto, Fabio ha sempre nutrito una forte curiosità scientifica verso tutte le materie relative alle Scienze della Terra, appassionandosi negli ultimi anni anche al fenomeno dei sinkhole nel Lazio che lo ha visto estensore di un catalogo regionale unificato degli stessi. Il medesimo rigore e approfondimento lo metteva in tutti i lavori in cui si cimentava, anche quelli relativi alla libera professione che aveva praticato nella sua zona di residenza agli inizi della sua carriera. Da questo punto di vista viveva con entusiasmo il suo lavoro, affrontando con tenacia, con grande capacità di analisi, ma anche con una proverbiale serenità e sicurezza tutti gli imprevisti e le novità che gli si prospettavano, contagiando e rassicurando chi gli stava accanto. I colleghi della Regione Lazio lo ricordano immerso nelle sue carte fino a tardi, quando le guardie giurate lo invitavano a tornarsene a casa. Ricordiamo Fabio per la sua innata disponibilità e correttezza verso tutti noi, per la sua flemma, la calma con la quale non riusciva a mandarci in bestia nemmeno quando invece di concludere, rimetteva in discussione tutto il lavoro fatto fino a quel momento.

**Paolo Galli e Antonio Rossi**

# Indice

# Lectio Magistralis

# IL TERREMOTO DEL FRIULI: CONSIDERAZIONI SU UN EVENTO SINGOLARE

**M. Riuscetti**

Nei quasi 40 anni che sono passati dal 6 maggio 1976 sono molti gli eventi celebrativi che si sono succeduti in varie sedi istituzionali e scientifiche. Sono stati fondati musei, allestite mostre, pubblicati libri, organizzati congressi e scritti numerosi articoli.

Inevitabilmente la funzione commemorativa ha assunto peso sempre più prevalente rispetto alla funzione di contributo alla conoscenza che, invece, è fondamentale per insegnare a diminuire l'impatto sociale ed economico che avranno i futuri terremoti.

A ciò si aggiunga che anche le criticità e gli errori che pur ci furono sono stati sottaciuti perché non venisse offuscato l'esito complessivamente positivo della ricostruzione.

La singolarità che cercherò, sia pur brevemente, di delineare risiede nel fatto che il terremoto del Friuli si inserisce, ed in parte provoca, con il successivo terremoto dell'Irpinia-Basilicata di cui ricorre tra pochi giorni il trentaseiesimo anniversario, in un clima di notevoli cambiamenti e progressi sia scientifici che legislativi ed organizzativi come mai era accaduto in precedenza, salvo poi costringerci a constatare la loro labilità ed il lento ed apparente ritorno a condizioni che molto ricordano sotto vari aspetti le condizioni precedenti.

Ricordare i quasi 1.000 morti e la distruzione totale o parziale di 86.000 edifici, fabbriche, chiese è doveroso così come è comprensibile l'enfasi sui risultati della ricostruzione che, unica nella storia della Repubblica, può essere accostata a quella del secondo dopoguerra (anche se, a mio parere, la meravigliosa ricostruzione della Sicilia orientale dopo il terremoto del 1693 è qualcosa di insuperato e forse insuperabile). Ciò avverrà anche nell'anno che sta per iniziare con numerose iniziative già annunciate ed altre che sicuramente seguiranno. In questa sede è più appropriato ed utile dare enfasi alla funzione conoscitiva di cui dicevo poc'anzi.

Cerchiamo allora di collocare il terremoto del 1976 con particolare riguardo agli aspetti sismologici *lato sensu*.

Va innanzitutto rilevato che l'evento, come tutti gli altri che lo precedettero nel secolo scorso, avvenne in una zona "non sismica". La prassi normativa vigente dal 1909 (anno della prima legge in materia ) si limitava a prescrivere l'osservanza della regolamentazione alle "aree colpite da terremoto" di fatto dopo il 1909. Tale prassi continuò per decenni (fino al 1962), nonostante le norme venissero spesso riviste, migliorate ed adeguate al progredire delle conoscenze e delle tecniche costruttive (come, ad esempio, il cemento armato).

Ciò consentì che si continuasse ad ignorare il pericolo sismico per circa 70 anni in regioni come la Sicilia orientale, colpita nel 1693 da quello che forse può essere considerato il più forte terremoto nella storia dell'Europa continentale. Anche se le conseguenze possono sembrare poco rilevanti data che la normativa sismica, in un Paese intensamente antropizzato da secoli, si sarebbe dovuta applicare solamente alle nuove costruzioni, si pensi invece alla gran mole di costruito e ricostruito dopo la seconda guerra mondiale. Venne sprecata dunque una grande (e speriamo irripetibile) occasione di mettere in sicurezza una gran parte, soprattutto, delle maggiori città italiane.

Le Scienze della Terra, per quanto riguarda gli aspetti sismologici, erano agli inizi degli anni '70 in uno stato di notevole arretratezza. La Sismologia, ad esempio, veniva insegnata in pochissime università. La quasi totalità dei geologi si rifacevano alle poche informazioni fornite come parte dei corsi di Fisica Terrestre e, dove esistevano, di quelli di Geofisica Applicata. Non dimentichiamo che la maggior parte delle cattedre di Geologia erano occupate da laureati in Scienze Naturali, Chimica e financo Farmacia.

Si accettava, senza che ne venisse grande scandalo, che il titolare di una cattedra geofisica di Palermo dichiarasse che il terremoto del Bélice (1968) fosse dovuto alla grande quantità di magnetite, contenuta nelle rocce profonde della Sicilia occidentale, il cui campo magnetico era stato perturbato dall'intensa attività solare di quel gennaio. Per inciso egli era lo stesso autore di un testo, adottato per il suo corso, in cui tra le rocce ad alta suscettività magnetica erano segnalate le ghiaie magnetiche (sic!) che altro non erano che la pirrotite che in tedesco si chiama Magnetkies, parola composta, appunto da Magnet e Kies (ghiaia).

Il grosso della dotazione strumentale dell'Istituto Nazionale di Geofisica (la Vulcanologia sarà aggiunta in seguito) era costituito da 14 Wiechert con orologi a pendolo su cui era basata la rete nazionale integrata in maniera non organica da osservatori di varia natura e gestione spesso affidata alla buona volontà di religiosi secondo una tradizione ottocentesca. Erano presenti reti sismiche locali moderne a Napoli e Genova e stazioni sismiche di buona qualità a Trieste, L'Aquila, Messina. Alcune erano dedicate alla vulcanologia (Napoli), altre facevano parte della rete americana per il controllo delle esplosioni nucleari sotterranee dell'Unione Sovietica (Trieste e L'Aquila).

Lo stato generale del sistema risultava evidente nella "guerra degli epicentri" (la definizione è di Massimiliano Stucchi) che si scatenava dopo ogni terremoto forte abbastanza da essere registrato in più punti del territorio nazionale. Ricordo, per inciso, che tra gli epicentri proposti nella notte del 6-7 maggio 1976 per la scossa delle 21:00 era anche il Golfo di Genova!

Nella prima metà degli anni '70, però, qualcosa aveva iniziato a perturbare l'immobilità del sistema che governava le Scienze della Terra: in sede internazionale era stato lanciato il Progetto Internazionale Geodinamica come conseguenza della nascita della rivoluzionaria teoria della Tettonica a zolle. Ad esso aveva aderito l'Italia in cui il C.N.R. aveva deciso di riorganizzare la ricerca pubblica con lo strumento dei progetti finalizzati. Il progetto finalizzato venne così definito: *"Il Progetto Finalizzato è un insieme coordinato di attività di ricerca, sviluppo e dimostrazione di prototipi relativi a prodotti, processi e servizi, di durata definita, volto all'acquisizione di conoscenze e innovazioni, trasferibili al sistema produttivo, al tessuto economico sociale e al contesto politico-giuridico del Paese, relative a tematiche considerate prioritarie nel quadro della programmazione economica nazionale"*. La risposta che tentò di dare il sistema fu quella di mascherare ciò che si era sempre fatto ignorando di fatto gli scopi dei progetti finalizzati. Venne varato un ponderoso piano di ricerche organizzate su grandi sezioni crostali (le geotraverse). Tutto venne spazzato via in una tempestosa assemblea a Roma, al C.N.R., dove molti ricercatori dopo veementi critiche (che a dire al vero trovarono deboli risposta nei baroni increduli di fronte a tanta mancanza di rispetto) chiesero ed ottennero di riscrivere il progetto finalizzandolo alla costruzione di un quadro organizzativo e di conoscenze volta alla riduzione dei rischi sismico e vulcanico.

Lascio alla penna di Paolo Rumiz (La Repubblica, 1999) la descrizione di ciò che fu il Progetto Finalizzato Geodinamica: *"Non c'è scienziato che non parli con nostalgia di quegli anni. Si mobilitano risorse, scendono in campo geologi, ingegneri, storici. Cadono steccati, baronie. L'interazione di cervelli dà frutto, il patrimonio edilizio del Paese comincia a essere monitorato. La protezione civile si mette agli ordini della scienza. L'Italia diventa avanguardia, compie un balzo di venti' anni"*.

Forse c'è un po' di sopravvalutazione ma certamente fu chiaramente indicata la volontà di rendere immediata la ricaduta sociale della ricerca tradizionalmente perseguita attraverso l'istituto delle consulenze professionali mediante i quali lo Stato centrale e le sue ramificazioni territoriali compravano i risultati di ricerche da essi in precedenza finanziate; ciò in nome di una capziosa difesa del diritto alla proprietà intellettuale.

Tra i fatti di sistema grandemente positivo fu, a mio avviso, l'approccio multidisciplinare ed in particolare quello tra le discipline praticate dai "geocosi" (come Giuseppe Grandori scherzosamente definiva gli scienziati della Terra) e gli ingegneri.

Si partiva da una situazione (in un *excursus* breve come questo alcune semplificazioni sono inevitabili) in cui ad esempio le indagini macrosismiche venivano generalmente effettuate da geologi che difficilmente erano in possesso del necessario sapere in materia di Scienza e Tecnica delle costruzioni (e d'altra parte, quando gli autori erano gli ingegneri, i danni erano considerati come variabile indipendente dalle condizioni geo-morfologiche dei siti) e per l'Ingegneria (non solo in Italia) il terremoto era compiutamente rappresentato, a fini pratici, da un'accelerazione orizzontale di picco e relativa frequenza: fisica della sorgente e differenze tra *near-* e *far-field* erano bellamente ignorate. Se le azioni rilevate sembrano incompatibili con questo semplicistico modello, la reazione era (e purtroppo lo è ancora) quella di proporre l'aumento dei valori di accelerazioni orizzontali di progetto. Si vuole ignorare che nelle aree epicentrali le accelerazioni verticali possono superare ampiamente il valore di *g* come è noto a chiunque abbia letto trattati, anche antichi, di sismologia elementare.

Si cercò, inoltre, di gestire il progetto nel modo più democratico possibile in un mondo ad esso tradizionalmente e pervicacemente impervio (esemplare, a questo proposito il nome del primo presidente del C.N.R.: il Maresciallo d'Italia Pietro Badoglio). Continui e continuamente stimolati erano i confronti ed i congressi anche in corso d'opera nei quali si discutevano i risultati, si decidevano, quando necessario le correzioni di rotta anche al di là di quanto previsto nei progetti iniziali riducendo al minimo le riunioni monodisciplinari al fine di ottenere un'effettiva integrazione a partire anche dallo stesso linguaggio, si decidevano gli indirizzi delle attività future.

I risultati diretti ed indiretti, con un'attenta ottimizzazione delle poche risorse disponibili, furono importanti sia a livello scientifico che organizzativo ed esattamente nello spirito e nella lettera di quanto previsto nella definizione di Progetto Finalizzato più sopra ricordata.

Tra i primi sono la definizione su tutto il territorio nazionale della pericolosità sismica (una mappa del genere in California veniva definita mappa di rischio!) con grande attenzione al rapporto costi/benefici ed integrando i dati del catalogo sismico, rapidamente redatto, con le informazioni di carattere sismotettonico e neotettonico provenienti dai relativi sottoprogetti; il miglioramento della normativa tecnica; la costruzione di strumenti di comunicazione moderni per la diffusione delle conoscenze ritenute elemento fondamentale per un'efficace politica di difesa dai terremoti.

Tra i secondi: l'importante e riconosciuto contributo alla definitiva approvazione della legge in materia di protezione civile che ha un impianto originale rispetto a quelle di altre legislazioni europee dando ampio spazio alle azioni di prevenzione oltre a quelle di gestione delle emergenze; la gemmazione dei gruppi nazionali per la difesa dai terremoti e per il rischio vulcanico; l'impulso alla creazione di una rete sismica nazionale supportata da un Istituto Nazionale di Geofisica e Vulcanologia adeguatamente finanziato e dotato di personale; l'istituzione della Commissione Grandi Rischi a supporto scientifico dell'organizzazione civile di cui fa parte integrante, intesa, almeno inizialmente, come interfaccia con la comunità scientifica di ricerca attiva nei settori relativi ai grandi rischi.

Un importante riconoscimento della qualità del lavoro svolto ci fu all'assemblea generale dell'IUGG di Canberra, dove la relazione italiana venne a lungo applaudita e, fatto inusuale, fu riconosciuta con comunicazione scritta dalla presidenza dell'associazione.

Affermare che allora si misero le basi per un duraturo consolidamento di metodi, filosofia e strutture sarebbe eccessivo. La catastrofe de L'Aquila credo abbia minato le convinzioni anche dei più ottimisti ma di essa non voglio parlare se non per rilevare il singolare destino di una città sede dei due più importanti processi imperniati sui rapporti tra scienza e società (terremoto e Vajont) e sulla natura ed utilità della previsione.

Oggi si è tornati improvvidamente alla vecchia separatezza disciplinare, la normativa è, a mio avviso, eccessivamente severa ma i provvedimenti importanti per migliorare la sicurezza della gran parte del patrimonio edilizio pubblico e privato mancano o sono timidi, saltuari e male indirizzati; la ricerca risente della crisi finanziaria delle università e della drastica e per alcuni versi stolta riduzione del rimpiazzo del personale in quiescenza o emigrato, l'autolesionista prevalenza del finanziamento della ricerca applicata (si badi bene: applicata, non finalizzata) che riduce le possibilità di avere autentica innovazione a favore di quella tecnologica che può essere utile sul breve termine soprattutto per i committenti che sono sollevati da oneri che sarebbero loro ma che nel tempo produrrà una difficilmente recuperabile capacità di tenere il passo con Paesi maggiormente consapevoli dell'importanza strategica di ricerca e formazione di alto livello, i servizi tecnici statali continuano ad essere nello stato denunciato quasi 40 anni fa nella nota relazione Barberi-Grandori al Senato (Barberi e Grandori, 1980), le Regioni tra le strette finanziarie e le molte ed irrisolte questioni concernenti i poteri trasferiti, concorrenti, negati non sono in grado di risolvere problemi accumulati in decenni.

Infine un rapido cenno alla regione nel cui territorio ci troviamo. Nel 1976 era ancora vivo il ricordo della catastrofe del Vajont (1963) che l'aveva colpita sia pur marginalmente. Era inoltre ben presente alla classe dirigente ciò che stava avvenendo nel Bélice. Per questi motivi si richiesero allo Stato provvedimenti inediti che, insieme con la grande solidarietà nazionale ed internazionale che garantì un continuo e largamente sufficiente flusso di finanziamenti, portarono a completare la ricostruzione in un decennio. Fatto mai avvenuto prima e mai ripetuto dopo esclusa, forse, la ricostruzione dopo la seconda guerra mondiale. Va detto che uno dei fattori decisivi del successo fu la possibilità di dotarsi rapidamente di leggi *ad hoc* derivante dal regime speciale della Regione Friuli Venezia Giulia (Riuscetti, 1996).

La legge regionale sulla Protezione Civile del 1986 fu largamente ispirata dal Progetto Finalizzato Geodinamica che in Friuli ebbe il suo battesimo del fuoco e ad essa si rifà anche la successiva legge nazionale finalmente uscita dalle pluriennali secche parlamentari. Essa ancor oggi dimostra la sua validità anche se alcuni aspetti innovativi e fondamentali sono stati progressivamente trascurati.

Proprio in virtù della legge del 1986 la Direzione Regionale della Protezione Civile si assunse il compito di sostenere finanziariamente, senza incertezze, il progetto di ricerca degli enti regionali consorziati (Università ed O.G.S.) per la realizzazione della Mappa Regionale del Rischio Sismico. Successivamente diede il contributo per la realizzazione del progetto ASSESS, sempre della stessa compagine, per determinare in maniera speditiva il quadro della vulnerabilità degli edifici scolastici richiesto dal Governo in conseguenza del disastro di San Giuliano.

Per tre anni, inoltre, contribuì alla realizzazione di un ciclo di aggiornamento professionale in tema di *Seismic Risk Management* ben noto a molti dei partecipanti al congresso che vi hanno insegnato. Ad esso hanno partecipato appartenenti agli ordini professionale degli ingegneri e dei geologi nonché tenici della Regione

Queste ricerche e quelle da esse direttamente derivate per i provvedimenti di emergenza diventati patrimonio del Corpo Nazionale dei Vigili del Fuoco e per la ricognizione dei danni hanno avuto larga eco in ambito UNESCO che li ha proposti per l'utilizzo in molti Stati (Nepal, Laos, Indonesia).

Va detto che esse non hanno avuto altrettanto riconoscimento nella nostra regione dove l'apprezzabile sostegno alla ricerca che per molti anni era continuato pur nel frequente succedersi degli assessori alla Protezione Civile si è malamente interrotto con la sostituzione del vertice tecnico della Direzione Regionale.

Evidentemente, ancora una volta, con il passare del tempo l'attenzione ai problemi delle catastrofi si attenua e si azzera. Eppure la Mappa del Rischio Sismico, che giace nei cassetti degli uffici regionali, dice prima o poi ci ritroveremo ad affrontare un'emergenza simile a quella del 1976 in qualche altra parte della regione e dovremo piangere per non aver approfittato del trascorso periodo di calma per migliorare le difese e diminuire gli impatti negativi su uomini e cose.

Chi ha avuto ed ha il potere di intervenire avrà magari la possibilità di trarre vanto dal successo della prossima ricostruzione invece di essere chiamato a rispondere per non aver operato come doveva e poteva per evitare la catastrofe. Forse è questo l'insegnamento più amaro che ci lascia la storia dei 40 anni.

**Bibliografia**

Barberi F. e Grandori G.; 1980: *Difendersi dai terremoti – La lezione dell'Irpinia*. CNR – Progetto Finalizzato Geodinamica, Roma.

Riuscetti M.; 1996: *Il terremoto del Friuli: scenario di una ricostruzione improbabile in Italia*. In: Bonfanti P. (a cura di), Friuli 1976-1996. Contributo sul modello di ricostruzione, Forum, Udine, pp. 49-60.

Rumiz P.; 2009: *I miracoli di S. Emidio*. La Repubblica del 26/8/2009, Roma.

# Tema 1

## Geodinamica

# sessione 1.1

## Geologia dei terremoti e sismicità

**Convenor: E. Eva e P. Galli**

# COULOMB FAILURE STRESS TRANSFER AND FAULT INTERACTION AT ETNA VOLCANO: SOME CASE-HISTORIES IN THE TIMPE FAULT SYSTEM

**R. Azzaro, V. Maiolino, M. Palano**
*Istituto Nazionale di Geofisica e Vulcanologia, Osservatorio Etneo - Sezione di Catania, Catania*

**Introduction.** In this study we adopt a well-established approach based on the Coulomb failure stress transfer theory to study fault interaction processes at Mt. Etna. Coulomb stress transfer analyses have been applied to this area in order to verify the interaction between magma sources represented by intrusions in the central part of the volcano and tectonic structures located on its flanks. Modelled case-histories showed that volcanic influence have a significant role in promoting or inhibiting fault activity, both before the onset of flank eruptions (Gresta *et al.*, 2005; Mattia *et al.*, 2007; Currenti *et al.*, 2008; Gonzàlez and Palano, 2014) and after the end, when dynamics due to stress readjustment at the scale of the volcanic edifice are usually relevant (Bonanno *et al.*, 2011; Bonaccorso *et al.*, 2013).

By contrast, "fault contagion" seems to be a possible mechanism of interaction at Etna. Seismic activity migrating from fault to fault during seismic swarms in the eastern sector of the volcano is documented in several cases (e.g., Gresta *et al.*, 1987, Patanè *et al.*, 2003; Barberi *et al.*, 2004), and poses the question if the main source of stress perturbation remains the "volcanic system" or not. On the other hand, evidence for interaction between nearby faults following strong earthquakes ($M \geq 4.0$) has been historically observed in the Timpe system, the main seismogenic zone of the Etna region (Azzaro, 2004).

In our analysis we consider couples of earthquakes close in space and time – from hours to one month and 3-6 km apart, respectively – whose causative fault can be recognized by the occurrence of coseismic surface faulting (Azzaro, 1999). We performed tests by considering the Coulomb failure stress change from fault to fault as well as the role of the regional and local stress fields on the "optimal faults".

It has to be stressed how the application of this approach at Etna may shed light on the mechanics of faulting but also represent an complementary tool for short-term earthquake rupture forecast, in order to improving seismic hazard assessment in a densely populated area of the volcano (Azzaro *et al.*, 2013b).

**Active tectonics and seismicity.** Mt. Etna is a Quaternary basaltic stratovolcano located along the eastern coast of Sicily between two first-order tectonic elements: the Apenninic-Maghrebian Chain and the Hyblean Foreland (Branca *et al.*, 2011) (Fig. 1a). This area is characterised by intense geodynamics involving the entire scale of the volcano, with the main process being represented by flank instability which affects the eastern sector of the volcanic edifice. The continuous ESE seaward sliding indeed represents the result of the interaction among regional stress regime, magma intrusion and basement geology (Azzaro *et al.*, 2013a). In fact, the northern and western sectors of the volcano lie over metamorphic and sedimentary rocks belonging to the frontal nappes system of the Apenninic-Maghrebian Chain, whereas the southern and eastern ones (i.e. the unstable sector) overlie marine clays of Quaternary age, deposited on the flexured margin of the northward-dipping downgoing Hyblean Foreland (Lentini *et al.*, 2006). Evidence of active tectonics is mostly distributed over the unstable sector, with a number of volcano-tectonic features controlling dynamics of this area. In particular, the three main faults zones are distinguished from the north to the south (Fig. 1): i) the Pernicana fault, ii) the Tremestieri-Trecastagni fault system and iii) the Timpe fault system (TFS). Since the role played by these tectonic systems in the geodynamics at a local scale is not relevant in this study, in the following we focus on TFS by describing the main features.

TFS crosses the central part of the eastern flank in form of a wide belt of mainly extensional structures, showing well-developed morphological scarps interrupted by hidden sections of the fault (Azzaro *et al.*, 2012). The Moscarello and S. Leonardello faults dissect the lower part of the eastern flank with a NNW-SSE trend and are characterized by prevailingly vertical

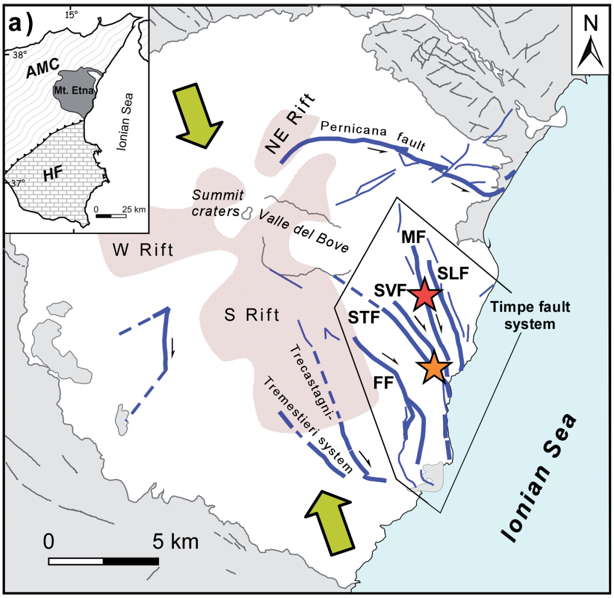


Fig. 1 – Active fault map of Mt. Etna. The main seismogenic structures are in bold; abbreviations indicate: FF, Fiandaca fault; MF, Moscarello f.; SLF, S. Leonardello f.; STF, S. Tecla f.; SVF, S. Venerina f. The contour of the rift zones is in brown; arrows indicate the horizontal regional σ1 stress field (from Patanè and Privitera, 2001). Stars stand for the 1865 earthquakes case-history: red, July event; orange, August event. Inset map a) shows the simplified geological setting of eastern Sicily: AMC, Apenninic-Maghrebian Chain; HF, Hyblean Foreland.

movements. The Fiandaca, S. Tecla and S. Venerina faults displace the middle-low part of the eastern flank with a NW-SE strike and show prevailing right-lateral features. Their intense tectonic activity is confirmed by high slip-rates, varying from 1.0 to 4.3 mm/yr (see Azzaro *et al.*, 2013a for an overview), as well as complex pattern of ground deformation, decennial time series (GPS, SAR) showing inside TFS kinematic domains with different velocities and displacements (Bonforte *et al.*, 2011). Basically, the fairly constant mid-term (decennial) ESE seaward sliding is interrupted by sudden short-term (months to year) accelerations related to flank eruptions.

These faults are highly seismogenic representing the sources of the strongest earthquakes reported in the local seismic catalogue for the last centuries (CMTE Working Group, 2014). With a long-term behavior (~200 years) characterised by a mean recurrence time of about 20 years for severe/destructive events (epicentral intensity $I_0 \geq$ VIII EMS, corresponding to magnitude $M_w \geq 4.6$), the seismic potential of the Timpe fault system is highly significant in terms of local seismic hazard (Azzaro *et al.*, 2013b). It has to be stressed that these shallow earthquakes are accompanied by extensive phenomena of surface faulting, with end-to-end ruptures up to 6.5 km long and vertical offsets up to 90 cm (Azzaro, 1999). The coseismic evidence provides reliable information on the geometry of the causative fault segment and associated kinematics.

In a more general framework, these earthquakes are the strongest events of a seismicity located mainly within the first 7 km of crust (Patane *et al.*, 2004; Alparone *et al.*, 2011; Alparone *et al.*, 2013; Alparone *et al.*, 2015), while the western sector of Etna is characterized by higher focal depths (10-30 km) and lesser seismic rate (Sicali *et al.*, 2014).

**Coulomb stress changes modeling.** It has long been recognized that while an earthquake produces a net reduction of regional stress, earthquakes also are responsible of stress increase, therefore resulting in i) a redistribution of the stress in the surrounding rock volume and ii) an alteration of the shear and normal stress on surrounding faults. Depending on the critical state of failure, sites of positive static stress changes (≥ 0.1 bars) may be foci of future events (Stein, 1999). Spatial and temporal relationships between stress changes and earthquakes are commonly explained through the Coulomb failure stress change defined as (Reasenberg and Simpson, 1992):

$$\Delta CFS = \Delta\tau + \mu\,(\Delta\sigma_n + \Delta P)$$

where $\Delta\tau$ is the shear stress change computed in the direction of slip on the fault, $\Delta\sigma_n$ is the normal stress changes (positive for extension), $\mu$ is the coefficient of friction and $\Delta P$ is the pore pressure change (King *et al.*, 1994; Harris, 1998; King and Cocco, 2000). For simplicity, we considered here a constant effective friction model (Beeler *et al*., 2000; Cocco and Rice 2002), which assumes that ΔP is proportional to the normal stress changes ($\Delta P = -B\Delta\sigma_n$, where $B$ is the Skempton parameter):

$$\Delta CFS = \Delta\tau + \mu' \Delta\sigma_n$$

where $\mu'$ is the effective friction ($\mu' = \mu(1 - B)$). As above mentioned, the fault is brought closer to failure when ΔCFS is positive.

**Application to Mt. Etna: some preliminary results.** In this study, by using the Coulomb 3.3 code (Toda *et al*., 2011), we performed some tests on selected couples of strong earthquakes striking the eastern flank of Mt. Etna in order to verify if a simple fault interaction exists.

Calculations are made in a homogeneous half-space with elastic moduli appropriate for a volcanic domain in the shallow crust (average rigidity modulus of 15 GPa, Poisson's ratio $\upsilon = 0.25$, and effective friction $\mu' = 0.4$). More in details, rigidity modulus value was obtained from recent seismic velocity tomographies (e.g., Chiarabba *et al*., 2000; Patanè *et al*., 2003; Alparone *et al*., 2012) and density models (Schiavone and Loddo, 2007), while the values of $\upsilon$ and $\mu'$ have been selected according to the results of tests performed by Gresta *et al*. (2005).

In order to evaluate the Coulomb stress change, we considered two different perspectives: i) seismic rupture migrating from fault to fault and ii) influence of the regional and local stress fields on the "optimal faults". Regarding the latest point, computations were made by adopting the following static stress fields: the background regional stress field (hereinafter PP2001) described in Patanè and Privitera (2001), and the local stress field estimated for the southeastern flank of Etna during the 2002-2003 eruption (Barberi *et al*., 2004). Moreover, in order to derive a sort of mid-term stress field for our study area, we are compiling a database of more than 100 focal plane solutions, spanning from 1989 to 2014, by collecting data from literature (e.g. Patanè and Privitera, 2001; Alparone *et al*., 2012; De Lorenzo *et al*., 2010; Saraò *et al*., 2010) and online database (http://sismoweb.ct.ingv.it/Focal/).

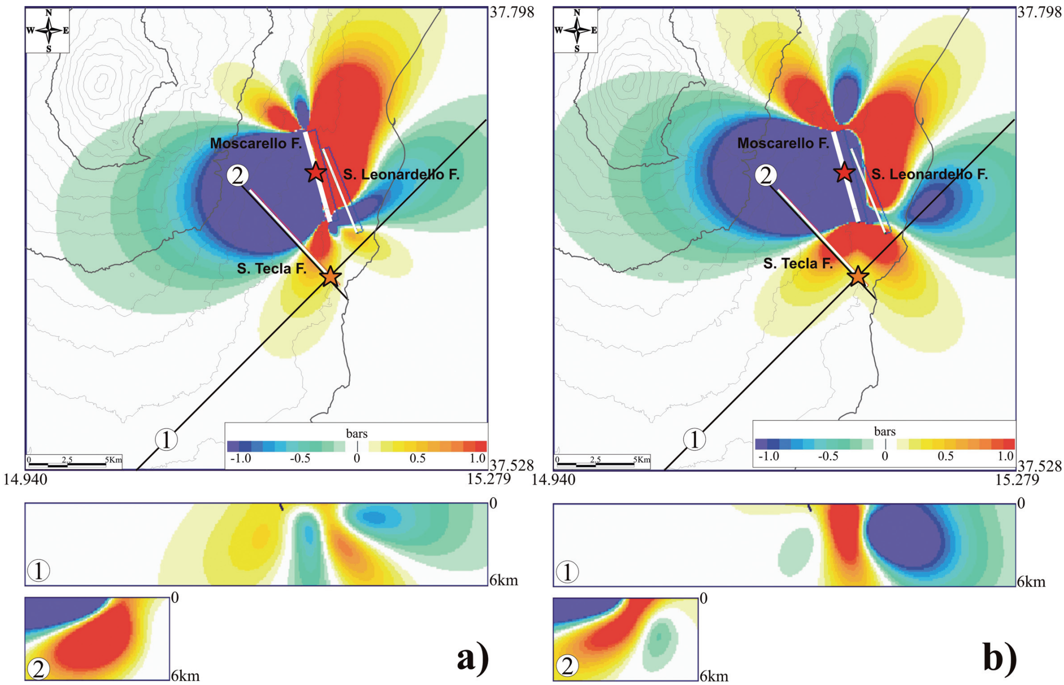


Fig. 2 – Distribution of the ΔCFS due to the Moscarello fault (source, red star) with respect to the S. Tecla fault (receiver, orange star). The areal distribution is calculated at a depth of 0.4 km. Maps and vertical sections are related to: a) dip-slip kinematics; b) right-lateral strike-slip kinematics.

Fig. 2 reports some preliminary results related to the July 19, 1865 earthquake (epicentral intensity $I_0$ IX EMS, $M_w$ 5.1) occurring along the Moscarello fault, which was followed the month later by another strong shock striking the S. Tecla fault ($I_0$ VIII EMS, $M_w$ 4.6). We calculated the ΔCFS caused by the Moscarello fault (source) on the S. Tecla fault (receiver). Results are reported as areal distribution at a depth of 0.4 km and along two vertical sections related to a receiver fault with dip-slip (Fig. 2a) and right-lateral strike-slip (Fig. 2b) kinematics. We observe that the southern segment of the S. Tecla fault which ruptured during the August 19, 1865 earthquake, falls within the lobe with increase of stress (red areas), where the rupture is favored.

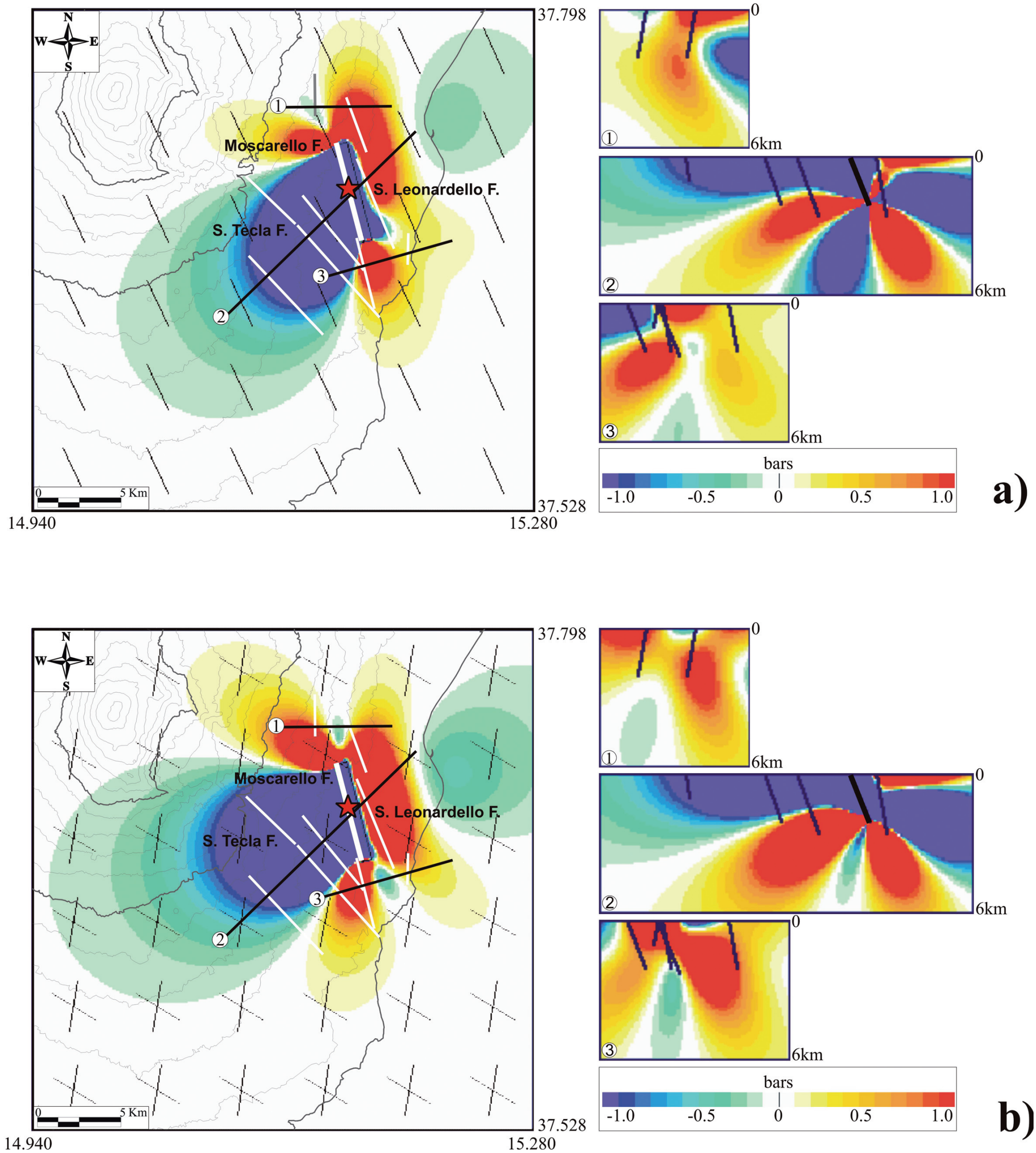


**Fig. 3** – Distribution of the ΔCFS due to the Moscarello fault by adopting the regional PP2001 stress field. The areal distribution is calculated at a depth of 0.4 km. Maps and vertical sections are related to optimally oriented a) normal faults and b) strike-slip faults.

By taking into account the slip historically observed in the field along the Moscarello fault and the PP2001 stress, we modelled the areal distribution of ΔCFS at a depth of 0.4 km as well as for three different sections crossing TFS (Fig. 3). In particular, we show two different computations considering faults that could be "encouraged" to slip, with dip-slip (Fig. 3a) and strike-slip kinematics (Fig. 3b), respectively. We observe that some faults, or parts of them, fall within lobes with increase of stress (red areas), where the rupture should be favored, while faults, or parts of them, that are located in areas in which the ΔCFS is negative (blue areas), are those potentially inhibited to slip.

Also in this computation, we observe that the southern section of the S. Tecla fault, where the August 1865 earthquake nucleated, is characterized by a positive ΔCFS, confirming the observations inferred from the previous computation.

These results, although preliminary, suggest that the August 19, 1865 earthquake could be potentially "triggered" by a stress transfers mechanism. Further tests on other case-histories might indicate if the stress transfer represents a common mechanism during faulting at Etna and therefore, provides useful constraints on the processes controlling it.

**References**


Alparone S., Barberi G., Bonforte A., Maiolino V. and Ursino A.; 2011: *Evidence of multiple strain fields beneath the eastern flank of Mt Etna volcano (Sicily, Italy) deduced from seismic and geodetic data during 2003–2004*. Bull. Volcanol., **73**, 869-885, doi: 10.1007/s00445-011-0456-1.

Alparone S., Barberi G., Cocina O., Giampiccolo E., Musumeci C. and Patanè D.; 2012: *Intrusive mechanism of the 2008–2009 Mt. Etna eruption: Constraints by tomographic images and stress tensor analysis*. J. Volcanol. Geotherm. Res., **229-230**, 50-63, doi: 10.1016/j.jvolgeores.2012.04.001.

Alparone S., Bonaccorso A., Bonforte A. and Currenti G.; 2013: *Long-term stress-strain analysis of volcano flank instability: The eastern sector of Etna from 1980 to 2012*. J. Geophys. Res. Solid Earth, **118**, doi: 10.1002/jgrb.50364.

Alparone S., Cocina O., Gambino S., Mostaccio A., Spampinato S., Tuvè T. and Ursino A.; 2013: *Seismological features of the Pernicana–Provenzana fault system (Mt Etna, Italy) and implications for the dynamics of northeastern flank of the volcano*. J. Volcanol. Geotherm. Res., **251**, 16-26, doi: 10.1016/j.jvolgeores.2012.03.010.

Alparone S., Maiolino V., Mostaccio A., Scaltrito A., Ursino A., Barberi G., D'Amico S., Di Grazia G., Giampiccolo E., Musumeci C., Scarfì L., and Zuccarello L.; 2015: Instrumental seismic catalogue of Mt. Etna earthquakes (Sicily, Italy): ten years (2000-2010) of instrumental recording. Ann. Geophys., **58** (4), doi: 10.4401/ag-6591.

Azzaro R.; 1999: *Earthquake surface faulting at Mount Etna volcano (Sicily) and implications for active tectonics*. J. Geodyn. **28**, 193-213, doi: 10.1016/S0264-3707(98)00037-4.

Azzaro R.; 2004: *Seismicity and active tectonics in the Etna region: constraints for a seismotectonic model*. In: Bonaccorso A., Calvari S., Coltelli M., Del Negro C., Falsaperla S., (eds.) Mt. Etna: volcano laboratory, American Geophysical Union, Geophysical monograph, **143**, pp. 205-220.

Azzaro R., Branca S., Gwinner K. and Coltelli, M.; 2012: *The volcano-tectonic map of Etna volcano, 1:100.000 scale: morphotectonic analysis from high-resolution DEM integrated with geologic, active faulting and seismotectonic data*. It. J. Geosci. (Boll. Soc. Geol. It.), **131** (1), 153-170.

Azzaro R., D'Amico S., Peruzza L. and Tuvè T.; 2013b: *Probabilistic seismic hazard at Mt. Etna (Italy): the contribution of local fault activity in mid-term assessment*. J. Volcanol. Geotherm. Res., **251**, 158-169, doi: 10.1016/j.jvolgeores.2012.06.005.

Azzaro R., Bonforte A., Branca S. and Guglielmino, F.; 2013a. *Geometry and kinematics of the fault systems controlling the unstable flank of Etna volcano (Sicily)*. J. Volcanol. Geotherm. Res., **251**, 5-15, doi: 10.1016/j.jvolgeores.2012.10.001.

Barberi G., Cocina O., Maiolino V., Musumeci C. and Privitera E.; 2004: *Insight into Mt. Etna (Italy) kinematics during 2002-2003 eruption as infered from seismic stress and strain tensors*. Geophys. Res. Letters, **31**, L21614, doi: 10.1029/2004GL020918.

Beeler N.M., Simpson R.W., Hickman S.H. and Lockner D.A.; 2000: *Pore fluid pressure, apparent friction and Coulomb failure*. J. Geophys. Res., **105**, 25,533-25,542, doi: 10.1029/2000JB900119.

Bonaccorso A., Currenti G., and Del Negro C.; 2013: *Interaction of volcano-tectonic fault with magma storage, intrusion and flank instability: a thirty years study at Mt. Etna volcano*. J. Volcanol. Geotherm. Res., **251**, 127-136, doi: 10.1016/j.jvolgeores.2012.06.002.

Bonanno A., Palano M., Privitera E., Gresta S. and Puglisi G.; 2011: *Magma intrusion mechanisms and redistribution of seismogenic stress at Mt. Etna volcano (1997-1998)*. Terra Nova 23, 339-348, doi: 10.1111/j.1365-3121.2011.01019.x.

Branca, S., Coltelli, M., Groppelli G. and Lentini, F.; 2011: *Geological map of Etna volcano, 1:50,000 scale*. It. J. Geosci. (Boll. Soc. Geol. It.), **130**, 265-291, doi: 10.3301/IJG.2011.15.
Chiarabba C., Amato A., Boschi E. and Barberi F.; 2000: *Recent seismicity and tomographic modeling of the Mount Etna plumbing system*. J. Geophys. Res., **105** (B5), 10,923-10,938, doi: 10.1029/1999JB900427.
Cocco M. and Rice J.R.; 2002: *Pore pressure and poroelasticity effects in Coulomb stress analysis of earthquake interactions*. J. Geophys. Res., **107** (B2), 2030, doi: 10.1029/2000JB000138.
Currenti G., Del Negro C., Ganci G. and Williams C. A.; 2008: *Static stress changes induced by the magmatic intrusions during the 2002–2003 Etna eruption*. J. Geophys. Res., **113**, B10206, doi: 10.1029/2007JB005301.
De Lorenzo S., Giampiccolo E., Martinez-Arevalo C., Patanè D. and Romeo A.; 2010: Fault plane orientations of microearthquakes at Mt. Etna from the inversion of P-wave rise times. J. Volcanol. Geotherm. Res., 189, 247-256, doi: 10.1016/j.jvolgeores.2009.11.011.
Gonzalez P. J. and Palano M.; 2014: Mt. Etna 2001 eruption: *New insights into the magmatic feeding system and the mechanical response of the western flank from a detailed geodetic dataset*. J. Volcanol. Geotherm. Res., **274**, 108-121, doi: 10.1016/j.jvolgeores.2014.02.001.
Gresta S., Glot J.P., Patanè G., Poupinet G. and Menza S.; 1987: *The October 1984 seismic crisis at Mount Etna. Part I: Space-time evolution of the events*. Ann. Geophys., ***5B***, 671-680.
Gresta S., Ghisetti F., Privitera E. and Bonanno A.; 2005: *Coupling of eruptions and earthquakes at Mt. Etna (Sicily, Italy): a case study from the 1981 and 2001 events*. Geophys. Res. Lett., **32**, L05306, doi: 10.1029/2004GL021479.
Harris R.A.; 1998: Introduction to special section: *Stress triggers, stress shadows, and implications for seismic hazard*. J. Geophys. Res., **103**, 24,347-24,358, doi: 10.1029/98JB01576.
King G.C.P. and Cocco, M.; 2000: *Fault interaction by elastic stress changes: New clues from eaarthquake sequences*. Adv. Geophys., **44**, 1-38, doi: 10.1016/S0065-2687(00)80006-0.
King G.C.P., Stein R. S. and Lin J.; 1994: *Static stress changes and the triggering of earthquakes*. Bull. Seismol. Soc. Am., **84**, 935-953.
Lentini F., Carbone, S. and Guarnieri P.; 2006: *Collisional and postcollisional tectonics of the Apenninic-Maghrebian orogen (southern Italy)*. In: Dilek, Y., Pavlides, S. (Eds.), Postcollisional tectonics and magmatism in the Mediterranean region and Asia. Geol. Soc. Am. Special Papers, **409**, pp. 57-81.
Mattia M., Patanè D., Aloisi M. and Amore M.; 2007: *Faulting on the western flank ofMt Etna and magma intrusions in the shallow crust*. Terra Nova, **19**, 89-94, doi: 10.1111/j.1365-3121.2006.00724.x.
Patanè D. and Privitera E.; 2001: *Seismicity related to 1989 and 1991-93 Mt. Etna (Italy) eruptions: kinematic constraints by fault plane solution analysis*. J. Volcanol. Geotherm. Res. **109**, 77-98, doi: 10.1016/S0377-0273(00)00305-X.
Patanè D., Cocina O., Falsaperla S., Privitera E. and Spampinato S.; 2004: *Mt Etna Volcano: A Seismological Framework*. In: "Etna Volcano Laboratory", Bonaccorso A., Calvari S., Coltelli M., Del Negro C., Falsaperla S. (Eds), AGU (Geophysical monograph series), 147-165.
Patanè, D., Chiarabba, C., De Gori, P., and Bonaccorso, A.; 2003: *Magma ascent and the pressurization of Mt. Etna's volcanic system*. Science, **299**, 2061-2063.
Reasenberg P. A. and Simpson R. W.; 1992: *Response of regional seismicity to the static stress change produced by the Loma Pietra earthquake*. Science, **255**, 1687-1690.
Saraò A., Cocina O., Privitera E., and Panza G.F.; 2010: *The dynamics of the 2001 Etna eruption as seen with full moment tensor analysis*. Geophys. J. Int., **181**, 951-965, doi: 10.1111/j.1365-246X.2010.04547.
Schiavone, D. and Loddo M.; 2007: *3-D density model of Mt Etna volcano (Southern Italy)*. J. Volcanol. Geotherm. Res. **164**, 161-175, doi: 10.1016/j.jvolgeores.2007.04.016.
Sicali S., Barbano M.S., D'Amico S. and Azzaro R.; 2014: *Characterization of seismicity at Mt. Etna volcano (Italy) by inter-event time distribution*. J. Volc. Geotherm. Res., **270**, 1-9, doi: 10.1016/j.jvolgeores.2013.11.011.
Stein R.S., 1999. *The role of stress transfer in earthquake occurrence*. Nature, **402**, 605-609.
Toda S., Stein R. S., Sevilgen V. and Lin J.; 2011: *Coulomb 3.3 Graphic-rich deformation and stress-change software for earthquake, tectonic and volcano research and teaching-user guide*. U.S. Geological Survey Open-file Report 2011-1060, 63 p., available at http://pubs.usgs.gov/of/2011/1060.

# ANALYZING SEISMOINDUCED EFFECTS AND FRAGILE DEFORMATION IN THE AVOLA VECCHIA AREA (SOUTHERN SICILY): IMPLICATION FOR ACTIVE TECTONICS AND SEISMICITY

**M.S. Barbano, C. Pirrotta, G. De Guidi, C. Farina**
*Dipartimento di Scienze Biologiche, Geologiche e Ambientali, Università di Catania, Italy*

**Introduction.** Although in active areas tectonics is considered the most probable trigger mechanism of fragile deformation of the rocky masses, seismic shock is another highly probable cause (Caputo, 2005; Montenat *et al.*, 2008). Indeed, strong earthquakes can trigger several soil deformation phenomena, such as liquefaction, ground fracturing and landslides, which can often cause more damage than the seismic shaking itself. Ground fracturing, which is among the most diffuse seismo-induced effects, can also contribute to increase terrain instability. Rocks and sediments can record such effects as evidence of paleoearthquakes.

The study of these markers of seismicity can be a useful tool to obtain data on ancient earthquakes occurring in a region. Indeed, although the recognition of off-fault seismo-induced structures does not provide precise and direct information on seismogenic fault and earthquake parameters (magnitude, intensity, fault length and elapsed time), it can give important information on the epicentral distance of the site, earthquake magnitude threshold and intensity reached at the site. Moreover, the finding of features dated before historical records, can be useful to extend the seismic catalogues back in time, to assess recurrence time of earthquakes and so to better characterize the seismicity of an area.

Eastern Sicily is considered among the most seismically active area in Italy. Several strong earthquakes with Maw 6.0–7.4 (Rovida *et al.*, 2011) have occurred in the last millennium and numerous Quaternary faults modified the landform. However, the lack of instrumental data for strong historical earthquakes, and poor exposures of faulted Quaternary sediments do not allow the unambiguous identification of active, seismogenic faults. An extensional belt running, for ≈ 370 km, from eastern Sicily to South Calabria, the Siculo Calabrian Rift Zone (SCRZ), is considered responsible of the crustal seismicity of these areas (Catalano *et al.*, 2008). This belt is composed by faults up to 50 km long and some of these are considered seismogenic only on few evidence of geological and structural studies and macroseismic data (Bianca *et al.*, 1999; Catalano *et al.*, 2008). Seismicity of south-eastern Sicily is tentatively related to some tectonic structures of the northern and western Hyblean Plateau. The 1169 and the 1693 earthquakes were located off-shore and associated with Malta Escarpment fault system since the strong tsunamis triggered by these events and the lack of surface faulting evidence on-shore (e.g. Azzaro and Barbano, 2000; Monaco and Tortorici, 2000; Argnani *et al.*, 2012). The Avola Fault segment has been considered responsible of the 9th January 1693 foreshock only on the basis of the damage area that extend along a narrow belt, on land, along the eastern edge of the Hyblean Plateau (Bianca *et al.*, 1999).

The 1169, 1542, 1693, 1848 and 1990 south-eastern Sicily earthquakes caused damage, numerous fatalities and triggered several ground failures, as reported by historical sources.

Geological evidence of liquefactions, correlated to some of the strongest earthquakes, were found in the Holocene deposits of the Mascali area and in the Catania Plain, both characterized by a continental fluviatile sedimentation environment (Guarnieri *et al.*, 2009). Moreover, Pirrotta and Barbano (2011) reported seismically induced deformation structures along the rocky coast of Vendicari (southeastern Sicily). Traces of seismically induced features can be particularly significant to assess earthquake recurrence time in areas that, like eastern Sicily, have poorly defined seismogenic sources.

In this study we analyse a seismically induced landslide along with some fractures affecting archaeological structures in the ancient site of Avola Vecchia, southwest of Syracuse (Fig. 1), and correlate them with historical and prehistorical events.

Avola Vecchia is located in the eastern coastal sector of the Hyblean Plateau, which is the emerged part of a gently deformed segment of the African continental margin representing

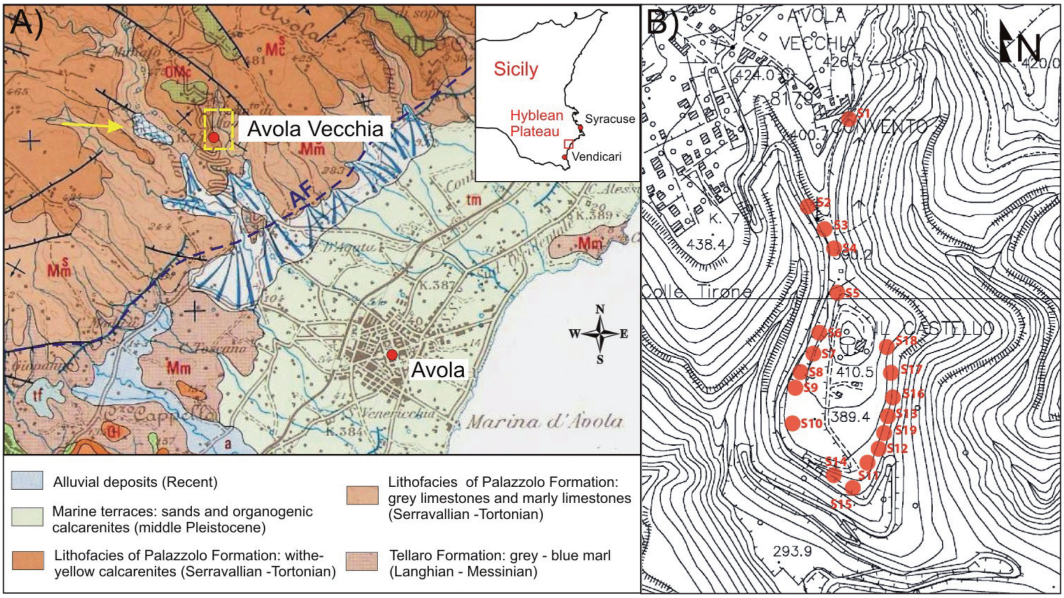


Fig. 1 – A) Geologic map (modified after Lentini *et al.*, 1984) and location of the studied area; AF is the Avola Fault; the yellow arrow marks the 1693 Mt. Ginisi landslide; B) Mt Aquilone and location of the caves with the mesostructural stations.

the Tertiary foreland of the Apenninic-Maghrebian Thrust Belt. NE–SW and NW–SE trending normal fault systems affect the outcropping Miocene terrain (Lentini *et al.*, 1984). In the studied area the main of these faults is the 20 km long, NE-striking E-dipping normal Avola Fault (AF in Fig. 1). The growth of this fault since 200-240 ky is hypothesized on geomorphological observation (Catalano *et al.*, 2008) but its recent activity has never been constrained.

Active tectonics of the eastern sector of the Hyblean Plateau is scantly documented. The most recent evidence consist in joint sets and grid-lock fracture systems affecting Late Pleistocene terraced deposits (yellow sands and bioclastic calcarenites) documenting the existence of an extensional tectonic regime (De Guidi *et al.*, 2013). However, present day active tectonics has never been documented for lacking of deformed Holocene terrains.

**Historical data**. The foundation of Avola, in an area previously inhabited by the Sicans, is perhaps connected to the history of the older town of Hybla Major (Di Maria, 1745) that was invaded by the Sicels in the 11th-9th centuries BC. The Greeks colonized the city in the 8th century BC. After the Syracuse domination (4th century BC), the Romans conquered Sicily in 227 BC. The Sicels' age is testified by numerous finds, especially pottery and dishes, found in the oven-shaped tombs resembling a beehive and characterizing the surroundings of Avola Vecchia and the near site of Cavagrande di Cassibile. The cave houses are a type of dwelling cave carved into the rock that marks the ancient Avola urban centre. They date back to the Byzantine-medieval period (6th-9th century AD) and people lived there until the 1693 earthquakes (Gringeri Pantano, 1996). The caves of the Sicels' necropolis along with the Byzantine-medieval cave houses are among the oldest testimony of civilization in the area. The older Hybla town disappeared in the early middle Ages, and the territory started to be repopulated during the Islamic domination of Sicily (9th-11th centuries AD). However, Avola Vecchia appeared only during the Norman or Hohenstaufen rule (12th-13th centuries), and persisted until the 1693, when two earthquakes destroyed it, as well as many of the southeastern Sicily towns. Not persisting more reasons to rebuild the city in an elevated site to protect themselves from the Saracens' incursions and to favoured maritime trade, the old city was abandoned and rebuilt in a new location along the coast (Fig. 1), following the geometrical and regular plan designed by the architect friar Angelo Italia (Gringeri Pantano, 1996).

Among the numerous historical sources, reporting the effects of the 1693 earthquakes in Avola Vecchia, we selected the two witness contemporary and reliable accounts by Dell'Arte (1699) and Di Maria (1745), who described in detail the effects of earthquakes on the city and on the territory.

"In Avola Vecchia, the January 9 at four-thirty (Italian time, used in the XVII century in Sicily) in the night (~21 GMT), a strong earthquake destroyed almost the whole quarters known as di Sopra and Marchi, ruining houses since foundations with the loss of 500 citizens. 40 hours after the first shock, on January 11 at 20 hours and a quarter (~13 GMT), the earthquake was so proud and terrible that destroyed the entire city. No stone remained upon stone, including caves, and people was not able to distinguish one house from the other houses" (Dell'Arte, 1699). The earthquake "has unhinged stones above which Avola was built; then destroyed throughout the whole city" (Di Maria, 1745). Five hundred people died for this shock. In Avola, the whole fatalities (9 and 11 January shocks) were 1,000 out of 6,225, in minor percentage than other Sicilian cities, because most of the inhabitants, were outdoors, having felt another slight shock at 16 hours (~9 GMT). The fortified castle, located on the acropolis of Mt Aquilone, was destroyed, although it had been rebuilt a first time after the December 10, 1542 earthquake, "which had ruined the castle and many houses" (Gallo, 1966). "The Mount called Gisini split, and almost half Mount, breaking away with fury, sank in the bed of the Valley called Carnevale, remaining under the portentous mass three mills with many people inside them" (Di Maria, 1745). The Mt Gisini landslide is further documented by an archive plan concerning the construction of a canal system to bypass the occlusion and provide water to the plantations and factories (Gringeri Pantano, 1996).

**Data analysis**. Aerial-photos interpretation, field survey and mesostructural analysis near Avola Vecchia allowed us to observe some devastating effects of the 1693 earthquakes still evident on the surface.

Mechanical discontinuities with decimetric spacing affect the calcarenites, marly limestones and limestones of Miocene age, outcropping at Mt Aquilone. Numerous of these fractures affect both the cave-tombs of the Sicels' necropolis and the Byzantine-medieval cave houses (Figs. 2A and 2B). Since they can give an evidence of active tectonics, we performed systematic and mesostructural analyses (stereographic projections and rose diagrams) of 137 fractures disturbing 19 caves of Mt Aquilone (Fig. 1B). These fractures are up to several metres long, often opened from few millimetres to several centimetres (Figs. 2B and 2C) and sometimes filled by re-crystallized calcite deposit. They show no, or few, evidence of shear motion, being originated as purely extensional fractures. This type of brittle features is known as "extensional joints" and they have been recognized as one of the most common deformational structures in every tectonic environment (Caputo, 2010 and references therein).

The joints are grouped in two orthogonal sets with main directions N45 and N140 (Fig. 2D). According to Caputo (2005), two orthogonal joint sets are due to stress swap mechanisms between $\sigma_2$ and $\sigma_3$ stress axes that occur locally causing stress field deformation. However, the prevalence of fractures with direction NE-SW indicates that the local tectonic maximum extension is almost NW-SE oriented (Fig. 2E), which is compatible with the regional stress field. This stress field is also responsible of the Avola fault (AF in Fig. 1A). It is worth noting that the study site is located on the footwall of the Avola Fault, which according to some authors may be active and could be the source of the 9 January 1693 earthquake (Monaco and Tortorici, 2000).

Nevertheless, other mechanisms such as seismic shacking can have triggered the fractures. Indeed historical accounts describe damage in the cave houses and "unhinged stones" during the 1693 earthquakes.

We have also compared the trend of the NE-SW fractures, with that of the slope at the location of each mesostructural station. A similitude between the two directions was observed

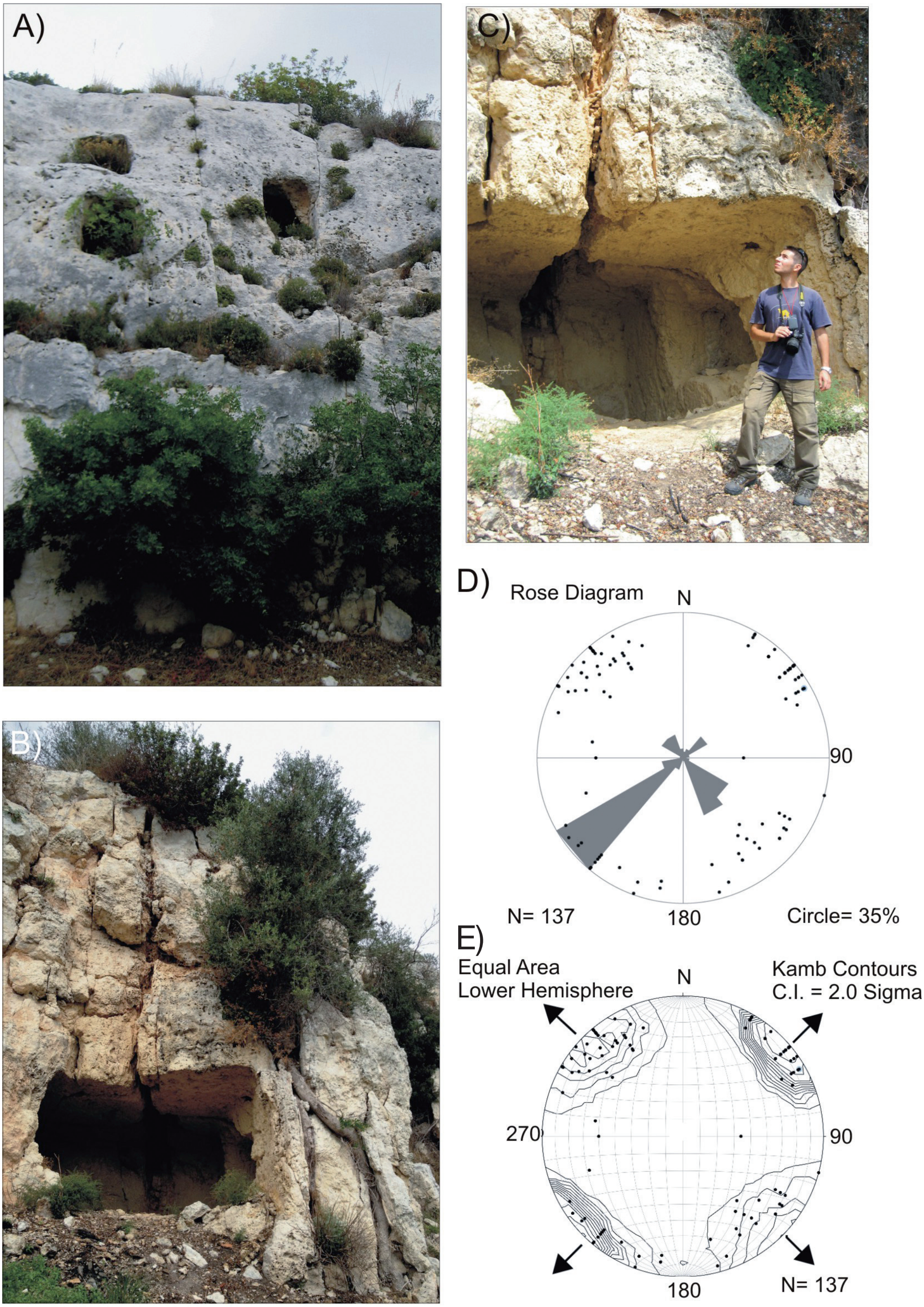


Fig. 2 – A) Fractures in the limestone affecting oven-shaped tombs in the Sicels' necropolis (11th-9th centuries BC); B) and C) open fractures in the calcarenite affecting cave houses dated back to the Byzantine-medieval period (6th-9th century AD); D) stereographic projections of the joints in the surveyed stations and rose diagram; E) stress inversion.

for the most of the stations indicating that the NE-SW set represents potential failure surfaces for future rockfalls. Moreover, the weakening of the rocky slope, along with the enlargement of the fractures, is likely enhanced by water circulation dissolving the limestone and by the presence of the caves. Therefore, seismic shaking, which in turn can drive slope instability, can be considered a cause for the rock fracturing superimposed on tectonic stress.

Seismically induced brittle deformation on rock, usually found close to active fault zones worldwide (Montenat *et al.*, 2008), is documented locally at Vendicari (10 km south from the study site) (Pirrotta and Barbano, 2011).

The Mt. Gisini landslide (Figs. 1 and 3) occurred to the west of Avola Vecchia. It was a planar translational rockslide, with a steep slip surface, involving a volume of 2 x 106 m$^3$ of sub-horizontally bedded Tortonian and Messinian calcarenite and marly limestone (Gringeri *et al.*, 2002). The accumulation, about 250 m wide and 370 m long, is around 60 m high above the valley bottom. Despite the high degree of fracturing, the rock stratification remains sub-horizontal. The landslide produced the obstruction of the Miranda river causing a dam belongs to type II (spanning the entire valley) according to the classification of landslide dams by Costa and Schuster (1988) (Nicoletti and Parise, 2002). Nowadays the landslide body is re-incised by the Piscitello stream that creates a V valley on it. The erosion processes on the downstream face have triggered a secondary landslide on the downstream side of the same landslide body. The Mt. Gisini landslide seems to have reached the position of minimum potential energy and, therefore, the probability of a further failure seems low (Nicoletti and Parise, 2002).

**Discussion**. The Avola Vecchia area shows several effects of active tectonics and earthquake shaking. We have observed brittle deformational structures and seismically induced features such as the Mt. Gisini landslide.

Fig. 3 – The Mt. Gisini landslide that dammed the River Miranda on 11 January 1693, and destroyed three mills killing people.

The occurrence of landslides and ground fracturing during strong earthquakes in eastern Sicily is also illustrated both by the historical accounts, reporting the observation of such phenomena in several places of this region, and by previous field works that studied similar seismically induced structures (Nicoletti and Parise, 2002; Guarnieri *et al*., 2009; Pirrotta and Barbano, 2011).

The large and inactive landslide occurred near Avola Vecchia is described by historical accounts as related to the 1693 earthquake. Other landslides were surveyed in the same area and in southeastern Sicily. Since this is a seismic region but commonly considered no prone to slide failure, these landslides are considered earthquake-triggered (Nicoletti and Parise, 2002). The landslides testify the occurrence of seismic events with magnitude greater than 5 and intensity greater than IX, that are the thresholds for which these seismo-induced features may develop in a site (e.g. Pirrotta and Barbano, 2011). According to empirical relationship between source parameters and epicentral distance of the site where landslides developed during historical earthquakes in eastern Sicily, the triggering earthquakes occurred at a distance lower than 20 km, considering the threshold parameters, or at a longer distance but with a higher magnitude than the threshold (Pirrotta *et al*., 2007).

The study of joint sets and grid-lock fracture systems, allows documenting the existence of an extensional tectonic regime, which is still active since fractures affect historical and archaeological man-made structures. The obtained stress orientations are in good agreement with the regional extensional tectonic stress field and support the recent activity of the Avola fault located close to Mt. Aquilone (Fig. 1A). Since the joints can be related and reopened either because of coseismic shaking, or for slope instability, additional surveys and analysis need to validate their connection to the recent stress field.

**Conclusion.** Coeval sources describe with certainty a landslide triggered by the January 11, 1693 Sicilian earthquake near Avola Vecchia. The landslide occurred west of the town, at Mt. Ginisi, along the Miranda river, which was the economic and productive focus of the territory hosting five mills. The landslide destroyed three mills and dammed the river. Near Avola Vecchia, at Mt. Aquilone, we have recognized several fractures in rock masses as well as in anthropogenic caves (the so-called cave houses) and oven-shaped tombs, dating back to the Byzantine period and Sicels' age, respectively. The mesostructural analysis of the rock masses showed that fractures are mainly classifiable as joints and that some of them are due to the tectonic stress field. The fact that fractures affect man-made structures confirms that in southern Sicily a WNW-ESE extensional regime is still active. Some fractures are due to seismic shaking and slope gravity effects, suggesting that several earthquakes have affected the area. Therefore, with the aim to provide new and useful information on ancient earthquakes, we plan to extend structural and morphometric analyses in other site of the Avola area and to date landslides and fractures. This data can help to better define the seismic framework in Sicily having a strong seismic activity but poorly defined seismogenic sources.

**Acknowledgements.** The research was supported by University of Catania PRA grants.

## References

Argnani A., Armigliato A., Pagnoni G., Zaniboni F., Tinti S., Bonazzi C.; 2012: Active tectonics along the submarine slope of south-eastern Sicily and the source of the 11 January 1693 earthquake and tsunami. Nat. Haz. Earth Syst. Scie., 12, 1–9, doi: 10.5194/nhess-12-1-2012.

Azzaro R., Barbano M.S.; 2000: Analysis of seismicity of Southeastern Sicily: a proposed tectonic interpretation. Ann. Geofis. 43, 171–188.

Bianca M., Monaco C., Tortorici L., Cernobori L.; 1999: Quaternary normal faulting in southeastern Sicily (Italy): a seismic source for the 1693 large earthquake. Geophysical Journal International, 139 (2), 370-394.

Caputo R.; 2005: Stress variability and brittle tectonic structures. Earth-Sci. Rev. 70, 103–127

Caputo R.; 2010: Why joints are more abundant than faults. A conceptual model to estimate their ratio in layered carbonate rocks. J. Struct. Geol., 32, 1257–1270.

Costa J.E., Schuster R.L.; 1988: The formation and failure of natural dams. Geol. Soc. Am. Bull., 100,1054–1068.

Catalano S., De Guidi G., Monaco C., Tortorici G., Tortorici L.; 2008: Active faulting and seismicity along the Siculo–Calabrian Rift Zone (Southern Italy) Tectonophysics 453, 177–192.
Dell'Arte P.; 1699: Storia dell'Antica Avola e del terremoto dell'anno fatale 1693.
De Guidi G., Caputo R., Scudero S.; 2013: Regional and local stress field orientation inferred from quantitative analyses of extension joints: Case study from southern Italy. Tectonics, 32 (2), 239-251.
Di Maria F.; 1745: Ibla rediviva. 1989 Reprint. Pro Loco, Avola,160 pp.
Gallo C.; 1966: Poblemi ed aspetti storici della ricostruzione a Noto e nella Sicilia orientale dopo il terremoto del 1693. Archivio Storico Siciliano, serie III, 15, 89-190.
Gringeri Pantano F.; 1996: La città esagonale. Avola: L'antico sito, lo spazio urbano ricostruito. Sellerio, Palermo, 269 pp.
Gringeri Pantano F., Nicoletti P.G., Parise M.; 2002: Historical and Geological Evidence for Seismic Origin of Newly Recognized Landslides in Southeastern Sicily, and Its Significance in Terms of Hazard. Environ. Manag., 29 (1), 116–131
Guarnieri P., Pirrotta C., Barbano M.S., De Martini P.M, Pantosti D., Gerardi F., Smedile A.; 2009: Paleoseismic investigation of historical liquefactions along the Ionian coast of Sicily. J. Earth. Eng., 13, 68–79.
Lentini F., Carbone S., Grasso M.; 1984: Carta geologica della Sicilia Sud-Orientale. Scale 1:100.000. S.EL.CA., Florence.
Monaco C., Tortorici L.; 2000: Active faulting in the Calabrian arc and eastern Sicily. J. Geodyn., 29, 407-424.
Montenat C., Barrier P., Ott d'Estevou P., Hibsch C.; 2008: Seismites: an attempt at critical analysis and classification. Sedim. Geol., 196, 5–30.
Nicoletti P.G., Parise M.; 2002: Seven landslide dams of old seismic origin in southeastern Sicily (Italy). Geomorph.: 46 (3– 4), 203– 222.
Pirrotta C., Barbano M.S.; 2011: Analysis of deformation structures in Pliocene and Quaternary deposits of the Hyblean Plateaux (South-eastern Sicily). Tectonophysics. 499, 41-53.
Pirrotta C., Barbano M.S, Guarnieri P., Gerardi F.; 2007: A new dataset and empirical relationships between magnitude/intensity and epicentral distance for liquefaction in central-eastern Sicily. Ann. of Geoph,, 50, 763-774.
Rovida A., Camassi R., Gasperini P., Stucchi M. (ed); 2011: CPTI11, the 2011 version of the Parametric Catalogue of Italian Earthquakes, Milano, Bologna, http://emidius.mi.ingv.it/CPTI.

# FEASIBILITY STUDY OF A NETWORK FOR THE MICROSEISMIC MONITORING OF THE NATURAL GAS FIELD OF "SANT'ALBERTO" (PO PLAIN, ITALY)

**S. Carannante[1], E. D'Alema[1], M. Buttinelli[2], M. Anselmi[2], S. Lovati[1], M. Massa[1], P. Augliera[1], G. Franceschina[1]**
[1] *Istituto Nazionale di Geofisica e Vulcanologia, Milano, Italy*
[2] *Istituto Nazionale di Geofisica e Vulcanologia, Roma, Italy*

**Introduction.** The natural gas reservoir named "Sant'Alberto" is located within the area of the "San Vincenzo" exploration license (Po Plain, Italy) owned by PoValley Energy (PVE), an oil and gas E&P company engaged in the production and development of hydrocarbon assets in northern Italy (http://www.povalley.com). In 2006, following an extensive geological and geophysical re-evaluation of the available gas fields, PVE presented to the Italian "Ministero dello Sviluppo Economico (MiSE)" (http://unmig.sviluppoeconomico.gov.it), the application for the homonymous hydrocarbon exploitation concession. The "Sant'Alberto" concession covers a 20 km$^2$ area and it is located 35 km NE of Bologna and 15 km SW of Ferrara, within the municipalities of Galliera, Malalbergo and San Pietro in Casale. The area is characterized by an elevated anthropogenic noise, due to the presence of important communication routes and of anthropic activities, both agricultural and industrial. As an example, the Bologna-Padova (A13) highway flanks the concession passing at about 1.5 km from the east side, while the homonymous railway line runs through it. In this area, the exploration activities carried out by AGIP/ENI company starting from 1956, allowed to identify and put into production the

"San Pietro in Casale" gas field, in which 24 wells have been drilled. The historic production of the field, ended in 1995, amounts to 500 $MSm^3$ from 14 wells. In 2011, PVE started a new exploration phase by acquiring a 31-km line of 2D seismic survey. The results from these new seismic lines, confirmed the availability of a re-usable reservoir of about 50 $MSm^3$, deliverable in 12-15 years, from the exploration well named "Santa Maddalena 1 dir (SM1d)".

The development plan for the exploitation of the "Sant'Alberto" concession, currently under review by the Italian "Ministero dell'Ambiente e della Tutela del Territorio e del Mare (MATTM)" (http://www.va.minambiente.it), provides for the evaluation of various aspects related to the impact of this facility on the territory. As an example, detailed investigation concerning the possible presence of active faults near the reservoir and the possible presence of archaeological, historical or cultural sites located near the production facilities, have been required. In particular, in order to verify the possible relationships between the exploitation activities planned and induced seismicity, the INGV was commissioned to perform a feasibility study of a network for the monitoring of the local seismicity. It has been required that the seismic network meets the monitoring criteria specified in the recent MiSE report: "Indirizzi e linee guida per il monitoraggio della sismicità, delle deformazioni del suolo e delle pressioni di poro nell'ambito delle attività antropiche" (MiSE-DGRME, 2014). In this paper, we present the preliminary results obtained by the INGV team concerning the investigation about the presence of possible active faults nearby the reservoir and the planning of a microseismic network that allows to reach the detection thresholds specified in MiSE-DGRME (2014).

**Monitoring areas and network geometry.** Two crustal volumes of earthquakes detection are specified in MiSE-DGRME (2014): the inner domain of detection (DI) and the extended domain of detection (DE). DI is the crustal volume within which we expect to detect some type of induced seismicity so, within this volume, the planned monitoring network must reach the highest detection capability. According to MiSE-DGRME (2014), the surface projection of DI must be defined by extending horizontally the area corresponding to the surface projection of the reservoir. For oil and gas extraction activities without re-injection, a 3 km extension is required, and the same distance must be adopted in order to define the bottom of DI, by moving vertically, starting from the depth of the reservoir. The definition of DE is required in order to contextualize the monitoring performed by the microseismic network. In this volume, the planned network should improve the magnitude of completeness of the regional networks operating in the area of about 1 degree. For the "Sant'Alberto" reservoir, DE can be defined by extending DI both horizontally and vertically, for a distance of 5 km. We thus defined the surface projections of DI and DE as squared areas centered to the position of the SM1d well, and with areas of 8.6 x 8.6 $km^2$ and 18.6 x18.6 $km^2$, respectively (Fig.1, right panel). Moreover, being the reservoir located between 850 and 900 m depth, we defined the bottoms of DI and DE at 4.0 and 9.0 km depth, respectively.

At the present, in an area of 100x100 $km^2$ centered to the "Sant'Alberto" concession, the Italian National Seismic Network (RSN) features 12 stations. The minimum inter-station distance is about 21 km (Fig.1, left panel). In this region, the RSN shows a magnitude of completeness of about 2.0, and as an example, a $M_L$ 1.5 event has a 50% probability of detection (Shorlemmer *et al.*, 2010). In order to meet the requirements specified in MiSE-DGRME (2014), it is thus necessary to install in the area a microseismic network characterized by a higher detection capability. In this paper, we examine the possibility to detect and locate seismic events occurring in DI, with local magnitude of at least 0.5 unit, and seismic events occurring in DE, with local magnitude of at least 1.0 unit. A hypothetical network consisting of five stations, with an average inter-station distance of 4-5 km, has been considered (Fig.1, right side). The detection threshold is established by comparing simulated power spectra of earthquakes characterized by different values of magnitude and distance, with the power spectrum of the observed ambient noise. In order to minimize the influence of anthropic noise and to improve the network detection, we also consider the possibility to install at least one borehole sensor at 200 m depth.

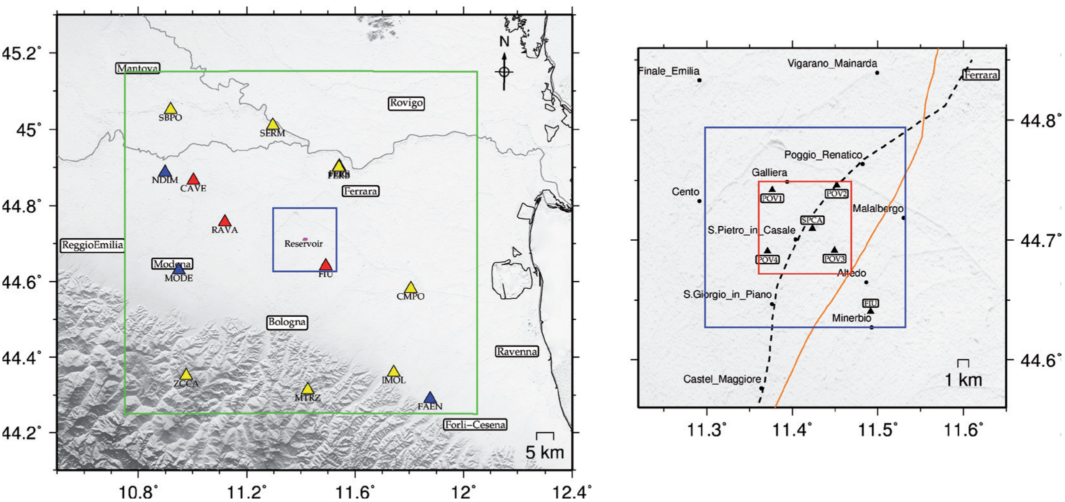


Fig. 1 – Left side: Station Distribution of National Seismic Network (RSN) in an area of about 100 x 100 km$^2$ (green box): velocimeters (red triangles), accelerometers (blue triangles) and six channels stations (yellow triangles). The center of the area, used to select the stations of the RSN, corresponds to surface projection of the reservoir (magenta line). The blue box underlines the extended domain of detection (DE) (cfr. MiSE-DGRME (2014) guidelines). Right side: Inner domain (red line) and the extended domain of detection (blue line). (cfr. MiSE-DGRME (2014) guidelines) with some of the main source of anthropic noise: highway (orange line) and railway line (black dotted line). The microseismic network composed of 5 temporary stations and the station FIU of RSN, is also shown.

**Geological and seismotectonic background.** The Po Plain represents the foreland of two mountain belts: the NNE-verging northern Apennines and the S-verging central Southern Alps. This architecture has been basically due to the convergence between the African and European plates (Carminati *et al.*, 2012). Since at least the recent 5 Ma, the Po Plain area underwent a continuous subsidence, which allowed the sedimentation of huge thicknesses of Plio-Quaternary foredeep terrigenous units (Fantoni and Franciosi, 2010; Consiglio Nazionale delle Ricerche, 1992). These units range from few hundred meters on top of the shallowest buried anticlines to several thousand meters (greater than 8000 m) in the depocenters between the main thrust fronts (Fig. 2). Since the 1950s of the last century those areas have been extensively investigated for hydrocarbons exploration purposes, with several oil and gas fields still actives (Bertello *et al.*, 2010; Casero, 2004). Thus, a great amount of underground data is present (mostly seismic profiles, well logs and structural maps, made available by the Italian Ministry of Economic Development -UNMIG- under the VIDEPI project, www.videpi.com). These data set allowed a refined interpretation of underground structures, which are mostly represented by blind ramp anticlines and anticlinal stacks belonging to the northern Apennines arcs, currently buried below the Plio–Quaternary sequence (Fig. 2). Several detailed stratigraphical analyses, based on geophysical well logs, were also conducted in order to deeply characterize the whole sedimentary cover down to the pre-foredeep basement units. The reconstruction of the sedimentary sequence, starting from the base of Pliocene sediments within the Po Plain, has been the historical target of geological literature (Pieri and Groppi, 1981; Cassano *et al.*, 1986; Casero *et al.*, 1990; Consiglio Nazionale delle Ricerche, 1992; RER and ENI-Agip, 1998; Fantoni e Franciosi, 2010; Vannoli *et al.*, 2014 and reference therein; Maesano *et al.*, 2015 and reference therein). Even if the large dataset show a complex geological variability, the general stratigraphy can be summarized in several group of units which have been coherently observed throughout the whole Po Plain basin (Montone and Mariucci, 2015 and reference therein; Bertello *et al.*, 2010 and reference therein). Those units are, from the top to the bottom: i) a Quaternary sequence made up by alluvial deposits, clays, silts, and sands (e.g., alluvial sediments, Sabbie

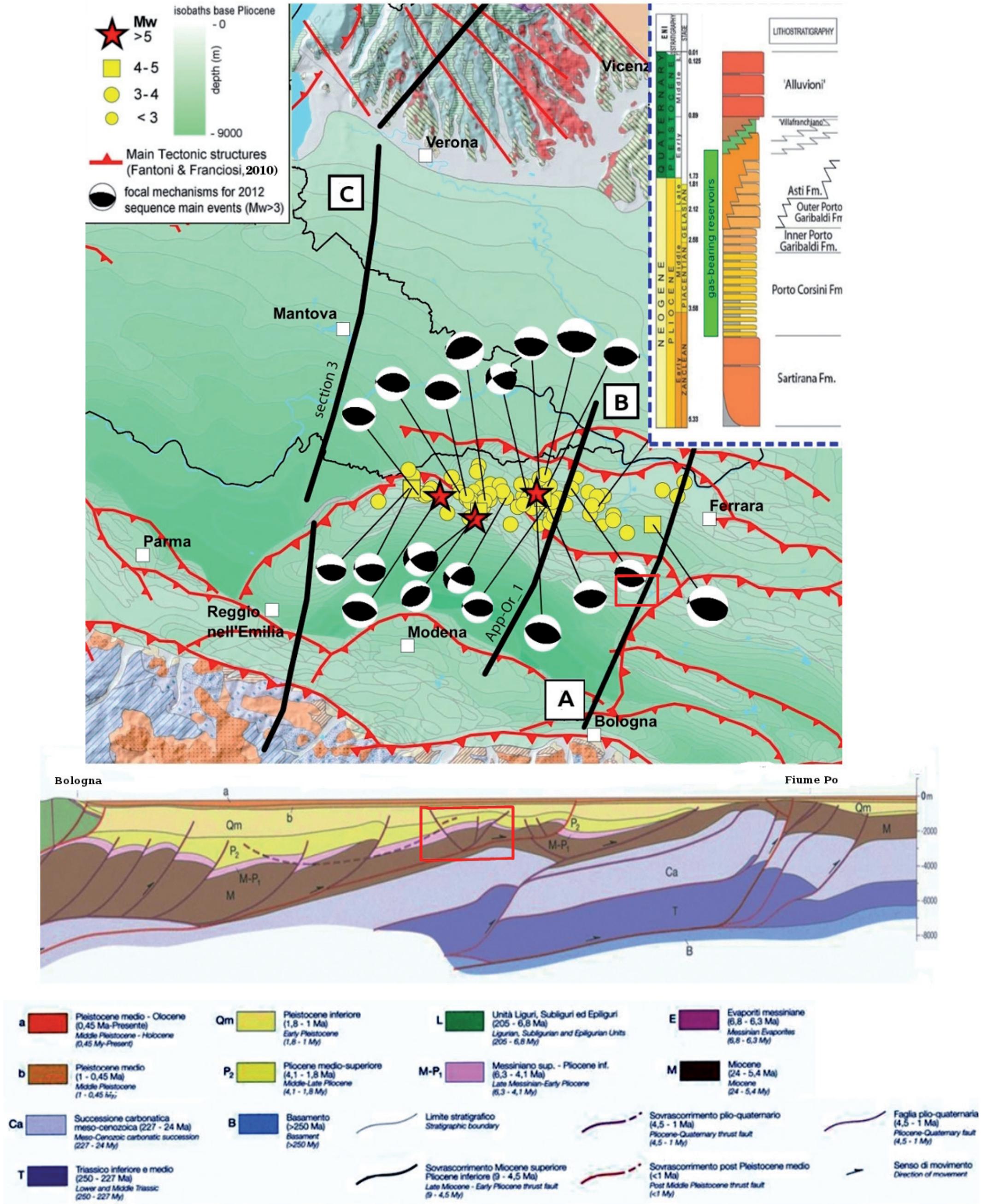


Fig. 2 – Structural setting of the study area with isobaths contours of Pliocene units below the whole Po Plain (as reported by Consiglio Nazionale delle Ricerche, 1992) and main tectonic lineaments (after Fantoni and Franciosi, 2010) with the main events of the 2012 seismic sequence (modified after Malagnini *et al.*, 2012). Some geological cross sections, well-known in literature, are also stressed: A) part of the section CC' from Boccaletti *et al.* (2004); B) geological cross section built on the interpretation of the App_Or_1 seismic profile (modified from Carminati *et al.*, 2010); C) geological cross section modified from Fantoni and Franciosi (2010). The general stratigraphy in the area of interest is summarized (box on the right-high corner), highlighting the presence of gas-bearing reservoir units (modified after Bertello *et al.*, 2010). The section A crosses the area considered in this paper: on the bottom, a snapshot of the section A with a red rectangle that highlights the Sant'Alberto structure.

di Asti, Ravenna Fm.); ii) a Pliocene group mainly characterized by clay, silt, and sand (e.g., Argille del Santerno, Portocorsini Fm., and Garibaldi Fm.); iii) a Messinian group consisting of sand, clay, and sandstone with gypsum (e.g., Gessoso-Solfifera and Colombacci Fms.); iv) a Flyschoid group consisting of syn- and post-orogenic terrigeneous sequences (e.g., Marne di Gallare, Marnoso-Arenacea and Cervarola unit); and v) a Meso-Cenozoic calcareous and marly sequence (e.g., Scaglia and Maiolica Fms.) present everywhere below the foredeep basin units. The whole Po Plain area have been historically interested by diffuse seismicity (Chiarabba *et al.*, 2005; ISIDe Working Group INGV, 2010). In addition the 2012 Emilia seismic sequence bring important information regarding the geometry of northern Apennine fold-and-thrust outer belt (Chiarabba *et al.*, 2014; Carannante *et al.*, 2015). The May 20 and 29, 2012 mainshocks-aftershocks seismic sequences concentrated within the Mesozoic–Tertiary carbonates (Govoni *et al.*, 2014 and reference therein) below the terrigenous sedimentary cover, compatibly with the reactivation of pre-existing normal faults inherited from the previous Mesozoic extensional tectonics (Chiarabba *et al.,* 2014). The structure of the "Sant'Alberto" gas reservoir, located on a blind ramp anticline, has been already highlighted, as an example, in Boccaletti *et al.* (2004). According to the recent literature concerning the relocation of the regional seismicity (Chiarabba *et al.*, 2014; Carannante *et al.*, 2015), this structure, does not appear to have been affected by the 2012 Emilia seismic sequence.

**Evaluations of ambient seismic noise.** The analysis of ambient noise has been performed by computing the power spectral density (PSD) of the seismic signal recorded in some test sites located within the surface projection of DI, and comparing the corresponding probability density functions (PDF) with the standard reference curves NHNM (New High Noise Model) and NLNM (New Long Noise Model) obtained by Peterson (1993). In particular, a seismic station (SPCA) was installed in the inner area of the SM1d well, in order to evaluate the day-night variation of the average level of ambient noise. The recorded signals are transmitted in real time to the INGV data acquisition center of Milan. To quantify the level of noise and its fluctuation, the signal is processed using the PQLX software (http:earthquake.usgs.gov/research/software/pqls.php).

Based on the algorithm developed by McNamara and Buland (2004), the software evaluates in real time the probability density function (PDF) of the power spectral density (PSD) for stationary random seismic data.

By comparing the observed PDF of ambient seismic noise with the reference curves of Peterson (1993), it results that, in the frequency band 1-3 Hz, the mean levels of ambient noise observed at SPCA are about 12 dB above the NHNM curve while at higher frequencies, the noise decreases up to 10-20 dB under the curve. Moreover, during the daily recording periods, the signal shows several transient disturbances. This site is thus characterized by elevated average levels of anthropic noise and by a high frequency of transients.

The characterization of the seismic noise of the area has been carried out by extending the noise measures in four additional sites located within the surface projection of DI. A measurement campaign, performed by means of four temporary stations that recorded simultaneous sequences of 1 hour ambient noise, was carried out. Fig. 3 shows the position of the employed stations. The analysis of results shows that all of the considered sites are affected by elevated levels of ambient seismic noise, with power spectra distributions generally comparable with the NHNM curve of Peterson (1993) in the range of frequencies: 1-20 Hz. Differences up to 10-20 dB are observed in the mean ambient noise levels within the investigated area, depending on the position of the considered site with respect to the anthropic sources of disturbance.

**Microseismic network design.** The analysis of noise presented in the previous section are employed for evaluating the sensibility of the network to be designed. For this purpose, we hypothesize that the areas where noise measurements have been carried out, can be characterized by different levels of noise, depending on the accuracy adopted in the selection of the installation site. We also hypothesize the possible installation of a borehole station at

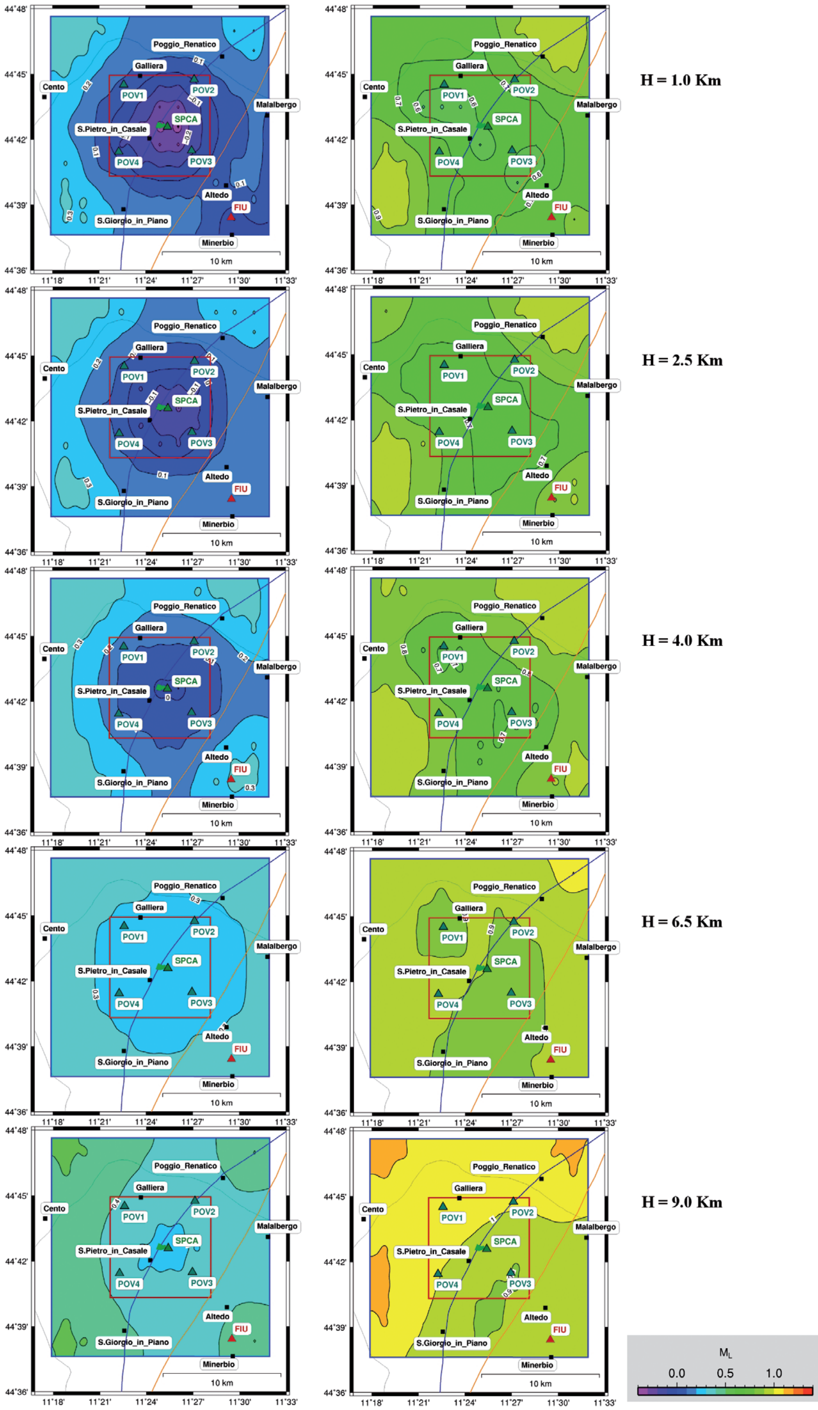


Fig. 3 – Detection (left side) and location (right side) threshold, as magnitude $M_L$ unit. Observed ambient noise levels are used for FIU, POV1 and POV4 stations, while for POV2 and POV3, modified ambient noise are simulated (the same seismic noise recorded at POV1 site). For the SPCA station a theoretical level of noise from borehole station at 200 m in depth, is also taken into account. From top to bottom, the above- mentioned distributions, in the extended domain, are shown at 1.0, 2.5, 4.0 , 6.5 and 9.0 km in depth. The detection threshold is evaluated by imposing that the seismic event was recorded by at least 3 stations of the network.

200 m depth in correspondence to SPCA. In accordance with ambient seismic noise estimates performed at borehole stations installed in the Po Plain in sites characterized by similar geological settings (Franceschina *et al.*, 2014), we hypothesize a decreasing rate of 0.1dB/m for the mean noise level in the frequency band: 1-20 Hz. In order to establish the detection threshold of the network, we used point source simulations of earthquakes characterized by different values of magnitude and distance. For each installation site, the power spectrum of the simulated earthquake was compared with the observed (or hypothesized) power spectrum of ambient seismic noise. The amplitude Fourier spectrum of S-waves, recorded at hypocentral distance *R*, was modeled according to Brune (1970, 1971). The seismic wave attenuation was introduced by considering a $R^{-1}$ dependence of geometrical spreading, a $f^{1}$ dependence of the quality factor, Q(*f*), and a constant value of the *k* parameter of Anderson and Hough (1984). A seismic sequence with maximum $M_L$ magnitude equal to 3.0, was recorded by the SPCA station during the test installation period. We employed the corresponding data to calibrate the simulation parameters. After that, point source simulations were carried out for seismic sources placed in 121 equally-spaced points of 5 regular grids, located within DE at 1.0, 2.5, 4.0, 6.5 and 9.0 km depth. The levels at 1.0, 4.0 and 9.0 km coincide with the depth of the "Sant'Alberto" gas field, the bottom of DI and the bottom of DE, respectively. A microseismic network, with inter-station distances between 3 and 5 km, composed of 5 stations installed in DI was hypothesized. In addition, in all simulations we considered the station FIU of National Seismic Network, located within the surface projection of DE at 9.4 km distance from SPCA. By adopting the network configuration reported in Fig. 3, consisting of stations POV1, POV2, POV3, POV4, SPCA and FIU, we considered three possible simulation scenarios, obtained with different combinations of the ambient noise levels. Noise levels were chosen as follows:

Case A: We adopted for all stations the noise levels really observed at the selected sites;

Case B: The noise level observed at the most favorable site, POV1, was artificially extended to the remaining installations;

Case C: As in case B, with the exception of the SPCA site, where a borehole installation at 200 m depth was hypothesized. In this case, a decreasing rate of 0.1dB/m was hypothesized for the mean level of noise in the frequency band: 1-20 Hz.

For each source-station couple, the power spectrum of a seismic signal of 4 s duration, generated by earthquakes with locale magnitudes ranging between -1.0 and 3.0, has been computed, and then compared with the corresponding power spectrum of the observed (or hypothesized) noise. A seismic event is assessed as detected when the signal to noise ratio is equal to 5 (~ 14 dB) in correspondence to the corner frequency of the source. We defined the detection threshold as the minimum magnitude at which an earthquake can be recorded by at least one station and the localization threshold as the minimum magnitude at which an earthquake can be localized. In this work we classified a seismic event as localizable if it is detected by at least 3 stations of the network.

The results obtained in cases A and B showed the need to install at least one borehole station in order to ensure the detection levels specified in MiSE-DGRME (2014) in the whole DI, also in the case of unfavorable noise conditions. The installation of a borehole station at 200 m depth ensures a general improvement of the detection threshold up to 4 km depth. In particular, the borehole station installed in correspondence of SPCA, is capable to detect $M_L$ -0.3 events, located at the depth of the reservoir. Also localization thresholds show a considerable improvement with $M_L$ values between 0.7 and 0.8 at the bottom level of DI. On the other side, Fig. 3 also shows that in these conditions, prescriptions indicated in MiSE-DGRME (2014) are not satisfied in the part of the extended domain of detection not included in DI. Localization thresholds greater than 1.0 are obtained in the deeper part of DE. Moreover, it is important to highlight that, under these conditions, the location of seismic events would be affected by remarkable errors due to the inadequate stations distribution. For a more accurate and homogeneous localization of seismic events occurring within the whole extended domain, it would be necessary the installation of at least three stations, properly distributed around the surface projection of the reservoir, at the same distance of FIU.

**Conclusions.** The goal of the paper is to summarize the analysis carried out in the area of the "Sant'Alberto" gas reservoir (Po Plain, Italy), concerning the presence of possible active faults nearby the reservoir, and the feasibility of a microseismic network that satisfies the features required in the MiSE document: "Indirizzi e linee guida per il monitoraggio della sismicità, delle deformazioni del suolo e delle pressioni di poro nell'ambito delle attività antropiche" (MiSE-DGRME, 2014).

Since the fifties of the last century, the great amount of data collected for hydrocarbons exploration purposes allowed a refined interpretation of the underground structures involved in area of the reservoir. These are mostly represented by blind ramp anticlines and anticlinal stacks belonging to the northern Apennines arcs, currently buried below the Plio–Quaternary sequence. Furthermore, the 2012 Emilia seismic sequence has allowed to outline with great detail the geometry of northern Apennine fold-and-thrust outer belt. In particular, recent works, concerning the relocation of the sequence, highlight that the whole structure of the "Sant' Alberto" reservoir, located on the back-limb of a ramp anticline, does not seem to be affected by the events of the 2012 Emilia sequence.

As regard to the planning of a microsesmic network in accordance with the criteria specified in MiSE-DGRME (2014), the present analysis shows that:

1. The area to be monitored is characterized by a strong anthropization, that produce high levels of ambient noise. The observed PSD of seismic noise are comparable with the NHNM curves of Peterson (1993).
2. According to the guidelines specified in MiSE-DGRME (2014), the internal domain of detection (DI) and the extended domain of detection (DE) correspond to crustal volumes of 8.6 x 8.6 x 4.0 $km^3$ and 18.6 x 18.6 x 9.0 $km^3$, respectively.
3. Due to the elevated levels of the observed ambient seismic noise, in order to ensure adequate detection thresholds in the whole DI, the network should include at least one borehole (200 m depth) station.
4. The installation of a borehole station (200 m depth), localized near the SM1d well, and an accurate selection of sites characterized by favorable levels of ambient noise, considerably improve the detection.

Hypothesizing favorable levels of the surface noise and a decreasing rate of 0.1 dB/m of the mean noise level recorded at depth, a minimal network composed of 5 stations installed within DI, integrated with a neighbor station of the RSN, allows to achieve $M_L$ detection thresholds of about 0.2 unit at the bottom of DI. In particular, in this case, it is possible to obtain a detection threshold $M_L$=-0.3 near the reservoir.

5. The above mentioned minimal network, is capable to localize $M_L$ 0.9 events occurring up to 4 Km depth, thus fulfilling the requirements specified in MiSE-DGRME (2014) for what concerns the internal domain of detection.
6. The above mentioned minimal network, shows a minimum localization magnitude $M_L$ 1.1 at the bottom of DE (9 km depth). The requested decreasing of about one unit of the completeness magnitude obtained with the regional networks operating in this area, can be allowed by installing at least three additional stations within the surface projection of DE.

**References**


Anderson J. G. and Hough S. E.; 1984: *A model for the shape of the Fourier amplitude spectrum of acceleration at high frequencies*, Bull. Seism. Soc. Am. 74, 1969-1993.

Bertello F., Fantoni R., Franciosi R., Gatti V., Ghielmi M. and Pugliese A.; 2010: *From thrust and fold belt to foreland: hydrocarbon occurrences in Italy,* in B.A. Vining and S.C. Pickering (Eds.). Petroleum Geology: From Mature Basin to New Frontiers, Proceedings of the 7th Petroleum Geology Conference, Geol. Soc., p. 113-126.

Boccaletti M., Bonini M., Corti G., Gasperini P., Martelli L., Piccardi L., Tanini C. and Vannucci G.; 2004: *Carta simotettonica della regione Emilia Romagna, 1:250.000 e note illustrative,* SELCA Editore, Firenze.

Brune J.N.; 1970: *Tectonic stress and the spectra of seismic shear waves from earthquakes*, J. Geophysical Res., 75, 4997-5009.

Brune J.N.; 1971: *Correction*, J. Geophysical Res., 76, 5002.

Carannante S., Argnani A., Massa M., D'Alema E., Lovati S., Moretti M., Cattaneo M. and Augliera P.; 2015: *The May 20 (MW 6.1) and 29 (MW 6.0), 2012, Emilia (Po Plain, northern Italy) earthquakes: New seismotectonic implications from subsurface geology and high-quality hypocenter location,* Tectonophysics, doi:10.1016/j.tecto.2015.05.015.

Carminati E., Scrocca D. and Doglioni C.; 2010: *Compaction-induced stress variations with depth in an active anticline: Northern Apennines, Italy*, J. Geophys. Res., 115, B02401, doi:10.1029/2009JB006395.

Carminati E., Lustrino M. and Doglioni C.; 2012: *Geodynamic evolution of the central and western Mediterranean: Tectonics vs. igneous petrology constraints,* Tectonophysics, doi:10.1016/j.tecto.2012.01.02.

Casero P., Rigamonti A. and Iocca M.; 1990: *Paleogeographic relationships durino cretaceous between the northern Adriatic area and the eastern Southern Alps,* Mem Soc Geol It 45:807–814 23.

Casero P.; 2004: *Structural setting of petroleum exploration plays in Italy,* Ital. Geol. Soc. Special Volume of the Italian Geological Society for the IGC 32 Florence-2004. 189.

Cassano E., Anelli L., Fichera V. and Cappelli V.; 1986: *Pianura Padana. Interpretazione integrata di dati geofisici e geologici,* 73° Congr. Soc. Geol. Ital., Roma, 29 September - 4 October 1986, AGIP, S. Donato Milanese, Milano, p. 27.

Chiarabba C., De Gori P., Improta L., Lucente F. P., Moretti M., Govoni A. and Nardi A.; 2014: *Frontal compression along the Apennines thrust system: The Emilia 2012 example from seismicity to crustal structure,* Journal of Geodynamics, 82, 98-109.

Chiarabba C., Jovane L., and Di Stefano R.; 2005: *A new view of Italian seismicity using 20 years of instrumental recordings,* Tectonophysics, doi:10.1016/j.tecto.2004.09.013.

Consiglio Nazionale delle Ricerche; 1992: *Structural model of Italy and gravity map, scale 1:500000*, in Progetto Finalizzato Geodinamica. Quad. Ric. Sci., vol. 114, 1 pp., Rome.

Fantoni R. and Franciosi R.; 2010: *Tectono-sedimentary setting of the Po Plain and Adriatic foreland,* Rendiconti Lincei, 21(1), 197-209.

Franceschina G., Augliera P., Lovati S.and Massa M.; 2014: *Surface seismic monitoring of a natural gas storage reservoir in the Po Plain (Northern Italy),* Bollettino di Geofisica Teorica e Applicata (submitted).

Govoni A., Marchetti A., De Gori P., Di Bona M., Lucente F.P., Improta L.,Chiarabba C., Nardi A., Margheriti L., Piana Agostinetti N., Di Giovambattista R., Latorre D., Anselmi M., Ciaccio M.G., Moretti M., Castellano C. and Piccinini D.; 2014: *The 2012 Emilia seismic sequence (Northern Italy): imaging the thrust fault system by accurate aftershocks location,* Tectonophysics, doi:10.1016/j.tecto.2014.02.013.

ISIDe Working Group (INGV, 2010), *Italian Seismological Instrumental and parametric database:* http://iside.rm.ingv.it

Maesano F.E., D'Ambrogi C., Burrato P. and Toscani G.; 2015: *Slip-rates of blind thrusts in slow deforming areas: Examples from the Po Plain (Italy),* Tectonophysics, doi:10.1016/j.tecto.2014.12.007.

Malagnini L., Herrmann R. B., Munafò I., Buttinelli M., Anselmi M., Akinci A. and Boschi E.; 2012: *The 2012 Ferrara seismic sequence: Regional crustal structure, earthquake sources, and seismic hazard,* Geophysical Research Letters, 39(19).

McNamara D.E. and Buland R.P.; 2004: *Ambient Noise Levels in the Continental United States,* Bull. Seism. Soc. Am., 94, 1517-1527.

MiSE-DGRME; 2014: Ministero dello Sviluppo Economico – Direzione Generale per le Risorse Minerarie ed Energetiche - Gruppo di lavoro CIRM, Indirizzi e linee guida per il monitoraggio della sismicità, delle deformazioni del suolo e delle pressioni di poro nell'ambito delle attività antropiche, Roma, 24/11/2014, http://unmig.sviluppoeconomico.gov.it/unmig/agenda/upload/85_238.pdf.

Montone P. and Mariucci M. T.; 2015: *P-wave Velocity, Density, and Vertical Stress Magnitude Along the Crustal Po Plain (Northern Italy) from Sonic Log Drilling Data,* Pure and Applied Geophysics, 1-15. ISO 690.

Peterson J.; 1993: *Observation and modeling of seismic background noise*, U.S.G.S. Tech. Rept., 93-322, 1-95.

Pieri M. and Groppi G.; 1981: *Subsurface geological structure of the Po Plain, Italy,* Pub. 414, del Progetto finalizzato Geodinamica (CNR), 13 pp.

RER, ENI-Agip; 1998: *Riserve idriche sotterranee della Regione Emilia-Romagna*, Publication Regione Emilia Romagna.

Schorlemmer D., Mele F. and Marzocchi W.; 2010: *A completeness analysis of the National Seismic Network of Italy*, J. Geophys. Res., 115, B04308, doi: 10.1029/2008JB006097.

Vannoli P., Burrato P. and Valensise G.; 2014: T*he seismotectonics of the Po Plain (northern Italy): tectonic diversity in a blind faulting domain,* Pure and Applied Geophysics, 1-38.

ViDEPI Project (Visibility of petroleum exploration data in Italy, http://unmig.sviluppoeconomico.gov.it/videpi/videpi.asp).

# THE ORIGIN OF THE ACTIVE CRUSTAL STRETCHING AT THE SOUTHERN EDGE OF THE CALABRIA ARC

**S. Catalano, F. Pavano, G. Romagnoli, G. Tortorici**
*Dip. di Scienze Biologiche, Geologiche e Ambientali, Sezione di Scienze della Terra, Università di Catania, Italy*

**Introduction**. In the central Mediterranean the SE-ward migration of the Calabrian arc and the coincident opening of the back-arc Tyrrhenian Basin dominated the post-Tortonian tectonic picture of the region. The current geodynamic models explain both the two processes as the consequence of the roll-back of the oceanic Ionian lithosphere, which drove the forward shifting of the arc with respect to the adjacent Sicily segment of the orogenic belt, colliding with the African continental margin. According to the models, the motions of the Calabrian arc was accommodated, to the west, by the back-arc extension and to the south by dextral motions along NW-SE oriented faults and oblique (righ-lateral) displacements along E-W trending ramps, breaching the previous thrust-nappes of the Sicily collision belt. Whether or not these geodynamics are still active and control the seismicity of the region are still open questions. As a consequence, the seismotectonic models are often contradictive, depending on the adopted reference geodynamic model. A distribution of seismogenic zones mimicking the arcuate shape of the orogeny and marking the separation between the seismogenic extensional features of southern Calabria and eastern Sicily is imposed in the models that start from the evidence of a still active arc migration (Ghisetti and Vezzani, 1982; Meletti and Valensise, 2004). On the other hand, seismotectonic models taking into account the fragmentation of the southern edge of the arc (Monaco and Tortorici, 2000; Catalano *et al.*, 2008a), in the Straits of Messina area, have been generally related to a recent modification of the geodynamic picture, due to the propagation of an incipient rift zone, extending from southern Calabria to eastern Sicily.

This paper aims to summarise the outlines of the Late Quaternary (< 1 Myr) deformation of eastern Sicily, at the southern edge of the Calabrian arc, to frame the active crustal extension of eastern Sicily, responsible for the high level regional seismicity, in the long-term geodynamic evolution of the Calabria arc migration.

**Active deformation at the southern edge of the Calabrian arc**. The active tectonic picture of the southern edge of the Calabrian arc is dominated by an incipient crustal stretching which is well constrained, in the Straits of Messina area, by both GPS data (D'Agostino and Selvaggi, 2004) and by the focal mechanism of the catastrophic 1908 earthquake (Cello *et al.*, 1982). The geological, structural and morphological data (Monaco and Tortorici, 2000; Catalano and De Guidi, 2003) evidence that the recent faults on the two sides of the Straits of Messina form an antithetic relay ramp, connecting the main west facing normal faults of southern Calabrian (Reggio Calabria and Armo Fault; a and b in Fig. 1) to the east facing Taormina Fault (c in Fig. 1), bounding the Ionian coast of the Peloritani Mountains. The fault belt of the Calabrian side of the Straits originated from the remobilisation of previous extensional features that have also controlled the Plio-Quaternary basins of the peri-Tyrrhenian margin of the arc. The morphological features (marine terraces, fault scarps, triangular facets) indicate that the reactivation of the southern Calabria fault belt started at least since 580 kyr B.P. and then progressively propagated to the south, towards the Straits of Messina region (Catalano *et al.*, 2008a). On the opposite side of the Straits, the off-shore NNE oriented Taormina Fault has controlled the uplift of a discrete segment of the Ionian coast of the Peloritani Mountains since about 125 kyr B.P. (Catalano and De Guidi, 2003). In the Taormina area, a synthetic relay ramp links the southern tip of the Taormina Fault to the on-shore active faults which propagated along the eastern flank of Mt. Etna (d in Fig. 1; Monaco *et al.*, 1997), in the last 125 kyr (Monaco *et al.*, 2000; Catalano *et al.*, 2004). The active faults flanking the Mt. Etna overstep the NNW oriented main extensional fault which was detected in the off-shore from Catania to the Hyblean Plateau (Western Fault of Bianca *et al.*, 1999; e in Fig. 1). This offshore structure originated from the reactivation of

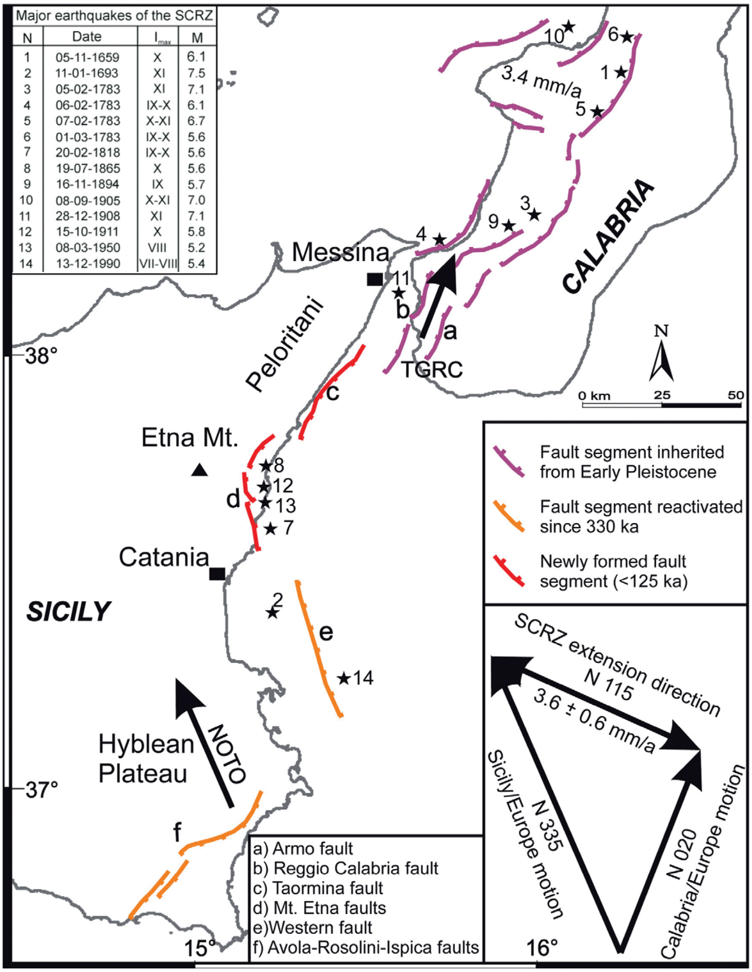


Fig. 1 – Age and distribution of active extensional fault in southern Calabria and eastern Sicily.

part of the Mesozoic Malta Escarpment and borders a series of eye-shaped half-grabens, which are infilled by up to 800 m thick syn-tectonic deposits, suggesting the long lived activity (~ 330 kyr; Bianca *et al.,* 1999) of the fault.

The southernmost extensional features of the region are located along the southeastern margin of the Hyblean Plateau (Avola and Rosolini-Ispica faults, f in Fig. 1). These faults replaced an Early Pleistocene contractional belt (Catalano *et al*., 2007) and accommodated the huge Late Quaternary tectonic uplift of the Hyblean Plateau (Catalano *et al*., 2010).

**South-eastern Sicily**. In south-eastern Sicily, the Western Fault and the Avola-Rosolini-Ispica faults border the eastern portion of the Hyblean Plateau (Siracusa Domain; SD in Fig. 2) that represents an uplifted mobile crustal block of the African Foreland. The tectonic boundaries of the Siracusa Domain consist of inverted tectonics that drove the Late Quaternary (< 850 kyr) motion of the crustal block. The western boundary of the Siracusa Domain is represented by a left-lateral shear zone, inherited from a previous dextral fault (Scicli Line; Ghisetti and Vezzani, 1982). The north-western margin of the mobile block consists of a NNW-verging thrust and fold belt that extends to the north, as far as the southern margin of Mt. Etna. These contractional features derived from the positive tectonic inversion of NE-oriented extensional basins (Simeto Graben and Scordia-Lentini Graben; Fig. 2), that originated in the 1.5-0.9 Ma time interval (Pedley *et al*., 2001), at the peak of the impressive emission of tholeiitic to alkaline volcanic products in the region.

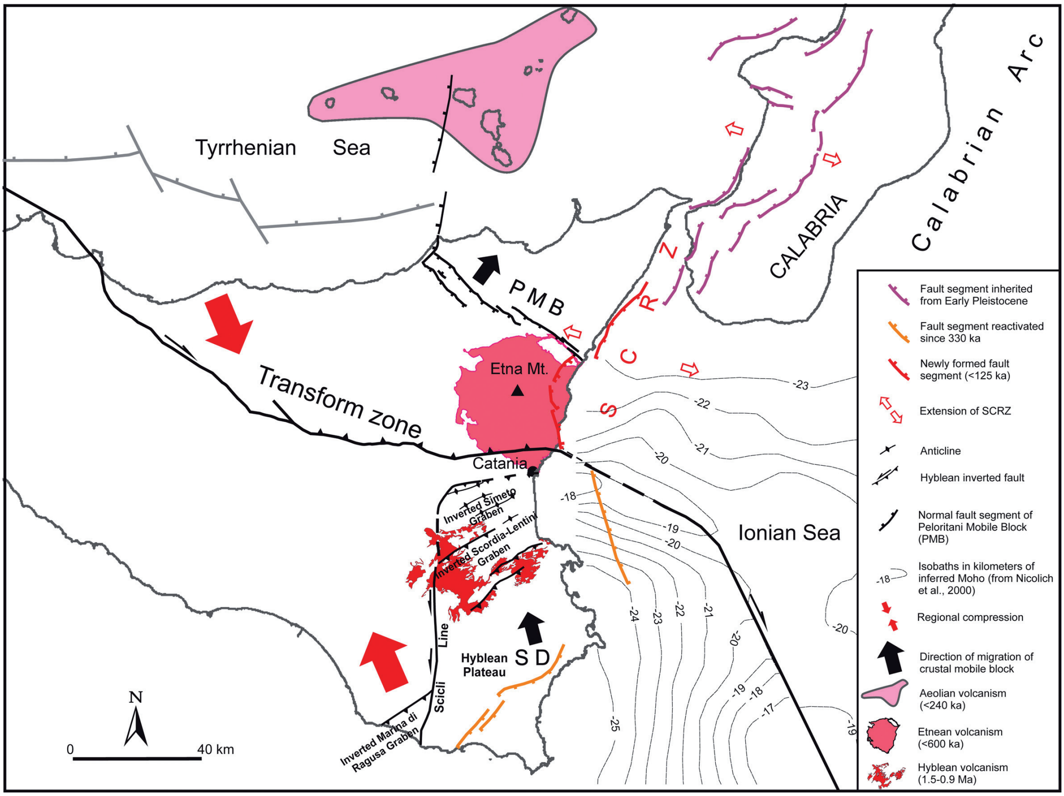


Fig. 2 – Main Quaternary tectonic and volcanic features of eastern Sicily.

The Siracusa Domain is contoured by a flight of Late Quaternary marine terraces, that have been assigned to the Oxygen Isotope Stages (OISs) from 21 (850 kyr) to 3 (60 kyr). The geometry of these marine platform constrain a regional scale tilting associated to a tectonic uplift, faster than the adjacent sectors, which was regularly increasing towards the NNW, in the direction of the active thrust and fold system controlling the northwestern margin of the block (Bonforte *et al.*, 2015). The rate of deformation measured along the bordering structures indicate that the amounts of contractional-rate along the northwestern border of the block, estimated at about 1.2 to 1.3 mm/a (Catalano *et al.*, 201), has been completely accommodated by the 1.4 mm/a rate of left-lateral motions along the western border (Scicli Line; Catalano *et al.*, 2008b) and by the 1.3 mm/a extension-rate, which has been measured along the southeastern edge (Avola Fault; Catalano *et al.*, 2010). The kinematics of the borders of the Siracusa Domain are consistent with the NNW-SSE oriented compression which has been obtained by inversion of seismological data (Musumeci *et al.*, 2005) and fit the residual GPS velocity relative to Eurasia, with respect to rest of the foreland domain (Bonforte *et al.*, 2015).

**Mt. Etna region**. In the Mt. Etna region, the contractional domain at the northern margin of the Hyblean Plateau is abruptly interrupted by a NW-SE oriented alignment, marked by dextral active fault segments, that represents the onshore prolongation of the Africa-Ionian tectonic boundary, recognised by seismic lines in the offshore of Catania (Fig. 2) (Nicolich *et al.*, 2000). The crustal significance of this tectonic boundary, already interpreted as a transform zone (Catalano *et al.*, 2004), is demonstrated by a N-S trending seismic line across the volcano (Cristofolini *et al.*, 1978) that shows a sharp increase of the depth of the Moho, almost corresponding to the location of the alignment. The southern portion of the seismic line, crossing the contractional domains, shows the continental crust of the African margin, flooring the southern flank of Mt. Etna. The northern prosecution of the seismic line pictures a thickened crust sector, which consists of two superimposed distinct crusts. This part of the seismic lines can be interpreted, taking into account that the cross-section cuts parallel to the hinge of the Ionian subduction zone. The deeper crustal horizon, whose top is at depth of 21 km, represents the flexured Ionian Crust (Vp = 7.5 - 6 km/s) and the upper crustal horizon consists of the Calabrian Arc continental crust (Vp = 6.0 km/s) and its sedimentary cover (Vp = 3.0 - 5.0 km/s). An intermediate, low-velocity layer (Vp=5.0-5.5 km/s), located at depth from 12 to 21 km is interleaved between the two superimposed crusts.

The evolution of the Etna volcanism was clearly controlled by the existence of the Africa-Ionian tectonic boundary. The earlier emissions of tholeiitic products, ranging in age from 540 kyr to 225 kyr, were in fact localised at the main transtensional features that were active along the southern margin of Mt. Etna (Catalano *et al.*, 2004), while the following emissions of the alkaline products (< 225 kyr) mainly developed within the extensional domain, to the north of the transform zone.

**North-eastern Sicily.** The north-eastern corner of Sicily, comprising the Peloritani and part of the Nebrodi Mountain Belts, form an uplifted crustal block (Peloritani Mobile Block; PMB in Fig. 2) that is now diverging from both the Sicily collision zone and the southern Calabria sector of the arc. The geodetic data in the Nubia reference frame (D'Agostino and Selvaggi, 2004) evidence that the NE Sicily diverges, with rates of about 5 mm/a along a N160 direction, from the rest of the Calabrian arc, which is still migrating towards the E. This relative motion is consistent with the rate and the direction of the extension obtained by the inversion of structural data on the fault planes in the Straits of Messina area, which are also fitting the focal mechanism of the 1908 event.

The geodetic measurements in NE Sicily also evidence a NNE-ward divergence of the PMB from the rest of island, at rates of about 5 mm/yr (see FOSS vs Nubia in D'Agostino and Selvaggi, 2004). Recent geological analyses carried out at the southern border of the PMB pointed out an active extensional fault belt, which remobilized segments of the previous NW-SE oriented dextral fault system, at the southern edge of the arc (Pavano *et al.*, 2015). This reactivated extensional feature has been related to the June-September 2011 seismic swarm in the area of Longi-Galati Mamertino. It consists of about 430 events that followed the 23/06/2011 event, characterized by a 4.1 magnitude (ISIDe Working Group, 2010). This main event provided a focal mechanism (Scarfì *et al.*, 2013) indicating a NNE-SSW oriented extension, matching that obtained by GPS data and structural analyses of rejuvenated fault planes (Pavano *et al.*, 2015).

The PMB is contoured by marine terraces, which have been referred to successive OISs from 15 (570 kyr) to the OIS 3 (60 kyr) (Catalano and Cinque, 1995; Catalano and De Guidi, 2003; Catalano and Di Stefano, 1997). They undercut a raised transgressive, neritic-to-batial marine sequence that ranges in age from 900 to 600 yr (Naso sequence; Catalano and Di Stefano, 1997). The Naso sequence pre-dates the tectonic uplift of the PMB that started, thus, at about 600 yr. Along the entire Tyrrhenian coast of the PMB the strandlines of the marine terraces show a constant elevation that constrain an almost uniform uplift-rate of about 1.1 mm/yr, since 600 kyr B.P.. In particular, the strandlines of the marine terraces cross undisturbed the main NW-SE dextral fault segments that dissect the region (e.g. Tindari Fault). Along the Tyrrhenian coast, the tectonic boundary of the mobile block is evidenced by a sharp decrease in the elevation of the marine terraces, ranging in age from the OIS 15 (570 kyr) to the OIS 3 (60 yr).

To the north of the mobile block, the active volcanic belt of the Eolian Islands, whose oldest products have been dated at about 225 kyr B.P. (Crisci *et al.*, 1991), is represented by the islands of Volcano, Lipari and Salina, that are located at the main releasing bends along a seismogenic NNW-SSE dextral shear zone (Catalano *et al.*, 2009).

**Discussion and conclusions.** The active extensional belt which extends from southern Calabria to the south-eastern Sicily is composed by two branches (southern Calabria and south-eastern Sicily) deriving from the reactivation of older faults, which are now linked by faults that

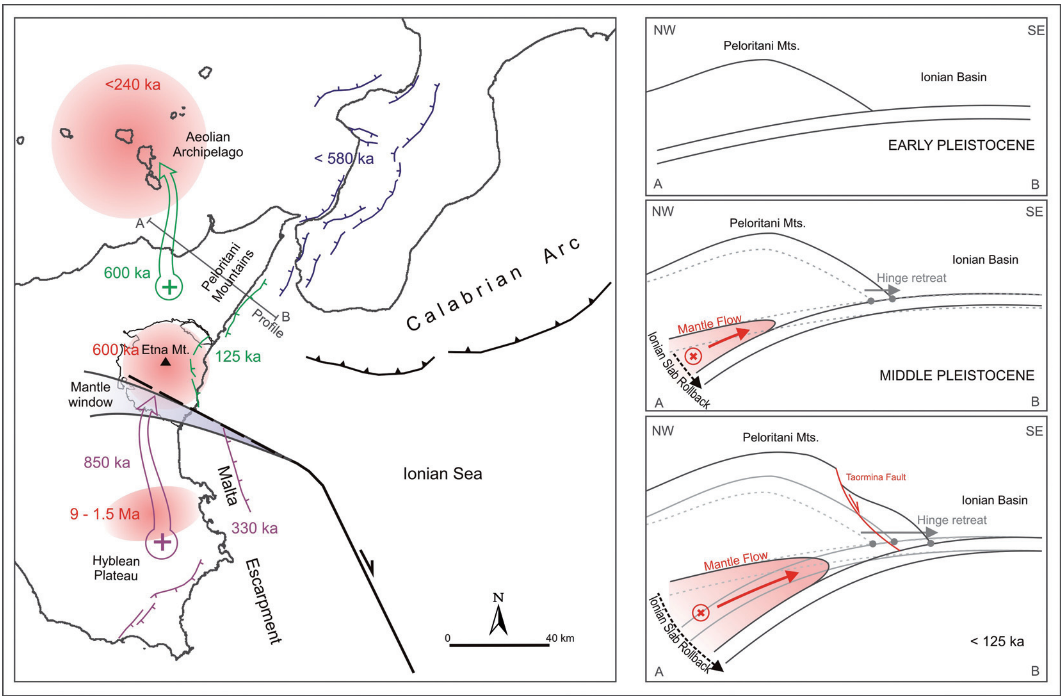


Fig. 3 – Sketch map illustrating the timing of the propagation of the mantle-flow beneath eastern Sicily and the relation with the volcanism and the crustal extension.

propagated since about 125 kyr from the eastern flank of Mt. Etna to the offshore of NE Sicily. Our investigations point out that an impressive tectonic uplifting, affecting isolated crustal blocks, associated with the development and the progressive migration of the volcanism, from the Hyblean Plateau to the Aeolian Islands, heralded the reactivation and the propagation of the normal faults in eastern Sicily.

The normal faults of south-eastern Sicily activated since ~330 kyr at the borders of a mobile crustal wedge that started to move and uplift since ~850 kyr. The normal faults of north-eastern Sicily propagated since ~125 kyr, along the margin of an actively uplifting crustal block which, in turn, started to move at ~600 yr. Our data also evidence that the mobilisation of block anticipated the onset of the volcanism at the leading edge of the moving crustal blocks (Fig. 3). This aspect, together with the mode and the rate of deformation along the bounding faults, suggest to relate the remobilization of the crustal blocks to upraising mantle wedges beneath these (see also Catalano *et al.*, 2010). It is remarkable that the process started at the main transform zone separating the subducting Ionian slab from the buoyant Hyblean continental crust, to the south of Mt. Etna. The opening of a mantle window along this transform zone has been proposed as the cause of the mantle plume which induced the Etna volcanism since 600 yr (Gvirtzman and Nur, 1999). This process matches the indication of a NE-ward remobilisation of the mantle beneath the continental crust of the adjacent Hyblean region, dragging the Siracusa Domain mobile block towards the Etna region since ~850 yr. The Etna volcanism started together with the remobilisation of the Peloritani Mobile Block that also marked the deactivation of the main dextral faults at the southern edge of Calabrian arc. The end of the strike-slip deformation could be strictly related to a NE-directed mantle flow fed by the mantle window. The activation of the flow paralleling the hinge of the Ionian subduction have supplied large volumes of materials, balancing the accommodation space due to the Ionian rolling back, thus causing the end of the dextral crustal shearing at the surface. The reconstructed tectonic evolution of eastern Sicily clearly points out that the propagation of the active normal faults of eastern Sicily occurred on the flank of the uplifted crustal blocks, 500 kyr after the onset of their remobilisation caused by the mantle perturbation. The crustal extension governing the propagation of the seismogenic normal faults of eastern Sicily can be thus interpreted as the delayed surface expression of an incipient active rifting which causes the gravity sliding of the crust from the uplifted mantle wedge towards the still retreating Ionian slab. In conclusion, active extension at the southern edge of Calabrian arc totally replaced the dextral crustal shearing in accommodating the Calabrian still active arc migration. This evidence candidates the extensional features of eastern Sicily as the main seismogenic sources of the region.

**References**

Bianca M., Monaco C., Tortorici L. and Cernobori L.; 1999. *Quaternary normal faulting in southeastern Sicily (Italy): A seismic source for the 1693 large earthquake*. Geophys. J. Int., 139, 370-394.

Bonforte A., Catalano S., Maniscalco R., Romagnoli G., Sturiale G., Tortorici G.; 2015. *Geological and geodetic constraints on the active deformation along the northern margin of the Hyblean Plateau (SE Sicily)*. Tectonophysics, 640-641, 80-89. doi:10.1016/j.tecto.2014.11.024

Catalano S. and Cinque A.; 1995. *L'evoluzione neotettonica dei Peloritani settentrionali (Sicilia nord-orientale): il contributo di una analisi geomorfologica preliminare*. Studi Geologici Camerti, Vol. Spec. 1995/2, 113-123.

Catalano, S. and De Guidi, G.; 2003. *Late Quaternary uplift of northeastern Sicily: relation with the active normal faulting deformation*. Journal of Geodynamic, 36, 445-467.

Catalano S., De Guidi G., Romagnoli G., Torrisi S., Tortorici G. and Tortorici L.; 2008b. *The migration of plate boundaries in SE Sicily: influence on the large-scale kinematic model of the African Promontory in Southern Italy*. Tectonophysics, 449, 41-62.

Catalano S., De Guidi G., Monaco C., Tortorici G., Tortorici L.; 2008a. *Active faulting and seismicity along the Siculo-Calabrian rift zone*. Tectonophysics, 453, 177-192.

Catalano S. and Di Stefano A.; 1997. *Sollevamenti e tettogenesi pleistocenica lungo il margine tirrenico dei Monti Peloritani: integrazione dei dati geomorfologici, strutturali e biostratigrafici*. Il Quaternario, 10 (2) 6pp

Catalano S., Romagnoli G., De Guidi G., Torrisi S., Tortorici G., & Tortorici L.; 2007. *Evoluzione neogenico-quaternaria della Linea del Tellaro: relazioni con la dinamica del Plateau Ibleo (Sicilia SE)*. Rend. Soc. Geol. It., 4 (2007), Nuova serie, pp. 177-180, 2ff. GIGS Urbino 12-13 marzo 2007.

Catalano S., Romagnoli G. and Tortorici G.; 2009. *The Late Quaternary crustal deformation of NE Sicily: evidence for an active Mantle diapirism*. Riassunti estesi delle comunicazioni pp. 152-154. GNGTS 28° Convegno Nazionale Trieste 16-19 Novembre 2009, Consiglio Nazionale delle Ricerche.

Catalano S., Romagnoli G., and Tortorici G.; 2010. *Kinematics and dynamics of the Late Quaternary rift-flank deformation in the Hyblean Plateau (SE Sicily)*. Tectonophysics, 486 pp.1–14. ISSN: 0040-1951, doi: 10.1016/j.tecto.2010.01.013.

Catalano S., Torrisi S., Ferlito C., 2004. *The relationship between Late Quaternary deformation and volcanism of Mt. Etna (eastern Sicily): new evidence from the sedimentary substratum in the Catania region*. J. Volcanol. Geotherm. Res. 132, 311-334.

Catalano S., Torrisi S., Tortorici G., Romagnoli G.; 2011. *Active folding along a rift-flank: the Catania region case history (SE Sicily)*. Journal of Geodynamics, 51, 53-63. ISSN: 0264-3707 doi:10.1016/j.jog.2010.08.001.

Cello G., Guerra I., Tortorici L., Turco E., Scarpa R., 1982. *Geometry of the neotectonics stress field in southern Italy: geological and seismological evidence*. J. Struct. Geol., 4, 385-393.

Crisci G.M., De Rosa R., Esperanca S., Mazzuoli R. and Sonnino M.; 1991. *Temporal evolution of a three component system: the Island of Lipari (Aeolian Arc, southern Italy)*. Bull. Volcanol., 53, 207-221.

Cristofolini R., Patane G. and Rasà R.; 1978. *Studio morfostrutturale del versante orientale etneo*. Mem Soc. Geol. It., 19, 613-620.

D'Agostino N. and Selvaggi G.; 2004. *Crustal motion along the Eurasia-Nubia plate boundary in the Calabrian arc and Sicily and active extension in the Messina Straits from GPS measurements*. J. Geophys. Res. 109, B11402.

Ghisetti F. and Vezzani L.; 1982. *Different styles of deformation in the Calabrian Arc (Southern Italy); implication for a sismotectonics zoning*. Tectonophysics 85, 149-165.

Gvirtzman Z. and Nur A.; 1999. *The formation of Mount Etna as the consequence of slab rollback*. Nature, 401: 782-785.

ISIDEe Working Group (INGV); 2010. *Italian seismological Instrumental and parametric database*: http://iside.rm.ingv.it.

Meletti C. and Valensise, G.; 2004. *Zonazione sismogenetica ZS9 – App. 2 al Rapporto Conclusivo del Gruppo di Lavoro per la redazione della mappa di pericolosità sismica (Ordinanza PCM 20-03-2003 n. 3274)*. http://zonesismiche.mi.ingv.it/documenti/App2.pdf.

Monaco C., Bianca M., Catalano S., De Guidi G., Tortorici L.; 2002. *Sudden change in the Late Quaternary tectonic regime in eastern Sicily: evidences from geological and geomorphological features*. Boll. Soc. Geol. It., Volume speciale n.1, 901-913.
Monaco C., Tapponnier P., Tortorici L., Gillot P.Y.; 1997. *Late Quaternary slip rates on the Acireale-Piedimonte normal faults and tectonic origin of Mt. Etna (Sicily*). Earth Planet. Sci. Lett. 147, 125-139.
Monaco C. and Tortorici L.; 2000. *Active faulting in the Calabrian arc and eastern Sicily*. J. Geodyn., 29, 407-424.
Musumeci C., Patanè D., Scarfì L. and Gresta, S.; 2005. *Stress Directions and Shear-Wave Anisotropy: Observations from Local Earthquakes in Southeastern Sicily*, Italy. Bull. Seism. Soc. Amer., 95 (4), 1359-1374.
Nicolich R., Laigle M., Hirn A., Cernobori L. and Gallart, J.; 2000. *Crustal structure of the ionian margin of Sicily; Etna volcano in the frame of regional evolution*, Tectonophysics, 329, 121-139.
Pavano F. Romagnoli G., Tortorici G., Catalano S.; 2015. *Active tectonics along the Nebrodi–Peloritani boundary in northeastern Sicily (Southern Italy)*. Tectonophysics, 659, 1-11. doi:10.1016/j.tecto.2015.07.024
Pedley H.M., Grasso M., Maniscalco R., Bencke B., Di Stefano A., Giuffrida S., Sturiale G.; 2001. *The sedimentology and Palaeoenvironment of Quaternary temperate carbonates and their distribution around the northern Hyblean Mountains (SE Sicily)*. Boll. Soc. Geol. It., 121, 233-255.
Scarfì L., MessinaA., Cassisi C.; 2013. *Sicily and southern Calabria focal mechanism database: a valuable tool for local and regional stress-field determination*. Annals of Geophysics, 56, 1-16.

## GRAVIQUAKES AND ELASTOQUAKES

**C. Doglioni[1,2], E. Carminati[1,2], P. Petricca[3] and F. Riguzzi[4]**
*[1] Dipartimento di Scienze della Terra, Università Sapienza, Roma, Italy*
*[2] Istituto di Geologia Ambientale e Geoingegneria, CNR, Roma, Italy*
*[3] GFZ-German Research Centre for Geosciences, Potsdam, Germany*
*[4] Istituto Nazionale di Geofisica e Vulcanologia, Roma, Italy*

Fault activation is crucial for the understanding of earthquakes and their prediction. Earthquakes are usually interpreted as the rupture of an asperity along a fault, when the shear stress overcomes the fault strength. But why do faults move episodically? Why is seismicity not more randomly distributed if an earthquake is simply associated with an asperity, which should be smeared out after fault motion? The origin of the earthquake recurrence or seismic cycle, consisting of a long interseismic period followed by a coseismic (and postseismic) period, remains quite obscure. The length of the interseismic period between two earthquakes along the same fault has been proposed to be controlled by a number of physical parameters, e.g., the relative velocity between the two walls of the fault, the composition of the crust, the mineralogy and foliation of the fault rocks, the morphology and length of the fault plane, the thermal state, the friction on the fault, the fluid pore-pressure, etc.. All these parameters entail first a long, static accumulation of energy during the interseismic period, which is eventually radiated coseismically when the friction on the fault has overcome. In this article we contribute to this topic with a geological model to explain the activation of a crustal fault, where the aforementioned physical parameters could determine the timescale of the recurrence or the magnitude. In particular, we investigate the role of the brittle-ductile transition (BDT) in the evolution of crustal seismicity. The BDT depth generally represents the lower limit of most crustal seismicity. We propose a model that links the continuous ductile deformation at depth with the brittle episodic behavior of shallow crustal layers, and show how the BDT may play a triggering role in fault movement. The model is tested numerically and applied to two areas where normal fault and thrust related earthquakes occurred, i.e., in the central Apennines (2009) and Taiwan (1999). GPS interseismic and coseismic data, dissipated energy from the two cases are shown to be consistent with model predictions, where normal faults and thrusts have opposite behavior. Similar to the effects of the lithostatic load, which enhances the rupture of normal faults and inhibits faulting along thrusts (Carminati *et al.*, 2004), the two types of faulting are asymmetric in terms of geological and mechanical behavior (Doglioni *et al.*, 2011).

We model a fault cross-cutting the brittle upper crust and the ductile lower crust. In the brittle layer the fault is assumed to have stick–slip behavior, whereas the lower ductile crust is inferred to deform in a steady-state shear. Therefore, the brittle–ductile transition (BDT) separates two layers with different strain rates and structural styles. This contrasting behavior determines a stress gradient at the BDT that is eventually dissipated during the earthquake. During the interseismic period, along a normal fault it should form a dilated hinge at and above the BDT. Conversely, an over-compressed volume should rather develop above a thrust plane at the BDT. On a normal fault the earthquake is associated with the coseismic closure of the dilated fractures generated in the stretched hangingwall during the interseismic period. In addition to the shear stress overcoming the friction of the fault, the brittle fault moves when the weight of the hangingwall exceeds the strength of the dilated band above the BDT. On a thrust fault, the seismic event is instead associated with the sudden dilation of the previously over-compressed volume in the hangingwall above the BDT, a mechanism requiring much more energy because it acts against gravity. In both cases, the deeper the BDT, the larger the involved volume, and the bigger the related magnitude. We tested two scenarios with two examples from L'Aquila 2009 (Italy) and Chi-Chi 1999 (Taiwan) events. GPS data, energy dissipation and strain rate analysis support these contrasting evolutions. Our model also predicts, consistently with data, that the interseismic strain rate is lower along the faultsegment more prone to seismic activation (Doglioni *et al.*, 2011).

Earthquakes deliver in few seconds the elastic energy accumulated in hundreds of years. Where and when will be the next earthquake remains a difficult task due to the chaotic behavior of seismicity and the present lack of available tools to measure the threshold of the crustal strength. However, the analysis of the background strain rate in Italy and the comparison with seismicity shows that larger earthquakes occur with higher probability in areas of lower strain rate. We present a statistical study in which a relationship linking the earthquake size (magnitude) and the total strain rate (SR) is found. We combine the information provided by the Gutenberg–Richter law (GR) of earthquake occurrence and the probability density distribution of SR in the Italian area. Following a Bayesian approach, we found a simple family of exponential decrease curves describing the probability that an event of a given size occurs within a given class of SR. This approach relies on the evidence that elastic energy accumulates in those areas where faults are locked and the SR is lower. Therefore, in tectonically active areas, SR lows are more prone to release larger amount of energy with respect to adjacent zones characterised by higher strain rates. The SR map of Italy, compared with 5 years seismicity supports this result and may become a powerful tool for identifying the areas more prone to the next earthquakes (Riguzzi *et al.*, 2012).

We find that geodetic strain rate (SR) integrated with the knowledge of active faults points out that hazardous seismic areas are those with lower SR, where active faults are possibly approaching the end of seismic cycle. SR values estimated from GPS velocities at epicentral areas of large historical earthquakes in Italy decrease with increasing elapsed time, thus highlighting faults more prone to reactivation. We have modelled an exponential decrease relationship between SR and the time elapsed since the last largest earthquake, differencing historical earthquakes according to their fault rupture style. Then, we have estimated the characteristic times of relaxation by a non-linear inversion, showing that events with thrust mechanism exhibit a characteristic time (~990 yr) about three times larger than those with normal mechanism. Assuming standard rigidity and viscosity values we can infer an average recurrence time of about 600 yr for normal faults and about 2000 yr for thrust faults (Riguzzi *et al.*, 2012).

The fault activation (fault on) interrupts the enduring fault locking (fault off) and marks the end of a seismic cycle in which the brittle-ductile transition (BDT) acts as a sort of switch.

We suggest that the fluid flow rates differ during the different periods of the seismic cycle (interseismic, pre-seismic, coseismic and post-seismic) and in particular as a function of the tectonic style. Regional examples indicate that tectonic-related fluids anomalies depend on the stage of the tectonic cycle and the tectonic style. Although it is difficult to model an increasing permeability with depth and several BDT transitions plus independent acquicludes may occur in the crust, we devised the simplest numerical model of a fault constantly shearing in the ductile deeper crust while being locked in the brittle shallow layer, with variable homogeneous permeabilities. The results indicate different behaviors in the three main tectonic settings. In tensional tectonics, a stretched band antithetic to the normal fault forms above the BDT during the interseismic period. Fractures close and fluids are expelled during the coseismic stage. The mechanism reverses in compressional tectonics. During the interseismic stage, an over-compressed band forms above the BDT. The band dilates while rebounding in the coseismic stage and attracts fluids locally. At the tip lines along strike-slip faults, two couples of subvertical bands show different behavior, one in dilation/compression and one in compression/dilation. This deformation pattern inverts during the coseismic stage. Sometimes a pre-seismic stage in which fluids start moving may be observed and could potentially become a precursor (Doglioni *et al.*, 2014).

We propose that the brittle-ductile transition (BDT) controls the seismic cycle. In particular, the movements detected by space geodesy record the steady state deformation in the ductile lower crust, whereas the stick-slip behavior of the brittle upper crust is constrained by its larger friction. GPS data allow analyzing the strain rate along active plate boundaries. In all tectonic settings, we propose that earthquakes primarily occur along active fault segments characterized by relative minima of strain rate, segments which are locked or slowly creeping. We discuss regional examples where large earthquakes happened in areas of relative low strain rate. Regardless the tectonic style, the interseismic stress and strain pattern inverts during the coseismic stage. Where a dilated band formed during the interseismic stage, this will be shortened at the coseismic stage, and vice-versa what was previously shortened, it will be dilated. The interseismic energy accumulation and the coseismic expenditure rather depend on the tectonic setting (extensional, contractional, or strike-slip). The gravitational potential energy dominates along normal faults, whereas the elastic energy prevails for thrust earthquakes and performs work against the gravity force. The energy budget in strike-slip tectonic setting is also primarily due elastic energy. Therefore, precursors may be different as a function of the tectonic setting. In this model, with a given displacement, the magnitude of an earthquake results from the coseismic slip of the deformed volume above the BDT rather than only on the fault length, and it also depends on the fault kinematics (Doglioni *et al.*, 2015a).

Earthquakes dissipate energy stored by pressure gradients at plate boundaries and still represent a major issue both for public safety and for their mechanisms. We assume that the lateral variations of the viscous-plastic basal mantle drag are determining the tectonics at plate boundaries and the deformation is transferred from the lithosphere base at the Earth's surface. Due to the brittle nature of the upper crust, the shallow deformation occurs episodically, i.e., releasing in few seconds the energy accumulated in hundreds of years. We focus our study on the earthquakes generated by normal faults, which are widespread in several geodynamic environments, such as continental rifts, backarc basins, mid-ocean ridges, orogens and strike-slip settings. Earthquakes modify Earth's gravitational energy. It was pointed out that the coseismic gravitational energy variation might be few orders of magnitude larger than the radiated seismic wave energy, which is usually referred as 'seismic energy'. Unlike thrust or reverse faults, gravity favours normal faulting since the maximum stress axis is parallel to the lithostatic load. In fact, contrary to thrust faults, normal fault rupture tends to propagate upward. In extensional environments, the differential stress necessary to generate rock failure is on average 5–6 times smaller than that required in contractional tectonic settings. Accordingly, normal fault-related earthquakes never reached the magnitudes (e.g., >Mw 8.5) recorded in strike-slip and contractional settings and have a higher b-value of the Gutenberg-Richter power law. The elastic rebound is commonly considered as the main model for earthquake generation, being inferred as the mechanism dissipating the elastic energy accumulated during the interseismic period. This is likely true for contractional and strike-slip tectonic settings, but in tensional environments, the influence of gravitation may rather be dominant. In this paper we discuss some basic parameters that control the energy dissipation in shallow crustal extensional settings, such as the involved volume, the dip of the normal fault and the static friction. Natural examples will be taken from the Apennines belt and other geodynamic settings, characterized by widespread extensional fault activity and related earthquakes. In addition we address the energy partitioning of earthquakes comparing the potential energy stored by the volume involved during the coseismic collapse with that inferred from earthquake magnitude. Regardless its origin (elastic or gravitational), potential energy has been demonstrated far greater, indicating that, in the energy budget, the available energy is far larger than that released by earthquakes waves. Therefore most of the energy must be dissipated by other geological phenomena (shear heating, heat flow and fracturing above all), consistently with previous works. It was also shown that all earthquakes gradually decrease the global gravitational energy, which is transformed into heat flow. However, as intuitively expected, in extensional tectonic settings the gravitational potential energy is decreasing, whereas it is increasing in contractional tectonic environments.

In an upper crust having average density of 2.5 g/cm$^3$, the vertical (lithostatic) load increases by about 25 MPa/km. Below 1–1.5 km depth, the crust is under horizontal compression even in extensional settings, i.e., the sigma 1 is vertical and corresponds to the lithostatic load, whereas the sigma 2 and 3 stress axes are horizontal but still contracting rocks. Therefore, say at 10 km depth, both sigma 2 and 3 must be positive and lower than 250 MPa. With the progression of the stretching, sigma 2 and 3 decrease, providing a larger differential stress that may eventually evolve into rupture and fault activation. This determines the collapse of the normal fault hangingwall, dissipating mostly gravitational potential energy, being the elastic component a minor factor in the fall, if any. In a simplified two-layers stretching crust, within the brittle upper crust, the faults are generally locked or slowly creeping, and the deformation is mostly assumed to be stick-slip. During the secular interseismic period of lithospheric stretching, the ductile lower crust is permanently shearing and thinning by viscous flow and deformation is inferred as a continuous process. The brittle-ductile transition (BDT) is on average located in the middle Earth's crust. When a brittle fault merges into a ductile shear zone crosscutting the whole crust, the BDT is characterized by a pressure gradient because the brittle upper crust is mostly locked, whereas the viscous-plastic lower crust is sheared steadily (Fig. 1). Since the steady deformation of the ductile lower crust has to be transferred upward, it was proposed that the stretching could be accommodated in the brittle realm by dilation in a wedge conjugate to the episodically active normal fault (Fig. 1). In that wedge, millimetric open fractures are inferred to develop. These fractures may be partly filled by cement, and partly by fluids, as shown in logs of hydrocarbon exploration boreholes and as predicted by analogue modelling. This mechanism has also been defined as dilatancy, i.e., the phenomenon in which fractures and cracks form and open when rocks are stressed. This dilated wedge is inferred due to the strain partitioning and the pressure gradient between the ductile lower crust and the brittle upper crust. The occurrence of the dilated wedge from the geological model is also supported by the fact that the hangingwall of a normal fault could not collapse without a corresponding vacuity at the base of the activated fault segment (Fig. 1). A 10–15 km thick brittle crust needs only about 100–150 MPa to fail under extension. Moreover, once rocks are broken (e.g., by fracturing in limestone), they lose their elastic component, and fractures may be filled or unfilled by cement (Fig. 1), depending on fluids circulation, carbonate compensation depth, temperature, pressure, $CO_2$ content in the system, etc. During the initial stage of collapse, fluid pressure increases, supporting the existence, in pre-coseismic stages, of open fractures filled by fluids, becoming squeezed by the fall of the fault hangingwall.

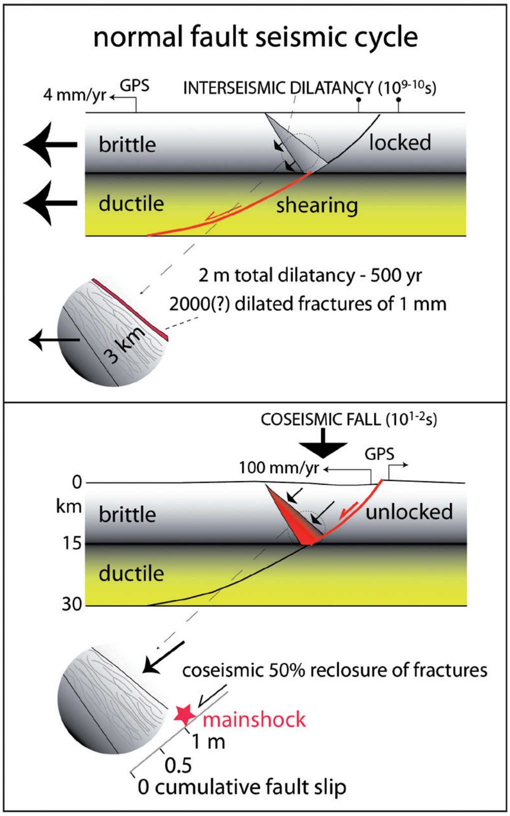


Fig. 1 – Geological model of the seismic cycle associated to a normal fault. During the interseismic period, while the lower crust shears steadily, the brittle upper crust is locked and a dilating wedge is inferred. The width of this triangle is here hypothetically imaged to affect an antithetic section to the locked fault, say 3 km thick. Partial sealing of the fractures due to fluids circulation may be expected. The remaining open fractures allow the fall of the hangingwall at the coseismic stage, when the fault plane and the dilated wedge cannot sustain anymore the upper suspended block. The coseismic collapse of the hangingwall could recover for example only half of the total extension. Note that the mainshock is located along the fault at the upper tip of the dilated wedge, consistently with the seismological observations showing that the mainshock is located slightly above the rupture zone [e.g., like in the L'Aquila, April 6 6.3 Mw earthquake, after Doglioni *et al*. (2015b)].

In the hypothetical case the upper crust was made of low strength material, the deformation in the upper crust would rather occur in steady state, without generation of pressure gradients. In this situation, in the low-temperature upper crust, the fault would continuously creep and the conjugate dilatational wedge of Fig. 1 would not form. Therefore, the inferred dilated conjugate wedge reaches its maximum expression when the fault in the brittle crust is completely locked. Intermediate cases should possibly exist between these two end-members, and it is evident that the crust consists of multilayers having strength variability, hence generating multiple stress gradients.

The opening of fractures and the fluids permeating them gradually weaken the dilated wedge, which should increasingly lose strength during the interseismic stage. Therefore, the suspended hangingwall is lying on the fault on one side, and is bounded on the other side by the dilated wedge. When the fault and the conjugate wedge will not be any more sufficiently strong to support the hangingwall, the sudden collapse will generate the earthquake (Fig. 1). Therefore, from the BDT to the surface there may be accumulation of elastic and gravitational potential energy in a "suspended" volume. The volume times its density gives the mass of the hangingwall wedge. The hangingwall will collapse when the weight of this volume will overtake the strength of the fault plane and of the dilated wedge. At the coseismic stage the wedge will partly recover, by fracture closure, the dilation accommodated during the interseismic period (Fig. 1). This is proposed to be accompanied by expulsion of fluids that permeated the fractures. Alternatively, the fall of the hangingwall may be diluted in time during the interseismic stage generating continuous microseismicity in case of lower fault dip, possibly associated with lower friction. The Mw 6.3 April 6, 2009 L'Aquila earthquake can be taken as a case history for this model. During the 4-5 months preceding the quake, a series of foreshocks occurred in the volume of the hangingwall and along the inferred dilated wedge.

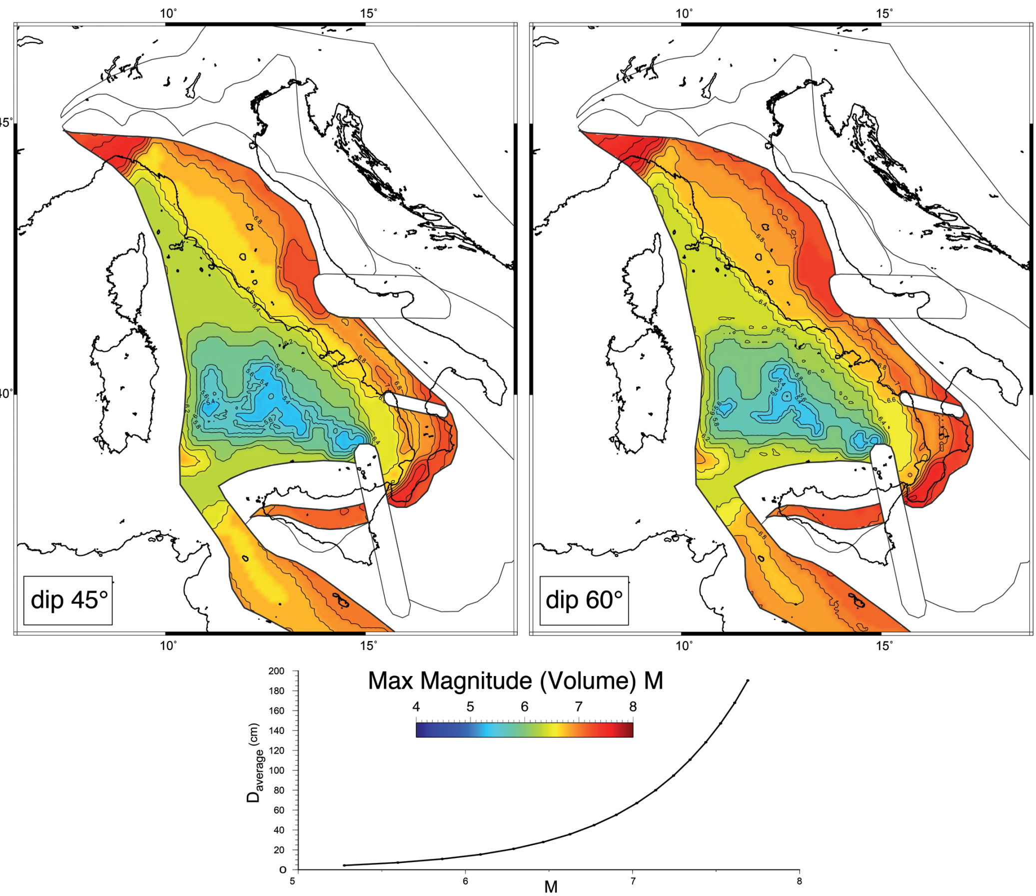


Fig. 2 – The maps show the maximum magnitude (M) expected by gravitational collapse along normal faults in the Italian area and surroundings undergoing extensional tectonics, assuming a slip (D) increasing with magnitude as reported in the lower diagram. The values are inferred assuming the collapse of the volumes computed in the previous figure (45° left and 60° right). It is hypothesized a constant static friction, and normal fault planes activated during an earthquake seem to have in average a mean maximum length three times the depth of the hypocentre. Normal fault earthquakes have their maximum magnitude close to the brittle-ductile transition (BDT), which is deeper where the surface heat flow is lower. The deeper the BDT, the larger the volume and the higher will result the graviquake magnitude. These maps of the extensional areas affecting the central Mediterranean, are only a preliminary attempt to relate brittle volumes and maximum potential magnitude, if active normal faults are present (after Petricca *et al.*, 2015).

The model predicts that the dilated wedge formed during the interseismic will be contracted during the coseismic stage. An example of this inversion occurred during the 1986 Kalamata (south Peloponnesus) normal fault-related earthquake, which was associated with several compressional focal mechanisms.

We discuss the mechanics of crustal normal fault-related earthquakes, and show that they represent dissipation of gravitational potential energy (graviquakes) and their magnitude increases with the involved volume (delimited by the seismogenic fault and an antithetic dilated wedge in its hangingwall), and the fault dip. The magnitude increases with the deepening of the brittle-ductile transition (BDT), which in turn enlarges the involved volume. The fault dip seems rather controlled by the static friction of the involved crustal layers. We apply the model to the extensional area of the Italian peninsula (Fig. 2), whose geodynamics is controlled by the Alpine and Apennines subduction zones. The latter has a well-developed backarc basin and a large part

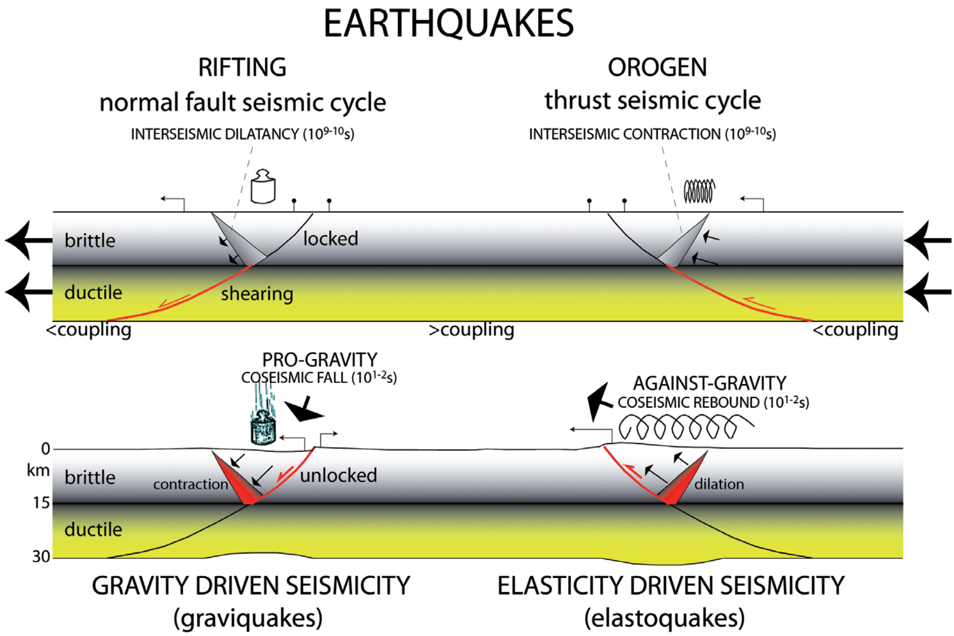


Fig. 3 – Simplified classification of earthquakes as a function of their energy source. Earthquakes are distinguished depending on whether they are generated by gravity in extensional tectonic settings or by elastic rebound in strike-slip and contractional tectonic environments (after Doglioni *et al.*, 2015b).

of the accretionary prism is affected by on-going extensional tectonics, which is responsible for most of peninsular Italy seismicity. Analysing the seismic record of the Apennines, the length of seismogenic normal faults tends to be at most about 3 times the hypocentre depth. We compile a map of the brittle-ductile transition depth and, assuming a fixed 45° or 60° fault dip and a dilated wedge developed during the interseismic period almost perpendicular to the fault plane, we compute the maximum volume of the hangingwall collapsing at the coseismic stage, and estimate the maximum expected magnitude. Lower magnitude values are obtained in areas with thinner brittle layer and higher heat flow. Moreover, lower magnitude relative to those theoretically expected may occur in areas of higher strain rate where faults may creep faster due to lower frictional values (Petricca *et al.*, 2015).

Earthquakes are dissipation of energy throughout elastic waves. Canonically is the elastic energy accumulated during the interseismic period. However, in crustal extensional settings, gravity is the main energy source for hangingwall fault collapsing. Gravitational potential is about 100 times larger than the observed magnitude, far more than enough to explain the earthquake. Therefore, normal faults have a different mechanism of energy accumulation and dissipation (graviquakes) with respect to other tectonic settings (strike-slip and contractional), where elastic energy allows motion even against gravity (elastoquakes), Fig. 3. The bigger the involved volume, the larger is their magnitude. The steeper the normal fault, the larger is the vertical displacement and the larger is the seismic energy released. Normal faults activate preferentially at about 60° but they can be shallower in low friction rocks. In low static friction rocks, the fault may partly creep dissipating gravitational energy without releasing great amount of seismic energy. The maximum volume involved by graviquakes is smaller than the other tectonic settings, being the activated fault at most about three times the hypocentre depth, explaining their higher b-value and the lower magnitude of the largest recorded events. Having different phenomenology, graviquakes show peculiar precursors (Doglioni *et al.*, 2014, 2015b).

**References**

Carminati E., Doglioni C. and Barba S.; 2004: *Reverse migration of seismicity on thrusts and normal faults*. Earth Sci. Rev., 65, 195–222.

Doglioni C., Barba S., Carminati E. and Riguzzi F.; 2011: *Role of the brittle-ductile transition on fault activation*. Phys. Earth Planet. Int., 184, 160–171.

Doglioni C., Barba S., Carminati E. and Riguzzi F.; 2014: Fault on-off versus coseismic fluids reaction. Geoscience Frontiers, v. 5, issue 6, pp. 767–780, doi.org/10.1016/j.gsf.2013.08.004

Doglioni C., Barba S., Carminati E. and Riguzzi F.; 2015: *Fault on-off versus strain rate and earthquakes energy*. Geoscience Frontiers 6, 265-276, doi: http://dx.doi.org/10.1016/j.gsf.2013.12.007

Doglioni C., Carminati E., Petricca P. and Riguzzi F.; 2015b: *Normal fault earthquakes or graviquakes*. Scientific Reports Nature, 5, 12110 doi:10.1038/srep12110.

Petricca P., Barba S., Carminati E., Doglioni C. and Riguzzi F.; 2015: *Graviquakes in Italy*. Tectonophysics, 656, 202–214, doi:10.1016/j.tecto.2015.07.001

Riguzzi F., Crespi M., Devoti R., Doglioni C., Pietrantonio· G. and Pisani A.R.; 2012: *Geodetic strain rate and earthquake size: New clues for seismic hazard studies*. Phys. Earth Planet. Int., 206-207, 67–75.

Riguzzi F., Crespi M., Devoti R., Doglioni C., Pietrantonio G. and Pisani A.R.; 2013: Strain rate relaxation of normal and thrust faults in Italy. Geophys. J. Int., doi: 10.1093/gji/ggt304

## LOST EARTHQUAKES BETWEEN ANTIQUITY AND MIDDLE AGE. ARCHEOLOGICAL INDICATION FROM VOLCEI (SOUTHERN APENNINE)

**P. Galli[1], A. Lagi[2]**

*[1] Dipartimento della Protezione Civile Nazionale, Roma, Italy*

*[2] Ministero per i Beni e le Attività Culturali, Ufficio Patrimonio Mondiale UNESCO, Roma, Italy*

**Introduction.** Although the Italian seismic compilations are among the best and back-in time extended catalogues of the world, with earthquakes on record even before the Common Era (e.g., 461 BC in Rome), we have surely lost the memory of dozen strong events of the historical period, mostly in the first millennium AD. In the lack of written sources, the only way to infer the occurrence of an ancient earthquake in a settlement is to gather as much evidence as possible from archaeological excavations. This happens usually by investigating the existence of collapses/ restorations/ reconstructions of buildings, the general re-organization of the urban texture or, even, the abandonment of the settlement. Exceptionally, this goal is achieved thanks to the discovery of epigraphs mentioning more or less explicitly the effects of the earthquake.

Here we present the case of Buccino, the former Roman *municipium* of Volcei, a settlement located since the Iron Age close to the Apennine divide, between Campania and Basilicata regions (Fig. 1). This sector of the chain is dominated by active NE-SW extension, mainly accommodated by NW-SE normal faults which sourced some among the strongest earthquakes of the Apennines. Indeed, Buccino was heavily damaged (8 MCS degree) by the 1980 Irpinia earthquake (Mw 6.9), with the thirty-year reconstruction activities providing an amazing opportunity to rediscover the buried remains of the Roman town. As the seismic history of Buccino was known to be quite destructive, at least relatively to the past six centuries [e.g., earthquakes in 1466, 1561 and 1857; Is 8-10 MCS: Galli *et al*. (2006), Castelli *et al*. (2008), Galli and Peronace (2014)] the recognition of widespread, seismically induced damage to the ancient structures was not an unexpected discovery, allowing the extension of our information well behind the memory of the written Modern sources.

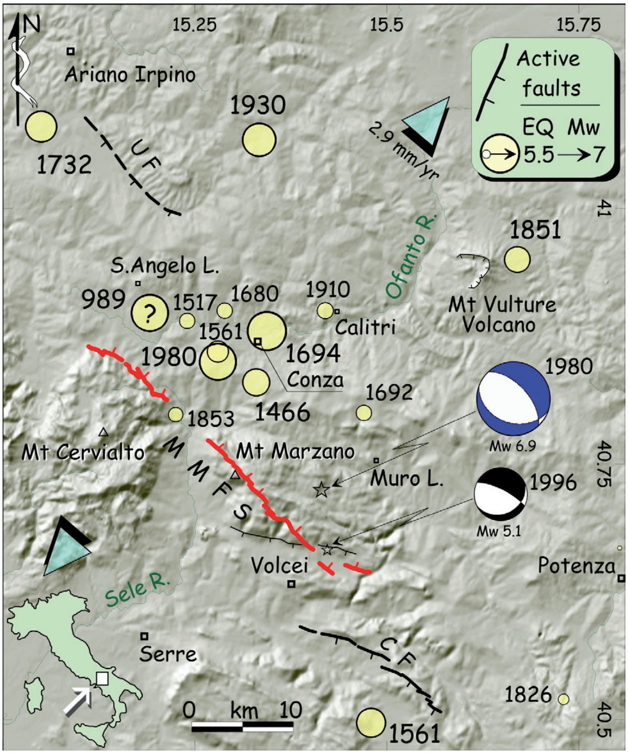


Fig. 1 – Historical earthquakes distribution and seismogenic faults around Buccino/Volcei. Note the epicenters cluster in the hanging wall of the Mount Marzano Fault System (MMFS), which is responsible for the strongest earth shaking in Buccino, together with the Caggiano Fault (CF) and the still unknown structure that sourced the Mw 7.1, 1857 earthquake (outside this map). Normal faults accommodate NE-SW extension (see 1980, 1996 focal mechanisms), currently rated at ~3 mm/yr by GPS studies (from Galli and Peronace, 2014).

**The late third century BC event (Santo Stefano sanctuary area).** Due to the presence of everlasting soil creep and earth flow, the sacred area of Santo Stefano (NE of Buccino), occupied since the 8$^{th}$ century BC, actually provided not-univocal indication of coseismic damage. However, these might consist of widespread collapses and destruction layers of 4$^{th}$ century BC buildings, indicating an abrupt end of the settlement on the terraces occupied by the sanctuary and by the necropolis in the last decades of the 3$^{rd}$ century BC. In the uppermost terrace, a farm was built over the sanctuary walls, suggesting the overall abandonment of the sacred site, which was successively buried by alluvial and colluvial deposits.

**The first century AD event (Volcei).** During the reconstruction works following the 1980 earthquake, many indications of coeval collapses, *butti* (stacks of archeological debris), fills and leveling of destroyed buildings were found everywhere in Buccino. Moreover, there was evidence of restoring and/or rebuilding of several houses, with the reutilization of architectural elements from the previous buildings, such as architraves and epigraphs, beside the existence of a coeval epigraph mentioning explicitly the restoration made after a collapse due to an earthquake. In the whole, all the indications point to an event falling in the second half of the 1$^{st}$ century AD, as summarized in the forthcoming points (see Fig. 2 for sites location).

- Forcella palace. Here the indications consist in a dumping grave containing domestic pottery (lamps and dishes) datable within the first half of the 1$^{st}$ century AD. As no *sigillata chiara* A pottery (early second half of 1$^{st}$ century AD) was found within the grave, the dumping age should falls at the onset of the second half of the 1$^{st}$ century AD.
- Castle. Over the southern side of the main 12$^{th}$ century Norman tower (i.e., *Mastio*, resting over the basement of a Roman temple), the excavations found a broad, wall-supported rubble fill, made by domestic material, bricks, tiles and limestone blocks. The fill, which was sealed upward by a concrete pouring, contains *sigillata italica* and *Africana chiara A* pottery, the latter datable at the end of the 1$^{st}$ century AD (max 60-70 AD). At the bottom of the fill, a coin of Emperor Tiberius (23-30 AD) provides a certain post *quem term* for

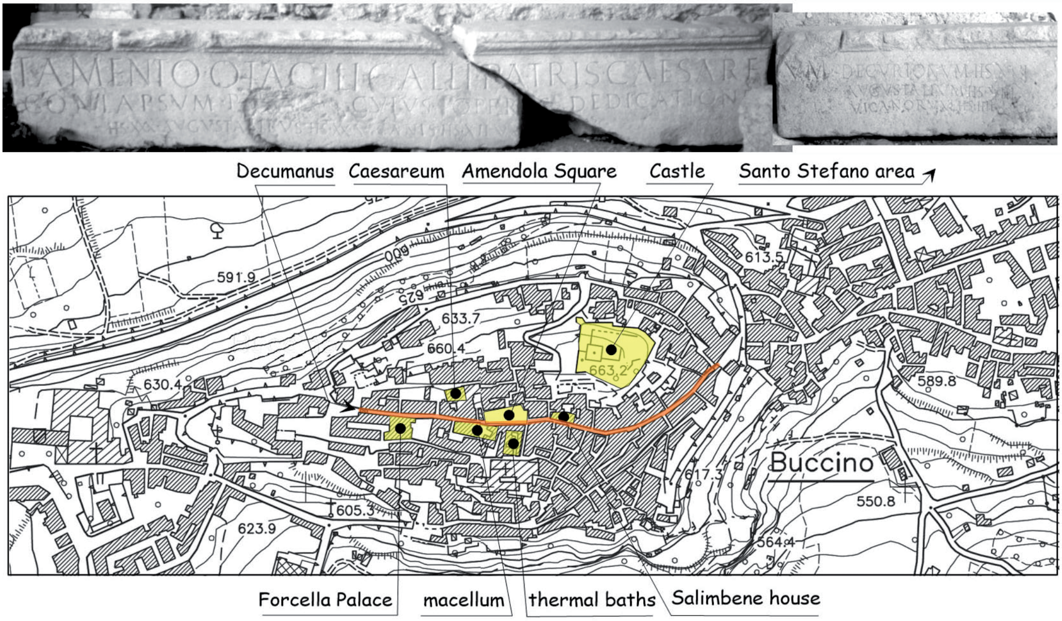


Fig. 2 – Map of Buccino showing the main archaeological sites attesting the 1st century AD earthquake. Upper panel is the photomosaic of the epigraph of Otacilius Gallus attesting the collapse of the *Caesareum* (photo by PG).

the rubbles mass which, in turn, was likely leveled between the late 1st and the early 2nd century.

- Sotto San Nicola street. Here another dumping grave of both building and domestic rubble has been found. It contains vases and lamps datable within the first half of the 1st century AD (*i.e., sigillata italica, pareti sottili*), being thus coeval with the Castle area fill.
- Amendola square. In this place three different dumping graves, all overlaid by a restoration floor, contain pottery shards with *pareti sottili* (early 1st century AD). Amongst these, the relic of a pot was found, with the skeleton of a dormouse still inside. At least one of the building facing the *Decumanus* was restored in the 2nd century AD, when also a *porticus* with four pillars was added to the house. One of the pillar supported a Osco-Latin epigraph, likely recalling the restoration of a nearby *vicum venerlum* [sic] in the 2nd century (G. Camodeca and A. La Regina, pers. comm.). We dated some charred materials belonging to the wooden structure of the *porticus*, which was finally buried by the whole collapse of this building in the Early-High Middle Age. The calibrated age (110-330 AD, 2σ cal.) fits the period of general restoration of the town, providing the *ante quem* term for the collapse.
- Thermal baths. Between the 1st and the 2nd century AD, the thermal baths were restored, their orientation was changed, whereas the floors were completely remade with mosaics.
- Macellum. In the same period, in the area of the *macellum* the two *tholoi* were dismantled, the *macellum* itself was abandoned, its remains were leveled and occupied by new workshops.
- Salimbene house. During the archaeological excavation, the abrupt collapse of a 1st century BC room ceiling has been found and removed. This has allowed to observe that the *incannucciato* ceiling collapse rest directly over the mortar floor, where it buries pottery shards of the 1st century AD (Fig. 3, left panel).
- Caesareum temple. Here, in the same period, an *opus caementicium* cistern was built for supporting the damaged retaining wall of the temple. Damages to this temple are testified also by an epigraph, as hereafter described.


Fig. 3 – Left panel, collapse of the *incannucciato* ceiling (unit 24) and of the plaster (25) over a mortar floor (30). Wall 21 is instead the foundation of a medieval wall which was carved within the previous Roman collapse. This medieval wall collapsed later, and its relics were found inside an adjacent room. Right panel, Amendola Square *insula*. View of the final collapse of the porticated house over the *Decumanus* (see the *basoli* in the upper side) before the roof removal (photos by PG).

- <u>Epigraph of Otacilius Gallus.</u> This epigraph (Fig. 2), probably an architrave, recalls the collapse of the Caesareum, which was built around 50-60 BC. The text is: OTACILIVS EX TESTAMENTO OTACILI GALLI PATRIS CAESAREVM/ [TERRAE MOTV] CONLAPSVM P(ecVnia) [S(Va) R(estitVit)]. CVIVS OPER[IS] DEDICATIONE/ [DEDIT DECVRIONIBVS] (sestertios) XXX, AVGVSTA[L]IBVS (sestertios) XX, VICANIS (sestertios) XII, VX[ORIBVS]/ DECVRIONVM (sestertios) XVI, AVGVSTALIVM (sestertios) VIII, VICANORVM (sestertios) IIII. If the integration of the missing text is correct (Bracco, 1977), the Caesareum was destroyed by an earthquake occurred before the end of the $1^{st}$ century AD, and then restored by Otacilius in the $2^{nd}$ century (G. Camodeca, pers. comm.).

In the whole, the archaeological data evidence an abrupt discontinuity within the urban texture of the Roman Volcei, followed by a reconstruction phase focused between the $1^{st}$-$2^{nd}$ century AD. The great abundance of domestic pottery, tiles, bricks, stones in the dumping graves, summed to the existence of leveled rubble fills are the proof of extensive building collapses in the town. Moreover, the discovery of the pot with the dormouse, ready to be cooked when it was buried under the rubble, and the Otacilius' epigraph, attesting the collapse of the Caesareum, are strong indications concerning the occurrence of this event. At the end, a further indication which could be evocative of a tragedy related to this earthquake derives from the funerary monument of Gresia Tertia, located only 10 km away from Volcey. Here, recent archaeological investigations unearthed an epigraph datable within the $1^{st}$ century, where an *infelix mater* cries the death of her family, namely all the four sons and the father. Even if the cause is not declared, the simultaneous death of five person of the same family could really be related to the collapse of their house.

**The Early-High Middle Age event(s).** The evidence of this traumatic event are represented by the synchronous and total collapses of the buildings excavated below Amendola Square and in other neighboring *insulae*. Moreover, it is witnessed by the general abandonment of the surviving Late Antiquity buildings, which were still inhabited during the Langobardic period, and by the new urban topography that drifts apart from the Roman imprint, assuming a concentric path around the castle. It is difficult to provide a certain age for this earthquake, mainly because of the paucity of the Early Middle Age pottery. However, it could be constrained between the $7^{th}$-$8^{th}$ and the $12t^{h}$ century, even if we cannot exclude the occurrence of multiple events within this time span. The set of indications can be summarized as follow.

- Amendola square. The excavations have revealed the synchronous collapse of all the building surviving since the Late Roman times. Below the rubbles it has been possible to read the frozen history of these houses, with the different rezoning of each room during times, the wall restorations, the floors overlapping, the doorstep reutilization. The collapse affected all the masonry wall, the pillars of the *porticus* and the roofs which have been all found directly overlaying the floors (Fig. 3, right panel). This catastrophic collapse buried definitely also the *Decumanus* which was still in use and well mainteined at least during the $7^{th}$ century, as testified by the materials found in the ditches. At first glance, the collapse killed also a small sheep which was hit and buried by the rubble on the road *basoli*. The AMS collagen dating provided an age of 1034-1214 AD (2σ cal.). Inside the porticated building, beside the wall-plasters, the *incannucciato* ceiling, tiles and the masonry, it was possible to observe some walls and the four bricks-pillars which fell away from the road, burying *bande rosse* pottery (used all along the Early Middle Age).
- Salimbene house. An Early Middle Age cobble-wall was founded inside the fill burying the Roman buildings (Fig. 3). The pottery shards inside the foundation trench is the same as in Amendola Square, i.e. it contains *bande rosse* pottery. Therefore, this wall - successively collapsed over a nearby room - might suggest the onset of the reconstruction of the Early Middle Age Buccino after and over the earthquake rubble.

As aforementioned, the dating of these collapses is problematic. Indeed, whereas the pottery shards involved and buried by the collapses predate the second millennium, the AMS dating of the sheep buried under the rubble indicates the onset of the new millennium. This might suggest that an event occurred between the uppermost and lowermost limits of the two terms, i.e around 1000 AD. Indeed, on October 25, 989, a powerful earthquake hit this region (see Figliuolo and Marturano, 2002). Damage was recorded up to Ariano Irpino, and to the far-away town of Benevento. The strongest effects were focused on the broad upper Ofanto Valley, where coeval sources are complemented by archaeoseismic evidence, and supported in places also by radiocarbon dating of materials buried under the collapses (Galli, 2010). This suggests that Conza, Ronza, Montella, Rocca San Felice, Sant'Angelo dei Lombardi, and Frigento experienced severe damage, as Buccino likely did. However, this framework is complicated by the presence of a late historical source who mentions an earthquake occurred at the times of Pope Callistus II (1119-1124), the destructions of which were still visible in Buccino, in the "*horti...nella parrocchia de S Maria Sollitta...*" (from a drawing of B. Bardario, 1589; Biblioteca Angelica di Roma). The period of Pope Callistus fully matches the AMS age of the buried sheep, although it is not consistent with the time-span suggested by the pottery. Nevertheless, considering the high frequency of earthquake occurrence in this region (Galli and Peronace, 2014), we cannot exclude that more than one event hit Buccino just before and after 1000 AD, cumulating damage and collapses of the highly vulnerable Middle Age buildings. As a matter of fact, in one of the house below Amendola Square, the archaeologists unearthed a small lime furnace that was operating at the time of the collapse. The furnace overlays a thin abandonment level on the floor, suggesting that men were working inside an uninhabited house. Thus, an attractive hypothesis, that does not claim to be conclusive, is that while works were in progress for repairing the damage of the 989 earthquake, another event caused the complete collapse of the buildings around 1120 AD and the definitive burying of the ancient *Decumanus*.

**Discussion and conclusions**. An unexpected and tragic event, such as the Mw 6.9 Irpinia earthquake, allowed to rediscover the buried relics of the Roman *municipium* of Volcei. The further amazing circumstance is that below the ruins of the last earthquake the archaeologists have found a palimpsest of constructions/ collapses/reconstructions attributable to as many seismic events that, each time, have partly allowed the freezing of the buildings history below their own rubble. Although sometime the unraveling of this tangled skein of construction/ destruction events is a very hard task, we have collected several indications from different sectors of the town that suggest the occurrence of different earthquakes striking Volcei/ Buccino in the past. Leaving aside the destruction of the sacred structures of Santo Stefano, occurred in the late third century BC event in an area widely affected by earth flow and landslides, our data indicate a strong, destructive event occurred in the second half of the 1st century AD. This earthquake, which is unknown to the seismological compilations, could be related to the one found by means of paleoseismological analyses across the Mount Marzano Fault System (MMFS in Fig. 1; Galli and Peronace, 2014), i.e. the same structure that caused the 1980 earthquake. Alongside the archaeoseismic indications, this event is recorded by an epigraph that, although incomplete, clearly mention the collapse of the Caesareum. A very speculative hypothesis concerning this event is suggested by its concurrence with the so-called Pompei earthquake in 62 AD. As the strong earthquakes sourced by the Mount Marzano Fault System always induce high intensity effects in the Naples area (e.g., 7 MCS degree in both 1694 and 1980 events), it could be possible that the damage quoted by the historical sources in the ancient Pompei, as in Naples, Ercolano and Nocera (e.g., Seneca in his *Naturales quaestiones*) was the far-field effects of the same Irpinia earthquake that struck Volcei.

Another disruptive event, or perhaps two occurred close-in-time, is supported by the collapses and reconstructions datable around the year 1000 AD, that we have associated to the known 989 earthquake and/or to an unknown event around 1120.

More archaeoseismic indications related to later earthquakes, such as the 1466, 1561 and 1857 events, were not presented here, but together with those that we have discussed strengthen the ability of archaeoseismology in identifying and dating strong shaking events which are not recorded, or are poorly constrained in the current seismic compilation.

**References**

Bracco V.; 1977. *Inscriptiones Italiae, Civitates Vallum Silari et Tanagri, Regio III*, I, Roma, Poligr. Stato.

Castelli V., Galli P., Camassi R., Caracciolo C.H.; 2008. *The 1561 earthquake(s) in Southern Italy: new insights into a complex seismic sequence*. J. Earthq. Eng. 12 (7), 1054–1077.

Figliuolo B., Marturano A.; 2002. *Terremoti in Italia Meridionale dal IX all'XI secolo*. In: Marturano, A. (Ed.), "Contributi per la storia dei terremoti nel Bacino del Mediterraneo". Osservatorio Vesuviano, Istituto Italiano Studi Filosofici, Laveglia, Nocera Inferiore, NA, pp. 33-68.

Galli P.; 2010. *La storia sismica di Conza*. In: Ricciardi, E. (Ed.), Conza storia arte fede. Grafiche Pannisco, Calitri, pp. 23-70.

Galli P., Bosi V., Piscitelli S., Giocoli A., Scionti V.; 2006. *Late Holocene earthquakes in southern Apennines: paleoseismology of the Caggiano fault*. Int. J. Earth Sci. 95, 855–870.

Galli P., Peronace E.; 2014. *New paleoseismic data from the Irpinia fault. A different seismogenic perspective for southern Apennines (Italy)*, Earth Sci. Rev. 136, 175–201.

Seneca L. Annaeus. *Naturales quaestiones*, ed. D.Vottero (Classici latini), Torino 1989.

# LATE PLEISTOCENE REVERSE SURFACE FAULTING AT THE PECETTO DI VALENZA SITE (AL - NORTHERN ITALY): PRELIMINARY RESULTS

F. Livio[1], M.F. Ferrario[1], C. Frigerio[1], A.M. Michetti[1], A. Zerboni[2], L. Bonadeo[1], G. Fioraso[3], A. Irace[3], F. Brunamonte[1]

[1] *Dipartimento di Scienza ed Alta Tecnologia, Università dell'Insubria, Como, Italy*
[2] *Dipartimento di Scienze della Terra "A. Desio", Università degli Studi di Milano, Italy*
[3] *Istituto di Geoscienze e Georisorse (IGG), CNR, Torino, Italy*

**Introduction.** Notwithstanding the considerable investigation and research efforts produced almost 40 years ago for the Italian Nuclear Program, later published in the framework of the "Progetto Finalizzato Geodinamica" (e.g., Carraro, 1976; GSQP, 1976; Enel, 1984, 1985; CNR, 1992; Carraro *et al.*, 1995), the assessment of ground motion and surface faulting hazard in the Monferrato Arc is still poorly constrained. Since the western Po Plain shows subdued historical and instrumental seismicity, it is commonly regarded as a region characterized by a low seismic hazard (http://zonesismiche.mi.ingv.it/), and has been overlooked in the last 30 years from the paleoseismological point of view, while active tectonics studies flourished more to the east, basically due to the available record of strong seismic events during the Middle Ages and later (e.g., Magri and Molin, 1986; Serva, 1990; Benedetti *et al.,* 2000, 2003; Maesano *et al.,* 2001; Burrato *et al.,* 2003; Galadini *et al.,* 2005; Galli, 2005; Livio *et al.,* 2009, 2014). However, several lines of evidence strongly suggest that the seismotectonic potential of the study area is similar to the one known for the central and eastern part of the Po Valley (e.g., Serva, 1990; Michetti *et al.*, 2012; Bonadeo, 2014 and references therein; Turrini *et al.*, 2015).

The recent seismic crisis in Emilia clearly illustrates the need for revised seismic hazard assessment in northern Italy. In this line, the characterization of the maximum earthquake magnitude through paleoseismic analyses might represent a vital tool for mitigating seismic risks, in a region that seems unprepared to cope with the effects of strong earthquakes. In fact, high population density, clustering of industrial facilities, and the great deficit of seismic safety accumulated due to the lack of a proper seismic code (Stucchi *et al.*, 2012), make today the Po Plain one of the regions most exposed to seismic risk of the whole Italian peninsula.

This is particularly true for the Monferrato Arc, which, as noted above, is characterized by quite marginal seismicity according to the Italian Seismic Catalog. In this line, it is very important to remark that recent literature data describe geological features suggesting significant seismic potential in the western Po Plain. New observations, based on recently exposed stratigraphic sections at Cereseto and Ozzano Monferrato (Sassone *et al.*, 2015; Fig. 1b), reveal relevant evidence of Late Quaternary reverse faulting. Moreover, Giraudi (2014, 2015), based on fluvial terrace analyses and the revision of subsurface shallow stratigraphic data, identify previously unmapped Late Quaternary faults in the Vercelli Plain and Casale Monferrato *plateau*. In the following, we focus on the newly identified Pecetto di Valenza site, where recent paleoseismic surface faulting has been observed for the first time in the study area. We base our interpretations on data coming from an integrated and multidisciplinary analysis, including paleoseismology, pedostratigraphy and geomorphology, as already successfully applied in another case study in the Po Plain area (Livio *et al.,* 2014; Zerboni *et al.,* 2015).

**Geological and geomorphological setting.** The Monferrato Arc is the westernmost of the 3 major salients enclosing the most external structural fronts of the northern Apennines (Fig. 1). The tectonic activity of the Po Plain is closely related to the recent evolution of these structural belts, mainly buried below the Plio-Pleistocene infilling of the basin but emerging or very shallow along the Monferrato Arc (e.g., Mosca, 2006).

Study site (Pecetto di Valenza) is located in the easternmost Monferrato area, in a hilly area bordered by the Po and Tanaro River and encircled by the Valenza and Alessandria fluvial terraces, to the north and to the south of the site respectively. Miocene marls and conglomerates,

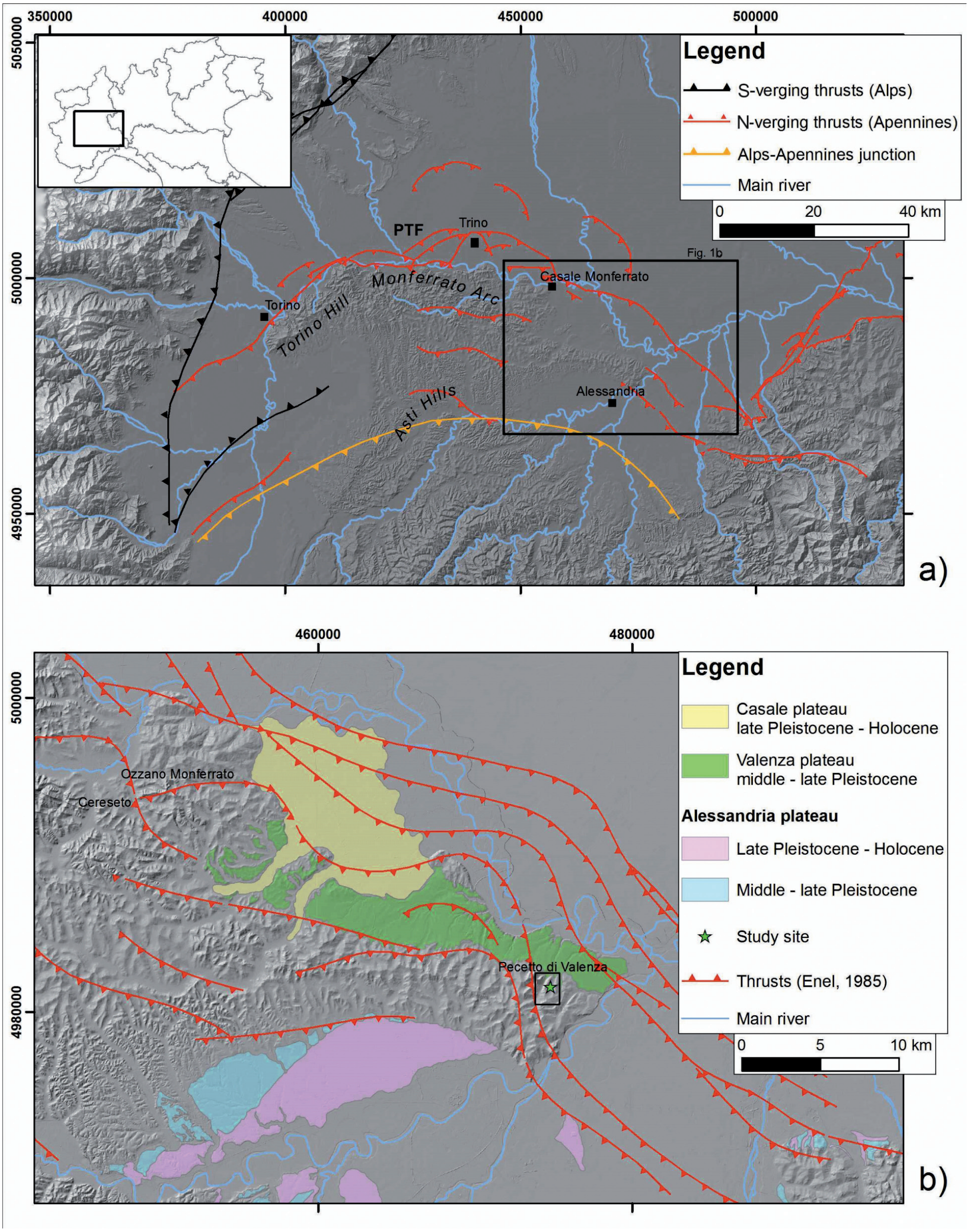


Fig. 1 – a) Simplified structural setting of the Monferrato Arc – western Po Plain area; PTF: Frontal Thrust, coordinates system UTM WGS84 – 32N; b) buried and outcropping thrust fronts along the eastern Monferrato (modified after Enel, 1985; Bonadeo, 2014) and main river terraces bordering the Monferrato hills. Black box indicates the area of Fig. 3.

unconformably lying upon Eocene marls, are deformed by ca. NW-SE trending thrusts and folds (ENEL - DCO, 1984), as observed in seismic reflection profiles.

At the study site, excavation works have exposed a reverse fault zone that displaces the late Miocene marly bedrock (Pecetto Fm.) and the overlying recent colluvial pedogenized deposits. This fact points to a recent landscape evolution of the site partially driven by active contractional tectonics.

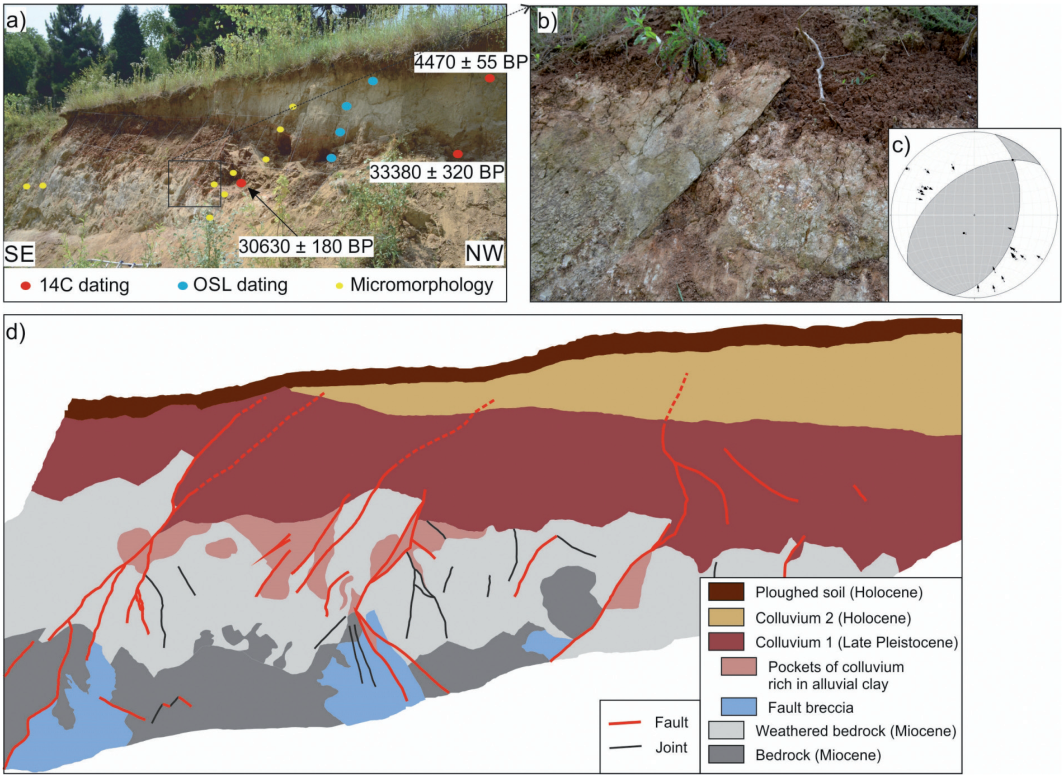


Fig. 2 – a) Perspective of the analyzed outcrop with the location of samples for different analysis; b) detail on a fault showing reverse slip and displacing the overlying colluvial unit; c) tangent-lineation diagram for fault data and kinematic analysis indicating a NW-SE directed principal stress; d) Log of the analyzed section.

**Results.** We made a detailed log of the exposed section (1:10 scale) including pedostratigraphic description of the colluvial units, structural data acquisition, sampling for radiocarbon, OSL dating and for soil thin-section micromorphology, presently still ongoing (Fig. 2).

We defined 5 Log units, including intact and weathered bedrock, a fault breccia and two stacked bodies of colluvial deposits, thickening upslope (Fig. 2), that point to a paleo-valley axis presently infilled by these deposits (Fig. 3).

Preliminary age constraints, coming from AMS dating, indicate two main colluvial phases ascribed at ca. 30 kyr BP and Holocene respectively (Fig. 2). The lowermost samples apparently indicate age reversal, thus pointing to reworking of pre-existing colluvial soils and deposits from the surrounding slopes. Moreover, several soil characteristics (e.g., illuviation, weathering, concretions etc.) indicate a strong and prolonged phase and/or phases of pedogenesis, thus supporting this possibility. This preliminary model needs to be validated by further analyses, including thin section soil micromorphology and comparison with OSL datings.

**Discussion.** The preliminary interpretation of the exposed section indicates the presence of a reverse fault zone, likely associated to Monferrato Arc thrusts system, controlling the morphology of the hills surrounding the exposed section (Fig. 3). Moreover, the data collected so far allow to state that this site show evidence of Late Pleistocene and possibly Holocene reverse surface faulting. This is the first site with documented evidence of coseismic displacement of very recent deposits in the whole Monferrato belt anyway.

The recent geomorphologic evolution of the basin, including an attested event of drainage piracy (Fig. 2), could be partly caused by tectonic-induced surface deformation together with climatically driven regional phases of gully erosion. A detailed pedostratigraphic study together

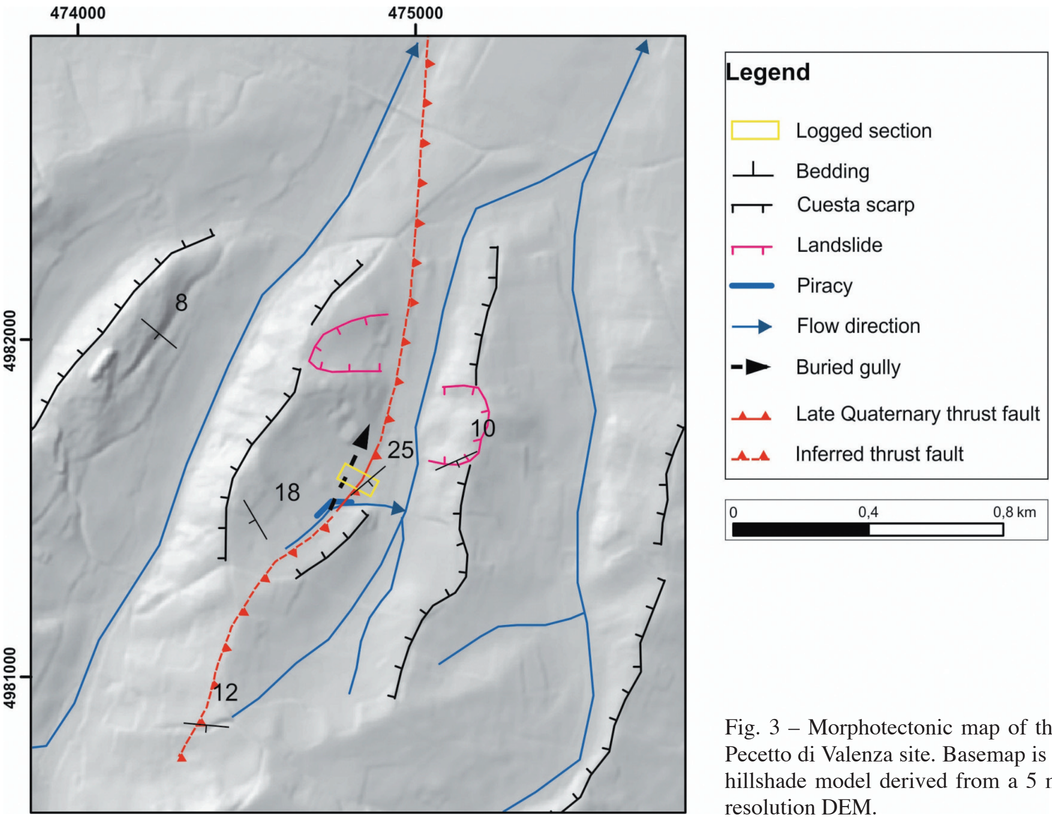


Fig. 3 – Morphotectonic map of the Pecetto di Valenza site. Basemap is a hillshade model derived from a 5 m resolution DEM.

with a collection of data over a wider region, could help in disentangle between different scenarios depicting the recent evolution of this sector of the Monferrato area. This site, in fact, has to be interpreted together with other key-sites located along the Monferrato Arc, showing evidence of recent tectonic activity. In particular, these preliminary results are consistent with the activity of the Valenza Deformation Zone a regional trasnpressional zone supposed to be active at least until the Late Pleistocene (Giraudi, 2015). Moreover, the following geological, geomorphic and geophysical evidence in the Po alluvial valley floor, possibly related to active tectonic shortening, is of particular value for the evaluation of the seismic potential of the area:

- the Trino Isolated Hill, representing the surficial expression of a Quaternary blind thrust (GSQP, 1976; Fig. 1a);
- the Quaternary, major, drainage changes that affected the fluvial network along the buried front of the Monferrato Arc (Forno, 1982; Carraro *et al.*, 1995; Irace *et al.*, 2009; Vezzoli *et al.*, 2010);
- the complex sequence of Mid-Pleistocene to Holocene fluvial units affected by progressive tectonic uplift (Dela Pierre *et al.*, 2003; Festa *et al.*, 2009; Giraudi, 2014, 2015);
- significant ongoing uplift rates based on long-term geodetic survey (e.g., Arca and Beretta, 1985);
- the evidence for Late Pleistocene to Holocene tectonic displacement described by Giraudi (2014, 2015) in the Casale Monferrato (Fig. 1a);
- newly exposed sections showing recent deposits affected by N-verging reverse faults described by Sassone *et al.* (2015; Fig. 1b) at the Cereseto and Ozzano Monferrato sites.

All these observations are lacking of absolute datings, an epistemic uncertainty that is still strongly limiting a reliable reconstruction of the recent landscape evolution of the area, including its tectonic and paleoseismic imprint. It is therefore reasonable to assume that the study of this and other sites, including different dating techniques, will therefore provide suitable constraints for the characterization of the style, rates and timing of active tectonics and earthquake faulting in the study area, and of the related seismic hazards.

**References**


Arca S. and Beretta G.P; 1985: *Prima sintesi geodetico-geologica sui movimenti verticali del suolo nell'Italia Settentrionale (1897–1957)*. Bollettino di Geodesia e Scienze Affini **XLIV (2),** 125–156.

Benedetti, L., Tapponnier, P., King, G. C., Meyer, B. and Manighetti, I.; 2000: *Growth folding and active thrusting in the Montello region, Veneto, northern Italy*. Journal of Geophysical Research: Solid Earth (1978–2012), **105(B1),** 739-766.

Benedetti, L. C., Tapponnier, P., Gaudemer, Y., Manighetti, I., and Van der Woerd, J.; 2003: *Geomorphic evidence for an emergent active thrust along the edge of the Po Plain: The Broni-Stradella fault*. Journal of Geophysical Research: Solid Earth (1978–2012), **108(B5)**.

Bonadeo L.; 2014: *Studio sismotettonico del settore della Pianura Padana occidentale compreso tra il Tortonese ed il fronte della Collina di Torino*. Università dell'Insubria. Ph.D. thesis pp. 178.

Burrato, P., Ciucci, F., and Valensise, G.; 2003: *An inventory of river anomalies in the Po Plain, Northern Italy: evidence for active blind thrust faulting*. Annals of Geophysics, **46(5),** 865-882.

Carraro F.; 1976: *Diversione pleistocenica nel deflusso del bacino piemontese meridionale: un'ipotesi di lavoro*. Gruppo Studio Quaternario Padano, **3**, 89-100.

Carraro F. Collo, G., Forno, M. G., Giardino, M., Maraga, F., Perotto, A., and Tropeano, D.; 1995; *L'evoluzione del reticolato idrografico del Piemonte centrale in relazione alla mobilità quaternaria*. In: (Polino, R., and Sacchi, R., editors). Atti del Convegno "Rapporti Alpi-Appennino" e guida alle escursioni (May 31-June 1st 1994, Peveragno, CN, Italy). Accademia Nazionale delle Scienze di Roma. 14, 445-461.

CNR, Consiglio Nazionale delle Ricerche; 1992: *Structural Model of Italy and Gravity Map*. Quaderni de "La Ricerca Scientifica", **114** (Progetto Finalizzato Geodinamica, vol. 3).

Dela Pierre F., Piana, F., Fioraso, G., Boano, P., Bicchi, E., Forno, M. G., and Ruffini, R.; 2003: *Carta Geologica d'Italia alla scala 1:50.000, Foglio 157 "Trino" e note illustrative*. APAT, Agenzia per la Protezione dell'Ambiente e per i Servizi Tecnici. Dipartimento Difesa del Suolo. Roma.

ENEL – DCO; 1984: *Progetto per la realizzazione di una centrale elettronucleare - Area Po2*

ENEL; 1985: *Interpretazione sismica a riflessione e rifrazione high-resolution , e ricostruzione strutturale, stratigrafica, tettonica e neotettonica. Rapporto finale, Gexon srl.*

Festa A., Dela Pierre, F., Irace, A., Piana, F., Fioraso, G., Lucchesi, S., and Forno, M. G.; 2009: *Carta Geologica d'Italia alla scala 1:50.000, Foglio 156 "Torino Est" e note illustrative*. ISPRA. Roma.

Forno M.G.; 1982: *Studio Geologico dell'altopiano di Poirino (Torino)*. Geografia Fisica e Dinamica Quaternaria, **5**, 129-162.

Galadini, F., Poli, M. E., and Zanferrari, A.; 2005: *Seismogenic sources potentially responsible for earthquakes with M≥ 6 in the eastern Southern Alps (Thiene-Udine sector, NE Italy)*. Geophysical Journal International, 161(3), 739-762.

Galli, P.; 2005: *I terremoti del gennaio 1117. Ipotesi di un epicentro nel Cremonese*. Il Quaternario, ***18***, 87-100.

Giraudi C.; 2014: *Quaternary studies as a tool to validate seismic hazard potential of tectonic structures: the case of the Monferrato thrust front (Vercelli Plain, NW Italy)*. Alpine and Mediterranean Quaternary, **27(1),** 5-28.

Giraudi C.; 2015: *Quaternary evolution of the plain between Casale Monferrato and Valenza: Implications for the tectonics of the Monferrato thrust front*. Alpine and Mediterranean Quaternary**, 28(1), 71 – 92.**

GSQP, Gruppo di Studio del Quaternario Padano; 1976: *Studio interdisciplinare del "Rilievo Isolato" di Trino (Bassa Pianura Vercellese, Piemonte)*. Quaderno n.**3**, Litografia Massaza and Sinchetto, Torino.

Irace A., Clemente, P., Piana, F., De Luca, D. A., Polino, R., Violanti, D., and Petricig, M.; 2009: *Geologia e Idrostratigrafia Profonda della Pianura Padana Occidentale*. Regione Piemonte. **111** p., 61 tables. La Nuova Lito. Firenze. 2009.

Livio F. A. Berlusconi, A., Zerboni, A., Trombino, L., Sileo, G., Michetti, A. M. and Spötl, C.; 2014: *Progressive offset and surface deformation along a seismogenic blind thrust in the Po Plain foredeep (Southern Alps, Northern Italy)*. Journal of Geophysical Research – Solid Earth, **199(10)** 7701-7721, 10-2014.

Magri, G., and Molin, D.; 1986: *I terremoti del 3 Gennaio 1117 e del 25 Dicembre 1222*. ENEA-RTI PAS-ISPGEOL-LO,(86), 2.

Maesano, F.E., D'ambrogi C., Burrato, P., & Toscani, G.; 2001: *Long-term geological slip rates of the Emilia thrust front (Northern Apennines) from 3D modelling of key buried horizons*. Geophysical Journal International, 154, 72-88.

Michetti A.M., Giardina, F., Livio, F., Mueller, K., Serva, L., Sileo, G., and Fioraso, G.; 2012: *Active compressional tectonics, Quaternary capable faults, and the seismic landscape of the Po Plain (N Italy)*. Annals of Geophysics. **55(5**), 2012.

Mosca P.; 2006: *Neogene basin evolution in the Northern Po Plain (NW Italy). Insights from seismic interpretation, subsidence analysis and low temperature (U-Th)/He thermocronology.* PhD Thesis. VU University Amsterdam. 190 pp.
Sassone P.; 2015: *Strutture recenti nord-vergenti a basso angolo in Val Cerrina (Monferrato Casalese): nuove segnalazioni*. Abstract Volume 26, pp. 41-42. AIQUA Congress 2015, Torino.
Serva L.; 1990: *Il ruolo delle scienze della terra nelle analisi di sicurezza di un sito per alcune tipologie di impianti industriali; il terremoto di riferimento per il sito di Viadana (MN).* Bollettino della Società Geologica Italiana, **109(2),** 375-411.
Stucchi M., Meletti C., Bazzurro P., Camassi R., Crowley H., Pagani M., Pinho R. and Calvi G.M.; 2012: *I terremoti del maggio 2012 e la pericolosità sismica dell'area: che cosa è stato sottostimato?,* Progettazione Sismica, **3**, 63-73.
Turrini C., Angeloni, P., Lacombe, O., Ponton, M., and Roure, F.; 2015: *Three-dimensional seismo-tectonics in the Po Valley basin, Northern Italy*. Tectonophysics, doi: 10.1016/j.tecto.2015.08.033
Vezzoli, G., Forno, M. G., Andò, S., Hron, K., Cadoppi, P., Rossello, E., & Tranchero, V.; 2010: *Tracing the drainage change in the Po basin from provenance of Quaternary sediments (Collina di Torino, Italy)*. Quaternary international, ***222*(1),** 64-71.
Zerboni, A., Trombino, L., Frigerio, C., Livio, F., Berlusconi, A., Michetti, A. M., and Spötl, C.; 2015: *The loess-paleosol sequence at Monte Netto: a record of climate change in the Upper Pleistocene of the central Po Plain, northern Italy.* Journal of Soils and Sediments, ***15*(6),** 1329-1350.

## INTENSITY-BASED SOURCE INVERSIONS OF THE M8 EARTHQUAKES OF BIHAR-NEPAL (1934) AND OF ASSAM (1897); FAST KF SCENARIO OF THE M7.8 GORKHA, 2015 EARTHQUAKE

**F. Pettenati, L. Sirovich, D. Sandron**
*Istituto Nazionale di Oceanografia e di Geofisica Sperimentale - OGS, Trieste, Italy*

**Introduction and seismotectonic context.** We apply the KF algorithm (Sirovich, 1996) in the inverse mode (Sirovich and Pettenati, 2004) and in the direct mode (Pettenati et al., 2011) to three earthquakes of the Himalaya-Assam region of the suture between the Indian subcontinent and Eurasia. Nonlinear intensity-based automatic source inversions are performed of the $M_S$ 8.1 Shillong, 1897 and of the $M_S$ 8.2 Bihar-Nepal, 1934 (Hough and Bilham, 2008) earthquakes and we calculate the fast KF parametric scenario of MMI intensities for the moment magnitude M7.8 Gorkha 25 April, at 06.11.26 UTC, 2015 earthquake.

The collision between the Indian subcontinent and Eurasia, with crust shortening and underthrusting of the Indian subcontinent beneath the Himalayas and in part beneath the Tibetan Plateau accounts for the tectonic structure of the central area of collision (the Himalayan chain) and of its lateral sectors. In particular, Molnar and Tapponnier (1975) and Tapponnier *et al.* (1986) comment on the major strike-slip faults, bounding Tibet and emanating from it, that seem to accommodate rapid eastward extrusion of Tibetan crust out of the way of India's and southern Tibet's northward advance. This large-scale phenomenon explains both the composition of the Himalaya (made by slivers of the ancient Indian subcontinent), and the present seismic activity of the chain and of Assam. It will be seen later, however, that underthrusting is still active in southern Assam.

Almost one hundred years ago, Argand (1924) understood that the altitude of the Tibetan Plateau should be due to a long underthrusting - perhaps complete - of the Indian subcontinent beneath Tibet, causing a double thickness of the crust and implying very shallow dipping fault zones below the plateau. Nowadays, it is thought that this underthrusting was not complete, but the interpretation by Argand (1924) remains a milestone. Then, in 1975, Molnar and Tapponier (1975) noted that no intermediate or deep earthquakes had been reliably located in the Himalayas. Lyon-Caen and Molnar (1984) suggested 50 to 80 km or more of underthrusting beneath northern Tibet, Brandon and Romanowicz (1986) measured only 50 to 60 km underthrusting. Indian crust surely was underthrusted beneath southernmost Tibet, and one of the troubling uncertainties still is - however - the magnitude of this underthrusting. Then, according to Molnar (1989), crustal thickening accounts for only part of Tibet's high altitude; its high uniform elevation would be supported by buoyancy and also by a hot upper mantle.

The Himalayan convergence is a unique case of continental subduction and both the Himalaya and the Assam earthquakes are driven by the convergence of approximately 20 mm/yr between India and the Himalaya. One part of the India's penetration is absorbed by local crustal thickening, while a significant fraction of the India-Eurasia convergence is absorbed by extrusion of material out of its way (e .g., Molnar and Tapponnier, 1975). This last mechanism is mostly relevant for the region of the $M_S$ 8.1, 1897 Shillong earthquake. The rest of the northward movement of the Indian subcontinent (approximately 20 mm/yr more) mainly causes the contraction of the Tibetan plateau (e.g.: Feldl and Bilham, 2006; Ader *et al.,* 2012).

The principal tectonic structure of underthrusting is the Main Himalayan Thrust (MHT), a sub-horizontal plane directly connected with the subduction of India beneath the Asian continent. The shallow-dipping MHT detachment is responsible of the Himalaya growth with a series of crustal ramps from the base of the detachment to the surface; from south, from the youngest to the oldest these ramps are: the Main Frontal Thrust (MFT, formed at the beginning of Pleistocene, still the most active), the Main Boundary Thrust (MBT) and the Main Central Thrust (MCT). odels of seismic coupling suggest that the MHT is fully locked up to the surface portion called the ain Frontal Thrust (MFT) (Ader *et al*., 2012; Sapkota *et al*., 2013).

Four strong earthquakes struck the Himalayan seismic belt approximately in one hundred years: the moment magnitude M8 Kangra, 1905 and the $M_S$ 8.2 Bihar-Nepal, 1934 (Hough and Bilham, 2008; Ambraseys and Douglas, 2004); the M8.5 Assam, 1950 (Raghukanth, 2008), and the M7.6 Kashmir, 2005. The Kangra, 1905 and Bihar-Nepal, 1934 are related to the main thrust of Himalaya growth MHT. In 1505, a huge earthquake of M8.8 struck the Himalayan belt between the meizoseismal areas of the Kangra, 1905 and Gorkha, 2015 events (Feldl and Bilham, 2006).

Fig. 1 shows a tectonic sketch of the area of study with: (A) the surface rupture of MFT found by Sapkota *et al*. (2013), with the hypothesis by Dixit *et al*. (2015, in press); (B) the best-fitting source of the 1934 earthquake obtained from the present inversions; (C) the central source used for the fast KF scenario of the M7.8 Gorkha, 2015 earthquake (see Fig. 3). The positions of the MFT, the MBT and the MCT Thrusts in Fig. 1 are taken from Stephenson *et*

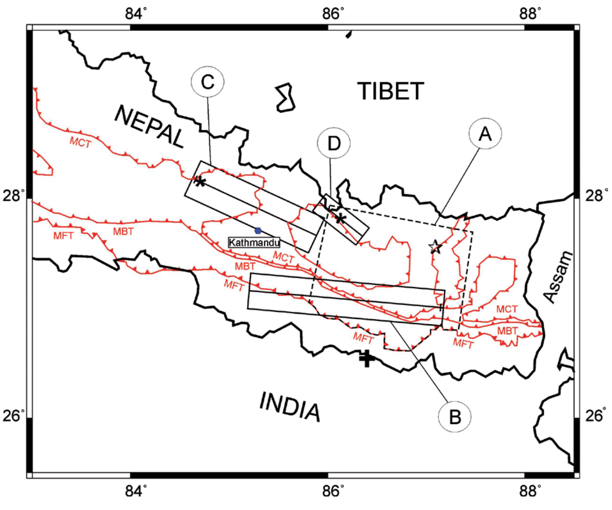


Fig. 1 – Tectonic sketch of the area of study. The star is the epicenter of the $M_S$ 8.2, 1934 Bihar-Nepal earthquake (Chen and Molnar, 1977); black cross: same, by Singh and Gupta (1980). The polygons/rectangles are the projections of: A) the source of the 1934 earthquake according to the surface rupture of MFT found by Sapkota *et al*. (2013) and to the hypothesis by Dixit *et al*. (2015, in press); B) the best-fitting source of the 1934 earthquake obtained from the present inversions; C) the central source used for the fast KF scenario of the M7.8 Gorkha, 2015 earthquake (asterisk: epicenter); D) as (C) for the strong aftershock (M7.3) of 12 May, 2015 (not shown in this paper).

*al.* (2001; Fig. 1) and Amatya and Jnawali (2006). The South Tibetan Detachment normal fault zone is not depicted in Fig. 1, for simplicity.

In the following, we conform the fault-plane solutions of various authors to the convention of the fault plane dipping to the right of the positive direction of the strike (ranging 0°-360°) with the rake angle seen from the hanging wall and measured counterclockwise from 0° to 360° between the positive direction of the strike and the direction of the slip vector. We mention this kind of data in the following order: strike-, dip-, and rake-angle.

We come now to the $M_S$ 8.2 Bihar-Nepal, 1934 earthquake. Dunn *et al.* (1939) erroneously imagined a strike-slip sense of motion along a west-northwest striking fault from the intensity observations. Chen and Molnar (1977) did not follow this interpretation. Rather, they: i) started from low-angle thrust faults found from fault-plane solutions of more recent earthquakes in the India-Nepal border region by Fitch (1970) and Molnar *et al.* (1973); ii) assumed a mechanism of this type, and iii) calculated the following source parameters: 27.55°N epicentral latitude, 87.09°E epicentral longitude, M = 8.3. This epicenter was adopted by all subsequent studies up to that of Sapkota *et. al.* (2013) [its position in Fig. 4 by Hough and Bilham (2008) is wrong].

Singh and Gupta (1980) claim they used nine first motions from long-period records to attempt the calculation of the fault-plane solution, but only eight are seen in their fig. 2. They reached the questionable result of 100°, 30°, 40°, that implies a thrust plane dipping 30° almost south with 100°-ward directivity. Then, Hough e Bilham (2008) assumed the epicenter by Chen and Molnar (1977) and took into account «the region of maximum shaking intensity and subsidence as proxy measures of the centroid of the 1934 earthquake» (Hough e Bilham, 2008; page 776) in a semi-quantitative reasoning to draw the projection of the inferred rupture for the 1934 Bihar-Nepal earthquake. They also proposed up-dip rupture, with propagation from east to west (opposite to the direction calculated by Singh and Gupta (1980)); on an expert judgment basis, they chose a 90° rake-angle and admit that «Our preferred rupture is not well constrained». Unfortunately, in Hough and Bilham (2008) there are some typos and for this reason we cannot include their source in Fig. 1. Recently, Dixit *et al.* (2015, in press) moved the rectangular projection of Hough e Bilham (2008) to match the surface rupture of MFT found by Sapkota *et al.* (2013) and obtained the polygon (A) shown in Fig. 1 for the 1934 earthquake.

In conclusion, the present automatic KF source inversion is the first attempt of constraining quantitatively the approximate area of main moment release and fault slip of the 1934 earthquake using only the MSK intensities reported by Ambraseys and Douglas (2004).

Finally, the meizoseismal area of the $M_S$ 8.1, 1897 Shillong earthquake is out of the Himalayan belt and south of the so called Assam syntaxis, mostly in the Assam territory, in small part in Bangladesh. This zone is in rapid upheaval and bordered, south-ward, by a north-dipping thrust (see fig. 1A in Sapkota *et al.*, 2013.)

**Source inversion of the $M_S$ 8.1 Shillong, 1897 earthquake.** Fig. 2A shows the MSK intensities of the $M_S$ 8.1 Shillong, 1897 earthquake reported by Ambraseys and Douglas (2004) within 120 km from the epicenter in 31 towns and villages (dots). Fig. 2B shows the synthetic intensities and the beach ball diagram that was produced by the minimum variance model (column 3 of Tab. 1) in the KF inversion (interpolation as in Fig. 2A). The verification of this result with measurements-based inversions is not possible. In the case of the 1934 earthquake, we just saw however that measurements-derived geometry and kinematics can give questionable results for earthquakes of the early instrumental era. The match of Fig. 2B is striking. The geometry and kinematics of column 3 of Tab. 1 is almost in perfect agreement with the seismotectonic situation shown by Sapkota *et al.* (2013) in their fig. 1A; we refer to the presence of an active thrust dipping north in the Assam territory close to the border with Bangladesh, with the epicenter of 1897 on the side of the hanging wall. This tectonic structure coincides with the northerly dipping E-W trending Dauki thrust (Sarma (2014); 250 km long, Evans (1964)) which borders south the Garo, Khasi and Jainta Hills in Assam, close to the Assam-Bangladesh border.

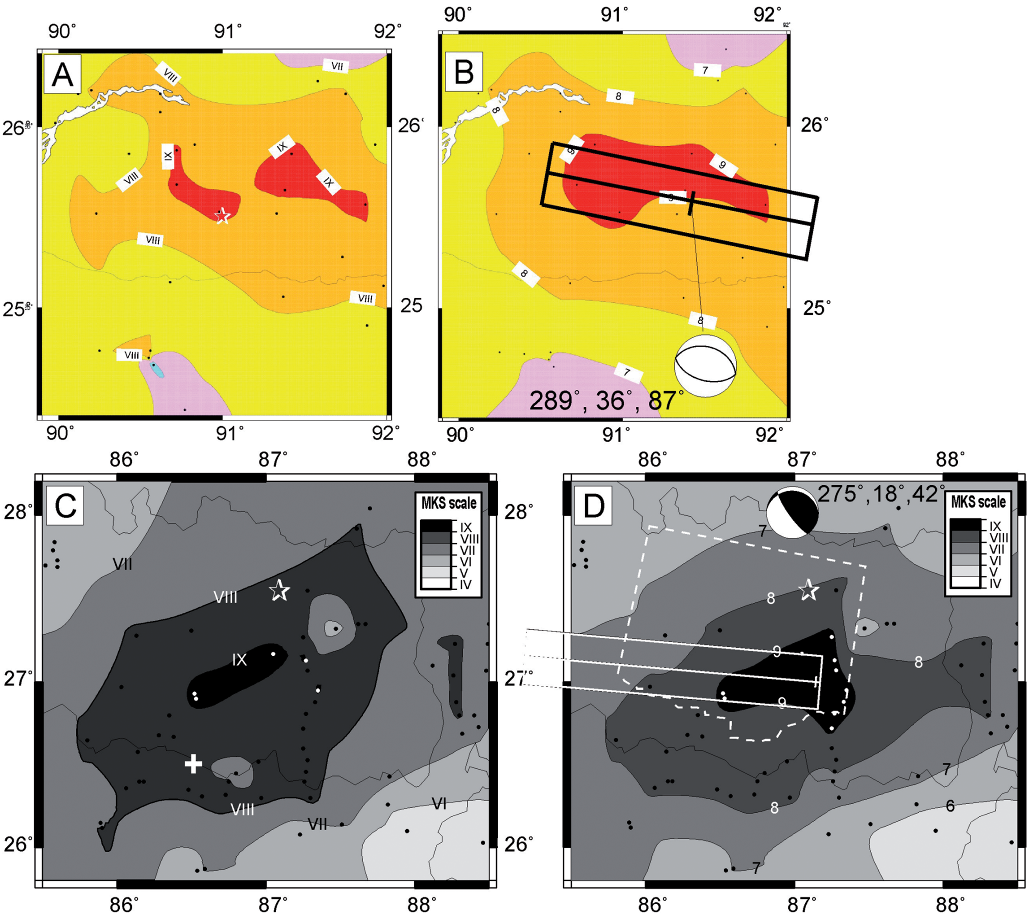


Fig. 2 – A) Field intensities (MSK scale, 31 data) of the $M_S$ 8.1, 1897 Shillong earthquake; the isoseismals were traced with the n-n bivariate interpolation scheme (Sirovich *et al.*, 2002). B) Synthetic intensities and the beach ball diagram that was produced by the minimum variance model of column 3 of Tab. 1; interpolated as in (A). C) Same as in Fig. 2A, 65 data, MS 8.2, 1934 Bihar-Nepal earthquake (star and cross as in Fig. 1). D) Synthetic intensities and the beach ball diagram as in Fig. 2B for the MS 8.2, 1934 Bihar-Nepal earthquake (see Tab. 2, column 3) (polygon and rectangle as in Fig. 1).

A different interpretation was proposed by Bilham and England (2001). They interpret the Shillong Plateau as a pop-up structure; for them, the causative fault is a SSW-dipping plane close to the auxiliary one in the beach ball in Fig. 2B (drawn in white to emphasize the limitation of the KF standard procedure).

**Source inversion of the $M_S$ 8.2 Bihar-Nepal, 1934 earthquake.** Fig. 2C shows the MSK intensities of the $M_S$ 8.2 Bihar-Nepal, 1934 earthquake reported by Ambraseys and Douglas (2004) in 65 towns and villages (dots) within 120 km epicentral distance. Fig. 2D shows the synthetic intensities and the beach ball diagram that was produced by the minimum variance model of column 3 of Tab. 1 (interpolation as in Fig. 2C). The match of Fig. 2D is good. In this case we can compare our results with two instrumental epicenters (we refer to those by Chen and Molnar (1977) and by Singh and Gupta (1980)) and with one fault-plane solution (Singh and Gupta, 1980). Then, there is a precious amount of palaeo-seismic data by Sapkota *et al.* (2013) who found the 1934 co-seismic rupture of a segment of MFT (refer to the wavy path of the southern side of polygon (A) in Fig. 1). By the way, the findings by Sapkota *et al.* (2013) definitely contradict the results offered by Singh and Gupta (1980). The projection of our source

Tab. 1 - Intensity-based KF inversion, $M_S$ 8.1 Shillong, 1897.

| Parameter | Ranges explored | Inversion results |
|---|---|---|
| Latitude [°] N | 25.20 – 25.80 | 25.61 ± 0.08 |
| Longitude [°] E | 90.00 – 92.00 | 91.42 ± 0.11 |
| Strike [°] | 0 - 359 | 289 ± 11 |
| Dip [°] | 0 - 90 | 36 ± 4 |
| Rake [°] | 0 - 179 | 87 ± 16 |
| Depth [km] | 20 - 45 | 40.9 ± 1.9 |
| Vs [km/s] | 3.50 – 3.95 | 3.50 ± 0.09 |
| Mach + | 0.50 – 0.95 | 0.50 ± 0.01 |
| Mach - | 0.50 – 0.95 | 0.59 ± 0.03 |
| Seismic Moment [N m] 1028 | 0.80 – 2.00 | 0.80 ± 0.09 |
| L + % | | 52 |
| ∑ r2 | | 8.5 |

Tab. 2 - Intensity-based KF inversion, $M_S$ 8.2 Bihar-Nepal, 1934.

| Parameter | Ranges explored | Inversion results |
|---|---|---|
| Latitude [°] N | 26.80 – 27.30 | 27.00 ± 0.16 |
| Longitude [°] E | 86.90 – 87.30 | 87.14 ± 0.14 |
| Strike [°] | 0 - 359 | 275 ± 16 |
| Dip [°] | 0 - 90 | 18 ± 11 |
| Rake [°] | 0 - 179 | 42 ± 14 |
| Depth [km] | 30 - 40 | 34.4 ± 8.2 |
| Vs [km/s] | 3.60 – 3.95 | 3.76 ± 0.16 |
| Mach + | 0.50 – 0.95 | 0.63 ± 0.10 |
| Mach - | 0.50 – 0.95 | 0.50 ± 0.06 |
| Seismic Moment [N m] 1028 | 0.80 – 2.00 | 1.32 ± 0.42 |
| L + % | | 99 |
| ∑ r2 | | 16 |

is compatible with the surface rupture found by Sapkota *et al*. (2013) once the inversion errors of Tab. 2 are considered (mostly latitude and strike errors) and the strongly listric shape of MFT is taken into account. The north-dipping plane of the best-fitting solution in Tab. 2 (dip angle = 18°±11°) is perfectly compatible with MFT. The rake angle of Tab. 2 (42°±14°) cannot be verified due to the lack of reference values. By the way, among the eight first motions shown in Fig. 2 by Singh and Gupta (1980) six are compatible with the mechanism of column three of Tab. 2; this confirms only that instrumental evidence is too scarce to constraint a reliable double-couple for verification purposes.

**4. Fast KF parametric scenario of intensities for the M7.8 Gorkha 25 April, 2015 earthquake.** We performed the exercise of forecasting the fast MMI intensity scenario of the Gorkha earthquake of 2015, that could have been calculated 24 hrs after the event using the KF

Tab. 3 - Parameters used for the fast KF scenario of MMI intensities for the M7.8 Gorkha, 2015 earthquake.

| Method/Agency | M | Depth [km] | Strike [°] | Dip [°] | Rake [°] | Lat. [°] N | Lon [°] E |
|---|---|---|---|---|---|---|---|
| Centroid MT (Mwc) | 7.76 | 10 | 295 | 11 | 108 | | |
| W-phase MT (Mww) | 7.81 | 23.5 | 290 | 7 | 101 | | |
| Centroid MT (Mwc) Harvard | 7.86 | 12 | 293 | 7 | 108 | 27.77 | 85.37 |
| GFZ | 7.8 | 18 | 304 | 5 | 112 | 28.18 | 84.72 |
| USGS | | | | | | 28.147 | 84.708 |

Tab. 4 - Ranges and calculation steps of the parameters adopted to forecast the fast KF scenario of the M7.8 Gorkha, 2015 earthquake.

| Parameter | Range | Step |
|---|---|---|
| Latitude [°] N | 28.00 – 28.20 | 0.04 |
| Longitude [°] E | 84.66 – 85.06 | 0.04 |
| Strike [°] | 285 - 305 | 5 |
| Dip [°] | 10 | |
| Rake [°] | 100 - 112 | 4 |
| Depth [km] | 12 - 21 | 3 |
| Vs [km/s] | 3.60 | |
| Mach + | 0.60 | |
| Mach - | 0.60 | |
| M | 7.70 – 7.90 | 0.1 |
| L+ | 159 | |
| L- | 1 | |

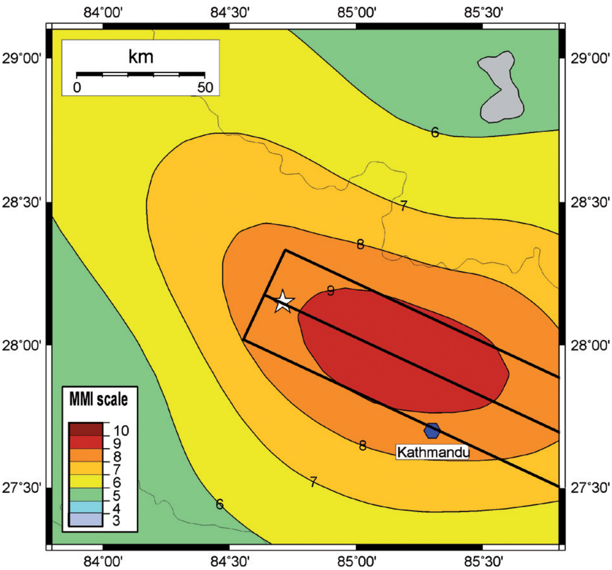


Fig. 3 – Fast KF parametric scenario (MMI intensities) for the M7.8 25 April, 2015 Gorkha earthquake, calculated on a regular grid with the source parameters available on April 26, 2015 (mean values from the 37,800 sources produced by Tabs. 3 and 4; see text).

algorithm in the direct mode and the information available on April 26, 2015 (see Tab. 3). We consider the suspected faults with their hypothesized mechanisms, and related uncertainties, and treat them parametrically. In the present post-event case, all hypocentral determinations and focal mechanisms, calculated by several international agencies shortly after the earthquake, were used. The discrepancies between the various data were treated as uncertainties. The combination between Tabs. 3 and 4 gave 37,800 sources.

**Conclusions.** The inversion of the Shillong, 1897 earthquake seems reliable because the synthetic match is striking and the source found is fully compatible with the seismotectonic situation of southern Assam presented in a fundamental paper (Sapkota *et al*., 2013).

The $M_S$ 8.2 Bihar-Nepal, 1934 earthquake offered the opportunity of one more verification of the automatic KF inversion technique. Its application to the intensities of this earthquake retrieved a source which is compatible with that obtained by authors who used instrumental data, field observations, palaeo-seismological logging of river-cut cliffs and trenches. Then, the KF inversion results are far better than those obtained by Singh and Gupta (1980) from instrumental data.

In general, our source inversions provide some constraints on our ideas of how the seismotectonics of Himalaya condition the present seismic hazard in the area within a tectonic process lasting 60-80 millions years.

The verification of the fast KF parametric scenario of the M7.8 April 25, 2015 Gorkha earthquake will be feasible when reliable site intensities will be available.

**Acknowledgements.** The inversion of the Shillong, 1897 earthquake was performed in cooperation with NORSAR. Susan Hough called our attention on Sapkota *et. al*. (2013) and provided a figure from Dixit *et al*. (2015, in press).

## References

Ader, T., J. P. Avouac, J. Liu-Zeng, H. Lyon-Caen, L. Bollinger, J. Galetzka, J. Genrich, Amatya, K. M., and B. M. Jnawali (2006), *Geological Map of Nepal (1994)*, Department of Mine and Geology, Lainchaur, Kathmandu, Nepal.

Ambraseys, N. N., and J. Douglas (2004), Magnitude calibration of north Indian earthquakes, *Geophys. J. Int.,* 159:165-206. doi: 10.1111/j.1365-246X.2004.02323.x

Argand, É (1924), La Tectonique de l'Asie, *Congrès Géologique International, Comptes rendus de la XIIIe session, en Belgique 1922*, Liège, 1924, 171-372.

Bilham R. and P. England (2001), Plateau 'pop-up' in the great 1897 Assam earthquake, Nature, 410, 806-809.

Chen, W.-P., and P. Molnar (1977), Seismic moments of major earthquakes and the average rate of slip in Central Asia, *Geophys. Res.,* 82, 2945–2969.

Dixit, A.M., A. Ringler, D. Sumy, E. Cochran, S.E. Hough, S.S. Martin, S. Gibbons, J. Luetgert, J. Galetzka, S.N. Shrestha, S. Rajaure, and D. McNamara (2015), Strong motion recordings of the M7.8 Gorkha, Nepal, earthquake sequence from low-cost, Quake Catcher Network accelerometers, *Seism. Res. Lett.,* in press.

Evans, P. (1964), The tectonic framework of Assam, *J. Geol. Soc. India,* 5, 88-96.

Feldl, N., and R. Bilham (2006), Great Himalayan earthquakes and the Tibetan plateau, *Nature*, 444 9, 165-170 doi:10.1038/nature05199.

Hough, S. E., and R. Bilham (2008), Site response of the Ganges basin inferred from re-evaluated macroseismic observations from the 1897 Shillong, 1905 Kangra, and 1934 Nepal earthquakes, J. Earth Syst. Sci., 117, S2, 773-782.

Lyon-Caen, H., and P. Molnar (1984), Gravity anomalies and the structure of western Tibet and the southern Tarim Basin, *Geophys. Res. Lett.,* 11, 1251-54.

Molnar, P, and P. Tapponier (1975), Cenozoic Tectonics of Asia: Effects of a Continental Collision, Science, New Series, 189, 4201, 419-426.

Pettenati, F., L. Sirovich, and D. Sandron (2011), Rapid simulation of seismic intensity for civil protection purposes; two recent cases in Italy, *Seism. Res. Lett., 82,* 3, 420-430. Doi: 10.1785/gssrl.82.3.420.

Raghukanth, S. T. G. (2008), Simulation of Strong Ground Motion During the 1950 Great Assam Earthquake, *Pure & Applied Geophysics*, 165, 9/10, 1761-1787. Doi: 10.1007/s00024-008-04-3-z.

Sapkota, S. N., L. Bollinger, Y. Klinger, P. Tapponnier, Y. Gaudemer, and D. Tiwari (2013), Primary surface ruptures of the great Himalayan earthquakes in 1934 and 1255, Nature Geosci., 6, 71-76 (http://dx.doi.org/10.1038/ngeo1669).

Sarma, K. P. (2014), Shillong Supergroup: a New Lithostratigraphic Unit in the Basement-Cover Precambrian Rocks of the Shillong Plateau, Northeast India, Int. J. Geol. Earth & Environ. Sci., 4 (2), 158-171 (http://www.cibtech.org/jgee.htm; last accessed 5 Oct., 2015).

Singh, D. D., and H. K. Gupta (1980), Source dynamics of two great earthquakes of the Indian subcontinent; the Bihar–Nepal earthquake of January 15, 1934 and the Quetta earthquake of May 30, 1935, *Bull. Seismol. Soc. Am. 70*(3), 757–773.
Sirovich, L., F. Pettenati, F. Cavallini, and M. Bobbio (2002), Natural-neighbor isoseismals, *Bull. Seismol. Soc. Am.*, 92, 1933–1940.
Sirovich, L., and F. Pettenati (2004), Source inversion of intensity patterns of earthquakes: A destructive shock in 1936 in northern Italy, *J. Geophys. Res., 109,* B10309, doi:10.1029/2003JB002919.
Stephenson, B. J., M. P. Searle1, D. J. Waters1, and D. C. Rex 158 (2001), Structure of the Main Central Thrust zone and extrusion of the High Himalayan deep crustal wedge, Kishtwar–Zanskar Himalaya, *Journal of the Geological Society, 158,* 637–652.

## SUBMARINE EARTHQUAKE GEOLOGY AS A TOOL FOR SEISMIC HAZARD ASSESSMENT IN THE CALABRIAN ARC

**A. Polonia[1], S. Romano[1], L. Gasperini[1], S.C. Vaiani[2], G. Gasparotto[2], E. Colizza[3], L. Torelli[4]**
[1] *Institute of Marine Sciences (ISMAR-CNR), Bologna, Italy*
[2] *Dipartimento di Scienze Biologiche, Geologiche e Ambientali, University of Bologna, Italy*
[3] *Dip. di Matematica e Geoscienze, Universita' degli Studi di Trieste, Italy*
[4] *Dipartimento di Fisica e Scienze della Terra "Macedonio Melloni", University of Parma, Italy*

**Introduction.** Paleoseismology is the investigation of individual earthquakes from their geological signatures such as those produced directly along the rupture plane, and those produced indirectly (landslides and, in general, mass wasting processes in the vicinity of faults). If datable material is recovered from stratigraphic horizons that experienced successive ruptures, slip rate and time separation between large earthquakes can be reconstructed. Earthquake geology has been widely applied to major continental faults in the Calabrian Arc over the past decades (Valensise and Pantosti, 1982; Galli *et al.*, 2003, 2008, 2015). While paleoseismology has become a primary tool for seismic hazard evaluation on land, only few paleoseismological studies have been attempted on submarine fault systems, mainly because of the limited resolution of the available geophysical techniques used at sea. Rapid developments in imaging and sampling techniques have now made such studies possible. Submarine paleoseismological studies have the following advantages compared to those undertaken on land: (i) marine sedimentation is generally more continuous in time and space, allowing for regional stratigraphic correlations; (ii) offshore data can be acquired more quickly. Innovative techniques have been developed which makes submarine paleoseismology feasible (Polonia *et al.*, 2012, 2013a, 2013b, 2015). They include (i) high-resolution morphobathymetric images of the seafloor, (ii) 3-D and pseudo-3D high resolution seismic reflection imaging, and (iii) detailed stratigraphic reconstruction of the sedimentary record. Although submarine geophysical data have lower resolution than classic paleoseismological trenching, they provide complete spatial coverage of fault structures, both horizontally and vertically. This will allow accurate long time-scale, high-resolution reconstruction of fault-zone evolution. During the last years, we applied such methodology to the submerged Calabrian Arc and surrounding areas of the central Mediterranean Sea during a number of oceanographic expeditions with R/V CNR Urania (2008, 2012, 2013, 2014, 2015).

**Interplay between seismic shaking, tsunamis and mass flows.** Submarine geohazards, such as major earthquakes, tsunamis, volcanic eruptions, volcanic flank collapse and submarine landslides, are isolated and exceptional events capable of producing large-volume turbidites that result from catastrophic submarine slope failures and the associated downslope mass transport of enormous quantities of sediment from continental shelves and slopes to the deep sea.

In this study, we analyse the interplay between tectonics and sedimentation along the Africa/Eurasian plate boundary in the Ionian Sea through an integrated approach involving

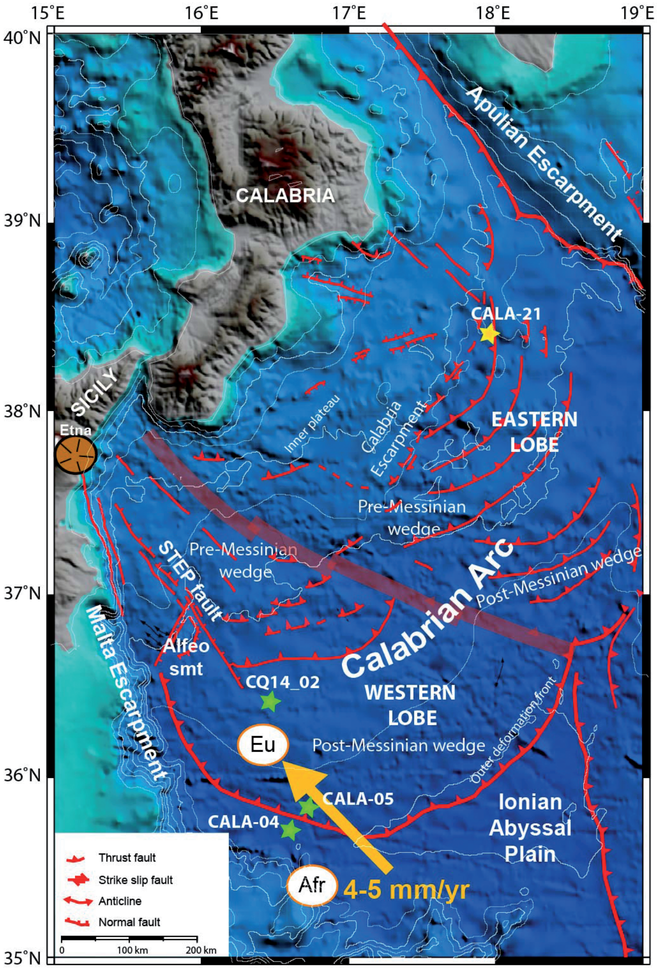


Fig. 1 – Geodynamic setting of the study area and structural map of the Calabrian Arc subduction system in the Ionian Sea as derived from the interpretation of available seismic data (Polonia *et al.*, 2011) integrated with multibeam bathymetry data. Yellow arrow indicates Europe (Eu) and Africa (Afr) slip vector in the Afr reference frame. Yellow and green stars indicate core location.

the interpretation of geophysical data at different scales (Polonia *et al.*, 2011, 2012) and well-targeted sediment samples. The Calabrian Arc region has been struck repeatedly by destructive historical earthquakes (Rovida *et al.*, 2011) often associated with tsunamis (Tinti *et al.*, 2004). In our approach, high penetration multichannel seismic data unravelled the overall geometry and tectonic evolution of the subduction complex while single fault strand dynamics have been reconstructed through the analysis of high-resolution geophysical data. On the other hand, the integrated analysis of sediment samples collected in the abyssal plain and slope basins, highlight the occurrence of anomalous sedimentary deposits (i.e. turbidites, debris flow and mass wasting deposits) and the likely relationships between active tectonics and sedimentation.

The multidisciplinary investigation of the effects of historical earthquakes on marine sedimentation through the analysis of the turbidite record (Polonia *et al.*, 2013a, 2013b, 2015) suggests that major historical earthquakes recorded in the area triggered slope instabilities and multiple turbidity currents. These findings suggest that seismically/tsunami triggered turbidites represent more than 90% of sedimentation in the deep basin. Marine sediments may thus be considered as seabed archives of paleo-earthquakes capable of reconstructing seismicity back in time, during several earthquake cycles (10,000-30,000 years).

**Calabrian Arc seismo-turbidites.** Gravity cores contain the eastern Mediterranean hemipelagic sequence interbedded with redeposited units characterized by coarse and/or graded layers. Three major turbidite sequences have been analysed in three different cores

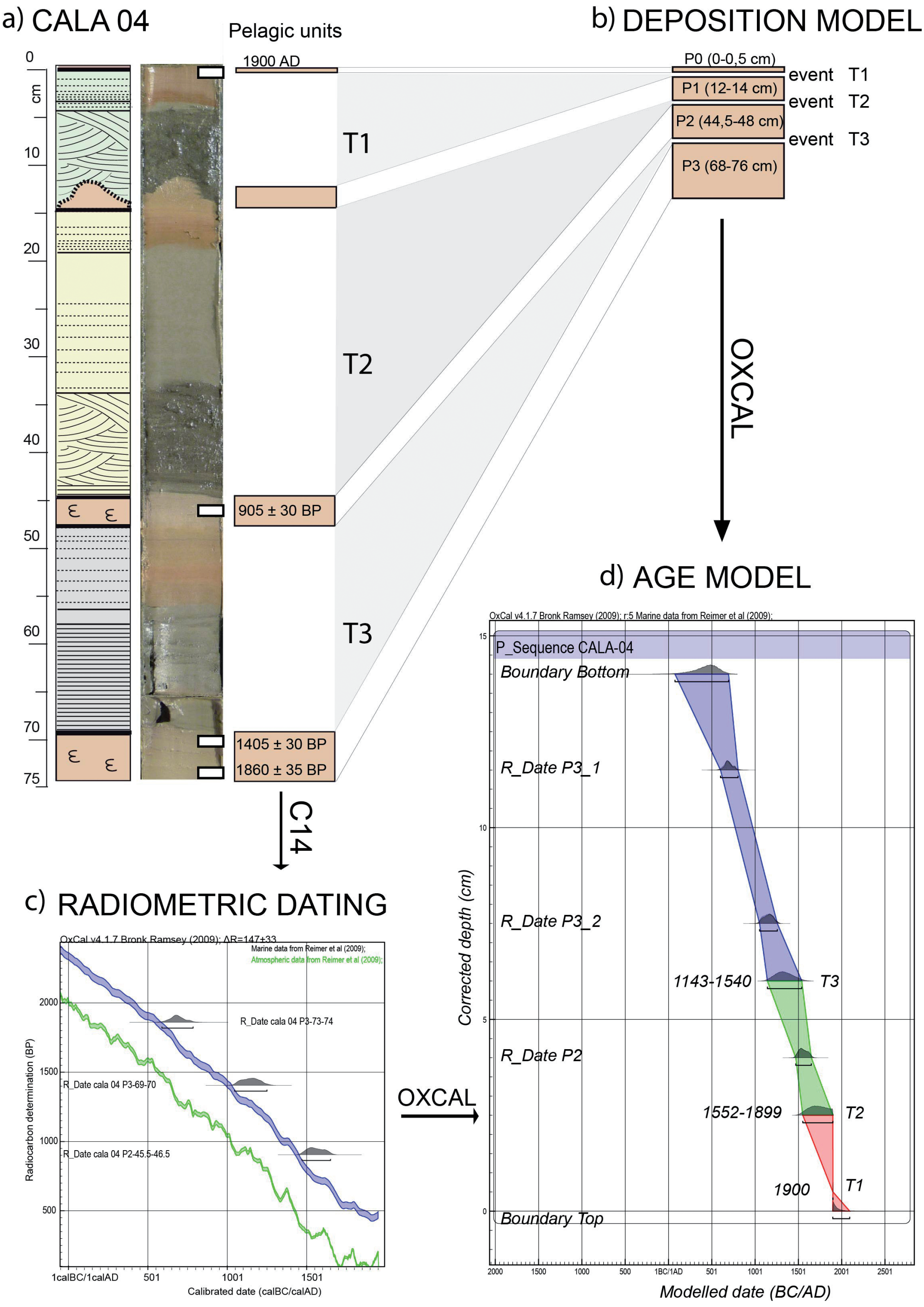


Fig. 2 – Core CALA 04 in the western Ionian Sea and age modelling results: a) stratigraphic log, photograph and pelagic units with samples for radiometric datings; b) deposition model built subtracting the thickness of the turbidites from the total core. Turbidite beds represent the “instantaneous sedimentary events” whose age is derived through interpolation within the OxCal modelling; c) calibrated radiometric dates (2 σ) of the pelagic units using a ΔR147±33. d) age model built using the P_Sequence (a Bayesian model of deposition) implemented in the computer program OxCal 4 [modified from Polonia *et al.* (2013a)].

in the Western Ionian Sea offshore the Messina Straits region (Fig. 1). Sedimentological and micropaleontological findings together with radiometric dating below and/or above key-layers outlined that turbidite emplacement may be related with the occurrence of major earthquakes in the area, such as the AD 1169, 1693 and 1908 events (Fig. 2). Sediment composition deduced by mineralogical analysis and SEM observations unravel the source region of the different turbidite beds and identify the links between sedimentary or tectonic preconditioning factors and the occurrence of the catastrophic event (Polonia *et al.*, 2013a).

The surveying techniques and approaches used in this study have therefore the potential of documenting earthquake ruptures of fault segments, extending the earthquake record far before the known history. Moreover, the regional analysis of sediment samples is useful to understand if the recurrence time of major catastrophic events is constant and which portions of the Calabrian Arc have experienced great earthquakes in the past thus improving hazard evaluations and the fundamental understanding of earthquake process in this highly populated region of the central Mediterranean.

The recurrence of mass-flow units within sapropel S1, an organic carbon-rich lower Holocene marker bed in the Eastern Mediterranean Sea, was used to reconstruct seismicity back in time (6000-10000 yrs BP) in the Calabria offshore (Fig. 1). Nine turbidite beds interrupt anoxic conditions during the deposition of sapropel S1 (Fig. 3). Turbidite structure and composition, as well as comparison with historical seismoturbidites, suggest a seismic triggering for such mass flows events. The pelagic units bracketing turbidite beds were radiometrically dated and age modelling provided the emplacement age of each turbidite. In this way, we compiled a catalogue of mass flow events during sapropel S1 deposition, a time span long enough to include several earthquake cycles and allow reliable seismic and tsunami hazard assessment in this area. Our results are in good agreement with paleoseismological studies onland (Galli *et*

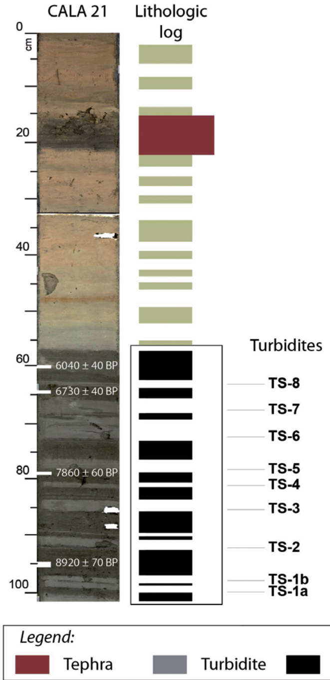


| | (1) Age of turbidites deduced through sapropel sediment thickness and sedimentation rate<br>Age (Cal BP) | (2) Age of turbidites deduced through OxCal age modeling<br>Modeled Age (Cal BP) | |
|---|---|---|---|
| **TOP S1 (kyr cal BP)** | **6000** *(This study:* sed. rate within S1=0.065mm/yr) | (2a) **6000** *(This study)* | (2b) **TS higher probability ages from age modeling** |
| **TS-8** | 6925 | 7195-6513 | 6950 |
| **TS-7** | 7225 | 7853-7053 | 7150 |
| **TS-6** | 7375 | 8220-7263 | 7850 |
| **TS-5** | 7835 | 8368-7798 | 8180 |
| **TS-4** | 8135 | 9085-8117 | 8350 |
| **TS-3** | 8515 | 9447-8367 | 9030 |
| **TS-2** | 9205 | 9601-8936 | 9400 |
| **TS-1b** | 9875 | 10200-9462 | 9620 |
| **TS-1a** | 9970 | 10200-9963 | 10150 |
| **BOTTOM S1 (kyr cal BP)** | **10200** | **10200** | |

Fig. 3 – Age model for core CALA 21 in the eastern Ionian Sea offshore Calabria. Left side: photograph and stratigraphic log from the base of sapropel S1 to the core top. Right side: age of turbidite beds within sapropel S1 calculated using: thickness of sapropel sub-units and average sedimentation rate (column 1); OxCal age modelling (column 2) [modified from Polonia *et al.* (2015)].

*al*., 2003, 2015). Average recurrence of seismoturbidites, deduced considering chronology and number of turbidites, is about 500 yrs which is in good agreement with the average frequency of major earthquakes in Calabria during historical time. However, age modelling performed on the entire Holocene sequence suggests that recurrence time is not constant, but rather it varies between 100 and 700 yrs with periods of higher frequency of seismic events.

**The AD 1908 Messina earthquake and tsunamis.** The AD 1908 seismo-turbidite consists of three different stacked turbidites, suggesting that seismic shaking triggered at least three slope failures. The first failure, that sources the basal stack, occurred in a deeper environment because of more marine geochemical proxies and the absence of inner shelf foraminifera. This deeper slope failure was followed by two additional failures, with sources apparently located closer to the coast, as indicated by more entrained material from shallow water. The Straits area is where the first cable break occurred and where the Ionian fault was described (Polonia *et al*., 2012, 2014).

The 1908 earthquake seafloor rupture displacement, which is reported to be on the order of 1 m (Loperfido, 1909; Valensise and Pantosti, 1982), can drive a runup of the same amplitude or a bit more (Okal and Synolakis, 2004). It follows that part of the 11 m 1908 tsunami runup must have been triggered by landslides. This is in agreement with the observation of the stacked seismo-turbidite, three submarine cables breaks downslope along the margin (Ryan and Heezen, 1965) and models that include a composite source (e.g. earthquake and landslide) (Tinti *et al*., 2008; Tappin *et al*., 2008; Favalli *et al*., 2009). The location of slope failures, however, is highly debated (see Billi *et al*., 2009 and references therein). The AD 1908-stacked seismo-turbidite that we observed in our cores suggest that more than one slope failure occurred after the earthquake. These sediment failures can be considered the likely source, together with seismic shaking, for the generation of the AD 1908 tsunami.

**The AD 365 Crete earthquake.** Destructive earthquakes/tsunamis have affected repeatedly the circum Mediterranean highly populated coastal regions. A record of these past events can be provided by large-volume turbidites or megaturbidites, detected in the marine sedimentary record. Megaturbidites have been identified in the Ionian basin (central Mediterranean) that is located between two tectonically active subduction zones (i.e. the Calabrin Arc to the north and the Hellenic Arc to the east). The uppermost megabed, has been named "Homogenite" (Kastens and Cita, 1981) or "Augias turbidite" (Hieke, 1984). Its well defined stratigraphic position, above the regional marker sapropel bed S1, has been interpreted as evidence that it was deposited in a single, basin-wide event capable to put into suspension simultaneously sediment at a basin-wide scale. Absence of absolute dating of the megabed and of a detailed chronostratigraphy of the deposits above and below the turbidite, have allowed a number of different correlations of this megaturbidite with the 3500 yr BP Minoan eruption of Santorini and related tsunamis in the Aegean Sea (Kastens and Cita, 1981), with the 7.600 ± 130 yr B.P. collapse of a flank of the Etna Volcano (Pareschi *et al*., 2006) or with a major earthquake in the Mediterranean Sea (Vigliotti, 2008).

Based on studies of sediment cores we collected from the Ionian seafloor (mineralogy, micropaleontology, elemental and isotopic geochemistry and radiocarbon dating), we show that the Homogenite/Augias turbidite (HAT), up to 20-25 m thick, was related to multi-source turbidity flows triggered by the AD 365 earthquake and tsunami (Polonia *et al*., 2013b). We were able to reconstruct the different units deposited in response to the 365 AD Cretan earthquake/tsunami and the results confirm that the HAT is a unique instance of deep sea tsunami deposit. Backwash flows and related gravity-driven processes are the primary means of downslope sediment transport. An older similar deep sea megaturbidite was deposited in the Ionian Sea about 15.000 years B.P., implying a large recurrence time of such extreme sedimentary events in the Mediterranean Sea.

**Conclusions.** The Ionian Sea is a landlocked basin where convergence between Africa and Eurasia produced the emplacement of two opposite verging subduction/rollback systems (i.e. the Calabrian and the Hellenic Arcs). It is one of the most seismically active regions in the Mediterranean Sea and has been struck repeatedly by destructive historical earthquakes, often associated with tsunamis. Slab tearing in a pre-collisional setting is reflected in dynamic topography with high uplift rates of the coastal mountain belts, accompanied with a great sediment discharge to the continental margins. This increases the susceptibility to mass failures implying a strong interplay between active tectonics, seismic shaking, mass flows and tsunami generation.

We investigated the effects of historic earthquakes on abyssal marine sedimentation through the analysis of the turbidite record in tectonically controlled basins. Holocene resedimented units in the deep Ionian Sea represent more than 90% of the total thickness of the sedimentary record. We dated the most recent turbidite sequences using different radiometric methods and the results suggest that turbidite emplacement was triggered by major historic earthquakes and tsunamis recorded in the region (i.e. AD 365 Crete and AD 1169, 1693 and 1908 Italian earthquakes).

Textural, micropaleontological, geochemical and mineralogical signatures reveal that turbidite beds are stacked sandy units, which have different compositions suggesting coeval multiple failures. They are characterized by organic-rich sandy layers, containing a mixture of lithic clasts, plant fragments and displaced benthic foraminifera derived from several sources and bathymetric ranges. Structure and composition of each turbidite unit, combined with geochemical and isotopic analysis on organic carbon, are being refined to unravel the relative contribution of seismic shaking and tsunami wave loading on mass flow processes generation.

Average recurrence of seismoturbidites within sapropel S1, deduced considering chronology and number of turbidites, is about 500 yrs, and appears to be constant also before and after its deposition. This is in good agreement with the average frequency of major earthquakes in Calabria during historical time. However, age modelling performed on the entire sequence suggests that recurrence time is not constant, but rather it varies between 100 and 700 yrs.

These findings enable us to extend back in time the paleoseismic catalogue of major seismic events in the Calabrian Arc during a time span of about 10.000 yrs. Turbidites may be considered as the sedimentary earthquake code within the background pelagic sedimentation. Deciphering this code aims at reconstructing paleo-seismicity during several earthquake cycles, a time span long enough to perform reliable seismic and tsunami hazard assessment in tectonically active coastal regions.

## References

Billi A., R. Funiciello, Minelli L., Faccenna C., Neri G., Orecchio B., and Presti D., 2009. *Reply to comment by Andrea Argnani et al. on "On the cause of the 1908 Messina tsunami, southern Italy"*. Geophysical Research Letters, 36, L13308. doi:10.1029/2009GL037499.

Hieke W., 1984, *Thick Holocene homogenite from the Ionian abyssal plain (Eastern Mediterranean)*: Marine Geology, v. 55, p. 63–78.

Kastens K.A., and Cita M.B., 1981, *Tsunami-induced sediment transport in the abyssal Mediterranean Sea*: Geological Society of America Bulletin, v. 92, p. 845–857.

Favalli M., Boschi E., Mazzarini F., Pareschi M.T., 2009. *Seismic and landslide source of the 1908 Straits of Messina tsunami (Sicily, Italy)*. Geophysical Research Letters 36 :. L16304. doi:10.1029/2009GL039135.

Galli P., Bosi V.; 2003. *Catastrophic 1638 earthquakes in Calabria (southern Italy): new insights from paleoseismological investigation*. Journal of Geophysical Research 108, B1. http://dx.doi.org/10.1029/2001JB001713.

Galli P., Galadini F., Pantosti D.; 2008. *Twenty years of paleoseismology in Italy*, Earth Sciences Reviews, 88, 89-117, doi:10.1016/j.earscirev.2008.01.001.

Galli P., Peronace E.; 2015. *Low slip rates and multimillennial return times for Mw 7 earthquake faults in Southern Calabria (Italy)*. Geophysical Research Letters, 42, doi: 10.1002/2015GL064062.

Loperfido, A.: 1909. *Livellazione geometrica di precisione eseguita dall'IGMI sulla costa orientale della Sicilia, da Messina a Catania, a Gesso ed a Faro Peloro e sulla costa occidentale della Calabria da Gioia Tauro a Melito di Porto Salvo*. C.R. Accademia Naz. Lincei, 35, 131-155.

Okal, E.A., Synolakis C.E., 2004. *Source discriminants for near-field tsunamis*. Geophysical Journal International 158, 899–912.

Polonia A., Torelli L., Mussoni P., Gasperini L., Artoni A., Klaeschen D.; 2011. *The Calabrian Arc subduction complex in the Ionian Sea: Regional architecture, active deformation, and seismic hazard*, Tectonics, 30, TC5018, doi:10.1029/2010TC002821.

Polonia A., Torelli L., Gasperini L., Mussoni P.; 2012. *Active faults and historical earthquakes in the Messina Straits area (Ionian Sea),* Nat. Hazards Earth Syst. Sci., 12, 2311-2328, doi:10.5194/nhess-12-2311-2012.

Polonia A., Panieri G., Gasperini L., Gasparotto G., Bellucci L.G. Torelli L.; 2013a. *Turbidite paleoseismology in the Calabrian Arc Subduction Complex (Ionian Sea)*: Geochemistry, Geophysics, Geosystems, v. 14, no. 1, doi 10.1029/2012GC004402.

Polonia A., Bonatti E., Carmelenghi A., Lucchi R.G., Panieri G., and Gasperini L.; 2013b. *Mediterranean megaturbidite triggered by the AD 365 Crete earthquake and tsunami: Scientific Reports*, 3, Article number 1285, doi:10.1038/srep01285.

Polonia A., Torelli L., Gasperini L., Romano S., Vaiani S.C., Artoni A.; 2014. *Active Tectonics and Seismic/Tsunami Hazard in the Messinian Straits Region: the Ionian and Alfeo/Etna Fault System*. Atti del 33° Convegno Nazionale GNGTS, Bologna 25-27 Novembre 2014. Tema 1: Geodinamica 163-168.

Polonia A., Romano S., Çağatay M.N., Capotondi L., Gasparotto G., Gasperini L., Panieri G., Torelli L.; 2015. *Is repetitive slumping during sapropel S1 related to paleo-earthquakes?*: Marine Geology, v. 361, p. 41–52.

Ryan W.B.F., and Heezen B.C., 1965. Ionian Sea submarine canyons and the 1908 Messina turbidity current. Geological Society of America Bulletin 76, 915-932.

Rovida A., Camassi R., Gasperini P., Stucchi M., (Eds.); 2011. *CPTI11, la versione 2011 del Catalogo Parametrico dei Terremoti Italiani*. Istituto Nazionale di Geofisica e Vulcanologia, Milano, Bologna, http://emidius.mi.ingv.it/CPTI, doi:10.6092/INGV.IT-CPTI11.

Tappin, D. R., 2008. *The 1908 Messina tsunami. Some comments on the source: Earthquake, subamrine landslide or a combination of both?*, Eos Trans. AGU, 89 (53), Fall Meet. Suppl., Abstract S41D-07.

Tinti S., Maramai A., Graziani L.; 2004. *The new catalogue of the Italian tsunamis. Natural Hazards 33, 439–465.*

Tinti, S. *et al*., 2008. *Quale sorgente per il maremoto del 28 Dicembre 1908 nello Stretto di Messina? Terremoto, frana sottomarina o entrambe?,* in 27° Convegno Nazionale,191– 192, Gruppo Naz. di Geofis. Della Terra Solida, Trieste, Italy.

Valensise G. and Pantosti D.*;* 1982. *A 125-Kyr-long geological record of seismic source repeatability: the Messina Straits (southern Italy) and the 1908 earthquake (MS 71)*, Terra Nova, 4, 472- 483.

Vigliotti L., 2008, *Comment on "Lost tsunami" by Maria Teresa Pareschi et al.*: Geophysical Research Letters, v. 35, p. L02608.

# sessione 1.2

## Processi tettonici attivi: osservazioni e modelli interpretativi

Convenor: A. Del Ben e A. Argnani

# LOCAL EARTHQUAKE TOMOGRAPHY IN THE JUNCTION BETWEEN SOUTH-EASTERN ALPS AND EXTERNAL DINARIDES USING THE SEISMIC DATA OF THE CE3RN NETWORK

**L. Colavitti[1], L. Tiberi[1], G. Böhm[2], G. Costa[1], A. Gallo[1]**

[1] *University of Trieste, Department of Mathematics and Geosciences, Seismological Research and Monitoring Group, Trieste, Italy*

[2] *National Institute of Oceanography and Experimental Geophysics, Section of Geophysics, Trieste, Italy*

**Introduction.** The main force responsible of tectonic activity in south-eastern Alps is given by the collision between Adriatic microplate and Eurasian plate. This motion has a fundamental role in geodynamic evolution due to the convergence rate between Adria and Eurasian plate estimated greater than 2 mm/yr (Platt *et al*., 1989).

The largest historical earthquakes occurred in the region between Italy and Slovenia are reported in Burrato *et al*. (2008) and Galadini *et al*. (2005). Several large earthquakes hit the studied region in historical times, most of them were distributed in the Friuli Venezia Giulia region, as two events recorded in Tramonti in 1776 and 1794, but the most important earthquake that spread its effects in wide region was the 1511 Idrija event that represents the most destructive event that occurred so far in the region of the junction between south-eastern Alps and the External Dinarides, as reported in the catologues (Ribarič, 1982).

In general, the area of Friuli Venezia Giulia region is characterized by a moderate seismicity, in fact the most important instrumental seismic event recorded in the area was the destructive 1976 Friuli earthquake with $M_s$=6.5 (Aoudia *et al*., 2000), that was widely studied thanks to the large amount of collected seismometric data. In Veneto region, seismicity normally decreases and the only destructive earthquake instrumentally recorded was the Cansiglio event with Mw=5.9 (Sirovich and Pettenati, 2004).

Evidences that the collision is still active nowadays and the main seismogenic structures are located in the proximity of the political boundaries between Italy and Slovenia is also shown by the main shock of Bovec in April 1998 with $M_s$=5.7 (Bajc *et al*., 2001) and, later, in July 2004, with the event of Kobarid ($M_s$=4.9), which generated a sequence that lasted until the end of November 2004 (Bressan *et al*., 2009).

It is evident that, in an area with complex seismogenic structures, the use of 1-D velocity model might not be sufficient, so defining a 3-D velocity model represents a better solution to understand the inner structure of the Earth. For this reason, we used the travel-time tomography technique to obtain an accurate 3-D velocity model: in this work, we used a Cat 3-D software to perform the travel time tomography and a non-linear location tool to define the position of the events.

**Data set.** For the input parameters of our tomographic analysis it is fundamental to have a complete data set of available and accurate events in the area where potentially destructive events are located in the closeness of the political boundary between Italy and Slovenia. For this reason, seismic data were recorded by the Transfrontier network (Costa *et al*., 2010), which is called Central Eastern European Earthquake and Research Network (CE3RN). This network was born thanks to a prolific cooperation of the governmental institutions of Italy, Austria, Slovenia and recently, Croatia, which decide to share in real time their seismological data for scientific purposes and for Civil Defense. The main importance of the CE3RN is to ensure a very good recording of the seismic events that occur very close to the political borders and that otherwise would be recorded in non-homogeneous way only by national networks; in this sense, the example of recent strong earthquakes demonstrated that this integration of services is essential for a rapid and efficient intervention (Bragato *et al*., 2010).

In Fig. 1a, the black rectangle shows the area of our investigation (longitude east between 12.5° and 14.5°; latitude north between 46° and 46.5°) while, red triangles represent the seismic stations which belong to the CE3RN network. For this study, we used 52 seismic stations and analyzed 180 earthquakes, including the events with magnitude more than 3 between 2004 and

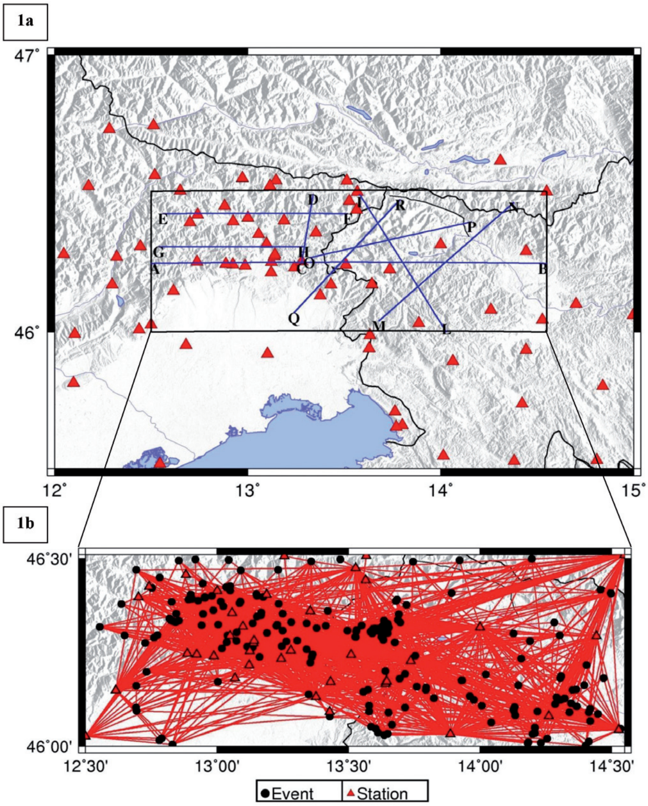


Fig. 1 – a: In the black rectangle the zone of our investigation is represented. The red triangles indicate the stations of the CE3RN, the blue lines the sections extrapolated from our model. b: Zoom of the study area: rays's coverage used for the tomographic inversion: with the red triangles are represented the stations included in our study area, while with the black dots are shown the event located using Non-Linear Location technique.

2013 and the full seismicity of the year 2011. In overall, we identified 1960 phases (1350 P and 610 S) manually picked to avoid false detection that can be generate by the automatic STA/LTA trigger algorithm. All the data were recorded by Antelope®, a software which represents an integrated set of programs that are able to acquire, store and process seismic devices.

**Method.** We applied the Local Earthquake Tomography (LET) technique that represents an important tool for the Earth's investigation. In this study, we used earthquake location method and travel time tomography combined in an iterative procedure.

For event location, we adopted the Non-Linear Location NLLOC (Lomax *et al.*, 2009) that is a technique used to locate the events using the 3-D velocity model resulting from the tomographic inversion. This technique is formed by a set of programs for the creation of the grid location, the computation of travel times and the probabilistic, non-linear location of structures for 3-D data volume.

As travel time tomography we adopted the software Cat3D, Computer Aided Tomography for 3-D models, developed by OGS (CAT 3D, User Manual, 2014) which computes the tomographic inversion of seismic waves travel times on 3-D models. In previous works, this software was mainly used for investigations in the field of exploration geophysics (Böhm *et al.*, 2006, 2009), while in other recent investigation (Tiberi, 2014), it is applied on seismological data. The main difference between active seismic and seismological applications is represented by the positions of sources, which in the first case are well defined, while for seismological purposes, they represents the unknowns parameters with high uncertainty.

As inversion algorithm for the velocity estimation, in this work we adopted the SIRT (Simultaneous Inversion Reconstruction Technique) technique; this method is part of series expansion methods, on which the investigated area can be divided on elements with constant velocity, called pixel in 2-D or voxel in 3-D. The ray which links the source (earthquake location) with the receiver (station position) is composed by several segments, whose associated travel time $t^i$ is defined by:

$$t^i = d_1^i s_1 + d_2^i s_2 + d_3^i s_3 + \cdots + d_m^i s_m = \sum_{j=1}^{m} d_j^i \ s_j$$

where $d_j$ represents the single straight line of the ray $i$ which belong to the single pixel $j$, $s_j$ is the slowness of the same pixel and $m$ is the total number of pixels in the model. To minimize time residuals, SIRT method uses an iterative procedure which leads to convergence.

In formulas,

$$\Delta s_j = \frac{1}{N} \sum\nolimits_{i=1}^{N} \left( \frac{\Delta t^i d_j^i}{\sum_{j=1}^{N} (d_j^i)^{\,2}} \right)$$

where $\Delta s_j$ is the upgraded velocity of pixel $j$, $\Delta t^i$ is the time residual associated to ray $i$, $N$ is the number of rays (travel times) and $M$ is the number of pixels in the model. The computation of ray paths in the model follows the principle of minimum time, using an iterative algorithm based on Snell's law (Böhm *et al*., 1999a).

**Initial model, data processing and reliability of the tomographic system.** As we can see in Fig. 1b, the rays distribution is not homogeneous in the considered area. The greater ray density reflects the higher seismicity of the area, distributed in the center of the model, with the most intense activity concentrated along the Friuli region and in correspondence of the geologic junction between southern Alps and External Dinarides.

We adopted the 1-D velocity structure computed by Costa *et al*. (1992) as initial velocity model. Futhermore, the Friuli plain constitutes an important part of our zone and obviously does not represent a seismic area, therefore we constrained, for the first layers, some voxels of the model with the velocity values coherent with real data considering the geological information by Slejko *et al*. (1987).

The volume of our investigation, whose dimensions are 180 x 60 x 51 km, is discretized by 18 voxels along X direction, 6 voxels along Y direction and 60 layers in depth, obtaining a spatial resolution of 10 x 10 km in two horizontal directions and 0.85 km in the vertical component, which it coincides with the half of thinnest layer of the base model. The choice of this grid, which we called "base grid", represents a compromise between two opposite requirements: the resolution and the reliability of the model.

In this work, inside the tomographic process, we used the staggered grids method (Böhm *et al*., 1999b), which provides a high resolution velocity model by summing and averaging different inversions obtained from low resolution but well-constrained in a base grid that has been perturbed in the space. In our case, we applied two shifts in both horizontal directions ($x$, $y$) and one shift in vertical direction $z$.

In tomographic inversion, the homogeneity of earthquake's distribution is fundamental to obtain a reliable 3-D velocity model. The reliability of tomographic system (model discretization and ray geometry) can be computed in different ways. The ray density represents only a simple method to evaluate the reliability of the model, while the map of null space is a more complex and expensive in computation time.

Nevertheless, null space evaluation is the most correct methodology to measure the reliability of a tomographic system; it utilizes the single value decomposition technique (SVD) (Stein and Wysession, 2003) in which the instability of the system is defined by the presence of singular values equal or close to zero. After defining a threshold value, it is possible to map the null space values in the whole model, by summing the squares of the elements of each column of the diagonal matrix of the singular values.

To verify the consistency of the inversion quality, we adopted the checkboard test, which represents one of the most popular test used to verify the inversion's quality. This technique consists of creating a model on which velocities are distributed between low (in our case,

-10%) and high values (in our case, +10%) on a checkboard pattern superimposed to the final tomographic model. Using the same acquisition geometry in terms of sources (earthquakes) and receivers used for the inversion, it is possible to create a new set of travel times used for a new inversion whose result will point out the resolvability of the system. In our analysis, looking the results of the differences between the checkboard pattern and the computed inverted model, we observe velocity values of the misfit very close to zero in a rather wide zone at the middle of the model.

At each tomographic iteration, we calculated the root mean square of time residuals (the difference between computed and picked travel times). In our case, we stopped the procedure after 4 iterations because the solution in terms of variation of seismic events locations seems immediately stable and reliable (absolute values around 0.15 s in term of root mean square of time residuals, corresponding to an error of 2.5% with respect to the picked times on the whole model).

In the final tomographic model, only 5 of a total of 180 earthquakes showed a variation in X-Y direction greater than 10 km; moreover, the most part of these events are located at the borders of the working area; while, as we can expect, in the central part, the variation of seismic events location during tomographic iterations is almost nil. Furthermore, the path of variation of these events is more scattered in X-Z respect to X-Y direction, according to theoretical assumptions for which the uncertainty in the vertical component is always bigger than the errors in the horizontal ones.

**Results and discussion.** Fig. 2 displays the final velocity model, which represents the inversion result associated to the minimum root mean square in terms of time residuals; it shows how the P-velocity changes at four different depth: 4, 8, 12 and 16 km. First, we can observe that the greater the depth of investigation, the smaller will be the imaging of the inner Earth solved because the studied zone is not homogeneously covered by the rays. In fact, we can find very few events that occur below 20 km, in according to the seismicity distribution of our area.

In particular, in Figs. 2a and 2b, we can observe an anomalous body in the western sector with P velocity values around 7 km/s beneath central Friuli, at a depth between 4 and 8 km, in agreement with a tomographic investigation already performed (Amato *et al.*, 1990) and that probably suggests the presence of a structure at a depth of 6 km, which could represent a wedge of metamorphic rocks (Chiarabba and Amato, 1994).

Other important aspects are represented by the presence of some anomalous bodies in eastern part of the model, corresponding to External Dinarides in western Slovenia, where we find P velocity in a range between 6.5 and 7 km/s at a depth from 4 to 12 km (Figs. 2a, 2b, 2c) which seems to follow the characteristic trend oriented in NW-SE direction of dinaric thrusts. Finally, in Fig. 2d we can observe that the crustal roots of External Dinarides are deeper than those of the southern Alps, in according to the interpretation of recent active geophysical investigations (Brückl *et al.*, 2007).

In the investigation area, we extracted some sections from 3-D final velocity model (Fig. 1a); here we report only two sections: the E-F section in in south-eastern Alps domain and the M-N section, which results to be perpendicular respect to the trend of dinaric faults.

Final tomographic results were compared to geological sections performed for the Friuli Venezia Giulia area to verify the existence of a direct connection between the interpretation of geological sections and the trend of velocity values in Earth's interior. Different geological formations that we can find are summarized in the stratigraphic column (Tab.1) available from a work of Ponton (2010).

In particular, the section E-F (Dogna-Forni di Sopra) represents a longitudinal section between Carnia's sector and Julian Alps, which includes a portion of important crustal thickness of bedrock. Other important structural element in the central part of the section is the But-Chiarsò line, which appears as an inverse fault with a high angle.

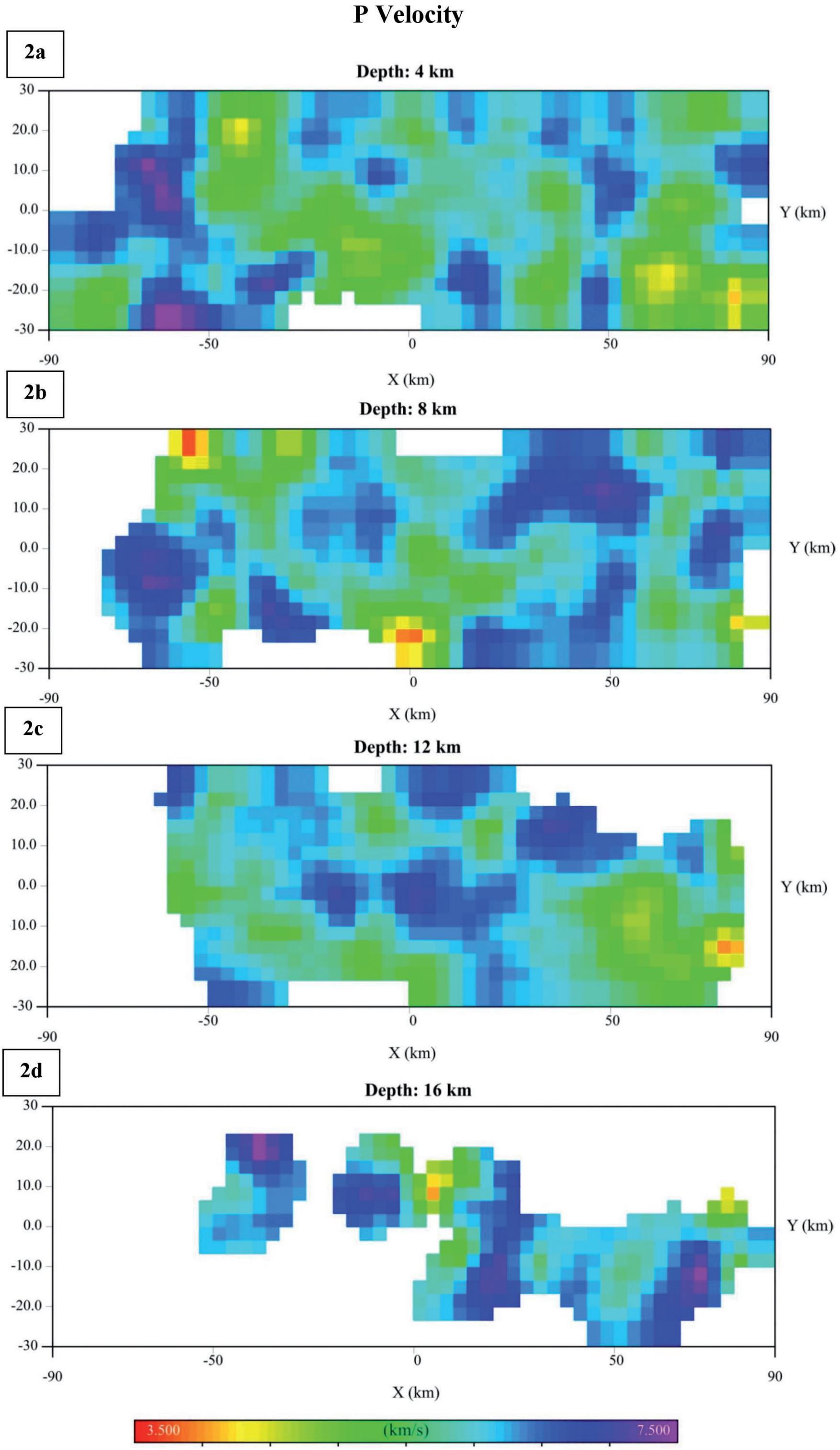


Fig. 2 – a, b, c, d) Representation of P velocity values at 4, 8, 12 and 16 km superimposed by P velocity ray density.

Tab. 1 - Geologic formations existing in the investigation area (Ponton 2010, modified). For the colors corresponding to name abbreviations, see the stratigraphic column reported at the bottom of Fig. 3a.

| Name | Geologic period | Geologic formations |
|---|---|---|
| TR 3 | Upper Triassic (Norico-Retico) | Fm. Monticello; Dol. Principale; Organic laminates; Dolomia di Forni; Fm. Dachstein |
| TR 2 | Upper Triassic (Carnico) | Fm. Santa Croce and Travenanzes |
| TR 1 | Lower-Upper Triassic | Fm. Val Degano; Dol. Sciliar and Dol. Cassiana; Anisian-Carnic terrigenous; Anisian platform; Fm. Werfen |
| PZ 2 | Upper Permian | Fm. a Bellerophon |
| PZ 1 | Upper Permian | Arenaria della Val Gardena; Pemic-Carboniferous succession; Fm. Dimon; Fm. Hochwipfel; Ordovician-Devonian limestones; phyllites and schists |

In our model (Fig. 3a), a positive value of P velocity around 7 km/s at a depth of about 12 km could be correlated to the geological bedrock. Moreover, it is also possible to distinguish some P velocity regions (with a range of P values between 6 and 6.5 km/s) which could be related to a portion of basement that is interposed in the Triassic dolomitic formations.

The interpretation of geological section Dogna-Forni di Sopra (Ponton, 2010 modified) seems to be coherent with our model because the bedrock is posed at 12 km of depth and is interrupted by the ramps of dinaric's thrusts as we can deduct from geophysical and geodynamical investigations in the Italian (Cati *et al.*, 1989) and Slovenian (Placer, 1999) area. Furthermore, the interpretation of the discontinuity of the two high P velocity anomalies of our model at a depth between 5 and 10 km, could reflect a high component of strike-slip fault of But-Chiarsò line detected by Ponton (2010). This fault system divides the section in two domains: the eastern part, that is moved in north direction along Fella-Sava line and the western part, which is moved in south direction, following Tagliamento line.

In Fig. 3b, we report the model of the section M-N which goes from the village of Bate, near Nova Gorica, at the boundary between Italy and Slovenia, to the village of Zell in southern Austria. For the sector in western Slovenia, we do not have a lot of investigations to take a comparison, except for a work of Michelini *et al.* (1998), whose investigation touches in a very small part our area. The section M-N is perpendicular respect to the main active faults in Slovenia and crosses the dextral strike-slip system of Idrija fault. In general, in our model, we can observe P velocities basically higher compared to the values found for the Friuli Venezia Giulia area; in particular some high P velocity zones with values around 7 km/s which could be in the closeness of the main dislocations of the strike-slip fault. In the eastern part of this section, the lack of data below 10 km of depth is due to the poor ray's coverage in that zone.

**Conclusions.** The goal of this work was to provide a 3-D velocity model of the upper crust for the area between south-eastern Alps and External Dinarides with the technique of Local Earthquake Tomography based on first arrivals. The investigated zone has always been interested by moderate seismicity both in historical and instrumental time. In particular, the seismic sequence in the western Slovenia characterized by recent events, has shown that the geodynamical process which controls the crustal thickening is nowadays active.

The Transfrontier network allowed the production of a 3-D velocity model without political boundaries even if the obtained results are highly influenced by inhomogeneity of rays's distribution. Comparing the 3-D velocity model obtained with geological sections available in the Friuli Venezia Giulia area, in west-east direction, the velocity model shows a positive anomaly which could indicate the Paleozoic bedrock and the intrusions within the most recent geological formations. In general, the results have confirmed the existence of an anomalous body with P velocity values around 7 km/s beneath central Friuli at a depth between 4 and 8 km

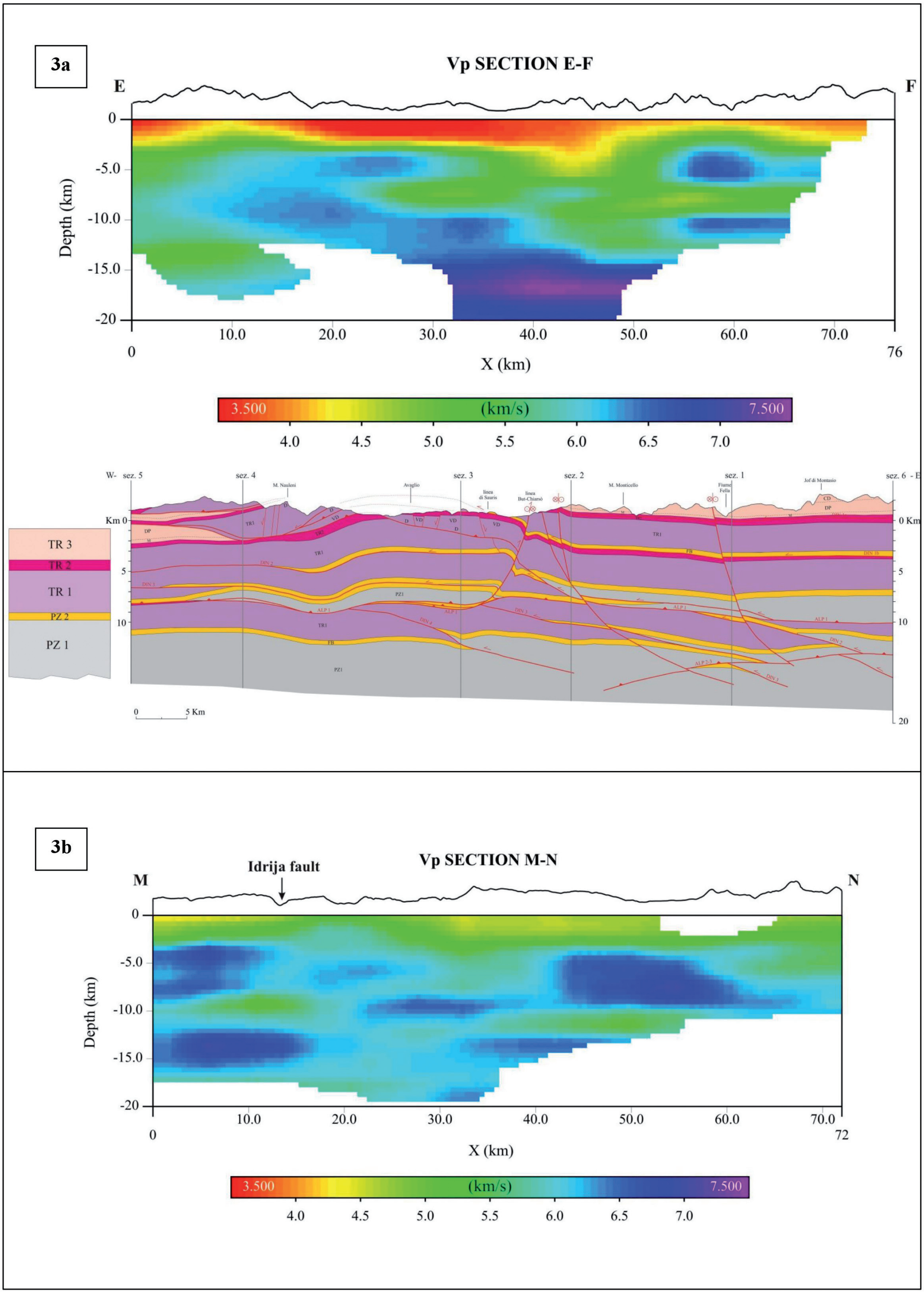


Fig. 3 – a: On the top, P velocity model for the section E-F superimposed by P ray density. In the bottom, it is shown the corresponding interpretation of geological section Dogna-Forni di Sopra with the simplified stratigraphic column (Ponton, 2010 modified). b: P velocity model for the section Bate (Slovenia)-Zell (Austria) superimposed by P-ray density. With the black arrow, is indicated the Idrija fault.

founded by an investigation performed by Amato *et al*. (1990) and probably connected to the region of 1976 Friuli earthquake. It has also been shown a section in Slovenia which crosses perpendicularly the main systems of fault, in particular the Idrija fault, to try to detect the highest discontinuities of External Dinarides.

**Acknowledgements.** We are very grateful to Dr. Maurizio Ponton to make available the geological sections used for this work.

## References

Amato A., De Franco R. and Malagnini L.; 1990: *Local souce tomography: application to italian areas*. Terra Nova, **2**, 596-608.

Aoudia A., Saraò A., Bukchin B. and Suhadolc P.; 2000: *The 1976 Friuli (NE Italy) thrust faulting earthquake: a reappraisal 23 years later*. Geophys. Res. Lett., **27**, 573-576.

Bajc J., Aoudia A., Saraò A. and Suhadolc P. 2001: *The 1998 Bovec-Krn mountain (Slovenia) earthquake sequence*. Geophys. Res. Lett. **28**, 1839-1842.

Böhm G., Rossi G. and Vesnaver A.; 1999a: *Minimum-time ray tracing for 3-D irregular grids*. Journal of seismic exploration, **8**, 117-131.

Böhm G., Galuppo P. and Vesnaver A.; 1999b: *Staggered adapted and stacked grids in seismic tomography*. In: EAGE 61st Conference and Technical Exhibition, Helsinki, Finland.

Böhm G., Accaino F., Rossi G. and Tinivella U.; 2006: *Tomographic joint inversion of first arrivals in a real case from Saudi Arabia*. Geophys. Prosp., **54**, 721-730.

Böhm G., Accaino F., Rossi G. and Tinivella U.; 2006: *Tomographic joint inversion of first arrivals in a real case from Saudi Arabia*. Geophys. Prosp., **54**, 721-730.

Böhm G., Okagoğlu N., Picotti S. and De Santis L.; 2009: *Western Ice Sheet evolution: new insights from a seismic tomographic 3D depth model in the Eastern Ross Sea (Antarctica)*. Marine Geology, **266**, 109-128.

Bragato P. L., Costa G., Horn N., Pahor J., Pesaresi D. and Lenhardt W. A.; 2010: *The usage of Antelope for acquiring and exchanging data in the southeastern Alps: present configuration and future perspectives*. In: 32nd European Seismological Commission General Assembly, Montpellier, France.

Bressan G., Gentile G. F., Perniola B. and Urban S.; 2009: *The 1998 and 2004 Bovec-Krn (Slovenia) seismic sequences: aftershock pattern, focal mechanisms and static stress changes*. Geophys. J. Int., **179**, 231-253, DOI: 10.1111/j.1365-246X.2009.04247.x.

Brückl E., Bleibinhaus F., Gosar A., Grad M., Guterch A., Hrubcová P., Keller G. R., Majdański M., Šumanovac F., Tiira T., Yliniemi J., Hegedűs E. and Thybo H.; 2007: *Crustal structure due to collisional and escape tectonics in the Eastern Alps region based on profiles Alp01 and Alp02 from the ALP 2002 seismic experiment*. J. Geophys. Res., **112**, B06308, DOI:10.1029/2006JB004687.

Burrato P., Poli, M. E., Vannoli P., Zanferrari A., Basili R. and Galadini F.; 2008: *Sources of Mw 5+ earthquakes in northeastern Italy and western Slovenia: an updated view based on geological and seismological evidence*. Tectonophys., **453**, 157-176.

CAT 3D Software (version 6.0); 2008: *Computer Aided Tomography for 3-D models*. User Manual, OGS Institute, Trieste, Italy.

Cati A., Fichera R. and Cappelli V.; 1989: *Northeastern Italy. Integrated processing of geophysical and geological data*. Mem. Soc. Geol. It., **40**, 295-308.

Chiarabba C. and Amato A.; 1994: *From tomographic images to fault heterogeneities*. Ann. Geofis, **37**, n°6, 14.

Costa G., Panza G. F., Suhadolc P. and Vaccari, F.; 1992: *Zoning of the Italian region with synthetic seismograms computed with known structural and source information*. In: Proc. 10th World Conference on Earthquake Engineering, Madrid, Spain, pp. 435-438.

Costa G., Moratto L. and Suhadolc P.; 2010: *The Friuli Venezia Giulia Accelerometric Network: RAF*. Bull. Earthq. Eng., **8**, 1141-1157.

Galadini F., Poli M. E. and Zanferrari A.; 2005: *Seismogenic souces potentially responsible for earthquakes with M 6 in the eastern Southern Alps (Thiene-Udine sector, NE Italy)*. Geophys. J. Int. **161**, 739-762.

Lomax A., Michelini A. and Curtis A.; 2009: *Earthquake Location, Direct, Global-Search Methods*. Encyclopedia of Complexity and Systems Science, **5**, 2449-2473.

Michelini A., Zivcic M. and Suhadolc, P.; 1998: *Simultaneous inversion for velocity structure and hypocenters in Slovenia*. Journal of Seismology, **2**, pp. 257-265.

Placer L.; 1999: *Contribution to the macrotectonic subdivision of the border region between southern Alps and External Dinarides*. Geologija, **41**, 223-255.

Platt J. P., Behrmann J. H., Cunningham P. C., Dewey J. F., Helman M. and Parish M.; 1989: *Kinematics of the Alpine arc and the motion history of Adria*. Nature **337**, 158-161, DOI: 10.1038/337158a0.

Ponton M.; 2010: *Architettura delle Alpi Friulane*. In: Museo Friulano di Storia Naturale, Pubbl. n. 52, Udine, Italy, pp. 9-69.

Ribarič V.; 1982: *Seimicity of Slovenia-catalogue of earthquakes (792 A. D. -1981)*. In: SZ SZRS, Publication Series A, 1-1, Ljubljana, 650 pp.
Sirovich, L. and Pettenati, F.; 2004: *Source inversion of intensity patterns of earthquakes: a destructive schock in 1936 northeastern Italy*. Journal of geophys. Res.: solid earth, **109**, DOI: 10.1029/2003JB002919
Slejko D., Carulli G. B., Carraro F., Castaldini D., Cavallin A., Doglioni C., Iliceto V., Nicolich R., Rebez A., Semenza E., Zanferrari A. and Zanolla C.; 1987: *Modello sismotettonico dell'Italia Nord-Orientale*. In: G. N. D. T., rendiconto n°1.
Stein S. and Wysession M.; 2003: *An Introduction to Seismology, earthquakes and earth structure*. Blackwell Publishing, 498.
Tiberi L.; 2014: *Crustal tomography of the Po Plain and calibration of location procedures*. Ph. D. Thesis in Geosciences, XXVI cycle, Università degli Studi di Trieste, 140 pp.

## MAPPATURA DELL'ANTICLINALE DI MIRANDOLA, ITALIA, MEDIANTE MISURE HVSR

**G. Tarabusi[1,2], R. Caputo[1]**
[1] *Dip. Fisica e Scienze della Terra, Università di Ferrara, Italia*
[2] *Istituto Nazionale di Geofisica e Vulcanologia, Roma, Italia*

I terremoti del maggio 2012 ($M_L$ = 5,9 e 5,8 oppure Mw = 6,1 e 5,9; *e.g.* Pondrelli *et al.*, 2012) hanno avuto origine da due segmenti dell'Arco Ferrarese che rappresenta il settore più avanzato dell'Appennino Settentrionale sepolto. Entrambe le faglie sono inverse e cieche e, nel volume sovrastante, generano un tipico processo plicativo per propagazione di faglia. La loro riattivazione, infatti, ha prodotto un'ampia deformazione della superficie terrestre con sollevamenti massimi nella zona epicentrale di ca. 20-25 cm (Bignami *et al.*, 2012; Salvi *et al.*, 2012; Caputo *et al.*, 2015). In un contesto geologico di subsidenza regionale e di forti apporti fluviali da parte del Po e dei suoi affluenti appenninici, le strutture deformative cosismiche vengono progressivamente sepolte e la topografia tendenzialmente 'pareggiata' dai continui processi fluviali. Il ripetersi di simili 'terremoti morfogenici areali' (Caputo, 2005) può essere ovviamente riconosciuto attraverso l'interpretazione di profili sismici a riflessione (generalmente effettuati per ricerche di idrocarburi; *e.g.* Pieri e Groppi, 1981; Boccaletti *et al.*, 2004) mettendo in evidenza le variazioni stratigrafiche cumulatesi nel tempo. Dal punto di vista morfologico, invece, il riconoscimento di tali strutture attive è molto più difficile, ma un'attenta analisi delle anomalie idrografiche può suggerire la loro individuazione (Burrato *et al.*, 2003; 2012). La sorgente sismogenica di Mirandola, già inserita nel DISS (2015) prima dei terremoti emiliani, si basava appunto su questo tipo di osservazioni, mancando tra l'altro nell'area specifica importanti terremoti storici probabilmente a causa dei lunghi tempi di ritorno.

Le esplorazioni sismiche e le indagini morfologiche hanno però entrambe dei forti limiti. Le prime, infatti, sono molto costose, non sempre disponibili e, soprattutto, sono spesso prive di informazioni sugli strati più superficiali perchè calibrate per target più profondi. Le seconde, invece hanno generalmente un largo margine di incertezza per le entità estremamente ridotte delle anomalie topografiche, in quanto rappresentative soltanto degli ultimi terremoti morfogenici. In alternativa ai due suddetti approcci, ma anche in modo complementare ad essi, con il presente lavoro ci siamo concentrati sul sottosuolo superficiale (ca. 100-200 m) che rappresenta un target di indagine cruciale per riconoscere l'attività recente di faglie sepolte. Per fare ciò è stata utilizzata una tecnica di indagine a basso costo, come le misure di rumore sismico a stazione singola, applicandola al settore di pianura padana in corrispondenza dell'anticlinale di Mirandola. Per le finalità del lavoro, quindi, sono state effettuate numerose misure tra il 2011 e il 2015, caratterizzate da una distanza variabile tra 100 m e 1 km (Fig. 1).

**Metodologia.** Le misure di sismica passiva sono state effettuate utilizzando un tromografo digital (Tromino(R)) che registra il rumore di fondo allo scopo di ricavare le frequenze di

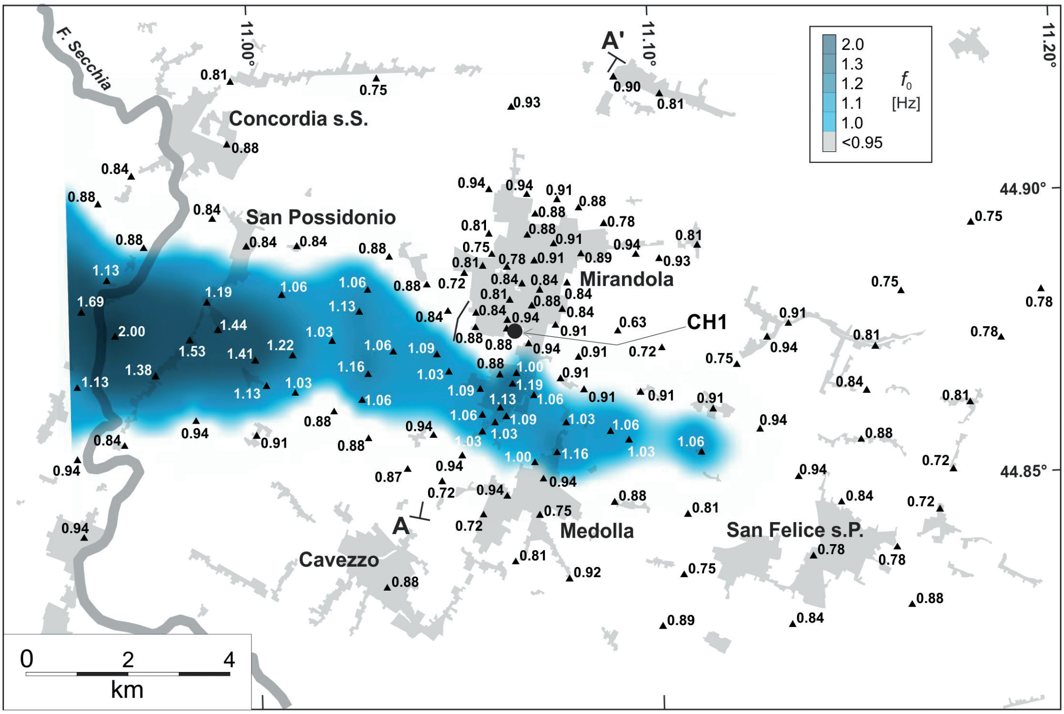


Fig. 1 – Distribuzione della frequenza naturale, $f_0$, ottenuto all'interno dell'area investigata. Il colore più intenso corrisponde ad un maggiore valore, e quindi ad una minore profondità della superficie caratterizzata dal contrasto di impedenza. I triangoli indicano i siti misurati mentre col cerchio nero è localizzato il sondaggio con *cross-hole* realizzato a Mirandola.

risonanza dei terreni, avendo cura che fossero rispettate le condizioni proposte nelle linee guida SESAME per ottenere misurazioni e risultati attendibili (Koller *et al.*, 2004; Bard *et al.*, 2005). La frequenza di risonanza fondamentale è in stretta realzione con l'amplificazione sismica locale che è oggi comunemente considerata come la principale causa di danno in occasione di un terremoto (*e.g.* Mucciarelli *et al.*, 2001; Gallipoli *et al.*, 2004).

Tale rumore di fondo, detto anche microtremore, è presente ovunque sulla superficie terrestre e può essere originato sia da fenomeni atmosferici che da attività antropiche. Esso è generalmente caratterizzato da oscillazioni molto piccole, con componenti spettrali che vengono scarsamente attenuate nello spazio e misurabili con tecniche di acquisizione dette passive.

Tutte le onde elastiche durante il percorso dalla sorgente al sito subiscono una certa attenuazione, che è essenzialmente di tipo geometrico, a causa dell'aumento di dimensione del fronte d'onda, e anelastico, a causa del comportamento in realtà non perfettamente elastico di tutte le rocce. In entrambi i casi l'attenuazione è funzione della frequenza; infatti, assumendo una velocità costante per tutte le frequenze, più è piccola la lunghezza d'onda (e quindi maggiore la frequenza), maggiore è il numero di cicli e quindi l'attenuazione che si verifica.

Tali informazioni sono incluse nelle registrazioni di microtremore assieme al rumore casuale e possono essere estratte utilizzando diversi metodi, tra cui quello proposto da Nakamura (1989; horizontal to vertical spectral ratio, HVSR). Questa tecnica viene oggi ampiamente utilizzata per determinare l'amplificazione sismica locale e per stimare le principali frequenze di risonanza che caratterizzano il sottosuolo più superficiale (fino a poche centinaia di metri di profondità). Entrambi i fattori risultano fondamentali nella progettazione antisismica.

Il metodo H/V assume i microtremori come principalmente costituiti da onde di Rayleigh, verticali e orizzontali, che vengono amplificate in conseguenza degli effetti di sito indotti dalla presenza di discontinuità stratigrafiche nel sottosuolo. Sulla base di una trasformata di Fourier, è quindi possibile ricostruire, nel dominio della frequenza, la distribuzione spettrale dei record, orizzontali e verticale (misurati nel dominio del tempo), e quindi calcolare la HVSR. La presenza di un picco nella curva HVSR attesta la presenza di una discontinuità meccanica lungo la verticale del sito di misura.

Il lavoro sul campo è stato realizzato con tre diversi strumenti e diverse prove sono state eseguite ripetendo le misurazioni su uno stesso sito in momenti distinti per la verifica della ripetibilità dei risultati. La frequenza di campionamento era 128 Hz con tempi di registrazione compresi tra i 30 e i 12 minuti, secondo quanto previsto dai criteri SESAME per una curva H/V affidabile alle frequenze di interesse (Koller *et al*., 2004; Bard *et al*., 2005). Il software Grilla (Micromed 2006, 2008) è stato utilizzato per elaborare con gli stessi criteri tutti i record nell'intervallo di frequenza 0-64 Hz, considerando finestre temporali di 20 s e una tecnica di smoothing basata su una finestra triangolare con ampiezza pari al 10%.

**Frequenze naturali e loro ampiezze.** Nei bacini di avanfossa fortemente subsidenti, come la Pianura Padana a partire dal Pleistocene medio, in corrispondenza delle culminazioni strutturali delle anticlinali per propagazione di faglia (fault-propagation folds), lo spessore dei depositi quaternari continentali è generalmente ridotto. Inoltre, questi depositi sono generalmente costituiti da successioni sedimentarie condensate o addirittura con lacune stratigrafiche e, in questa regione, si sovrappongono direttamente alle unità marine plioceniche (Pieri e Groppi, 1981; Boccaletti *et al.,* 2004; Martelli e Molinari, 2008). Di conseguenza, si verifica un contrasto di impedenza elevato a causa del brusco aumento, sia della velocità delle onde sismiche, sia della densità del materiale. Tali condizioni meccaniche sono particolarmente adatte ad essere rilevate attraverso le analisi HVSR.

In particolare, quando la variazione litologica è brusca e stratigraficamente ridotta a pochi metri, o anche meno, la curva HVSR presenta un elevato e marcato picco di amplificazione. Come comunemente accettato in letteratura, la frequenza del picco di amplificazione è in prima approssimazione proporzionale alla velocità delle onde di taglio del sovrastante corpo sedimentario e all'inverso della profondità della discontinuità secondo la formula (la cosiddetta equazione di risonanza)

$$f_0 = \frac{v_s}{4 \cdot h} \qquad (1)$$

In alcuni settori delle anticlinali sepolte, uno strato relativamente sottile di depositi marini del Pliocene superiore-Pleistocene inferiore (anche solo 20-30 m) potrebbe essere interposto tra la sovrastante successione sedimentaria continentale 'condensata' e le unità litologiche sottostanti. In questo contesto geologico, il contrasto di impedenza è in qualche modo distribuito o, eventualmente, suddiviso tra più di una superficie. In questo caso, l'analisi HVSR mostra due (o più) picchi ravvicinati o uno relativamente largo (Oliveto *et al*., 2004; Castellaro *et al*., 2005).

In linea di principio, più alto è il picco, maggiore è il contrasto di impedenza tra i due strati, mentre più è stretto il picco (cioè caratterizzato da una piccola gamma di frequenze), più è netta la variazione litologica nella colonna stratigrafica.

*Distribuzione areale*. Durante le campagne geofisiche sono state effettuate circa 150 misurazioni, di cui circa il 10% sono state scartate sulla base dei criteri SESAME, o per anomalie nello spettro di Fourier di una singola componente, o perché affette da disturbi di origine antropica. Di conseguenza, solo 136 misure sono state considerate e successivamente analizzate per le finalità di questo studio. Esse sono distribuite in tutta l'area indagata (Fig. 1), anche se con una densità variabile al fine di meglio evidenziare la geometria dell'anticlinale di Mirandola che rappresenta il caso di studio strutturale e stratigrafico del presente lavoro. Come sopra accennato, per ogni sito sono state considerate l'ampiezza del valore di picco della curva HVSR, *A*, e la frequenza corrispondente, $f_0$ (comunemente indicata come frequenza naturale). A questo proposito si noti che sono stati analizzati solo i picchi tra 0,2-0,4 e ~10

Hz, dal momento che picchi a frequenze più basse potrebbero essere anche influenzati dalle condizioni meteorologiche, mentre picchi a $f_0$ > 10 Hz sono associati a riflettori stratigrafici molto superficiali, di scarso interesse per lo scopo di questo studio.

La distribuzione di entrambi i parametri è stata oggetto di una ulteriore elaborazione che ha portato alla realizzazione di una mappa su cui è rappresentata una griglia con colori sfumati (*colour-shaded grid*), utilizzando il metodo di interpolazione *kriging* incluso in Golden Software Surfer (R). I risultati della campagna geofisica e la loro interpolazione documentano chiaramente la presenza di zone caratterizzate da fenomeni di risonanza, localmente molto importanti, e permettono di mapparne la distribuzione. In particolare, la Fig. 1 evidenzia la presenza di una fascia ristretta (2,5-3,5 km di larghezza), con andamento ESE-ONO, caratterizzata da valori $f_0$ delle curve HVSR maggiori di 1 Hz e fino a 2,0 Hz lungo la quale nel settore più centrale si verificano massimi locali in senso E-W. Un andamento simile può essere osservato anche interpolando il valore *A* con la stessa procedura descritta sopra. In questo caso, il valore discriminante selezionato è circa 2,5 e la rappresentazione in mappa conferma la presenza di un'area allungata ESE-ONO, caratterizzata da un notevole contrasto di impedenza (fino a 5,8) associato alla variazione nella successione stratigrafica sviluppata durante Pliocene-Quaternario in corrispondenza dell'anticlinale Mirandola. Assumendo, in prima approssimazione, che la velocità delle onde sismiche nelle unità sedimentarie superficiali (nei primi 100-150 m) sia lateralmente uniforme (o uniformemente variabile in profondità), la distribuzione delle frequenze naturali che è stata mappata è certamente dovuta ad una marcata variabilità (gradienti verso nord e verso sud e una progressiva diminuzione in direzione ESE) della profondità della superficie che dà origine alla risonanza (ossia caratterizzata da un significativo contrasto di impedenza).

*Profondità dell'interfaccia*. Una sezione geologica trasversale basata su profili di sismica a riflessione (Martelli e Molinari, 2008) e realizzata per indagare possibili serbatoi geotermici nella zona di Mirandola è rappresentata come riferimento in fig. 2. Sulla parte superiore del profilo sono anche riportate le curve HVSR ottenute da siti di misura posti ad una distanza massima di circa 200 m dalla traccia della sezione geologica (AA' in Fig. 1). Sono stati quindi lateralmente correlati i picchi maggiori e alcuni secondari al fine di ottenere una sezione pseudo-2D che rappresenta le principali superfici caratterizzate da un apprezzabile contrasto di impedenza. Come si può chiaramente osservare, c'è una buona concordanza tra la ricostruzione della geometria del sottosuolo dei corpi sedimentari pliocenici e quaternari e la posizione (cioè frequenza) e la forma dei picchi nelle diverse curve HVSR (Fig. 2a). In particolare, in corrispondenza della parte superiore della anticlinale Mirandola, le curve HVSR mostrano un picco marcato, localmente alto fino al valore di 5,8, progressivamente decrescente in ampiezza sia verso nord che verso sud, ossia spostandosi verso le due sinclinali contigue. Da un punto di vista meccanico e quindi sismologico, queste variazioni di HVSR (Fig. 2a) potrebbero essere dovute ad un contrasto di impedenza variabile lateralmente e correlato ad un aumento di rigidezza del corpo sedimentario al di sotto della interfaccia più superficiale in corrispondenza dell'anticlinale. Questo potrebbe essere una conseguenza i) della compattazione differenziale, ii) del contatto diretto con i livelli più antichi (cioè più compatti e più densi) a seguito della parziale erosione della parte superiore della successione sottostante e/o iii) di una sovrastante serie sedimentaria condensata. Seguendo lo stesso approccio, abbiamo anche cercato di correlare altri picchi secondari (Fig. 2a), che sottolineano la geometria a becco di flauto (*pinch-out*) dei corpi sedimentari che si depositano all'interno delle sinclinali sia a nord che a sud dell'anticlinale di Mirandola.

**Discussione.** È importante notare che in questo studio il quadro complessivo dell'anticlinale sepolta di Mirandola è stato ottenuto solo sulla base del gran numero di misurazioni a stazione singola che hanno permesso di correlare lateralmente la frequenza di picco e l'ampiezza delle curve HVSR e di attribuire un significato stratigrafico alle interfacce corrispondenti ai picchi osservati (Fig. 2).

Al fine di meglio definire e validare il modello sottosuolo qui proposto, sono state effettuate

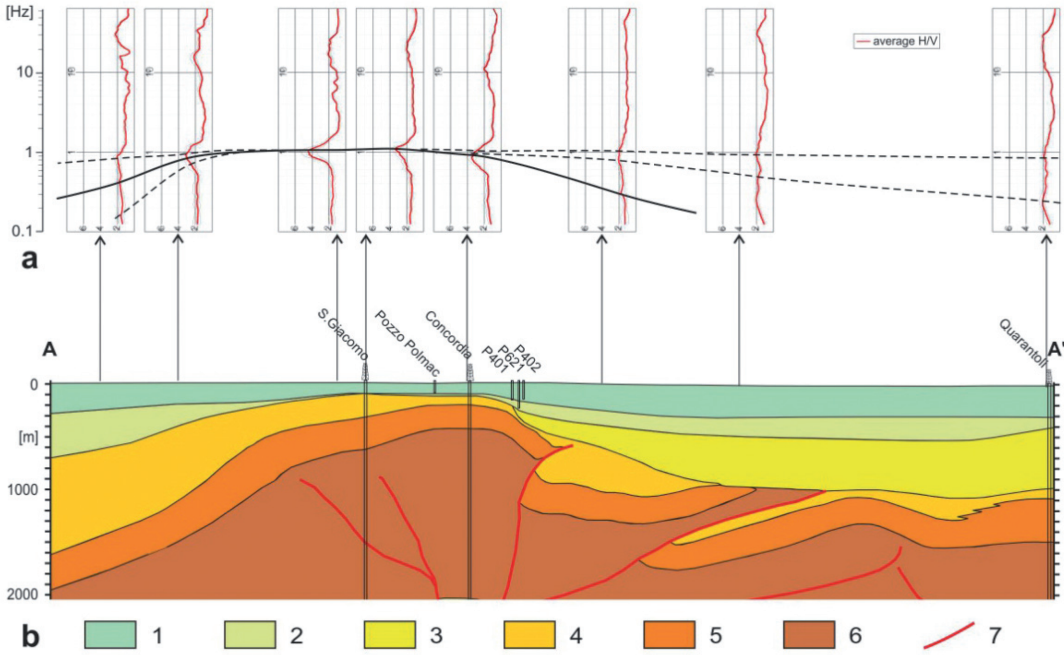


Fig. 2 – a) curve HVSR ottenute da siti indagati in un raggio di 200 metri dal profilo che attraversa l'anticlinale Mirandola (AA 'in Fig. 1). I maggiori picchi nei diversi grafici sono stati tentativamente correlati lungo il transetto suggerendo la possibile la sezione geologica (b) ottenuta da un profilo di sismica a riflessione e dati di pozzo (modificato da Martelli e Molinari, 2008). Legenda: 1) depositi continentali del Quaternario Medio-Superiore; 2) depositi marini del Pliocene Superiore - Pleistocene Inferiore; 3) Pliocene Medio; 4) Formazione del Santerno (Pliocene Inferiore); 5) Formazione di Porto Garibaldi (Pliocene Inferiore); 6) Formazione a Colombacci (Messiniano superiore); 7) principali faglie.

misure HVSR anche in corrispondenza di due carotaggi realizzati dalla Regione Emilia-Romagna fino a una profondità di 101 e 127 m, rispettivamente (Martelli *et al.*, 2013). In questi due siti è stata ricostruita la successione stratigrafica di dettaglio raggiungendo il Pliocene superiore, l'interfaccia sismica definita localmente come *pseudo-bedrock* (cioè $V_S \geq 600$ m/s), a circa 95 e 116 m, rispettivamente (Luca Martelli, com. pers.). Inoltre, in entrambi i siti è stato realizzato un secondo pozzo per poter svolgere un'indagine *cross-hole* allo scopo di misurare la distribuzione di velocità delle onde di taglio in profondità. Basandosi su un approccio di inversione semplificata (Castellaro e Mulargia, 2009), è stato possibile riprodurre le curve HVSR misurate e in particolare i più evidenti e significativi picchi in corrispondenza dell'interfaccia che i depositi continentali del Quaternario Medio da quelli marini del Quaternario Inferiore e del Pliocene Superiore. In Fig. 3 è riportato l'esempio di inversione da HVSR basandosi sui dati del carotaggio con *cross-hole* eseguito a Mirandola.

Inoltre, sulla base della inversione delle curve H/V là dove sono disponibili dati geotecnici o geofisici indipendenti (Castellaro e Mulargia, 2009), è stato anche possibile calcolare per siti selezionati la velocità delle onde di taglio nei primi 30 m ($V_{S30}$) e fino al *bedrock* ($V_{SH}$, dove H rappresenta una profondità compresa tra 75 e circa 150 m in corrispondenza della anticlinale). Entrambi i parametri sismici sono particolarmente importanti per la valutazione del fattore di amplificazione stratigrafica seguendo le cosiddette procedure semplificate (abachi) di uso comune, per esempio, negli studi di microzonazione sismica italiani (Gruppo di lavoro MS, 2008; Regione Emilia-Romagna, 2007).

Seguendo l'equazione di risonanza (1), una buona stima della velocità delle onde di taglio dei depositi sovrastanti la discontinuità litologica potrebbe consentire di definirne la profondità. I valori stimati della $V_{S30}$ e soprattutto della $V_{SH}$ variano da 190 a 220 m/s e da 290 a 320 m/

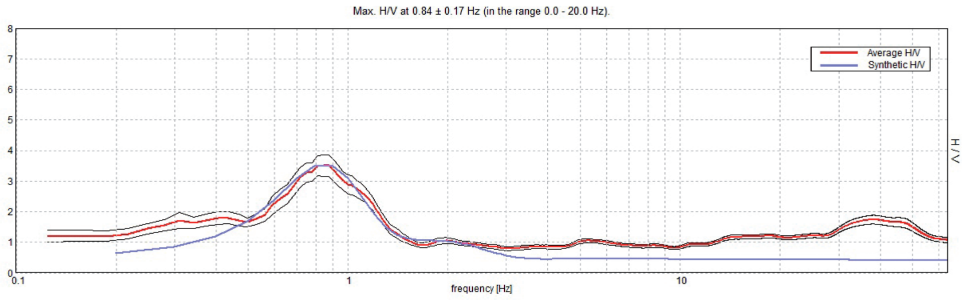


Fig. 3 – La curva HVSR (in rosso) ottenuta dalla misurazione eseguita in corrispondenza del sondaggio con *cross-hole* realizzato a Mirandola e la curva modellata (in blu) ottenuta utilizzando un modello di velocità semplificato a partire dai dati del *cross-hole*.

s, rispettivamente, nei due siti misurati di Medolla e Mirandola. Di conseguenza, è possibile dedurre che la profondità della discontinuità evidenziata dal valore della frequenza naturale, è compresa fra 75-90 m, sulla cresta della anticlinale di Mirandola (per esempio vicino San Giacomo Roncole; Fig. 1 e 2), e più di 150 m sia a nord che a sud lungo i due fianchi della piega e verso la periclinale orientale.

Anche se per successioni sedimentarie lateralmente eterogenee sarebbe necessario un numero molto maggiore di dati stratigrafici diretti (pozzi, carotaggi, ecc.) per stabilire un affidabile rapporto frequenza-spessore (e.g. Ibs von Seht e Wohlenberg, 1999; Gosar e Lenart, 2010), l'area indagata è caratterizzata da una stratigrafia tutto sommato solo poco variabile e quindi la taratura eseguita attraverso i due sondaggi della Regione Emilia-Romagna può essere considerata sufficientemente vincolata ai fini del presente studio.

Secondo i profili calibrati della velocità media e seguendo lo stesso approccio descritto in precedenza e utilizzato per correlare lateralmente le misure 1D HVSR (Fig. 2a), sono stati elaborati diversi transetti orientati NNE-SSW. I risultati di questo approccio applicato in modo sistematico e le relative proposte di correlazione tra i diversi picchi HVSR sono stati recentemente sottomessi dagli stessi autori. Tali correlazioni rendono possibile osservare un andamento sostanzialmente uniforme, marcato da alcune superfici principali (cioè caratterizzate da un evidente contrasto di impedenza) convergenti da nord e sud verso la culminazione della anticlinale. Questa geometria è evidenziata dai picchi di frequenza più pronunciati e relativamente elevati, che comunemente corrispondono alla profondità del cosiddetto *pseudo-bedrock* (cioè $V_S \geq 600$ m/s).

**Considerazioni conclusive.** L'amplificazione sismica è influenzata dalla rigidità del suolo e soprattutto dal contrasto di impedenza tra unità sismiche superficiali. Di conseguenza, le mappe di frequenza naturale sono della massima importanza perché permettono di riconoscere le aree caratterizzate da un elevato contrasto di impedenza in cui si prevede una maggiore amplificazione del moto del suolo in caso di scuotimento sismico. Se la frequenza di amplificazione di un terreno di fondazione è prossima a quella propria dell'edificio, può verificarsi un effetto detto di *doppia risonanza*, per cui il rischio per la costruzione di subire danni strutturali aumenta notevolmente (es Castellaro *et al.*, 2014). A questo proposito, le mappe di frequenza naturale e di amplificazione possono risultare importanti nella pianificazione urbanistica per definire le altezze degli edifici (ad esempio il numero di piani) a, consentendo così agli ingegneri di migliorare il comportamento antisismico di nuove costruzioni. L'amplificazione sismica infatti è considerata la prima causa di danni e di collasso durante un terremoto.

Con la presente ricerca è stata studiata e ricostruita la distribuzione dell'amplificazione naturale dovuta alla presenza di un contrasto impedenza nel sottosuolo, sia in termini di frequenza (Fig. 1) che di ampiezza del rapporto H/V (Tarabusi e Caputo, sottomesso). Ci si è concentrati sulla zona di Mirandola e dintorni per diversi motivi: in primo luogo, perché si tratta di un distretto industriale di dimensioni medio-piccole e, quindi, di particolare interesse economico e sociale per l'Italia; inoltre uno studio di microzonazione sismica di secondo livello era già stato commissionato dal Comune di Mirandola ed eseguito prima del terremoto dell'Emilia del 2012 (Tarabusi, 2012). In secondo luogo, il sottosuolo della zona è caratterizzato da una anticlinale per propagazione di faglia, in cui sia la faglia inversa che la piega associata risultano completamente sepolti dai depositi continentali del Pleistocene Medio-Superiore e olocenici (ad esempio Martelli e Molinari, 2008; Bonini *et al*., 2014). I movimenti verticali differenziali indotti dalla struttura tettonica cieca e in particolare quelli positivi (cioè sollevamento in corrispondenza della cerniera della piega) non sono infatti in grado di tenere il passo della subsidenza a scala regionale e degli elevati tassi di sedimentazione della Pianura Padana. Pertanto, si è voluta testare l'applicazione sistematica di una tecnica geofisica a basso costo, al fine di raccogliere informazioni utili sulla stratigrafia locale, relativamente poco profonda, nonché sulle sue caratteristiche sismiche. A questo proposito, i risultati ottenuti documentano chiaramente e indipendentemente la presenza di una superficie piegata nel primo sottosuolo dell'area di Mirandola; la cresta è orientata ESE-WNW con il culmine verso ovest e un andamento periclinalico verso est in perfetto accordo con la struttura tettonica ricostruita sulla base di profili sismici a riflessione. Pertanto, i risultati di questo approccio metodologico sono molto incoraggianti e potrebbero essere facilmente applicati ad altre regioni morfologicamente simili interessate da pieghe e faglie cieche.

**Bibliografia**

Bard P.-Y., Acerra C., Alguacil G., Anastasiadis A., Atakan K., Azzara R., Basili R., Bertrand E., Bettig B., Blarel F., Bonnefoy-Claudet S., Bordoni P., Borges A., Bøttger-Sørensen M., Bourjot L., Cara F., Caserta A., Chatelain J-L., Cornou C., Cotton F., Cultrera G., Daminelli R., Dimitriu P., Dunand F., Duval A.-M., Fäh D., Fojtikova L., de Franco R., di Giulio G., Grandison M., Guéguen P., Guillier B., Haghshenas E., Havskov J., Jongmans D., Kind F., Kirsch J., Koehler A., Koller M., Kristek J., Kristekova M., Lacave C., La Rocca M., Marcellini A., Maresca R., Margaris B., Moczo P., Moreno B., Morrone A., Ohrnberger M., Ojeda J.A., Oprsal I., Pagani M., Panou A., Paz C., Querendez E., Rao S., Rey J., Richter G., Rippberger J., Roquette P., Roten D., Rovelli A., Saccoroti G., Savvaidis A., Scherbaum F., Schisselé E., Spühler-Lanz E., Tento A., Teves-Costa P., Theodulidis N., Tvedt E., Utheim T., Vassiliadès J.-F., Vidal S., Viegas G., Vollmer D., Wathelet M., Woessner J., Wolff K. and Zacharapoulos S. (2005): *Guidelines for the implementation of the H/V spectral ratio technique on ambient vibrations measurements, processing and interpretation*. Deliverable D23.12 of the SESAME project, 62 pp, April 2005. Available at http://www.SESAME-FP5.obs.ujf-grenoble.fr

Bignami C., Burrato P., Cannelli V., Chini M., Falcucci E., Ferretti A., Gori S., Kyriakopoulos C., Melini D., Moro M., Novali F., Saroli M., Stramondo S., Valensise G. and Vannoli P. (2012): Coseismic deformation pattern of the Emilia 2012 seismic sequence imaged by Radarsat-1 interferometry. *Annals of Geophys*., **55**(4), 788-795, doi: 10.4401/ag-6157.

Boccaletti M., Bonini M., Corti G., Gasperini P., Martelli L., Piccardi L., Tanini C. and Vannucci G. (2004): *Seismotectonic Map of the Emilia-Romagna Region, 1:250000*. Regione Emilia-Romagna – CNR.

Bonini L., Toscani G. and Seno S. (2014): Three-dimensional segmentation and different rupture behavior during the 2012 Emilia seismic sequence (Northern Italy). *Tectonophys*., **630**, 33-42, doi: 10.1016/j.tecto.2014.05.006.

Burrato P., Ciucci F. and Valensise G. (2003): An inventory of river anomalies in the Po Plain, Northern Italy: evidence for active blind thrust faulting. *Ann. Geophys*., **46**(5), 865-882.

Burrato P., Vannoli P., Fracassi U., Basili R. and Valensise G. (2012): Is blind faulting truly invisible? Tectonic-controlled drainage evolution in the epicentral area of the May 2012, Emilia-Romagna earthquake sequence (northern Italy). *Ann. Geophys*., **55**(4), 525-531, doi: 10.4401/ag-6182.

Caputo R. (2005): Ground effects of large morphogenic earthquakes. *J. Geodyn*., **40**(2-3), 113-118.

Caputo R., Pellegrinelli A., Bignami C., Bondesan A., Mantovani A., Stramondo S. and Russo P. (2015): High-precision levelling, DInSAR and geomorphological effects in the Emilia 2012 epicentral area. *Geomorphology*, **235**, 106-117, doi: 10.1016/j.geomorph.2015.02.002

Castellaro S. e Mulargia F. (2009): Vs30 estimates using constrained H/V measurements. *Bull. Seism. Soc. Am*., **99**, 761-773, doi: 10.1785/0120080179.

Castellaro S., Mulargia F. e Bianconi L. (2005): Passive seismic stratigraphy: a new efficient, fast and economic technique. *J. Geotech. Environ. Geol*., **3**, 51-77.

Castellaro S., Padròn L.A. e Mulargia F. (2014): The different response of apparently identical structures: a far-field lesson from the Mirandola 20th May 2012 earthquake. *Bull. Earthq. Eng*., **12** (5), 2481-2493, doi: 10.1007/s10518-013-9505-9.

DISS WORKING GROUP (2015): *Database of Individual Seismogenic Sources (DISS), Version 3.2.0: A compilation of potential sources for earthquakes larger than M 5.5 in Italy and surrounding areas*. http://diss.rm.ingv.it/diss/, © INGV 2015 - Istituto Nazionale di Geofisica e Vulcanologia - All rights reserved, doi: 10.6092/INGV.IT-DISS3.2.0

Gallipoli M.R., Mucciarelli M., Gallicchio S., Tropeano M. e Lizza C. (2004): Horizontal to Vertical Spectral Ratio (HVSR) measurements in the area damaged by the 2002 Molise, Italy, earthquake. *Earthq. Spect.*, **20**(S1), S81-S93, doi: 10.1193/1.1766306.

Gosar A. e Lenart A. (2010): Mapping the thickness of sediments in the Ljubljana Moor basin (Slovenia) using microtremors. *Bull. Earthq. Eng.*, **8**, 501-518, doi: 10.1007/s10518-009-9115-8.

Gruppo di lavoro MS (2008): ICMS, Indirizzi e criteri per la microzonazione sismica. Conferenza delle Regioni e delle Province Autonome - Dipartimento della Protezione Civile, Roma, 3 vol. and Dvd, http://www.protezionecivile.it/cms/view.php?dir_pk=395&cms_pk=15833.

Ibs-von Seht M. e Wohlenberg J. (1999): Microtremor Measurements Used to Map Thickness of Soft Sediments. *Bull. Seism. Soc. Am.*, **89**(1), 250-259.

Koller M., Chatelain J.-L., Guillier B., Duval A.-M., Atakan K., Bard P.-Y. and SESAME Team (2004): Practical user guidelines and software for the implementation of the H/V ratio technique: measuring conditions, processing method and results interpretation. 13th World Conf. Earthq. Eng., Vancouver, August 2004, *Proceedings*, paper # 3132.

Martelli L. e Molinari F.C. (2008): *Studio geologico finalizzato alla ricerca di potenziali serbatoi geotermici nel sottosuolo del comune di Mirandola, Regione Emilia Romagna*. Internal Report, Servizio Geologico, Sismico e dei Suoli, Bologna, pp. 26.

Martelli L., Calabrese L., Ercolessi G., Severi P., Romani M., Tarabusi G., Pileggi D., Rosselli S., Minarelli L., Pergalani F., Compagnoni M., Vannucchi G., Madiai C., Facciorusso J., Fioravante V., Giretti D., Mucciarelli M., Priolo E., Laurenzano G., Bramerini F., Speranza E., Conte C., Di Salvo G., Giuffrè M., Zuppiroli M., Guidi F., Vona V., Manicardi A., Mengoli B., Ugoletti C., Ricci L. (2013): *Microzonazione sismica dell'area epicentrale del terremoto della pianura emiliana del 2012 (ORD. 70/2012)*. Atti 32° Convegno Nazionale GNGTS, Trieste. ISBN: 978-88-902101-7-4.

Micromed (2006): *Grilla ver. 2.2, spectral and HVSR analysis – user's manual*. Micromed, Treviso, pp. 47.

Micromed (2008): *An introduction to the phase velocity spectra module in Grilla*. Micromed, Treviso, pp. 16.

Mucciarelli M., Contri P., Mochavesi G., Calvano G. e Gallipoli M.R. (2001): An empirical method to assess the seismic vulnerability of existing buildings using the HVSR technique. *Pure. Appl. Geoph.*, **158**, 2635-2647.

Nakamura Y. (1989): A method for dynamic characteristics estimation of subsurface using microtremor on the ground surface. *Quart. Rep. Railway Tech. Res. Inst.* (RTRI), **30**, 25-33.

Oliveto A.N., Mucciarelli M. e Caputo R. (2004): HVSR prospections in multi-layered environments: an example from the Tyrnavos Basin (Greece). *J. Seismol.*, **8**, 395-406.

Pieri M. e Groppi G. (1981): Subsurface geological structure of the Po Plain, Italy. Consiglio Nazionale delle Ricerche, Progetto finalizzato Geodinamica, sottoprogetto Modello Strutturale, pubbl. N° 414, Roma, 13 pp.

Pondrelli S., Salimbeni S., Perfetti P. e Danecek P. (2012): Quick regional centroid moment tensor solutions for the Emilia 2012 (northern Italy) seismic sequence. *Ann. Geophys.*, **55**(4), 615-621, doi: 10.4401/ag-6146.

Regione Emilia-Romagna (2007): Delibera Assemblea Legislativa n. 112/2007 - Approvazione dell'atto di indirizzo e coordinamento tecnico ai sensi dell'art. 16, comma 1, della LR 20/2000 Disciplina generale sulla tutela del territorio, in merito a "Indirizzi per gli studi di microzonazione sismica in Emilia-Romagna per la pianificazione territoriale ed urbanistica".

Salvi S., Tolomei C., Merryman Boncori J.P., Pezzo G., Atzori S., Antonioli A., Trasatti E., Giuliani R., Zoffoli S. e Coletta A. (2012): Activation of the SIGRIS monitoring system for ground deformation mapping during the Emilia 2012 seismic sequence, using COSMO-SkyMed InSAR data. *Ann. Geophys.*, **55**(4), 796-802, doi: 10.4401/ag-6181.

Tarabusi G. (2012): *Microzonazione sismica del comune di Mirandola. Quadro conoscitivo del PSC di Mirandola*. http://www.comune.mirandola.mo.it/la-citta-e-il-territorio/piano-strutturale-comunale-psc, Studio di Geologia Tarabusi, QB_C_REL1, 26/01/2012, Bologna, pp. 57.

# GEOGUARD: UN NUOVO SERVIZIO DI MONITORAGGIO GEODETICO PER L'OSSERVAZIONE DI SEGNALI GEODINAMICI

S. Caldera[1], E. Realini[1], M. Reguzzoni[1,2], D. Sampietro[1], F. Sansò[1,2]
[1] *GReD srl, Lomazzo (CO), Italia*
[2] *DICA – Politecnico di Milano, Italia*

**Introduzione.** Lo studio dei processi geodinamici richiede spesso di attivare sistemi di monitoraggio, al fine di migliorare la conoscenza dei movimenti della crosta terrestre. Del resto lo stesso monitoraggio è anche utile per la mitigazione dei rischi naturali o dei rischi legati a cedimenti di strutture ed infrastrutture al fine di mitigarne gli effetti in termini di costi economici e sicurezza per la popolazione. Uno dei possibili approcci per controllare l'osservazione di tali processi consiste nella determinazione continua della posizione (e quindi dello spostamento) di una rete di punti posti sulla superficie e solidali con l'area di interesse. In particolare, a seconda dei movimenti da monitorare, possono essere definiti diversi requisiti sia in termini di risoluzione temporale (osservazioni di spostamento giornalieri, mensili, ecc.) sia in termini di risoluzione spaziale (numero di punti monitorati nell'area di studio), sia in termini di accuratezza delle osservazioni dello spostamento. Ovviamente i tre requisiti sopra elencati sono strettamente correlati tra loro, infatti elevate accuratezze nella misura permettono di osservare movimenti minori e quindi rendono di interesse anche maggiori risoluzioni sia temporali che spaziali.

Per la risoluzione di questi problemi le tecniche geodetiche come il posizionamento classico, il SAR o i sistemi GPS/GNSS Global Positioning System/Global Navigation Satellite System) rappresentano ormai una pratica comune. Tuttavia, ognuna di queste tecniche ha una serie di peculiarità: ad esempio il SAR permette di avere dati spazialmente ben distribuiti, ma ha una risoluzione temporale limitata dai passaggi dei satelliti e l'accuratezza delle osservazioni difficilmente scende sotto il centimetro.

Il posizionamento classico mediante l'utilizzo di stazione totale richiede invece la presenza di uno o più operatori, oppure la costruzione di costose strutture per l'installazione di stazioni totali automatiche. Nel primo caso la risoluzione spaziale del monitoraggio non può essere elevata, nel secondo caso non solo bisogna far fronte a elevate spese d'installazione, ma inoltre si possono monitorare solo punti visibili dalla stazione totale fissa. Inoltre, l'accuratezza delle misure può essere fortemente deteriorata dalle variazioni delle condizioni atmosferiche, con accuratezze anche inferiori ad 1 cm per elevate distanze tra stazione totale e punto da monitorare.

L'uso dei sistemi GPS/GNSS per monitorare le deformazioni viene tipicamente svolta installando una rete di ricevitori di qualità geodetica che garantiscono accuratezze dell'ordine dei millimetri con un giorno di latenza. Tuttavia, l'elevato costo dei ricevitori a doppia frequenza limita generalmente il numero dei punti monitorati.

Di recente sono stati usati in alternativa dispositivi GNSS a più basso costo che mostrano la possibilità di fornire buoni risultati. In questo lavoro viene proposto un servizio per il monitoraggio basato su ricevitori GNSS a singola frequenza a basso costo. Tale servizio presenta l'elevata accuratezza e risoluzione temporale dei sistemi GNSS ma, riducendo i costi, permette anche un'elevata risoluzione spaziale. Il ricevitore GNSS può essere affiancato da accelerometri MEMS (Micro Electro-Mechanical System) per l'analisi di possibili sismi di medio-alta intensità o da altri sensori, quali ad esempio pluviometri, termometri o barometri per eventuali correlazioni tra le deformazioni osservate e gli eventi atmosferici. L'analisi dei dati *raw* GPS, acquisiti in formato RINEX (Receiver Independent Exchange Format) è svolta da un sistema *cloud* all'interno del servizio stesso e all'utente finale vengono forniti, salvo diversa indicazione, direttamente le serie temporali delle deformazioni osservate.

In questo lavoro sono presentati, oltre all'architettura del servizio di posizionamento stesso, una serie di esperimenti di posizionamento relativo. Quest'ultimo è stato ottenuto processando dati con differenti pacchetti software che mostrano l'affidabilità dei ricevitori GNSS a basso costo per l'analisi di deformazioni.

Il principale risultato di questo lavoro può essere riassunto nel fatto che utilizzando un ricevitore GPS a basso costo u-blox e analizzando i dati con il software *free* e *open source* goGPS (Realini and Reguzzoni, 2013; Herrera *et al.*, 2015) è possibile individuare movimenti dell'ordine di pochi millimetri utilizzando basi corte, ovvero è possibile realizzare un servizio di monitoraggio.

**Il monitoraggio geodetico mediante sistemi GNSS.** Un sistema di monitoraggio geodetico consiste sostanzialmente nella determinazione continua della posizione di un certo insieme di punti nel tempo ed eventualmente nella generazione di un allarme quando viene superata una certa soglia sulla deformazione del sistema complessivo. Questo tipo di monitoraggio può essere realizzato tramite una rete di stazioni GNSS permanenti, come dimostrato da un'ampia letteratura sull'argomento (Roberts *et al.,* 2004; Chan *et al.,* 2006; Meng *et al.,* 2007; Watson *et al.,* 2007; Borghi *et al.,* 2009; Kaloop and Li, 2009; Fastellini *et al.,* 2011; Wang, 2011; Yi *et al.,* 2013). Tale letteratura mostra come con rete di diametro massimo di 10-15 km si possono raggiungere facilmente accuratezze millimetriche sulle coordinate delle stazioni che la costituiscono con una latenza giornaliera.

Il principale problema di questa soluzione è l'alto costo dei ricevitori geodetici, che porta ad una riduzione del loro numero all'interno della rete e di conseguenza al degrado dell'efficienza del sistema di monitoraggio dovuto alla bassa risoluzione spaziale. Recentemente la comunità geodetica ha rivolto l'attenzione sulla possibile applicazione di ricevitori a basso costo per sostituire, almeno in parte, i ricevitori geodetici all'interno di un sistema di monitoraggio (Heunecke *et al.,* 2011; Buchli *et al.,* 2012; Benoit *et al.,* 2014; Cina and Piras, 2014). Benchè i risultati ottenuti siano molto promettenti, la realizzazione di un sistema di monitoraggio a basso costo richiede anche l'utilizzo di pacchetti software adeguati. Il software *free* e *open source* goGPS è risultato essere in grado di svolgere questo compito. Vengono qui riportati i risultati di un esperimento preliminare basato sull'uso di un ricevitore a basso costo u-blox e su due basi corte di 70 m e di circa 2.8 km.

L'hardware utilizzato nell'esperimento consiste in due stazioni permanenti GNSS, per le quali è disponibile una lunga serie storica, e un ricevitore a basso costo nel punto da monitorare (tenuto fermo durante tutto l'esperimento). Più precisamente le due stazioni permanenti sono:

- MILA, che utilizza un ricevitore TOPCON Odyssey E con antenna TPSCR3 GGD CONE, posizionato presso il Campus Leonardo del Politecnico di Milano;
- PROV, che utilizza un ricevitore TOPCON Legacy E con antenna JAVAD RegAnt, posizionato presso la sede della Provincia di Milano.

Il ricevitore a basso costo era un u-blox EVK-6T (evaluation kit con modulo LEA-6T) con la sua antenna standard ANN-MS. L'antenna era fissata, attraverso un supporto magnetico, su una basetta metallica quadrata di lato 15 cm. La basetta era avvitata sopra una palina, a sua volta fissata all'angolo di una ringhiera sul tetto di un edificio del Politecnico di Milano (Fig. 1). L'antenna si trovava a circa 70 m dalla stazione di MILA e circa 2.8 km da quella di PROV. Il ricevitore, collegato all'antenna tramite un cavo coassiale di 5 m, era invece posizionato in un locale chiuso, accanto a un PC portatile che permetteva il download continuo dei dati.

I dati acquisiti dai vari ricevitori sono stati processati utilizzando i seguenti applicativi: Bernese GPS Software 5.2 (Dach *et al.,* 2007), Leica Geo Office Combined (LGO) e goGPS (http://www.gogps-project.org). Il primo è il software scientifico di riferimento della comunità geodetica, il secondo è un noto software commerciale della società Leica Geosystems, il terzo, come detto in precedenza, è un software free e open source, che dopo opportune modifiche è stato scelto come software di processamento per il servizio GeoGuard.

I dati acquisiti dalle due stazioni permanenti corrispondenti a 77 giorni di misura (da DOY 21/2014 a DOY 97/2014) sono stati inquadrati all'interno di IGb08, vincolando le stazioni di GRAS, GRAZ, MEDI, PADO, PFA2, TORI, WTZR e ZIMM alla soluzione ufficiale IGS. Nella compensazione sono state introdotte cinque stazioni aggiuntive appartenenti alla rete permanente EUREF (EPN). La compensazione della rete è stata realizzata da Politecnico di

Fig. 1 – Installazione dell'antenna ANN-MS del ricevitore u-blox EVK-6T sul tetto dell'edificio Nave (a sinistra) e dettaglio della basetta metallica usata come sostegno per il fissaggio dell'antenna (a destra).

Milano tramite il software Bernese, gestendo l'analisi dati tramite il tool RegNet (Biagi and Caldera, 2011).

A questo punto le osservazioni del ricevitore u-blox corrispondenti a 37 giorni di misura, con una frequenza di campionamento di 1 Hz, sono stati processati con i tre software prima citati, ottenendo soluzioni giornaliere. Poiché l'obiettivo di questo studio è il monitoraggio di deformazioni (qui il ricevitore u-blox è stato mantenuto fermo), la presenza di eventuali bias nella stima assoluta delle coordinate è di secondaria importanza. Di principale interesse è la stabilità della soluzione giornaliera nel tempo, ovvero la sua ripetibilità; questo indice è calcolato semplicemente come la deviazione standard delle coordinate stimate giorno per giorno per tutto il periodo di test. I risultati ottenuti sia per la base rispetto a MILA che per quella rispetto a PROV sono riportati in Tab. 1.

Tutte le soluzioni calcolate, indipendentemente dal software utilizzato, sono in singola frequenza e utilizzano le effemeridi trasmesse. Per quanto riguarda i ritardi atmosferici, per la troposfera è stato utilizzato il modello di Saastamoinen (1972) in tutti i software, mentre per la ionosfera è stato utilizzato il modello di Klobuchar (1987) in LGO e goGPS e il modello di Geckle e Feen (1982) nel Bernese. Infine, per quanto riguarda il fissaggio delle ambiguità,

Tab. 1 - Ripetibilità in mm delle soluzioni giornaliere nelle tre componenti (est, nord, up) rispetto alle due basi considerate nell'esperimento e usando i tre diversi software di processamento dati.

| | Base rispetto a MILA | | | Base rispetto a PROV | | |
|---|---|---|---|---|---|---|
| | σ(EST) | σ(NORD) | σ(UP) | σ(EST) | σ(NORD) | σ(UP) |
| Bernese | 0.7 | 0.8 | 0.4 | 0.8 | 0.6 | 1.0 |
| LGO | 0.9 | 0.8 | 0.6 | 0.9 | 0.8 | 1.3 |
| goGPS | 0.7 | 0.9 | 0.5 | 1.1 | 0.8 | 1.3 |

goGPS fa uso del metodo LAMBDA (Teunissen, 1995), Bernese del metodo SIGMA (Dach *et al.,* 2007) mentre per LGO, essendo un software commerciale, non si hanno esplicite indicazioni sul metodo utilizzato.

Allontanando la stazione permanente dal ricevitore singola frequenza ovviamente le accuratezza degradano. In particolare l'esperimento è stato ripetuto utilizzando sempre il software goGPS per distanze crescenti rispetto alla stazione permanente. L'accuratezza (in quota) sulla soluzione giornaliera scende da 0.5 mm per basi a 70 m a 4.2 mm per una base a 12 km fino a un massimo di 7.6 mm per una base da 15 km. La qualità del risultato sembrerebbe dipendere poco dal tipo di ricevitore (dual-frequency o single frequency low cost). Sarebbe invece dovuta principalmente alla capacità di eliminare i disturbi ionosferici/troposferici durante l'elaborazione (i risultati sono presentati in Fig. 2).

L'utilizzo di questo tipo di tecnologia può portare a numerosi vantaggi per il monitoraggio dei principali processi geodinamici. Infatti l'utilizzo di ricevitori GNSS singola frequenza permette di avere un'elevata risoluzione spaziale (ad esempio soluzioni giornaliere) combinata con la continuità dell'informazione, con un'elevata accuratezza dell'osservazione (dell'ordine del millimetro sulla singola misura, ma che può essere ulteriormente migliorata considerando appunto un adeguato filtraggio delle serie temporali) e infine una buona risoluzione spaziale (dovuta al fatto che l'utilizzo di ricevitori singola frequenza, decisamente più economici dei ricevitori di tipo geodetico, permette in linea di principio di costruire reti di monitoraggio con un gran numero di punti).

**Il Servizio GeoGuard.** I risultati riportati in Tab. 1 mostrano delle ripetibilità dell'ordine o addirittura inferiori al millimetro nelle tre componenti, con prestazioni leggermente migliori da parte del Bernese. Questo dimostra la fattibilità di un sistema di monitoraggio completamente a basso costo, sia dal punto di vista hardware (per esempio usando ricevitori u-blox) sia dal punto di vista software (per esempio usando goGPS), garantendo la possibilità di monitorare spostamenti 3D dell'ordine di 2-3 mm, almeno nel caso di basi corte. Ovviamente l'effettiva

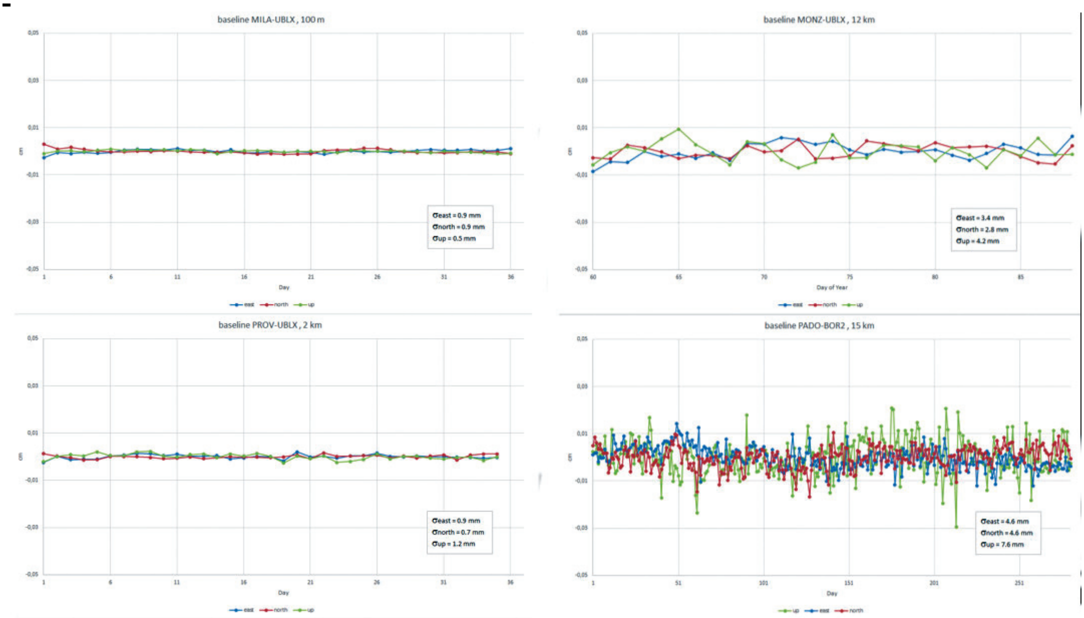


Fig. 2 – Ripetibilità in mm delle soluzioni giornaliere nelle tre componenti (est, nord, up) relative a basi a distanza crescente rispetto la stazione permanente.

realizzazione di un sistema di monitoraggio richiede lo sviluppo di un'unità di acquisizione, memorizzazione e trasmissione dei dati del ricevitore (possibilmente autonoma e in grado di funzionare anche in ambienti privi di rete elettrica e di telecomunicazione) e la disponibilità di un centro di calcolo in grado di processare i dati e generare eventuali allarmi. Un sistema di questo tipo, denominato GeoGuard (http://www.geoguard.eu/) è stato prodotto dalle due società GReD (http://www.g-red.eu) e Proteco (http://www.protecogroup.it).

In particolare il sistema GeoGuard è costituito da due componenti principali: la GeoGuard Monitoring Unit (GMU) e il GeoGuard Cloud. La GeoGuard Monitoring Unit (GMU) è sostanzialmente un device dotato di un ricevitore per la navigazione satellitare GNSS di nuova generazione, basato su tecnologia a singola frequenza che permette l'acquisizione e la trasmissione del dato. La rete di sensori è quindi composta da una o più GMU, integrate eventualmente con la strumentazione addizionale necessaria a rispondere a specifiche esigenze, come ad esempio sensori di temperatura e di pressione, accelerometri, ecc.

Il GeoGuard Cloud è invece il sistema che raccoglie e organizza i dati acquisiti, verifica l'integrità del flusso degli stessi, esegue l'elaborazione dei dati provenienti dal posizionamento e dalla rete di sensori, ne analizza i risultati e li invia al cliente finale.

La GMU è un'unità a controllo remoto specificamente progettata per operare in ambienti estremi e può essere alimentata in diverse modalità, ad esempio con un pannello solare che ne assicuri il buon funzionamento anche in condizioni di mancanza di rete elettrica. Il GeoGuard Cloud gestisce remotamente le GMU tramite una comunicazione bidirezionale, che consente sia l'acquisizione dei dati che il controllo remoto delle unità. Le GMU possono operare in una rete locale autonoma, connessa al GeoGuard Cloud attraverso un singolo punto esterno di collegamento. In dettaglio la singola GMU comprende:

- il modulo di elaborazione: comprende la CPU a microprocessore e l'unità di memorizzazione dati locale;
- il modulo di comunicazione: comprende le funzioni di comunicazione Ethernet, GSM / 3G LTE e collegamenti radio M2M;
- il modulo di posizionamento: è dotato di un ricevitore GNSS a singola frequenza e un accelerometro MEMS a 3 assi per rilevare posizione, orientamento e vibrazioni del dispositivo;
- il modulo di rilevamento: è dotato di I/O digitali ed analogici e di un bus di comunicazione "industry standard" per connettere qualsiasi sensore che possa essere necessario a rispondere a specifiche esigenze applicative;
- il modulo di alimentazione: fornisce l'alimentazione da corrente alternata (AC) e corrente continua (DC) da diverse fonti, tra cui il fotovoltaico.

La GeoGuard Cloud è invece la componente centrale del servizio GeoGuard: riceve ed elabora i dati della rete di sensori e fornisce le informazioni risultanti al cliente. Comprende le seguenti funzioni:

- l'interfaccia alla rete di sensori: riceve i dati grezzi di posizionamento GNSS e dei sensori, nonché i metadati dalla rete di sensori stessi;
- la gestione remota delle GMU: fornisce tutte le informazioni necessarie per la gestione del servizio, compresi i dati amministrativi e quelli relativi agli accordi con il cliente;
- l'elaborazione dei dati: è realizzata specificatamente per sfruttare al meglio le misure provenienti dai ricevitori GNSS e fornire analisi statistiche e di qualità relative alle osservazioni effettuate e ai risultati ottenuti (stima di trend e identificazione di discontinuità nelle serie temporali dei dati rilevati dai sensori), al fine di segnalare eventuali early warnings;
- l'interfaccia per l'utente finale che rende disponibili i risultati ottenuti in due diverse modalità: un'applicazione web che consente agli utenti finali di visualizzare i dati dei servizi GeoGuard; una API REST, che consente una rapida e facile integrazione dei servizi GeoGuard con eventuali sistemi informativi preesistenti.

GeoGuard si presenta quindi come un servizio innovativo end-to-end per il monitoraggio continuo delle infrastrutture critiche e dei rischi naturali dove l'utente finale non deve preoccuparsi dell'analisi dei dati raw GNSS ma solamente l'eventuale modellizzazione e interpretazione delle deformazioni.

**Bibliografia**

Benoit L., Briole P., Martin O., Thom C. (2014). *Real-time deformation monitoring by a wireless network of low-cost GPS*, Journal of Applied Geodesy, 8(2): 1-10.
Biagi L., Caldera, S. (2011). *The automation of permanent networks monitoring: remarks and case studies*, Applied Geomatics, 3(3): 137-152.
Borghi A., Aoudia A., Riva R. E. M., Barzaghi R. (2009). *GPS monitoring and earthquake prediction: A success story towards a useful integration*, Tectonophysics, 465(1): 177-189.
Buchli B., Sutton F., Beutel J. (2012). *GPS-equipped wireless sensor network node for high-accuracy positioning applications*, Wireless Sensor Networks, G. Picco, W. Heinzelman (eds), Lecture Notes in Computer Science, Springer Berlin Heidelberg, 179-195.
Chan W. S., Xu Y. L., Ding X. L., Dai W. J. (2006). *An integrated GPS-accelerometer data processing technique for structural deformation monitoring*, Journal of Geodesy, 80(12): 705-719.
Cina A., Piras M. (2014). *Performance of low-cost GNSS receiver for landslides monitoring: test and results*, Geomatics, Natural Hazards and Risk (pubblicato online), 3-20.
Dach R., Hugentobler U., Fridez P., Meindl M. (2007). *Bernese GPS software version 5.0*. Astronomical Institute, University of Bern.
Fastellini G., Radicioni F., Stoppini, A. (2011). *The Assisi landslide monitoring: a multi-year activity based on geomatic techniques*, Applied Geomatics, 3(2): 91-100.
Geckle W. J., Feen M. M. (1982). *Evaluation of the ionospheric refraction correction algorithm for single-frequency Doppler navigation using TRANET-II data*, PLANS'82-Position Location and Navigation Symposium, Atlantic City, NJ, 13-21.
Herrera A. M., Suhandri H. F., Realini E., Reguzzoni M., de Lacy M. C. (2015). *goGPS: open-source MATLAB software*, GPS Solutions (pubblicato online), DOI 10.1007/s10291-015-0469-x.
Heunecke O., Glabsch J., Schuhbaeck S. (2011). Landslide *monitoring using low cost GNSS equipment - experiences from two alpine testing sites*, Journal of Civil Engineering and Architecture, 5(8): 661-669.
Kaloop M. R., Li H. (2009). *Monitoring of bridge deformation using GPS technique*, KSCE Journal of Civil Engineering, 13(6): 423-431.
Klobuchar J. A. (1987). *Ionospheric time-delay algorithm for single- frequency GPS users*, IEEE Transactions on Aerospace and Electronic Systems, 23(3): 325-331.
Meng X., Dodson A. H., Roberts G. W. (2007). *Detecting bridge dynamics with GPS and triaxial accelerometers*, Engineering Structures, 29(11): 3178-3184.
Realini E., Reguzzoni M. (2013). *goGPS: open source software for enhancing the accuracy of low-cost receivers by single-frequency relative kinematic positioning*, Measurement Science and Technology, 24(11): 115010.
Roberts G. W., Meng X., Dodson A. H. (2004). *Integrating a global positioning system and accelerometers to monitor the deflection of bridges*, Journal of Surveying Engineering, 130(2): 65-72.
Saastamoinen J. (1972). Atmospheric *correction for the troposphere and stratosphere in radio ranging satellites*, The Use of Artificial Satellites for Geodesy, Wiley Online Library, 247-251.
Wang G. (2011). *GPS landslide monitoring: single base vs. network solutions - a case study based on the Puerto Rico and Virgin Islands permanent GPS network*, Journal of Geodetic Science, 1(3): 191-203.
Watson C., Watson T., Coleman R. (2007). *Structural monitoring of cable-stayed bridge: analysis of GPS versus modeled deflections*, Journal of Surveying Engineering, 133(1): 23-28.
Yi T. H., Li H. N., Gu M. (2013). *Recent research and applications of GPS-based monitoring technology for high-rise structures*, Structural Control and Health Monitoring, 20(5): 649-670.

# DATA BASE OF ITALIAN VELOCITIES AND STRAIN RATES AT PERMANENT GNSS SITES

**A. Caporali, M. Bertocco, J. Zurutuza**
*University of Padova, Italy*

**Introduction.** The knowledge of the present day deformation rates at the Earth's surface represents an important boundary condition for modeling deformation processes at depth, especially in areas such as Italy where the typical hypocentral depth is of the order of few tens of km. To reliably map the surface deformation on a regional scale the systematic timewise comparison of the coordinates of reference sites has proved to be a successful approach (see e.g. Caporali, 2003; Cenni *et al*., 2012; Nocquet, 2012; Serpelloni *et al*., 2005). In Italy there are over 400 permanent GNSS (Global Navigation Satellyte System) sites belonging to various Organizations which make the data freely available. In this paper we present the results of the analysis of such a network of 415 GNSS sites, with more to come as the time series become sufficiently long for a reliable estimate of the velocity. The University of Padova contributes to the GNSS activities: as Local Analysis Center of EUREF EPN is actively contributing to the maintenance of the European Reference Frame using state of the art software and analysis methods. The same analysis procedure and standards are used for processing on a weekly basis a network of over 450 permanent sites, which extends to cover surrounding countries. Consequently, updated time series of coordinates are regularly published on a dedicated web site (retegnssveneto.cisas.unipd.it) , under the auspices of the Regional Government of Veneto. This body of information forms the basis not only for updated coordinates of sites used in Real Time Kinematic surveying applications, but also for geodetic studies which can have a direct relation to seismicity and ground deformation.

The aim of this paper is to review how this information is generated, and how it can be packed into a convenient format (e.g. .kml or .shp) for layering with other databases, such as the DISS 3.1.1 of INGV. Our data base includes all the information which can be useful e.g. for seismic hazard or dynamic modeling, such as velocities in a rigorously defined reference frame, strain rates and derived values such as the regional stress drop. The information on statistical seismicity referred to the Seismic Zones ZS9 of Meletti *et al*. (2008) comes from the Catalogo Parametrico dei Terremoti Italiani CPTI04 (Gruppo di Lavoro CPTI04, 2004) updated with the more recentevents. The data and kml/shp files are freely available.

**From raw GNSS data to mean velocities.** We focus on accepted standards for data processing, which are based on the IGS (International GNSS Service http://igscb.jpl.nasa.gov) and EPN (European Permanent Network of EUREF http://epncb.oma.be and http://www.euref.eu ) to ensure implementation of state of the art reference frame, orbits, satellite clocks, antenna models, tropospheric modeling, elevation cutoff, and all those aspects of the processing which may affect the final coordinates at each epoch, and which make the processing products (weekly minimally constrained SINEX files representing the network adjustment) eligible for combination and stacking with other products (e.g. the weekly SINEX files of the EPN) (Lidberg *et al*., 2014). We use consistently the Bernese 5.2 software both for the daily/weekly processing and the multiyear analysis by normal equation stacking (Dach *et al*., 2013). The systematic processing of the Italian network started in 1996 with a very limited number of sites and with software, models and analysis procedures which have evolved in time. Only with GPSweek 1632 (April 17, 2011) consistent orbits, satellite clock models and antenna models, labeled IGb08 (Rebischung, 2012), were introduced. Normal equations prior to GPSweek 1632 use different analysis standards, and were therefore excluded from this analysis to ensure maximum compliance with the EPN Guidelines (Bruyninx *et al*., 2013).The velocities of the GNSS sites are defined in terms of mean slope of the time series of their coordinates. To this purpose the coordinates must be defined in a same reference frame across the time span of the coordinate time series. The state of the art reference frame is at this time the IGb08

(Rebischung, 2012), on which the orbits, satellite clocks and antenna models are based. Of particularly relevance for our work is the ETRF2000 (Boucher and Altamimi, 2011), which is related at any epoch to the IGb08 by a 14 parameter Helmert transformation. The ETRF2000 frame is defined, in compliance with the EU Directive INSPIRE on Conventional Reference Systems (INSPIRE, 2009), in such a way that the velocities of GNSS sites in a stable part of Europe are minimized. Because the reference GNSS sites used for datum definition may suffer from accidental discontinuities (e.g. antenna changes, coseismic offsets and similar) it is very important for consistency to adopt in the time series analysis conventional solution numbers, as published regularly by (Kenyeres, 2014) the EPN, to avoid that sudden jumps in the time series of reference sites affect those of other GNSS sites. Likewise a careful analysis of discontinuities in the time series of all the GNSS sites is necessary to ensure that the velocity which is computed for each site represents a long term coordinate change, in the given reference frame.The visualization of the time series of the GNSS sites we process is available at http://regegnssveneto.cisas.unipd.it/scidata and is directly linked to the .STA file used by the Bernese Software to track the history of each processed site, including coordinate discontinuities and setup of new solution numbers, edited periods and similar. The noise affecting the time series can be described by white noise and flicker phase noise (Caporali, 2003; Williams, 2003). This affects the estimate of the uncertainty in the velocities and is properly taken into account to correctly weigh the contributions of GNSS sites e.g. with different time histories. Estimating a realistic uncertainty in the velocity of each site is crucial to properly weight its contribution in the least squares collocation.

**From velocities to strain rates.** Next we address the spatial analysis of the velocities, and in particular their horizontal gradient, or 2D strain rate. To compute a strain rate it is necessary to identify an area containing a sufficient number of GNSS sites of known velocity. Although the minimum number of sites is three, the statistical reliability of the estimates and an appropriate monitoring of the uncertainties imposes that a larger number of sites is used. In general one can expect that comparing the sites which are nearest to each other, on the length scale of the deformation, leads to neglect the contribution of other sites which have a coherent signal. On the other hand, including sites spread on a large area relative to the scale length of the deformation, will tend to attenuate the deformation signal due to the loss of coherence. Consequently, for each seismic province containing a number of GNSS sites there must exist a typical distance defining an area of maximum coherence. Because the distribution of the GNSS sites is not optimized on the fault geometries, it is necessary to examine case by case the area on which the computation of horizontal deformation can be meaningfully carried out. Following previous work (Caporali *et al.*, 2011), in this paper we adopt least squares collocation as an optimal algorithm to map velocity into strain rate. This algorithm requires a covariance function with zero derivative at the origin and going to zero ad infinite distance. The scale distance of the fall off needs to be determined by the data themselves, as it is a statistical indication of the coherence of their signal content.

Because we are interested in deformation, we propose the use of the maximum shear strain rate (Savage and Simpson, 1996) as a coherence indicator. For example, for any given GNSS site of known velocity we compute by least squares collocation the shear strain rate using a covariance function with scale distance varying from 10 to 100 km at steps of say 10 km. We expect that the curve of the shear strain rate as a function of the scale distance is bell shaped, with the maximum at the scale distance which defines the maximum coherence. Failure to do so can be interpreted as an area subject to negligible deformation, or an area which is undergoing deformation but is occupied by GNSS sites unable to pick up the deformation. As a consequence, we discard sites for which the shear strain rate as a function of the correlation distance is not bell shaped, or such that within the optimal correlation distance there are less than three additional sites of known velocity.

The analysis of the velocities is made with a Matlab program. As input a file containing latitude, longitude, velocities in north, east, up and their standard deviations, and name of the GNSS site is required.

Least squares collocation is a minimum variance algorithm based on the mathematical model in Eq. 1:

$$\begin{bmatrix} v_n \\ v_e \end{bmatrix}_P = \sum_s C(d_{P,s}) \sum_{s'} \left[ C(d_{s,s'}) + W_{ss'} \right]^{-1} \cdot \begin{bmatrix} v_n \\ v_e \end{bmatrix}_{s'} \quad s, s' = station \quad indeces$$

$$\begin{bmatrix} \sigma^2{}_n \\ \sigma^2{}_e \end{bmatrix}_P = \left\{ I - \sum_s C(d_{P,s}) \sum_{s'} \left[ C(d_{s,s'}) + W_{ss'} \right]^{-1} C^T(d_{P,s'}) \right\} \cdot \begin{bmatrix} \sigma^2{}_n \\ \sigma^2{}_e \end{bmatrix}_{s'} \tag{1}$$

$$W_{ss'} = \frac{\frac{1}{\sigma^2{}_s}}{\sum_{s''} \frac{1}{\sigma^2{}_{s''}}} \delta_{ss'} \qquad C(d) = \frac{1}{1 + \left( \frac{d}{d_0} \right)^2}$$

Given a covariance function C(d), for example isotropic, dependent on the squared distance between any two points, the unbiased north and east velocity components at site P are computed by a weighted average of the velocities of all the GNSS sites, with weight dependent on the formal uncertainties of the measured velocities and the relative distance between the computation point and the contributing GNSS site. The velocities of the GNSS sites are assumed uncorrelated, so that the weight matrix W is diagonal. Eq. 1 represents the algorithm used to interpolate the scattered velocities of the GNSS sites to any point P within the network, and estimate the variance of the interpolated velocity, given the variances of the measured velocities (Caporali *et al.*, 2013).

To map the velocities into strain rates it is sufficient to differentiate the first equation in Eq.1 with respect to the north and east components:

$$\begin{bmatrix} v_{n,n} & v_{n,e} \\ v_{e,n} & v_{e,e} \end{bmatrix}_P = \sum_s \begin{bmatrix} \frac{\partial C}{\partial n} & \frac{\partial C}{\partial e} \\ \frac{\partial C}{\partial n} & \frac{\partial C}{\partial e} \end{bmatrix}_{P,s} \sum_{s'} \left[ C(d_{s,s'}) + W_{ss'} \right]^{-1} \cdot \begin{bmatrix} v_n \\ v_e \end{bmatrix}_{s'} \quad s, s' = station \quad indeces \tag{2}$$

We then obtain the strain rate matrix in geographical coordinates. The eigenvalues and eigenvectors are finally obtained by matrix diagonalization:

$$\dot{\varepsilon}_1 = \frac{v_{n,n} + v_{e,e}}{2} + \sqrt{\left( \frac{v_{e,e} - v_{n,n}}{2} \right)^2 + \left( \frac{v_{e,n} + v_{n,e}}{2} \right)^2}$$

$$\dot{\varepsilon}_2 = \frac{v_{n,n} + v_{e,e}}{2} - \sqrt{\left( \frac{v_{e,e} - v_{n,n}}{2} \right)^2 + \left( \frac{v_{e,n} + v_{n,e}}{2} \right)^2} \tag{3}$$

$$\sin 2\theta = \frac{v_{e,n} + v_{n,e}}{\dot{\varepsilon}_2 - \dot{\varepsilon}_1}; \cos 2\theta = \frac{v_{e,e} - v_{n,n}}{\dot{\varepsilon}_1 - \dot{\varepsilon}_2}$$

We take as positive the extensional strain rate and negative the compressional strain rate. The variances of the contributing velocities can likewise bemapped into variances of the strain rate components. In this way a control of the error propagation can be kept in a consistent manner.

As mentioned earlier, we constrain the scale distance $d_0$ in the covariance function by imposing that the shear strain rate, in the sense of Savage and Simpson (1996) is maximized:

$$\dot{\varepsilon}_g = \max(\dot{\varepsilon}_1, \dot{\varepsilon}_2, |\dot{\varepsilon}_1 + \dot{\varepsilon}_2|) \qquad (4)$$

This is accomplished by repeating, at each point, the calculation of the shear strain rate (Eq. 4) for values of $d_0$ spanning a range, e.g. 10-100 km, and choosing the value that maximizes the shear strain rate. A check is made that at least three GNSS sites exist within the selected scale distance from the computation point.

**Combining geodetic and seismologic data.** Once a reasonably detailed map of the deformation rates has been obtained on a regional scale by geodetic method, it is natural to ask how and to which extend this deformation does correlate with the statistical seismicity of the area. This theme is of particular relevance at this time, when finite element models of deformation at depth and at the surface are becoming available for the entire Mediterranean Region (Carafa *et al*., 2015), and models of seismic hazard include geodetic data (Slejko *et al.,* 2010; Cenni *et al.,* 2015). To this purpose the 36 Seismic Zones ZS9 of Meletti *et al*. (2008) (http://zonesismiche.mi.ingv.it/App2.pdf) are particularly useful, as a seismic catalogue is associated with each of them (Gruppo di Lavoro CPTI04, 2004). Consequently the Gutenberg Richter parameters of the statistical formula expressing the yearly number of events in the magnitude range (m, m+dm) as a function of magnitude m in each ZS9 are available. Caporali *et al*. (2011) have shown how the statistical seismicity, maximum expected magnitude and geodetic shear strain rate can be used, in conjunction with the empirical formulas of Wells and Coppersmith (1994) for rupture area and average displacements, to set an upper limit to the average stress drop which is to be expected in a given province.

The basic idea is to compute the strain rate associated to seismicity using the Gutenberg Richter parameters of that province, the empirical relations between magnitude m and Rupture Area (RA) and Average Displacement (AD) of Wells and Coppersmith (1996), and a maximum expected magnitude $m_{max}$. In our case we identify a seismic province with each of the 36 Seismic Zones of Meletti *et al*. (2008), we assume the b value and maximum catalogue magnitude as in Gruppo di Lavoro CPTI04 (2004) and assume that the maximum expected magnitude as equal to the maximum catalogue magnitude + 0.3. The a-value is computed for each seismic zone from the catalogue data, assuming the published b-value labeled b Co-04.4 (Caporali *et al*., 2011).

Imposing that the geodetic strain rate is not smaller than the seismic strain rate, computed with the Kostrov formula (Kostrov and Das, 1988) yields an upper limit on the static stress drop $\Delta\sigma$ of the seismic province:

$$\Delta\sigma \leq \Delta\sigma_g \equiv \frac{2\mu\dot{\varepsilon}_g}{10^{a_s}} \frac{10^{[a_{wc}+b_{wc}m_{max}]}-10^{[a_{wc}+b_{wc}m_{min}]}}{10^{[a_{wc}+(b_s+b_{wc})m_{max}]}-10^{[a_{wc}+(b_s+b_{wc})m_{min}]}} \frac{b_s+b_{wc}}{b_{wc}} \qquad (5)$$

where $a_{WC}=a_{RA}+a_{AD}$ and $b_{WC}=b_{RA}+b_{AD}$('WC' stands for 'Wells and Coppersmith'), m is the shear modulus (assumed 30 GPa) and $a_s$, $b_s$ are the Gutenberg Richter parameters of the seismic province .

This estimate of the static stress drop can be made at any point of a seismic province, and can serve as term of comparison for the stress drop computed from strong motion spectra of individual earthquakes.

**Interface to the DISS 3.1.1.** The output of the analysis is generated in tabular and pictorial form. Of particular interest are the kml files for use with Google Earth, as the output data can be visualized in conjunction with other layers, such as the DISS 3.1.1 of INGV (Basili *et al*., 2008). We remark that the scale of the plotting symbols has been optimized for a close-up visualization. Figs. 1-3 provide a full scale visualization so that the symbols appear small.

Fig. 1 shows an example of the ETRF2000 horizontal velocities of permanent GNSS sites in Italy and surrounding areas. For each site a GE 'balloon' is available, with all the relevant information. These include name, coordinates, velocities and standard deviations, principal strain rates (extension, compression, azimuth, shear and their uncertainties), the scale distance

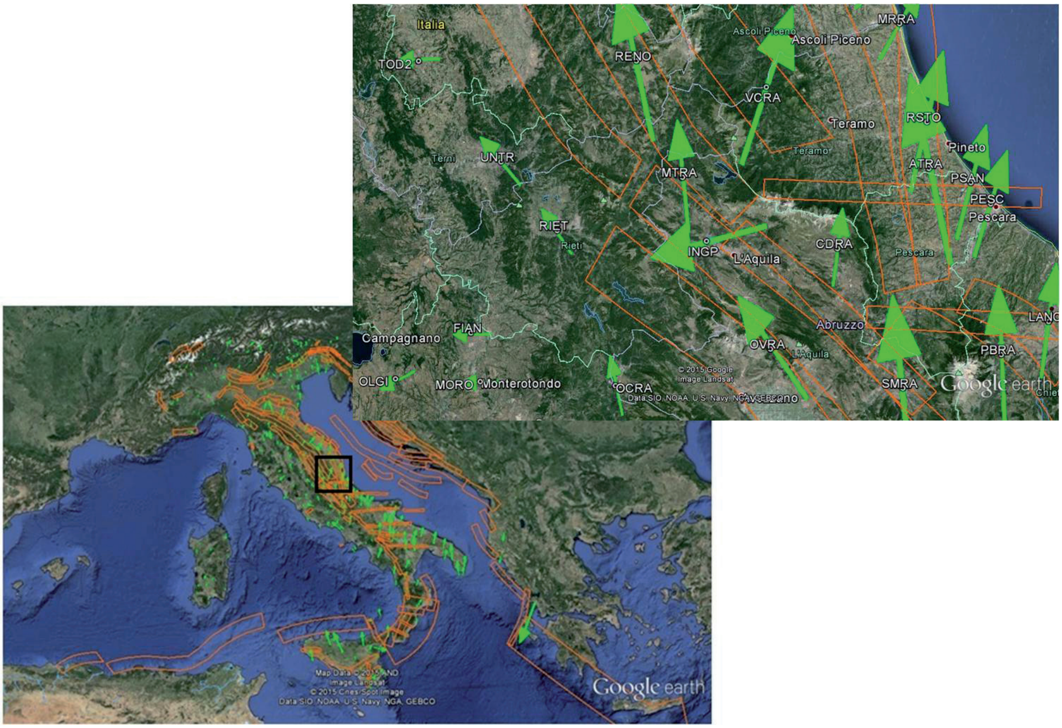


Fig. 1 – Map of horizontal velocities in the ETRF2000 frame (a); zoom on the area of L'Aquila (b).

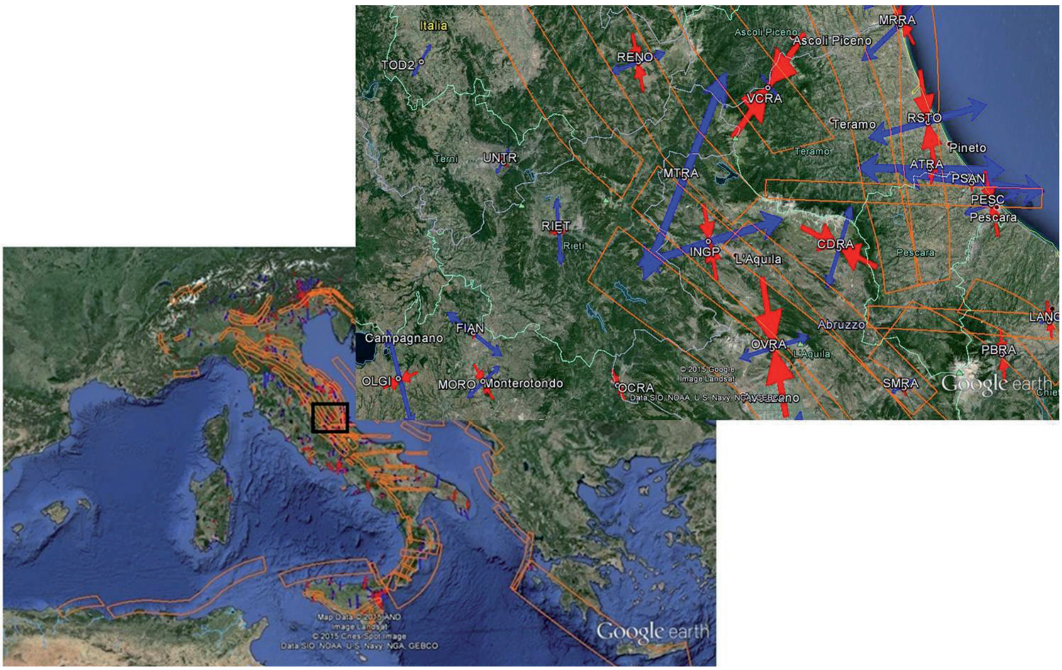


Fig. 2 – Map of the horizontal strain rates (red: compression; blue: extension) (a); zoom on the area of L'Aquila (b).

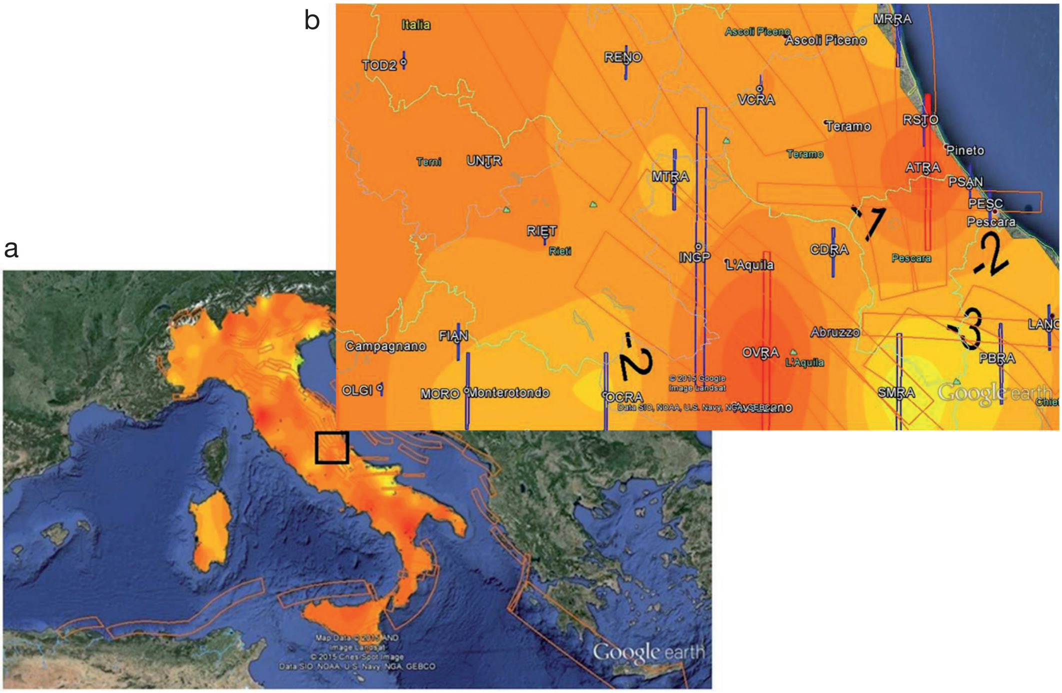


Fig. 3 – Map of the interpolated vertical movements (a); zoom on the area of L'Aquila (b).

used in the covariance function and the number of GNSSsites within that distance. We also provide links to the time series of that site and to the logsheet in IGS format. These logsheets are archived at the EPN Central Bureau, to emphasize that the Italian network is seen as a densification of a larger network on a European scale. Fig. 1 also shows as additional layer the geometry of the Composite Sources, as described in the DISS 3.1.1 DataBase.

Fig. 2 shows for the same area the deformation rates, computed at each site which satisfies our statistical criteria of reliability. The compressional strain ratesare marked in red and extension in blue.

Fig. 3 gives a contour map (in mm/yr) obtained by interpolating on a regular grid the vertical velocities of the GNSS sites and using the coastal profile as a mask. The map of individual velocities is also available as aseparate layer.

**Downloadable kml files.** We make available the following kml files, which are regularly updated every week together with the weekly processing of the network.

- italstrain.kml: map of the compressional and extensional eigenvalues of the strain rate tensor at the GNSS sites
- ital_hor_vel.kml; ital_ver_vel: horizontal and vertical velocities measured at the GNSS sites
- contour_vertical.kml: contour map of the vertical motion, in mm/yr., blanked outside the coastal line
- italstrain_balloon.kml: the balloon associated to each GNSS site, containing the numeric data and ancillary information (link to time series, station logsheet, contact, last update).

**Conclusions.** We have synthetically presented an updated database for velocities of 415 permanent GNSS stations in the Italian territory and the implied deformation maps. A basic feature of this work is the full compliance with the latest Guidelines as to processing techniques and reference frame, ensuring the maximum accuracy. Likewise the computation of the implied deformation rates is based on statistical algorithms which enable full error control and take into account the coherence properties of the input data, at different wavelengths, as an attempt to track the variable scale of the deformation. The interface visualization based on Google Earth enables a layering with other data bases which are particularly relevant, in particular the DISS of INGV.

**Acknowledgment.** This work is supported in part by a grant from the Cartographic Office of the Regione Veneto.

**References**

Basili, R., Valensise, G., Vannoli, P., Burrato, P., Fracassi, U., Mariano, S., Tiberti, MM., 2008. The database of individual seismogenic sources (DISS) version 3: summarizing 20 years of research on Italy's earthquake geology. Tectonophysics 453, 20-43, doi: 10.1016/j.tecto.2007.04.014

Boucher, C., Z. Altamimi, 2011. Memo : Specifications for reference frame fixing in the analysis of a EUREF GPS campaign V.8 http://etrs89.ensg.ign.fr/memo-V8.pdf

Bruyninx, C., Altamimi, Z., Caporali., A., Kenyeres, A., Stangl, G., and Torres, J.A., 2013. Guidelines for EUREF Densifications, vers.5, available online at ftp://epncb.oma.be/pub/general/Guidelines_for_EUREF_Densifications.pdf.

Caporali, A., 2003. Average strain rate in the Italian crust inferred from a permanent GPS network I. Statistical analysis of time series of permanent GPS stations. Geophysical Journal International, 155, 241-253.

Caporali, A., S. Barba, M. M. C. Carafa, R. Devoti, G. Pietrantonio, and F. Riguzzi, 2011. Static stress drop as determined from geodetic strain rates and statistical seismicity. J. Geophys. Res. 116, B02410, doi:10.1029/2010JB007671.

Carafa, M. C., S. Barba P. Bird 2015. Neotectonics and long-term seismicity in Europe and the Mediterranean region. J. Geophys. Res. Solid Earth 120/7 5311–5342 doi: 10.1002/2014JB01175

Cenni, N., E. Mantovani, P., Baldi M. Viti, 2012. Present kinematics of Central and Northern Italy from continuous GPS measurements. J. of Geodyn. 58, 62-72

Cenni, N., M. Viti, E. Mantovani, 2015. Space geodetic data (GPS) and earthquake forecasting: examples from the Italian geodetic network. Bollettino di Geofisica Teorica ed Applicata 56/2, 129-150

Dach, R., Hugentobler, U., Fridez, P., and Meindl, M., 2013. Bernese GPS Software 5.2 vers. 2013-07-18, available at http://www.bernese.unibe.ch/.

Gruppo di lavoro CPTI04, 2004. Catalogo parametrico dei Terremoti Italiani, versione 2004 (CPTI04), INGV, Bologna ed. by P. Gasperini, R. Camassi, C. Mirto and M. Stucchi, (http://emidius.mi.ingv.it/CPTI04/)

Inspire Working Group on Coordinate Reference Systems, 2009 http://inspire.ec.europa.eu/documents/Data_Specifications/INSPIRE_DataSpecification_RS_v3.2.pdf.

Kenyeres, A., 2014.European Dense Velocity Field Based on the Integration of the National Active GNSS Network Products, Paper presented at the 2014 EUREF Symposium, available online *http://www.euref.eu/symposia/2014Vilnius/03-07-Kenyeres.pdf*.

Kostrov, B.V., Das, S., 1988. Principles of Earthquake Source Mechanics, Cambridge University Press, Cambridge, UK, 286 pp.

Lidberg, M., Altamimi, Z., Bruyninx, C., Caporali, A., Dousa, J., Fernandes, R.M., Kenyeres, A., Stangl, G., Steffen, H., 2014. The EPN Working Group on Deformation Models, Paper presented at the 2014 EUREF Symposium, available online http://www.euref.eu/symposia/2014Vilnius/03-01-Lidberg.pdf.

Meletti, C., Galadini, F., Valensise, G., Stucchi, M., Basili, R., Barba, S., Vannucci, G., Boschi, E., 2008. A seismic source model for the seismic hazard assessment of the Italian territory. Tectonophysics, 450, 85-108.

Nocquet, J.M., 2012. Present-day kinematics of the Mediterranean: A comprehensive overview of GPS results. Tectonophysics 579, 220-242.

Rebischung, P., 2012: IGb08: an update on IGS08, IGSmail 6663, http://igscb.jpl.nasa.gov/pipermail/igsmail/2012/007853.html.

Savage, J.C, Simpson, R.W., 1996. Surface strain accumulation and the seismic moment tensor. Bull. Seism. Soc. Am. 87, 1345-1353.

Serpelloni E., Anzidei, M., Baldi., P., Casula, G., Galvani, A., 2005. Crustal velocity and strain-rate fields in Italy and surrounding regions: new results from the analysis of permanent and non-permanent GPS networks. Geophysical Journal International 161, 861-880.

Slejko, D., A. Caporali, M. Stirling, S. Barba, 2010. Occurrence probabilityof moderate to largeearthquakes, J. Seismol., 14, 27–51,doi:10.1007/s10950-009-9175-x.

Wells, D.L., Coppersmith, K.J., 1994. New empirical relationships among Magnitude, Rupture Length, Rupture Width, Rupture Area and Surface Displacement, BSSA 84, 974 – 1002.

Williams, S.D.P., 2003. The effect of coloured noise on the uncertainties of rates estimated from geodetic time series. J. of Geod., 76, 483–494.

# THE GPS VERTICAL KINEMATIC PATTERN IN THE ITALIAN PENINSULA: CHARACTERISTICS AND ANTHROPOGENIC – GEODYNAMIC IMPLICATIONS

**N. Cenni[1], P. Baldi[1], M.E. Belardinelli[1], S. Gandolfi[2], F. Loddo[3], E. Mantovani[4], M. Viti[4]**
*[1] Dipartimento di Fisica ed Astronomia, Università degli Studi di Bologna, Italy*
*[2] Dip. di Ingegneria Civile, Chimica, Ambientale e dei Materiali (DICAM), Università degli Studi di Bologna, Italy*
*[3] Istituto Nazionale di Geofisica e Vulcanologia, Sezione di Bologna, Italy*
*[4] Dipartimento Scienze Fisiche, della Terra e dell'Ambiente, Università degli Studi di Siena, Italy*

**Introduction.** The reconstruction of the present vertical kinematic pattern in the Italian peninsula is the aim of this work. The area is characterized by a complex tectonic setting driven by the interaction of Eurasian, Anatolian – Aegean, and African plates. Therefore the present kinematic patter observed in the area is principally driven from these geodynamic deformation. The most important sedimentary area are interested by natural subsidence and, in some cases by important anthropogenic phenomena, as for example groundwater pumping from a shallow well-developed multiaquifer system and gas production from onshore and offshore reservoirs, which introduce displacements superimposed to the tectonic ones. The magnitude of these anthropogenic displacements, especially in the vertical component, can be comparable or higher than the tectonic contribute and are characterized to important spatial and time variations. In order to reconstruct the present vertical kinematic pattern and its spatial and time variation we have analyzed the GPS observation acquired at several permanent stations located in the Italian peninsula and surroundings. The relatively high density of this network can provide a detailed spatial description of these movements. The relatively long observation time span (larger than 5-6 years) of several sites included in the network considered can give the possibility to investigate the existence and the magnitude of possible time variation in the vertical kinematic field. In some regions, as for example the Po Plain, the monitoring of the subsidence phenomena is realized by public Institutions as I.G.M.I. (Istituto Geografico Militare Italiano) or A.R.P.A. - E.R. (Agenzia Regionale per la Prevenzione e l´Ambiente dell´Emilia-Romagna) by different techniques: leveling, SAR and vertical extensometer. This, provide the possibility to combine and compare the results obtained analyzing GPS data with ones obtained with other techniques in the selected areas.

**Data analysis.** The present velocity field in the Italian peninsula and surroundings has been estimated using the GPS daily observation acquired with a sampling rate of 30 s from 632 permanent stations (Fig. 1). We have analysed the entire data set from January 1, 2001 to April 10, 2015. The phase and pseudo-code data of each continuous GPS site have been analysed by GAMIT software, version 10.4 and following (Herring *et al.,* 2015a) adopting a distributed procedure (Dong *et al.,* 1998). The whole network has been divided into 43 clusters, following a simple geographic criterion, while maintaining the shortest baseline as possible. The observation of the following common stations: AJAC, BRAS, CAGL, GRAZ, IENG, MATE, NOT1, WTZR e ZIMM (Fig. 1) have been included in each cluster. Loose constraints (100 m) have been assigned to the daily position coordinates of each station belonging to all clusters. The International GPS service for Geodynamics (IGS) precise orbital solutions from Scripps Orbit and Permanent Array Center have been included in the processing with tight constraints, such as the Earth Orientation Parameter. The Phase Centre Variation (PCV) absolute corrections for both ground and satellite antennas are included. The daily loosely constrained solutions of the 43 clusters obtained after GAMIT processing are combined into a unique solution by the GLOBK software (Herring *et al*., 2015b) and aligned into the ITRF2008 reference frame (Altamimi *et al*., 2012) by a weighted six parameters transformation (three translations and three rotations), using the ITRF2008 coordinates and velocities of the following 13 high-quality common IGS stations: BUCU, CAGL, GRAZ, IENG, LAMP, MARS, MATE, PENC, SFER, SOFI, TLSE, VILL, WTZR,YEBE and ZIMM (inset in Fig.1).

At the end of this procedure, the daily time series of the north, east and vertical geographical position components of each site included in the analysis are estimated. In order to obtain a

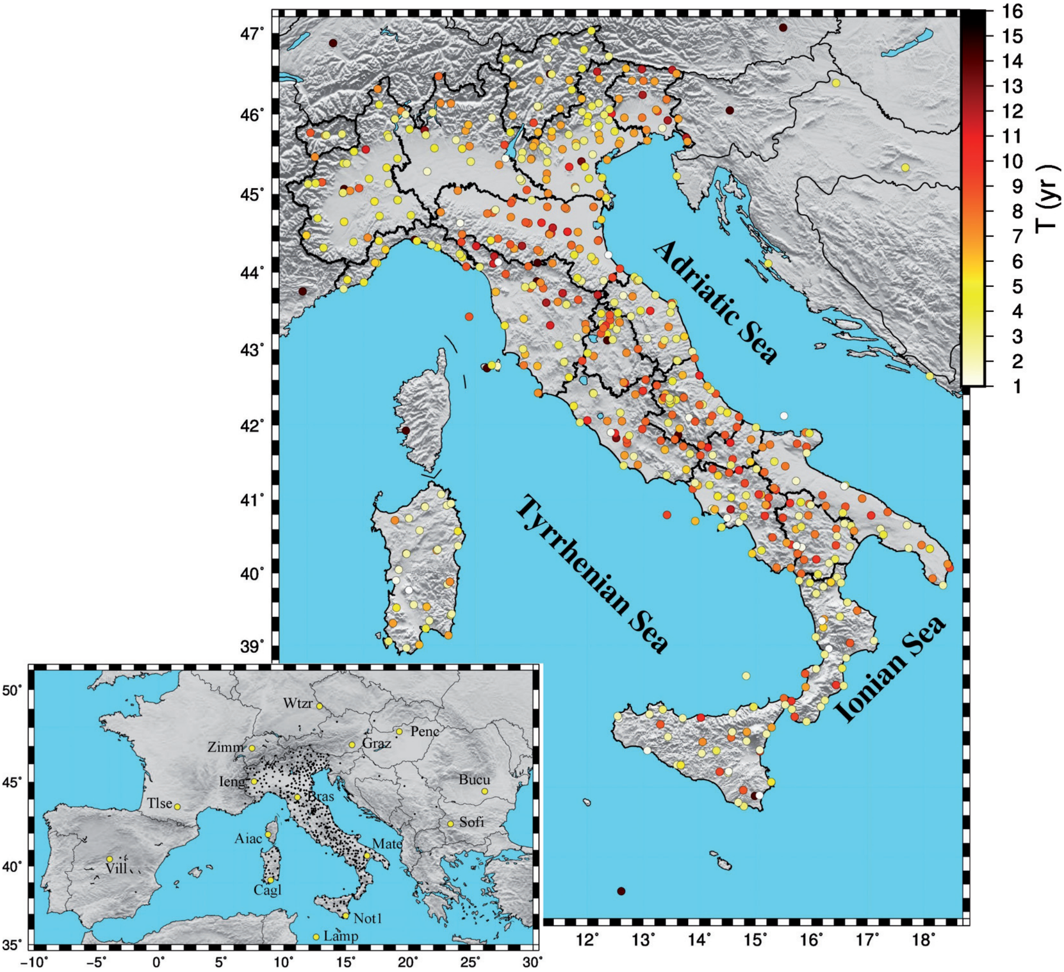


Fig. 1 – Locations of the permanent GPS stations used in this work. The colour of the circles indicate the observation time span of each single site considered, following the chromatic scale on the right. The inset shows the 13 IGS stations we have used to align the network here analyzed to the ITRF2008 reference frame (Altamimi *et al.*, 2012) and the common stations used in the distributed procedure.

reliable estimation of: average velocity, amplitude and periods of seasonal signals and noise the time series of the three position components are analysed with the same procedure as described in Cenni *et al*. (2012, 2013). This procedure is subdivided into the following five steps:

1 data cleaning: time series have been preliminarily analyzed in order to detect and remove outliers. We have considered as outlier the data with value or associated uncertainties greater than 3 times the weighted root mean square (wrms) of the series. The outlier epochs have been identified separately in each coordinate direction and then applied to all three components;

2 preliminary estimation: the time pattern of the daily position component $y_{1k}(t)$ ($k$=1, 2, 3, for the north, east and vertical component) has been modelled by the following relation:

$$y_{1k}(t_i)=A_{1k}+v_{1k}t_i+\sum_{j=1}^{N} g_{1kj}H(t_i-T\,j) \qquad (1)$$

where $A_{1k}$ and $v_{1k}$ are, respectively, the intercept and trend (or velocity) of the best fitting straight line, the $g_{1kj}$ terms are the $N$ instrumental or seismic steps eventually occurred at the $T_j$ epochs, $H$ is the Heaviside step function. These parameters are estimated by a weighted least square method, using as weights the uncertainties associated to the components estimated in the GAMIT processing;

3 spectral analysis: the residual time series obtained modelling the linear motion by means of the parameters estimated in the previous step (Eq. 1), are analyzed with a nonlinear least squares technique to estimate spectra following the Lomb (1976) – Scargle (1982) approach. The spectrum of each component is analyzed in order to estimate the period P of the principal signal, in the interval between seven days and half of the observation time span;

4 parameter estimation: the daily position component $y_{1k}(t)$ ($k$= 1, 2, 3, for the north, east and vertical component) has been modelled with the contribution of the principal periodic signal estimated in the spectral analysis phase. The daily time pattern of each component $y_{2k}(t)$, $k$= 1, 2 and 3 can be re-written as:

$$y_{2k}(t_i) = A_{2k} + v_{2k} t_i + \sum_{j=1}^{N} g_{2kj} H(t_i - T j) + B_{1k} \cos\left(\frac{2\pi t_i}{P}\right) + B_{2k} \sin\left(\frac{2\pi t_i}{P}\right) + \epsilon_k(t_i) \quad (2)$$

where $A_{2k}$ and $v_{2k}$ are the re-estimated intercept and constant velocity and $B_k = \sqrt{B_{1k}^2 + B_{2k}^2}$ is the amplitude of the principal periodic signal P. The $g_{2kj}$ terms are the re-estimated offset magnitudes for the $N$ identified discontinuities due to instrumental changes or seismic events eventually occurred at the $T_j$ epochs, $H$ is the Heaviside step function. As argued in several papers (e.g. Hackl *et al.*, 2011; Bos *et al.*, 2008, 2010; Santamaria-Gomez *et al.*, 2011; Williams, 2004), the noise $\varepsilon_k(t_i)$ in time series can be described as a power law process. Different methods have been developed to characterize noise in GPS time series and its impact on velocity uncertainties (Bos *et al.*, 2013; Hackl *et al.*, 2011; Santamaria-Gomez *et al.*, 2011; Williams, 2008). We have used the reformulated computation method of the Maximum Likelihood Estimation introduced to Bos *et al.* (2013) in order to estimate the characteristics of the noise and the realist uncertainties associated with velocity values.

**Vertical kinematic pattern.** The vertical velocity field shown in Fig. 2 indicates a very heterogeneous kinematic pattern in the Italian area, passing from uplift in most orogenic zones (Alps and Apennines) to subsidence in the Po, Arno and Venetian Plain. In the Alps, the rates are of the order of a few mm/yr, in agreement with previous estimates carried out by repeated levelling in the last century. At present, the uplift of that zone is attributed to the combined effects of tectonic shortening, postglacial isostatic rebound, flexural response to climate-driven denudation and rapid glacier shrinkage.

The permanent stations located on the Apennines chain are characterized by a moderate uplift (or stability) with rates lower than 1-2 mm/yr. This evidence is fairly compatible with the velocity pattern recognized by levelling campaigns performed by the Istituto Geografico Militare Italiano (I.G.M.I.) for about 130 years along routes covering the national territory (D'Anastasio *et al.*, 2006). This last investigation, performed along several lines crossing the chain from the Tyrrhenian to the Adriatic coasts, indicates maximum uplift rates in the range 1-3 mm/yr (under the assumption that most of the Tyrrhenian side of the central-northern Apennines is essentially stable). The uplift of the Apennines is consistent with the effects expected from the longitudinal shortening of the belt suggested to some authors as Mantovani *et al*. (2009, 2015a, 2015b) and Viti *et al*. (2015a, 2015b). Some isolated sites located on the Apennines chain are characterized to negative rates often due to anthropogenic local phenomena, as water pumping for civil and agricultural scope.

The present kinematic pattern observed in the central Apennines sector is also characterized a negative velocities observed from the sites located on the L'Aquila city and in the surroundings.

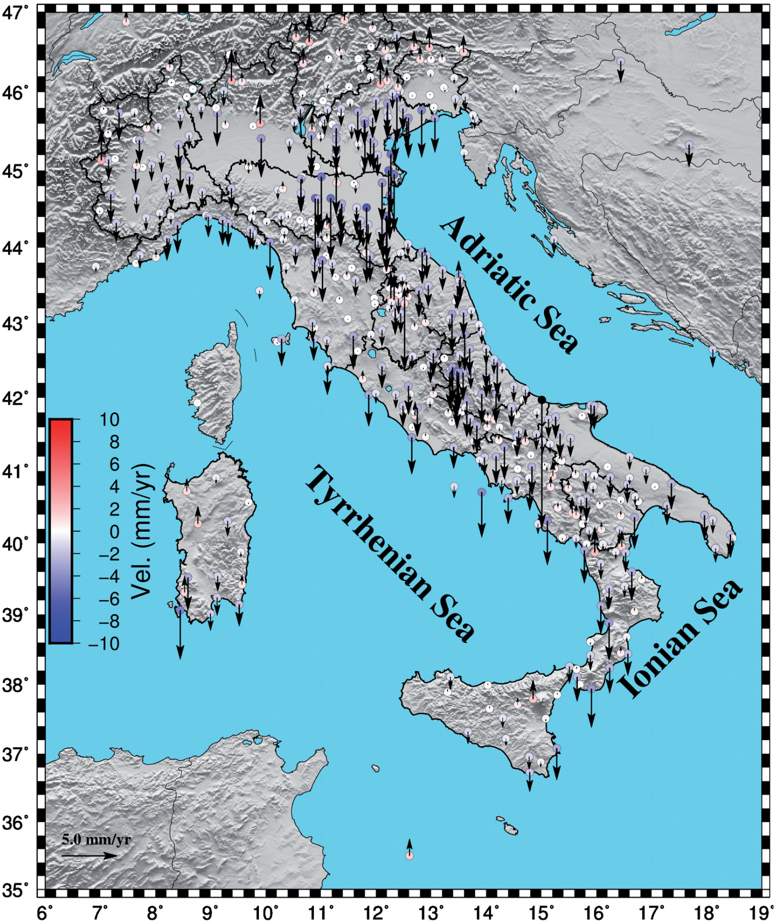


Fig. 2 – Vertical kinematic pattern obtained considering the stations with an observation time span longer than 2.5 years. The colours of circles indicate the velocity amplitudes, following the chromatic scale on the left.

In particular, the velocities of the permanent stations situated on the Tyrrhenian margin indicate stability or uplift, while the sites on the Adriatic sector are characterized with a subsidence pattern. We have formulated different hypothesis in order to explain this particular pattern, the study in order to find the more plausible are still in progress; preliminary results are discussed during the meeting.

Other interesting feature of the present vertical kinematic pattern showed in Fig. 2 it is be represented to the different movements of the sites located on the Tyrrhenian coast respect to the Adriatic sector. The permanent stations located on the first sector are characterized by negative rates between 2-4 mm/yr and the rates of the sites located on Sicily and south Calabrian area seem essentially stable (Fig. 2). Conversely the permanent stations situated on the Adriatic coasts are characterized with negative velocities lower than the Tyrrhenian margin or uplift. The present vertical kinematic fields observed in the Sardinia and Sicily islands are characterized to relatively low uplift, with some isolated sites with negative rates.

The Venetian and Po Valley are mostly characterized by subsidence as shown in Fig. 2. In the first zone, subsidence rates range between 2 and 4 mm/yr, while the highest rates are observed in the eastern sector of the Po Plain (Fig. 3) with rates roughly ranging from 3 to 8 mm/yr. In the western Po Valley vertical negative velocities are instead relatively lower (about 1–3 mm/yr). It can be noted that the transition from subsidence in the eastern zone to low subsidence (or stability) in the western sector fairly corresponds to the Giudicarie fault system and its southwestward prosecution. This relevant difference between vertical movements in the

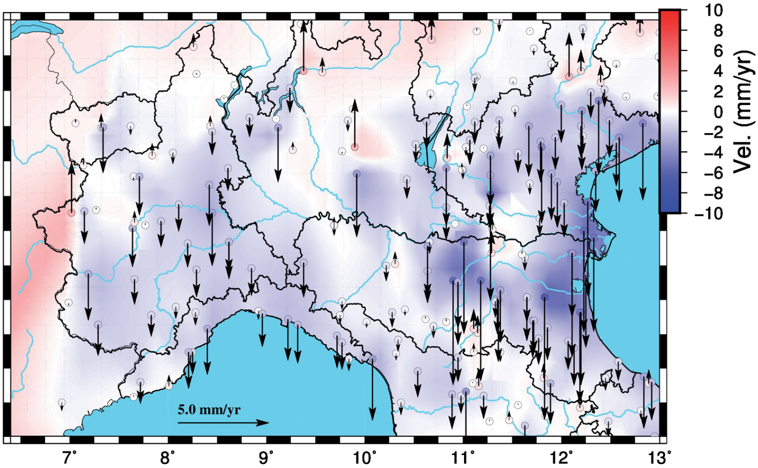


Fig. 3 – The present GPS vertical kinematic pattern in the Po Plain obtained considering the stations with an observation time span longer than 2.5 years. The contour map has been estimated using a geostatistical method over a regular spaced grid (15 km x 15 km). The magnitude of vertical rates can be deduced by the chromatic scale on the right.

two parts of the basin cannot be simply imputed to different anthropogenic effects or to ground settlement (Teatini *et al.,* 2011). The same pattern was highlighted by the results of repeated levelling measurements from 1897 to 1957 (Arca and Beretta, 1985), a period that preceded the strong increase of economic activities in the second half of the XX century. Such observations point out a dominant subsidence in the eastern Po Valley and a prevalent uplift in the western part of the valley. The similarity between the two vertical kinematic patterns, the actual obtained analyzing the GPS data and ones estimated using the data levelling acquired in the first half of XX century seems indicate that the effects of anthropogenic activities on the vertical movements it may be not only causes of this difference. This analysis suggests the existence of a tectonic contribution that produce a not negligible uplift in the eastern sector, as suggest to some authors (Cenni *et al.,* 2013). The comparison between the present kinematic pattern in the eastern sector of Po Plain (Fig. 3) and the results obtained previously with different observation time span and/or techniques (Baldi *et al.,* 2009, 2011; Bonsignore, 2007, 2008; Cenni *et al.,* 2013; Teatini *et al.,* 2013) indicates that the rates are stable or in some cases are decreasing. During the meeting we present the first results about a study regarding the time variation of the vertical velocity values observed in the Po Plain and possible correlations with tectonic processes, or other natural phenomena (e.g. changes in the rainfall trend) or anthropogenic activities.

**Acknowledgments.** We are grateful to the following Institutions: ASI, ARPA Piemonte, FOGER (Fondazione dei Geometri e Geometri Laureati dell'Emilia Romagna), FREDNET – OGS, LEICA – Italpos, NETGeo – Topocon, Regione Abruzzo, Regione Friuli Venezia Giulia, Regione Liguria, Regione Piemonte, Regine Umbria – Labtopo (University of Perugia), Regione Veneto, RING-INGV, Provincia Autonoma di Bolzano (STPOS), Provincia Autonoma di Trento (TPOS), STONEX, which have kindly made available GPS recordings. The figures have been carried out by the Generic Mapping Tools (Wessel and Smith, 1998).

## References

Arca S. and Beretta G.P.; 1985: *Prima sintesi geodetica-geologica sui movimenti verticali del suolo nell'Italia Settentrionale*. Boll. Geod. Sci. Aff., **44**, 125-156.

Altamimi, Z., Métivier, L. and Collilieux, X.; 2012: ITRF2008 Plate Motion Model. *Journal of Geophysical Research*, **117**, Article ID: B07402. http://dx.doi.org/10.1029/2011JB008930.

Baldi P., Casula G., Cenni N., Loddo F. and Pesci, A.; 2009: *GPS-based monitoring of land subsidence in the Po Plain (Northern Italy)*. Earth Planet. Science Letts., **288**, 204-212, doi:10.1016/j.epsl.2009.09.023.

Baldi, P., Casula, G., Cenni, N., Loddo, F., Pesci, A., Bacchetti, M.; 2011: *Vertical ad horizontal crustal movements in Central and Northern Italy*. Boll.Soc.Geol.It. (Ital. J. Geosci.), **52**, 4, 667-685.

Bonsignore, F.; 2007: *Il monitoraggio della subsidenza a scala regionale in Emilia-Romagna*. Proceedings of the meeting La subsidenza in Emilia-Romagna: Il monitoraggio tramite interferometria satellitare, esperienze a confronto. ARPA, Bologna, Italy. 3 dicembre 2007.

Bonsignore F.; 2008: *Il monitoraggio della subsidenza a scala regionale in Emilia-Romagna*. Arpa Rivista, **1**, 16-17.

Bos M. S., Fernandes R. M. S., Williams S. D. P. and Bastos L.; 2008: *Fast error analysis of continuous GPS observations*. J. Geod., **82(3)**, 157–166, doi:10.1007/s00190-007-0165-x.

Bos M.S., Bastos L. and Fernandes R.M.S.; 2010: *The influence of seasonal signals on the estimation of the tectonic motion in short continuous GPS time-series*. J. Geodyn., **49**: 205–209.

Bos M.S., Fernandes R.M.S., S.D.P. Williams and Bastos ; 2013: *Fast error analysis of continuous GNSS observations with missing data*. J. Geod., **87**: 351–360. doi: 10.1007/s00190-012-0605-0

Cenni N., Mantovani E., Baldi P. and Viti M.; 2012: *Present kinematics of Central and Northern Italy from continuous GPS measurements*. J. Geodyn., **58**, 62-72.

Cenni, N., Viti, M., Baldi, P., Mantovani, E., Bacchetti, M.,Vannucchi, A.; 2013: *Present vertical movements in central and northern Italy from GPS data: possible role of natural and anthropogenic causes*. Journal of Geodynamics, **71**, 74-85. doi: 10.1016/j.jog.2013.07.004.

D'Anastasio, E., De Martini, P.M., Selvaggi, G., Pantosti, D., Marchioni, A., Maseroli, R.; 2006: *Short-term vertical velocity field in the Apennines (Italy) revealed by geodetic levelling data*. Tectonophysics, **418**, 219–234.

Dong D., Herring T.A. and King R.W.; 1998: *Estimating regional deformation from a combination of space and terrestrial geodetic data*. J. Geod., **72**, 200-214.i

Hackl M., Malservisi R., Hugentobler U. and Wonnacott R., 2011: *Estimation of velocity uncertainties from GPS time series: Examples from the analysis of the South African TrigNet network*. J. Geophys. Res., 116, B11404, doi:10.1029/2010JB008142.

Herring T.A., King R.W., Floyd M.A. and McClusky S.C.; 2015a: *GAMIT Reference Manual, GPS Analysis at MIT, Release 10.6*. Department of Earth, Atmospheric and Planetary Sciences, Massachusset Institute of Technology, Cambridge MA.

Herring T.A., Floyd M.A., King R.W and McClusky S.C.; 2015b: *Global Kalman filter VLBI and GPS analysis program,* GLOBK Reference Manual, Release 10.6. Department of Earth, Atmospheric and Planetary Sciences, Massachusset Institute of Technology, Cambridge MA.

Lomb N. R.; 1976: *Least-Squares Frequency Analysis of Unevenly Spaced Data*. Astrophysical and Space Science, 39, pp. 447-462.

Mantovani E., Viti M., Babbucci D. and Tamburelli C; 2009: *A review on the driving mechanism of the Tyrrhenian-Apennines system: implications for the present seismotectonic setting in the Central-Northern Apennines*. Tectonophysics, **476**, 22-40.

Mantovani, E., Viti, M., Babbucci, D., Tamburelli, C., Cenni, N., Baglione, M. and D'Intinosante, V.; 2015a: *Present Tectonic Setting and Spatio-Temporal Distribution of Seismicity in the Apennine Belt*. International Journal of Geosciences, **6**, 429-454. http://dx.doi.org/10.4236/ijg.2015.64034 .

Mantovani, E., Viti, M., Cenni, N., Babbucci, D., Tamburelli, C., Baglione, M. and D'Intinosante, V.; 2015b: *Seismotectonics and Present Seismic Hazard in the Tuscany-Romagna-Marche-Umbria Apennines (Italy)*. Journal of Geodynamics, **89**, 1-14. doi: 10.1016/j.jog.2015.05.001.

Santamaría-Gómez, A., Bouin, M.N., Collilieux, X., Wöppelmann, G.; 2011: Correlated errors in GPS position time series: Implications for velocity estimates, J. Geophys. Res., **116**, B01405, doi:10.1029/2010JB007701.

Scargle J. D., 1982: *Studies in Astronomical Time Series Analysis II. Statistical Aspects of Spectral Analysis of Unevenly Sampled Data*. Astrophysical Journal, **263**, 835-853.

Teatini, P., Tosi L. and Strozzi T.; 2011: *Quantitative evidence that compaction of Holocene sediments drives the present land subsidence of the Po Delta, Italy*. J. Geophys. Res., **116**, B08407, doi:10.1029/2010JB008122.

Teatini, P., Tosi, L., Strozzi, T., Carbognin, L., Cecconi, G., Rosselli, R., Libardo, S.; 2012: *Resolving land subsidence within the Venice Lagoon by persistent scatterer SAR interferometry*. Phys. Chem. Earth, **40/41**, 72–77.

Viti, M., Mantovani, E., Babbucci, D., Tamburelli, C., Cenni, N., Baglione, M. and D'Intinosante, V.; 2015a: *Belt-Parallel Shortening in the Northern Apennines and Seismotectonic Implications*. International Journal of Geosciences, **6**, 938-961. doi: 10.4236/ijg.2015.68075

Viti, M., Mantovani, E., Babbucci, D., Cenni, N. and Tamburelli, C.; 2015b: *Where the Next Strong Earthquake in the Italian Peninsula? Insights by a Deterministic Approach*. Bollettino di Geofisica Teorica ed Applicata, Special Issue. (in press).

Wessel P. and Smith W.H.F.; 1998: *New, improved version of the Generic Mapping Tools released*. Eos Trans. AGU, **79**, 579.

Williams, S.D.P., Bock, Y., Fang, P., Jamason, P., Nikolaidis, R-M., Prawirodirdjo, L., Miller, M., Johnson J.; 2004:. *Error analysis of continuous GPS position time series*, J. Geophys. Res. **109**, B03412, doi:10.1029/2003JB002741.

Williams, S.D.P., 2008. CATS: GPS coordinate time series analysis software, GPS Solutions, **12(2)**, 147–153, doi:10.1007/s10291-007-0086-4.

# COMPLEX GEOMETRIES IN THE PLIO-QUATERNARY SEQUENCE IN THE WEST SARDINIAN MARGIN

**G. Guion[1], A. Del Ben[1], A. Mocnik[1], R. Geletti[2]**
[1] *DMG, University of Trieste, Trieste, Italy*
[2] *OGS, Trieste, Italy*

**Introduction.** During Autumn 2010 the R/V OGS Explora acquired a seismic dataset in the western Sardinian offshore within the framework of the WS10 project (Fig. 1). The acquired profiles covered a wide region between the west Sardinian shoreline and the oceanic Sardo-Provençal basin, crossing the entire Sardinian continental slope and platform. In the continental crust the data explore the entire sedimentary sequence and reach the geological basement, well depicting the rift and post-rift phases. Furthermore, many interesting information were outlined about the Messinian Salinity Crisis (MSC) that produced thick evaporite sequences in the deep basin. In the upper slopes and shelves around the Mediterranean Sea margins, as well as locally in the onshore, the MSC originated the erosional surface known as Messinian Erosional Surface (MES).

In this study we have focalized our analysis upon the Plio-Quaternary (PQ) sequence of the Sardinian shelf and upper slope. The base of the PQ sequence is generally clearly highlighted by the MES or, locally, by a thin seismic package of high amplitude reflectors that has been ascribed to Messinian evaporite of the Gessoso-Solfifera Fm (Geletti *et al.*, 2014). In the continental slope and in the deep basin, the MSC features are generally covered by the typical semi-transparent layer of Lower Pliocene; it, in its turn, is covered by the Upper Plio-Quaternary sediments, characterized by medium/high amplitude reflectors.

Also in the Sardinian shelf we can recognize the semi-transparent Lower Pliocene sequence, often onlapping the MES. It is covered by wavy sediment strata that we ascribe to the depositional and erosional effects of the sea bottom currents (contourites). Locally, the Plio-Quaternary sequence shows very peculiar geometries that need a different explanation. An investigation of the sediment geometries and a correlation with local events have allowed us to hypothesize the relationships between cause and effect of the observed features.

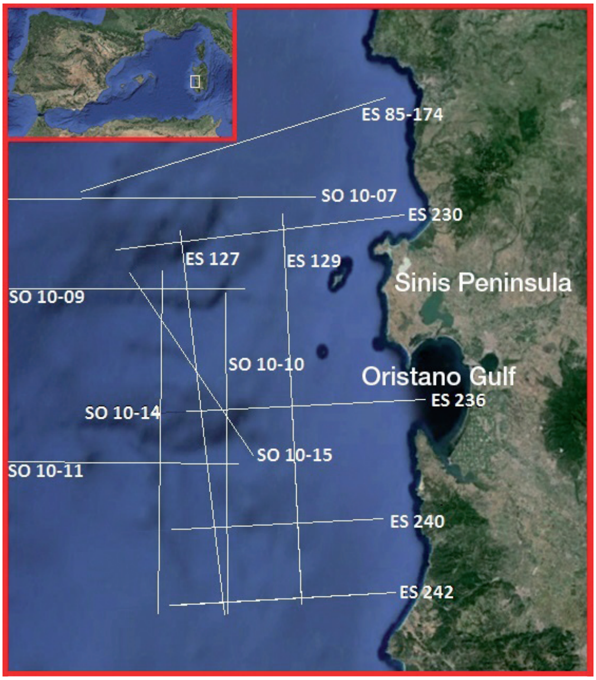


Fig. 1 – Map of the study area and position of the interpreted seismic profiles.

**Geological setting.** *Oligo-Miocene opening of the west Mediterranean basin.* A spreading phase between the African and European plates originated the development of the Tethyan oceanic crust (135 Myr). This process was followed by the subduction of the same oceanic crust and the consequent collision of the African and European plates.

The subduction of the oceanic crust under the European margin took place in the Oligo-Miocene; it is associated with the calc-alkaline volcanism of the Sardinia and with the opening of the back-arc basins of the west Mediterranean Sea. The tectonic process started in the Early Miocene (Maillard *et al.*, 1992) with the opening of the Valencia trough, related to the clock-wise rotation of the Balearic promontory. The rotation of the Corso-Sardinian microplate took place between 30 and 15 Myr (Cherchi and Montadert, 1982) producing the compressional phase of the Apennine Chain, while the north-east sector of the microplates was deformed in the present Calabria massif.

The west Mediterranean lithosphere is characterized by a variable thickness, as shown by seismic and gravimetric studies, which furnish values from 60 km in the oceanic basins to 80 km in the continent. The crustal thickness ranges between 10-15 km in the oceanic basins and 20-30 in the continent. About 16 Myr the Valencia through and the Ligure – Provençal basin were completely opened.

The Ligure-Provençal Basin [or Sardo-Provençal Basin, as called by Geletti *et al*. (2014)] is bounded by two continental margins that show an asymmetry due to the different sedimentary supplies from the French-Spanish and from the Corsica-Sardinian rivers (Geletti *et al*., 2014).

*Messinian Salinity Crisis and MES*. The MSC occurred in the whole Mediterranean Sea during the Late Miocene (5.33-6 Myr). The event was probably originated by the progressive approach of the African and European plates that caused the closure of the Strait of Gibraltar. This event determined a massive evaporation of water and the creation of a hypersaline lake. A salt layer precipitated with a thickness varying from 1.5 to almost 3 km, and an estimated volume of 1 million $km^3$.

In the Sardo-Provençal basin the MSC deposits correspond to an average 1.6 -2.1 km thick sequence of mainly evaporitic lithologies. They are divided, starting from below, in Lower Evaporite (LU), Salt/Mobile Unit (MU) and Upper Evaporite (UU) (Geletti *et al*., 2014). Clauzon *et al*. (1996) suggested that the evaporite precipitation took place in two steps: initially in the peripheral basins, after the first lowering of the sea level; then, a massive precipitation of halite (1.5 km) occurred in the deepest part of the basins. The MES (Margin Erosional Surface, as defined by Lofi *et al*., 2011) is the erosional truncation that affects the upper slope, the continental shelf and the onshore. The UU is covered by the Pliocene sequence that deposited after the end of MSC, when the Strait of Gibraltar re-opened and the water flood again in the Mediterranean basins.

The unconformity MES developed during the emersion of the Messinian or, more often, pre-Messinian sediments. In the Sinis Peninsula, which is the northern onshore of the Oristano Gulf, Messinian evaporitic deposits have been divided by Cornée *et al*. (2008) in four formations: 1) the Basal Marls and 2) the Capo San Marco Formations, both consisting in marls with foraminifers and bioclastic limestones deposited in marine conditions; 3) the Sinis Limestone Formation consisting in micritic limestone deposited under hypersaline lagoon conditions and 4) the Torre del Sevo Limestone Formation, consisting in limestone and dolomitic limestone, interpreted as a fully marine deposit. This last formation was affected by an emersion episode that determined an erosional surface. This sequence is overlain by the Pliocene marine unit.

*Plio-Quaternary sequence*. The Plio-Quaternary sediments of the studied area are fluvial-alluvial type and overlay the MES. Geletti *et al*. (2014) measured a sediment thicknesses from about 400 ms, in the Sardinia slope, to more than 1600 ms, in the deep basin.

The Plio-Quaternary sequence is usually characterized by two typical seismic facies: 1) at its base the Lower Pliocene semi-transparent pelagic marly sequence with volcanic pebbles and 2) the Upper Pliocene/ Quaternary sequence which shows an increased reflectivity (Geletti *et al*., 2014) due to the sediment coarsening. The PQ covers the MES unconformity, or the top of a thin basaltic plateau that was erupted at the end of the MSC (Lustrino *et al*., 2000). The Pliocene basalts are dated back to 5.5 Myr and are related with an extensional tectonics associated with the opening of the southern Tyrrhenian basin (Beccaluva *et al*., 1987; Fais, 1996).

After the Lower Pliocene transgression the area, already involved in the southern branch of the Oligo-Miocene Sardinian Rift, was partially covered by fluvial-alluvial sediments related to the start of the Campidano Graben rifting. A Middle Pliocene-Quaternary prograding complex deposited on the shelf (Fais *et al.*, 1996) and the sea bottom currents assumed a main role. The Upper Pliocene/ Quaternary sediments are generally scarce or absent, while in the western deep basin they are thicker because of the high sedimentation rate related to the rivers crossing the Gulf of Lions (Geletti *et al.*, 2014).

According to Cornée *et al.* (2008) a Pliocene basaltic flow was emplaced on an erosional surface transecting both Messinian and Early Pliocene deposits.

*Plio-Quaternary Magmatism in West Sardinia*. The Sardo-Provençal basin originated by the north-west subduction of the Tethys lithosphere. This caused the Oligo-Miocene calc-alkaline magmatism and the rotation of the Corso-Sardinian microplate, which reached its final stage about 18 Ma ago (Lustrino *et al.*, 2000).

A new volcanic phase took place during the Pliocene - Pleistocene Tyrrhenian opening: in the Sardinian onshore it is divided in two different periods: from 5.3 to 5.0 Myr and from 1 to 0.9 Myr (Lustrino *et al.*, 2000). Large volcanic structures, plateau and basaltic lava flows from individual small volcanoes were produced, with tholeiitic to transitional to alkaline chemistry.

**Seismic processing: multiple attenuation method.** *The multiples problem*. Multiples are signals generated by seismic waves repeatedly reflected between two seismic subsurface discontinuities. This phenomenon occurs when the seismic waves cross geological bodies that are characterized by large variations of the acoustic impedance: therefore, their paths are limited between interfaces with high reflection coefficients. The best example of multiples generation is the water column bounded by a top discontinuity with the air and the base with the sediments. The seismic waves crossing the water layer remain partially “trapped” and the repeated reflections are evidenced in seismic profiles as “ghost” reflectors. They will be not corresponding to real discontinuities present at pertinent depths. The occurrence of this phenomenon can obscure the presence of the primary reflectors, that are the purpose of a seismic acquisition.

Fortunately, the recognition of a multiple reflection shows consistently distinctive characteristics: they are regularly localized at a depth with a not random position and this makes easy their recognition. Furthermore, multiple signals often cross the primary reflectors, and this represents an unrealistic geological condition that suggests the multiple analysis. Finally, the multiple waves travel in shallower/slower sequences relatively to their depth: this allows their identification in velocity spectra.

*Multiple attenuation process applied to the seismic data set*. Since the studied area is sited on the west-Sardinian continental shelf and upper slope, the seismic profiles are affected by a shallow sea bottom. This implies the presence of strong multiple effects on the upper sedimentary sequence, that represent a major noise for the interpretation of data. Therefore we decided to reprocess the profiles to improve the possibility to recognize the primary signals.

In the f-k domain (frequency - wavenumber) the energy of primary and multiple reflections can be separated in two different quadrants (Yilmaz, 2001). To achieve this result we apply a correction of NMO using a velocity intermediate between those of primary and multiple reflectors: the primary signals will be over-corrected, while the multiples will be under-correct. Consequently, the multiples can be suppressed by resetting the dial with values greater than zero.

After the removal of multiples, we have to go back to the x-t domain through the inverse Fourier transform and to remove the incorrect NMO (NMO Removal) used for the primary reflections. At this point a standard process can be applied with all the steps normally used for the seismic processing: Deconvolution, Velocity analysis, correction of NMO and Migration (Fig. 2).

**Seismic interpretation.** Our interpretation of seismic data focused on the Plio-Quaternary sequence.

The base of PQ represents a very important and seismically clear horizon, which is represented by the MSC event. In the upper continental slopes and in the onshore Mediterranean regions the MSC is often highlighted by an erosional truncation caused by the drastic drop of the sea level:

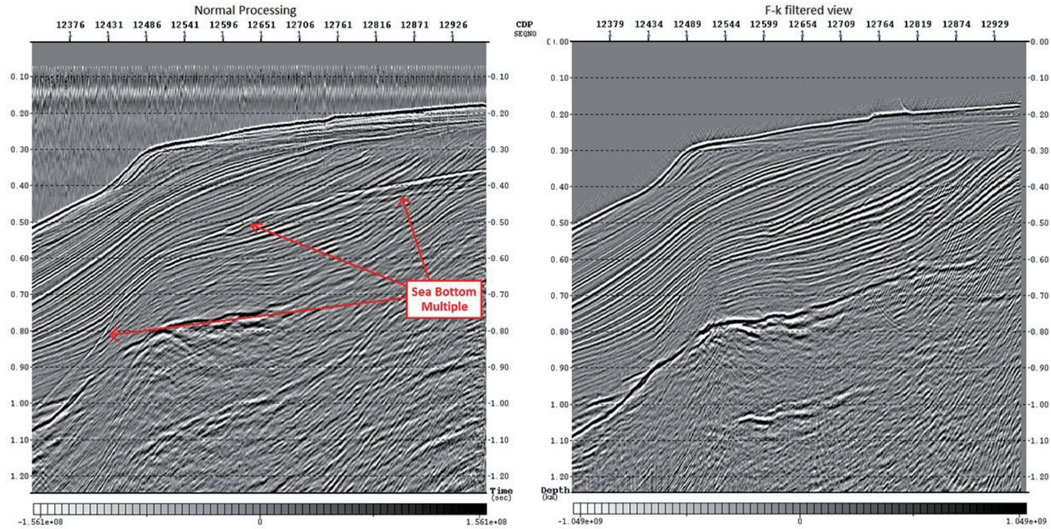


Fig. 2 – Part of stack seismic profile: comparison between the data before and after the multiple attenuated processing.

it is generally recognizable on the base of clear toplap termination. In some shallow basins the MSC is characterized by the deposition of the Gessoso-Solfifera Formation, whose top is generally a high amplitude reflector due to the high contrast of acoustic impedance between the PQ sediments and the gypsum layer. According to this regional conditions, in the west-Sardinian continental slope we recognize (example in Fig. 3) a clear erosional truncation (orange horizon on the left of Fig. 3) or, in any case, a high amplitude reflector which generally lays at the base of the semi-transparent Lower Pliocene. Locally we can see also a high amplitude seismic package that Geletti *et al*. (2014) ascribed to the Gessoso-Solfifera Formation.

Sometimes the MES results to be crossed by some conical buildings, locally outcropping on the sea bottom with a circular section, observed by Geletti *et al*. (2014) in the Mulibeam data and interpreted as volcanic bodies. Generally Lower Pliocene sediments onlap the top of these buildings and they show to be undeformed, so testifying a deposition following the magmatic activity. This magmatic activity could be assigned to the magmatic event occurred between 5.3-5.0 Myr in the SE Sardinian onshore, discussed by Lustrino *et al*. (2000). In some profiles the Pliocene sediments, laying above the volcanic buildings, show a smeared setting: this could be explained by a deformation due to the magmatic intrusion occurred after the deposition. This magmatic activity could be assigned to an event occurred between 0.9 and 0.1 Myr in northern Sardinia, as discussed by Lustrino *et al*. (2000). Also, this attribution would be coherent with the basaltic layer covering a Pliocene calcarenite described by Cornée *et al*. (2008) in the Sinis peninsula (Fig. 1).

As already outlined, a semi-transparent layer can be recognized on the Sardinian continental shelf and upper slope. It has been regionally interpreted on the whole Mediterranean Sea and has been joined to the marls of the Trubi Formation, representing the Lower Pliocene deposition after the re-opening of the Strait of Gibraltar at the end of the MSC. This sequence onlaps or concordantly overlays the MES. It is not homogenously present or recognizable on all the continental shelf, where it tends to thinning or, more often, it changes from the semi-transparent seismic facies to a more reflective package. In view of the total absence of calibrations this could have occurred due to a different sedimentary supply. In particular, we can observe that the higher reflectivity of the Plio-Quaternary sequence corresponds to some geometries characterized by undulations, inclination and changing thicknesses of the strata. Some internal erosional surfaces have been also recognized. These geometries can be related to mound drift, to

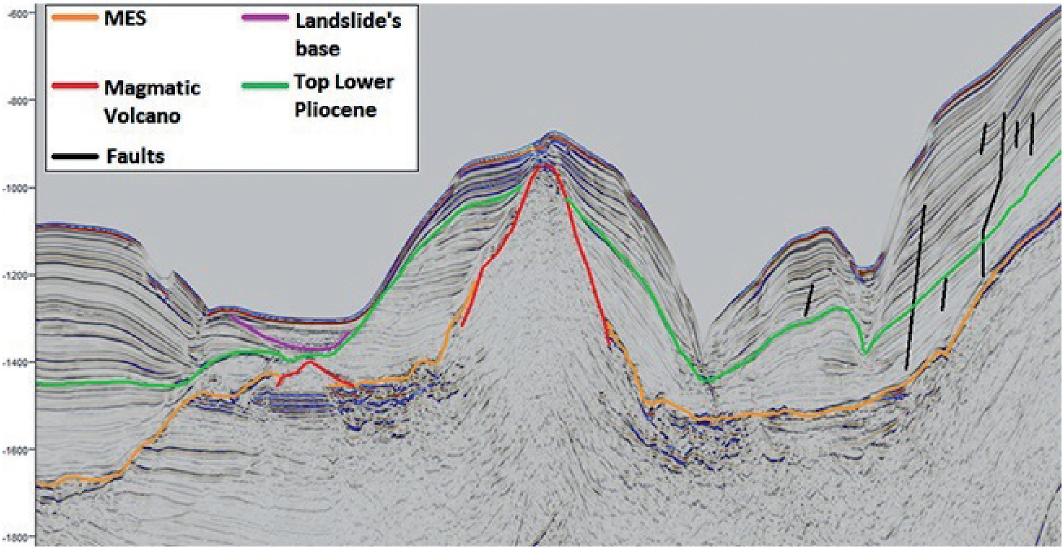


Fig. 3 – Interpreted seismic profile: the MES is clearly evidenced by erosional truncation (on the left) and by the high amplitude reflectors at the top of the Messinian sequence. The semi-transparent Lower Pliocene is covered by the Upper Pliocene/Quaternary sediments which show complex geometry probably due to the sea bottom currents effect. A main volcanic building crosses the PQ sequence and affects the sea bottom.

channel related patch drifts, to migrating sediment waves and internal erosional discontinuities that are attributable to the effects of sea bottom currents.

Along a seismic profile close to the shoreline, some peculiar geometries show a Plio-Quaternary sequence fractured in few blocks rotated over the MES. The inclined horizons seem to be not due to sea bottom currents, but probably to a local tectonic event. We are analyzing it using the Move software through a flattening of the strata and applying retro-deformation techniques. This approach allows the reconstruction of the original setting of the layers and to evaluate the possible correlation with local tectonics produced by a close magmatic event.

In the uppermost sediments some profiles evidence a prograding sequence that is locally evidenced with an enlargement of more than 10 km toward the basin of the continental shelf.

**Conclusion.** On the west Sardinian continental margin some characteristic geometries have been observed into the Plio-Quaternary sequence. Some multiple reflectors affected the seismic profiles caused by the shallow sea bottom in the continental shelf. These multiples were representing a noise partially covering the PQ primary reflectors. For this reason, a re-processing of the seismic data was applied. The de-multiplex processing, based on an f-k filtering, gave an improvement of the seismic signals and a better imaging of the structural features.

The interpretation of the data have highlighted a clear base of the PQ sequence, represented by the MES or, more locally, by the top of the Gessoso-Solfifera Formation. A Lower Pliocene semi-transparent sequence has been recognized in the upper slope and in the shallow platform; it is characterized by a change to a more reflecting seismic facies that has been ascribed to a different sedimentary supply. The overlaying sediments (Upper Pliocene-Quaternary) show a more reflecting facies, often joined to a strong effect of the sea bottom currents. Finally, a prograding sequence is locally present in the northern sector of the studied area, largely developed toward the basin.

The Plio-Quaternary layers are often crossed by some volcanic buildings directly overlaying the MES: their position inside the sediments and the (onlapping or smearing or pinching-out) terminations of the same sediments on the volcanic bodies makes difficult the evaluation of the age of this magmatic activity, regionally ascribed to the Tyrrhenian opening. These buildings on the Oristano offshore are probably associated to the Pliocene magmatic layer outcropping in the adjacent Sinis Peninsula.

A retrodeformation of a complex block geometries, recognized in a Plio-Quaternary marginal basin near the shoreline, seems to suggest a correlation between the fracture system and the coeval magmatic activity.

**Acknowledgements.** The authors gratefully acknowledge OGS-Trieste for the seismic data set used in this work, Shlumberger through the Petrel academic grant for interpretation software and Midland Valley through the Move Software Suite academic grant to the University of Trieste.

**References**

Beccaluva L., Brotzu P., Maciotta G., Morbidelli L., Serri G., Traversa G.; 1987, 80: *Cainozoic tectono-magmatic evolution and inferred mantle in the Sardo-Tyrrhenian area. The lithosphere in Italy*. Advanced in Science Research, Accad. Naz. Lincei, **80**, 229-248.

Cherchi A., Montadert L.; 1982. *Oligo-Miocene rift of Sardinia and the early history of the Western Mediterranean Basin*. Nature, **298**, 736-739.

Clauzon G., Suc J.P., Gautier F., Berger A., Loutre M.F.; 1996: *Alternate interpretation of the Messinian Salinity Crisis: controversy resolved?*. Geology, 24, pp. 363–366.

Cornnée J.J., Maillard A., Conesa G., García F., Saint Martin J.P., Sage F., Münch P.; 2008: *Onshore to offshore reconstruction of the Messinian erosion surface in western Sardinia, Italy: MSC implications*. Sediementary Geology, **210** (1-2), 48-60.

Fais F., Klingele E.E., Lecca L.; 1996: *Oligo-Miocene half graben structure in Western Sardinian Shelf (western Mediterranean): reflection seismic and aeromagnetic data comparison*. Marine Geology, **133**, 293-222.

Geletti R., Zugur F., Del Ben A., Buriola F., Fais S., Fedi M., Forte E., Mocnik A., Paoletti V., Pipan M., Ramella R., Romeo R., Romi A.; 2014: *The Messinian Salinity Crisis: New seismic evidence in the West-Sardinian Margin and Eastern Sardo-Provençal basin (West Mediterranean Sea)*. Marine Geology, **351**, 76-90.

Lofi J., Déverchére J., Gaullier V., Gillet H., Gorini C., Guennoc P., Loncke L., Maillard A., Sage F., Thinon I.; 2001: Seismic Atlas of the "*The Messinian Salinity Crisis" makers in the Mediterranean and Black Sea*. Geological Map of the World Ed., Paris, France.

Lustrino M., Melluso L., Morra V.; 2000: *The role of lower continental crust and lithospheric mantle in the genesis of Plio-Pleistocene volcanic rocks from Sardinia (Italy)*. EPSL, **180**, 259-270.

Maillard A., Mauffret A., Watts A.B., Torné M., Pascal G., Buhl P., Pinet B.; 1992: *Tertiary sedimentary history of the Valencia trough (western Mediterranean)*. Tectonophysics, **203**, 57-75.

Yilmaz O.; 2001: *Seismic Data Analysis*. SEG publication, S.M. Doherty Ed., Tulsa OK, USA.

## ANALYSIS OF GEOLOGICAL, SEISMOLOGICAL AND GRAVIMETRIC DATA FOR THE IDENTIFICATION OF ACTIVE FAULTS IN ABRUZZO AREA (CENTRAL ITALY)

**P. Luiso[1], V. Paoletti[1], G. Gaudiosi[2], R. Nappi[2], F. Cella[3], M. Fedi[1]**

[1] *Dipartimento di Scienze della Terra, Università degli Studi «Federico II», Napoli, Italy*

[2] *Istituto Nazionale di Geofisica e Vulcanologia, Sezione OV, Napoli, Italy*

[3] *Dipartimento di Scienze della Terra, Università degli Studi della Calabria, Arcavacata di Rende (CS), Italy*

**Introduction.** The aim of the study is to identify and better constrain the geometry of the seismogenic structures (active, outcropping and buried fault systems) in the Abruzzo area (central Italy), through an integrated analysis of geo-structural, seismic and gravimetric data.

The studied area is one of the most active zones from a geodynamic point of view of the Italian Apennines, characterized by the occurrence of intense and widely spread seismic activity.

The integrated analysis of structural, seismic and gravimetric data (Gaudiosi *et al*., 2012) of the areas was carried out through the use of Geographic Information System (GIS).

More specifically, the analysis consisted of the following main steps: (a) collection and acquisition of aerial photos, numeric cartography, Digital Terrain Model (DTM) data, geological and geophysical data; (b) generation of the vector cartographic database and alpha-numerical data; c) image processing and features classification; d) cartographic restitution and multi-layers representation.

Three thematic data sets have been generated: "faults", "earthquakes" and "gravimetric" data. The fault dataset was built by merging all Plio- Quaternary structural data extracted from the available structural and geological maps, and many geological studies (Boncio *et al.*, 2004; Galadini *et al.,* 2000, 2003; Falcucci *et al.*, 2011; Moro *et al.*, 2013). The earthquake data set consists of seismic data collected in the available historical and instrumental Catalogues (Gruppo di lavoro CPTI, 2004); CPTI11, Rovida *et al.*, 2011; ISIDE, INGV database). Seismic data have been standardized in the same format and merged in a single data set. As regards the gravimetric data set, we performed a *Multiscale Derivative Analysis* (MDA) of the gravity field, based on the good resolution properties of the *Enhanced Horizontal Derivative* (EHD) signal (Fedi *et al.*, 2005). The main results of our integrated analysis show a good correlation among faults, epicentral location of earthquakes and MDA lineaments from gravity data. Furthermore, 2D seismic hypocentral locations were correlated with the information yielded by the application of the DEXP method to gravity data (Fedi and Pilkington, 2012), to estimate strike, dip direction and dip angle of some faults of the areas.

**Seismotectonic framework of the area.** The central Apennines consists of a Mio-Pliocene thrust-and-fold belt that developed as the result of the convergence between the Hercynian European plate and the westward subducted Paleozoic Adriatic lithosphere (Patacca and Scandone, 2004). The opening of the Tyrrhenian basin and the flexural retreat of the lithospheric plate dipping below the Italian peninsula (Malinverno and Ryan, 1986; Royden *et al.*, 1987; Patacca *et al.*, 1990; Doglioni, 1991; Doglioni *et al.*, 1994) caused the E-W migration of the compressive front and, since the Mio-Pliocene, contemporary extentional tectonics affected the innermost portion of the Apennines chain previously controlled by compressive tectonics. The intra Apennine extension has also been characterized by a progressive northeastward migration determining an age of the extensional tectonic structures, progressively younger heading eastwards (Lavecchia *et al.*,1994; Bartole, 1995; Calamita *et al.,* 1999; Galadini and Messina, 2004). Since Pliocene, and during the entire Quaternary NW–SE trending faults have been responsible for the formation of several half-graben structures that currently match intermountain basins in which Plio-Quaternary continental sediments (up to 1,200 m thick in the case of the Fucino Plain) (Galadini and Messina, 1994) have been deposited. These include the Fucino, L'Aquila, Sulmona, Rieti, Leonessa and Norcia basins.

Normal and normal-oblique faults generally bound these depressions to the northeast. Changes during the Quaternary, however, affected the kinematic evolution of the (Patacca *et al.*, 1990; Cinque *et al.*, 1993; Pantosti *et al.*, 1993) central Apennines and are represented by the end of the activity of some normal faults, and by evidence of oblique-slip kinematics on faults previously characterised by normal movements (Galadini, 1999).To the west and northwest the boundary of the Abruzzi Apennines is represented by the contact between units overlain onto the Latium-Abruzzi carbonate and those belonging to the Umbro-Marchean Apennines; the surface trace of such contact is marked by the Olevano-Antrodoco- Sibillini Line (Patacca *et al.*, 1990; Bigi *et al.*, 1991a; Galadini, 1999; Pizzi and Scisciani, 2000; Centamore and Rossi, 2009; Pizzi and Galadini, 2009; Calamita *et al.*, 2011). East and SE of the Abruzzi Apennines, Oligo-Miocene flysch units of the Molise domain are separated from Latium-Abruzzi units by the Ortona-Roccamonfina Line, (Locardi, 1988; Di Bucci and Tozzi, 1991; Centamore and Rossi, 2009; Pizzi and Galadini, 2009). The persistence of the extensional activity during the Late Pleistocene–Holocene is demonstrated by the present seismicity with earthquakes of magnitudes up to 7.0 in past centuries (Working Group CPTI 2004) and by the numerous studies dealing with active tectonics and paleoseismology. The present tectonic regime shows that the

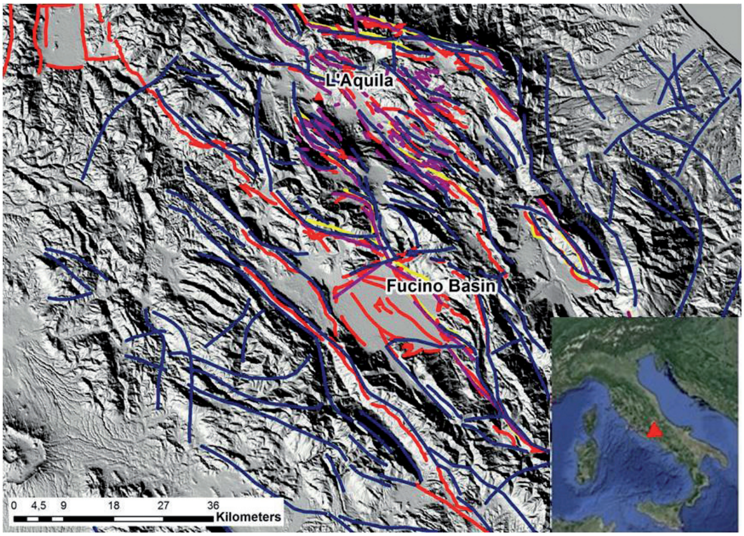


Fig. 1 – Map of the faults extracted from literature. Purple: from the CARG project (ISPRA); blue: from Neotectonic Map of Italy 1:500,000 (Ambrosetti *et al*., 1987); yellow: from Galadini *et al*. (2003); red: from ITHACA project (ISPRA).

Abruzzi Apennines are affected by almost two sets of NW-SE to N-S trending normal faults,. Focal mechanisms, geodetic data and borehole breakouts (Chiaraluce *et al*., 2003; D'Agostino *et al*., 2001; Mariucci *et al*., 1999) characterize the present stress field as NE-SW extension, related to the persistence of the back-arc extension. Such extension, mainly concentrated along the axial belt, generates NW–SE trending, mainly SW-dipping, seismically active normal faults, bounding graben and half-graben basins. Paleoseismological and historical data suggest that almost all the faults of the western fault set activated during historical time while there is no evidence of recent activation for most of the faults related to the eastern set (Galadini and Galli, 2000). For this reason, these structures have been defined as silent and are considered as probable seismic gaps (Galadini and Galli, 2000). The Abruzzi region was affected in the western active sector by large earthquakes in 1349 (Me = 6.5), (Me = 6.5), 1456 (Me = 7.0), 1461 (Me = 6.4), 1654 (Me = 6.1), 1703 (Me = 6.7), 1706 (Me = 6.7), 1762 (Me = 6.0) and 1915 (Mw = 7.0). The January 13, 1915 earthquake is one of the strongest seismic events in Italy, caused 30,000 victims within a large area surrounding the Fucino basin. The last seismic event occurred in the area on the April 6, 2009 (Mw=6.3) killing 309 people. This earthquake struck the town of L'Aquila, after several months of seismic activity focused in the Aquila basin. Thousands of aftershocks have been recorded. The relative hypocenters are located within the upper 10-20 km of the crust (Chiararaluce *et al*., 2011). Seismic activity in this region had been scarce during past few decades, with only three seismic swarms in 1985 (Mw=4.5), 1992 (Mw=3.9) and 1994 (Mw=4.4). The 7 May 1984 (Mw= 5.9) earthquake and its strong 11 May aftershock occurred near the southern end of the study region.

In historical times, the faults of the more external extensional alignment also remained blocked and silent (Galadini and Galli, 2000),with the only exception of the September 5, 1950 event (Mw 5.7) occurred near the city of Teramo. Further to the SE, two relatively large earthquakes occurred on the eastern flank of the Maiella Mt. on November 3, 1706 (Mw 6.6) and on September 26, 1933 (Mw 5.7). According to Lavecchia *et al*. (2010), these earthquakes have both been caused by E-verging reverse faulting underneath the Maiella Mt.

**Data analysis.** The analysis of the available geo-structural, seismic and gravimetric data of the studied area has been carried out under a Geographic Information System (GIS) environment (ArcGis 10.1).

The "fault" data set consists of a merge of the Plio-Quaternary structures extracted from the available geological and structural maps and from scientific papers (Fig. 1). The geological and structural maps of reference for our analysis have been the following: ITHACA catalogue

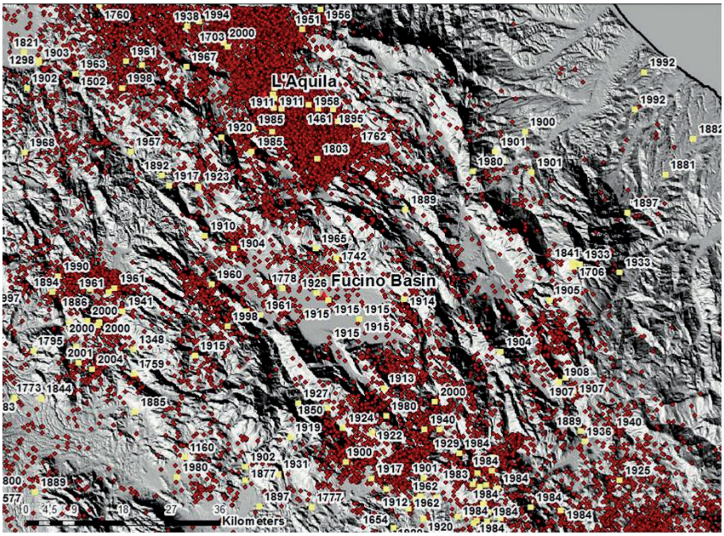


Fig. 2 – Map of earthquakes distribution: from ISIDE catalogue (in red), from CPT111 (in yellow).

(Italy Hazard from Capable Faults, ISPRA *project*), the "Neotectonic Map of Italy", 1:500,000 (Ambrosetti *et al.*, 1987), the geological sheets n.349, Gran Sasso, n.359, L'Aquila, n.368, Avezzano; n.369, Sulmona, 1:50.000 (ISPRA, CARG project); the Geological Map, 1:100,000, Sheet 1 (Vezzani and Ghisetti, 1998); moreover, the dataset was integrated with faults extracted by many scientic papers (Boncio *et al.*, 2004; Galadini *et al.* 2000; Galadini *et al.*, 2003; Falcucci *et al.*, 2011; Moro *et al.*, 2013). The final fault data set consists of the extracted lineaments, in vector format, which have been digitized and geocoded from the original maps in raster format. The selected faults are plotted on the shaded relief map of the Abruzzo area (Fig. 1). We created an associated attribute table containing for each fault: an ID number, geographical coordinates, age, slip rate, bibliography.

The "earthquake" data set includes the seismic events extracted from historical and recent available seismic catalogues (Fig. 2): the CPTI11 (Catalogue of Parametric Italian Earthquakes, Rovida *et al.*, 2011) that contains the historical Italian earthquakes and their seismic parameters (hypocenters; intensity value and equivalent magnitude) from year 1000 to 2006; the CPTI04 (Catalogue of Parametric Italian Earthquakes, Gruppo di Lavoro CPTI, 2004) including the Italian earthquakes and their seismic parameters (hypocenters; intensity value and equivalent magnitude) from year 217 b.C. to 2002; the ISIDE INGV database (Italian Seismological Instrumental and parametric data-base http://iside.rm.ingv.it/iside/standard/index.jsp) that contains all the revised Italian earthquakes recorded by the Italian permanent seismic network and their seismic parameters (hypocenters; intensity value and magnitude) since 1990. The earthquake layer have been created by selecting from the catalogues the seismic events with the best epicentral location. An associated attribute table that includes the date of earthquake, the focal parameters and geographic coordinates for each seismic event was created.

In this study we employed also the information deriving from the analysis of "gravimetric" data.

As known, potential fields may be seen as the superposition of effects due to sources of different depths and extents. The main difficulty to interpret the resulting field is due to the complex reciprocal interference of these different effects (Fedi *et al.*, 2007). To overcome this problem, we used a *Multiscale Derivative Analysis* (MDA), which employs the good resolution properties of the *Enhanced Horizontal Derivative* signal (EHD, Fedi *et al.*, 2005). EHD is a high-resolution edge estimator based on the horizontal derivative of a weighted sum of field vertical derivatives. We used the MDA to interpret the Bouguer anomalies of the central Italian regions. Gravity data extracted from the Bouguer Gravity Anomaly Map of Italy published by

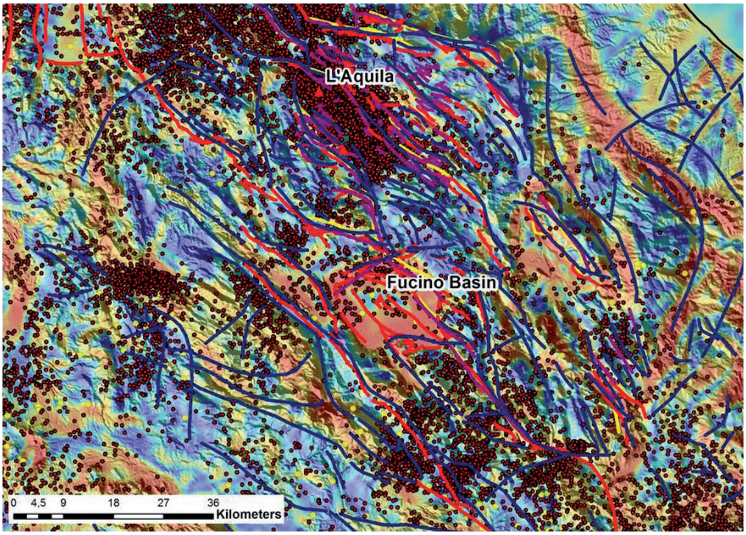


Fig. 3 – Map of three different thematic layers: faults, earthquakes and medium scale MDA overlapped on shaded relief of topography.

CNR (Carrozzo *et al.*, 1986; reduction density: 2.4 g/cm$^3$) were sampled with a step grid of 1 km. By including higher vertical derivatives, a better detail for shallower sources is obtained. For this study we computed MDA at three resolution scales to investigate structures of different depths and extents. However, in this paper the map obtained by computing a medium scale EHD, which yields insights about both shallow and deep structures has been used. A layer of gravimetric lineaments has been created with an associated attribute table in which they were entered, for each maximum MDA value, the correlation with the local topography, the probable fault and earthquakes associated.

The merge of the three different datasets (faults, earthquakes and gravimetric lineaments) in GIS environment is shown in Fig 3. GIS allows us to work with different types of data in a one geographic reference system with the elaboration of thematic information and the creation of 2D and 3D representations of geodynamic phenomena.

The analysis of the map (Fig. 3) shows a good correlation among earthquakes, faults and MDA lineaments along NW-SE and NNW-SSW alignments. These faults may be considered active.

Among the most important tectonic structures recognized in this paper, we have concentrated our investigation on the Fucino and l'Aquila basins. The L'Aquila basin is marked by MDA maxima with NW-SE and NE-SW strikes.

The Fucino basin seem to be surrounded by a series of MDA maxima in the same directions (NW-SE and NE-SW), but more evident. However, the MDA maxima could also be generated by the strong contribution of the topography and so the effect of the faults could be hidden. Thus, it is important to understand if the maxima are created by the topography or by a fault. For example, if we have a strong maximum, but there is no correlation with the topography (such as a relief) the maximum could be generated by a buried or outcropping fault. For this reason we have used the MDA medium scale map, where the topography effect is less evident.

In conclusion this study has highlighted four possible scenarios:

1) the existence of active faults, shown by a strong correlation among the epicentral location of seismic clusters matching the fault and MDA lineaments.
2) the existence of buried active faults, highlighted by a correlation of MDA maximum with an associated spatial distribution of epicentral location, but without correspondence with faults known from geological data;
3) the existence of inactive or silent faults, detected by the presence of faults reported in the geological datasets and literature which are correlated with a MDA maximum, but without correlation of spatial distribution of earthquakes;

4) the existence of faults identified by literature but not correlated with MDA anomaly; this could be due to faults putting in contact two lithologies with a similar density.

**Conclusion.** In this paper we performed a multiparametric data analysis (by integrating seismic, tectonic and gravity data) in the Abruzzo region, central Italy, with the aim of identifying active faults and investigating the neotectonic activity of these areas. As regards gravity data, a *Multiscale Derivative Analysis* (MDA) of the Bouguer anomalies of the areas allowed locating several linear and closed trends and identified new faults whose presence was not previously detected. The main results of the multiparametric analysis suggest a strong correlation among faults, seismicity and the MDA lineaments from gravity data, mainly along NW-SE and NNW-SSW alignments. These faults may be considered active.

Moreover, our study highlighted other possible scenarios as far as the correlation of faults, earthquakes and MDA lineaments is concerned: a) correlation between seismicity and MDA maxima that suggests the presence of buried active faults; b) correlation between faults and MDA maxima that suggests the presence of faults that are no more active; c) correlation between faults and earthquakes that suggests the presence of faults that put in contact two lithologies with similar density. Our results yield new insight into the existence of possible buried active faults, whose knowledge is useful to the definition of the areas' seismic risk.

**References**

Ambrosetti P., Bartolini C., Bosi C., Carraro F., Ciaranfi N., Panizza M., Papani G., Vezzani L., Zanferrari A.; 1987: *Neotectonic Map of Italy (Scale 1:500.000)* - C.N.R., P. F. Geodinamica.

Bartole R.; 1995: *The North Tyrrhenian –Northern Apennines post collisional system; constraints for a geodynamic model*. Terra Nova 7, 7–30.

Bigi G., Castellarin A., Coli M.,. dal Piaz G. V, Sartori R., Scandone P., Vai G. B.; 1991: *Structural model of Italy, scale 1:500,000,* Quad Ric. Sci., 114(3), 1 – 7.

Boncio, P., Lavecchia G., Pace B. ;2004: *Defining a model of 3D seismogenic sources for seismic hazard assessment applications: the case of central Apennines (Italy).* J. Seismol., 8, 407–425, doi:10.1023/B: JOSE.0000038449.78801.05.

Calamita F., Coltorti M., Pieruccini P., Pizzi A.; 1999: *Evoluzione strutturale e morfogenesi plio-quaternaria dell'Appennino umbro-marchigiano tra il preappennino umbro e la costa adriatica.*- Boll. Soc. Geol. It. 118, 125–139.

Calamita F., Satolli S., Scisciani V., Esestime P., Pace B.; 2011: *Contrasting styles of fault reactivation in curved orogenic belts: Examples from the Central Apennines (Italy)*, Geol. Soc. Amer, Bull., 123, 1097-1111. doi: 10.1130/B30276.1.

CARG-ISPRA: Istituto Superiore per la Protezione e la Ricerca Ambientale - *http://sgi.isprambiente.it/geoportal/catalog/content/project/carg.page*.

Carrozzo M. T., Luzio D., Margiotta C., Quarta T.; 1986: *Gravity anomaly map of Italy. Progetto Finalizzato Geodinamica* - Sottoprogetto: Modello Strutturale Tridimensionale: Rome, Italy, CNR

Cavinato G., Carusi C., Dall'Asta M., Miccadei E., Piacentini T.; 2002: *Sedimentary and tectonic evolution of Plio-Pleistocene alluvial and lacustrine deposits of Fucino Basin (central Italy)* - Sediment. Geol., 148, 29–59.

Centamore E., Rossi D.; 2009: *Neogene-Quaternary tectonics and sedimentation in the Central Apennines*. Ital. J. Geosci. (Boll. Soc. Geol. It.), **128** (1), 73-88.

Chiaraluce L., Ellsworth W.L., Chiarabba C., Cocco M.; 2003: *Imaging the complexity of an active normal fault system: the 1997 Colfiorito (central Italy) case study.*- Jour. Geophys. Res. **108**, 2294-2313. doi: 10.1029/2002JB002166.

Chiaraluce L., Valoroso L., Piccinini D., Di Stefano R., De Gori P.; 2011: *The anatomy of the 2009 L'Aquila normal fault system (central Italy) imaged by high resolution foreshock and aftershock locations,* - J. Geophys. Res. ,16 , B12311, doi:10.1029/2011JB008352.

Cinque A., Patacca E., Scandone P., Tozzi M.; 1993: *Quaternary kinematic evolution of the Southern Apennines. Relationships between surface geological features and deep lithospheric structures.* - Annali di Geofisica 36, 249–260.

D'Agostino N., Giuliani R., Mattone M., Bonci L.; 2001: *Active crustal extension in the central Apennines (Italy) inferred from GPS measurements in the interval 1994-1999.*- Geophys. Res. Lett., **28**, 2121-2124.

Di Bucci D., Tozzi M.; 1991: *La linea "Ortona-Roccamonfina": revisione dei dati esistenti e nuovi contributi per il settore settentrionale (media Valle del Sangro),* - Studi Geol. Cam., Vol. Spec. **1991/2**, CROP 11, 397-406.

Doglioni C.; 1991: *A proposal for the kinematic modelling of W dipping subductions: possible applications to the Tyrrhenian-Apennines system.* - Terra Nova 3, 423e434.

Doglioni C., Mongelli F., Pieri P.; 1994: *The Puglia uplift (SE Italy): an anomaly in the foreland of the Apenninic subduction due to buckling of a thick continental lithosphere*.- Tectonics 13, 1309 1321.

Falcucci, E., Gori, S., Moro, M., Pisani, A.R., Melini, D., Galadini, F., Fredi, P.; 2011: *The 2009 L'Aquila earthquake (Italy): what next in the region? Hints from stress diffusion analysis and normal fault activity*. Earth Planet. Sci. Lett. 305, 350-358.

Fedi M., Cella F., Florio G., Rapolla A.; 2005: *Multiscale Derivative Analysis of the Gravity and Magnetic Fields of the Southern Apennines (Italy) - CROP PROJECT:* Deep Seismic Exploration of the Central Mediterranean and Italy Edited by I.R. Finetti, 2005 Elsevier B.V.

Fedi M., Florio G., Cella F.; 2007: *Toward a Full Multiscale Approach to Interpret Potential Fields* – EGM International Workshop Innovation in EM, Grav and Mag Methods:a new Perspective for Exploration Capri, Italy, April 15 – 18, 2007.

Fedi M., Pilkington M.; 2012: *Understanding imaging methods for potential field data* - Geophysics77(1), G13–G24.

Galadini F., Galli P.; 1999: *The Holocene paleoearthquakes on the 1915 Avezzano earthquake faults (central Italy): Implications for active tectonics in Central Apennines,* - Tectonophysics 308, 143–170, doi 10.1016/S0040-1951(99)00091-8.

Galadini F., Galli P.; 2000: *Active tectonics in the Central Apennines (Italy)—Input data for seismic hazard assessment, Natural Hazards 22*, 225–268, doi 10.1023/A:1008149531980.

Galadini F., Galli P., Moro M.; 2003: *Paleoseismology of silent faults in the central Apennines (Italy): the Campo Imperatore fault (Gran Sasso Range fault system)* - Ann. Geophys. 46, 793–813.

Galadini F., Messina P.; 2004: *Early-Middle Pleistocene eastward migration of the AbruzziApennine (central Italy) extensional domain* - J. Geodyn., 37, 57 – 81.

Gaudiosi G., Alessio G., Cella F., Fedi M., Florio G., Nappi R.; 2012*: Multiparametric data analysis for seismic source identification in the Campanian area: merging of seismological, structural and gravimetric data* - Bollettino di Geofisica Teorica ed Applicata Vol. 53, n. 3, pp. 283-298; September 2012, DOI 10.4430/bgta0050.

ISIDe Working Group INGV; 2010: *Italian Seismological Instrumental and parametric database*. http://iside. rm.ingv. it.

ITHACA-ISPRA: *Istituto Superiore per la Protezione e la Ricerca Ambientale*, - http://www.isprambiente.gov.it/it/progetti/suolo-e-territorio-1/ithaca-catalogo-delle-faglie-capaci.

Lavecchia G., Brozzetti F., Barchi M. R., Keller J., Menichetti M.; 1994:*Seismotectonic zoning in east-central Italy deduced from the analysis of the Neogene to present deformations and related stress fields* - Soc. Geol. Am. Bull. 106, 1107–1120.

Lavecchia G., Brozzetti F., Barchi M., Keller J., Meinichetti M.; 1994: *Seismotectonic zoning in east–central Italy deduced from the analysis of the Neogene to present deformations and related stress fields*. Geol. Soc. Amr. Bull. 106, 1107–1120

Lavecchia G., Boncio P., Brozzetti F., De Nardis R., Di Naccio D., Ferrarini F., Pizzi A., Pomposo G.; 2010: *The April 2009 Aquila (Central Italy) seismic sequence (Mw 6.3): a preliminary seismotectonic picture*- Guarnieri, P. (Ed.), Recent Progress on Earthquake Geology. Nova Publishers, ISBN 978-1-60876- 147-0, pp. 1e17.

Locardi E., Nicolich R.; 1988: *Geodinamica del Tirreno e dell'Appennino centro-meridionale: la nuova carta della Moho*- Mem. Soc. Geol. Ital., 41, 121 – 140.

Malinverno A., Ryan W.B.F.; 1986: *Extension in the Tyrrhenian Sea and shortening in the Apennines as result of arc migration driven by sinking of the lithosphere*. Tectonics, 5, 227–254.

Mariucci M.T., Amato A., Montone P.; 1999: *Recent tectonic evolution and present day stress in the Northern Apennines (Italy)*- Tectonics 18 (1), 108–118.

Michetti A.M., Brunamonte F., Serva L., Vittori E.; 1996: *Trench investigations of the 1915 Fucino earthquake fault scarps (Abruzzo, central Italy): geological evidence of large historical events.* - J Geophys Res 101(B3):5921–5936

Moro, M., Gori S., Falcucci E., Saroli M., Galadini F., Salvi S.; 2013: *Historical earthquakes and variable kinematic behaviour of the 2009 L'Aquila seismic event (central Italy) causative fault, revealed by paleoseismological investigations*. Tectonophysics 583, 131-144.

Patacca E., Sartori R., Scandone P.; 1990: *Tyrrhenian basin and Apenninic arc: kinematic relations since Late Tortonian times* - Memorie Società Geologica Italiana 45, 425e451.

Patacca E., Scandone P.; 2004: *The Plio-Pleistocene thrust belt-foredeep system in the Southern Apennines and Sicily (Italy)* - Geology of Italy, edited by U. Crescenti *et al*., pp. 93 – 129, Ital. Geol. Soc., Florence, Italy.

Pantosti D., Schwartz D.P., Valensise G.; 1993: *Paleoseismology along the 1980 surface rupture of the Irpinia fault: implications for earthquake recurrence in the Southern Apennines,Italy* - J. Geophys. Res. 98, 6561–6577.

Pizzi A., Scisciani V.; 2000: *Methods for determining the Pleistocene-Holocene component of displacement on active faults reactivating pre-Quaternary structures: examples from the central Apennines (Italy)* - Journal of Geodynamics 29, 445–457.

Pizzi A., Galadini F.; 2009: *Pre-existing cross-structures and active fault segmentation in the northern-central Apennines*.Tectonophysics, **476**, 304-319. doi: 10.1016/j.tecto.2009.03.018.
Rovida A., Camassi R., Gasperini P., Stucchi M. (eds.); 2011: CPTI11, the 2011 version of the Parametric Catalogue of Italian Earthquakes. Milano, Bologna - http://emidius.mi.ingv.it/CPTI, *DOI:10.6092/INGV.IT-CPTI11*.
Royden L. H., Patacca E., Scandone P.; 1987: *Segmentation and configuration of subducted lithosphere in Italy: An important control on thrust-belt and foredeep- basin evolution* - Geology, 15, 714 – 717.
Vezzani L., Ghisetti F,; 1998: *Carta geologica dell'Abruzzo, 1:100000,* SELCA, Via R. Giuliani, Firenze.

## A GEOPHYSICAL TRANSECT ACROSS THE CENTRAL SECTOR OF THE FERRARA ARC: PASSIVE SEISMIC INVESTIGATIONS – PART II

**A. Mantovani, N. Abu Zeid, S. Bignardi, G. Santarato**
*Dipartimento di Fisica e Scienze della Terra, Università degli Studi di Ferrara, Italy*

**Introduction.** The architecture of the Po Plain foredeep filling, from Pleistocene onward, is characterized by a generally "regressive" trend, interrupted by lesser fluctuations, evidenced by the transition from offshore Pliocene deposits to marine-marginal and then to alluvial Quaternary sediments (Ricci Lucchi, 1986; Amorosi and Colalongo, 2005; Amorosi, 2008).

The great number of subsurface data collected during hydrocarbon explorations and water research (AGIP Mineraria, 1959; Aquater, 1976, 1978; Aquater-ENEL, 1981; Pieri and Groppi, 1975, 1981; RER & ENI-AGIP, 1998; Boccaletti *et al*., 2004, 2011; Ferrara province - RER 2007) allowed to map the main quaternary unconformities: the most recent surface, at regional scale, is the base of the Upper Emiliano-Romagnolo Synthem (AES; Boccaletti *et al*., 2004) which is made up of a series of different depositional cycles whose limits are placed in correspondence of the bottom of the "transgressive" marine deposits. The 'transgressive' portion of each cycle is characterized by the presence of fine materials (*e.g*. floodplain, marsh and coastal plain clays) with subordinated sandy intercalations. Instead, the 'regressive' sequence consists of alluvial plain deposits (*e.g*. fine sediments of overflowing river) where channel sands are subordinated in the form of isolated lenticular bodies. On the top of each cycle, the channel sands become abundant, thus forming laterally wider bodies (RER & ENI-AGIP, 1998; ISPRA, 2009).

The studies conducted by the Regione Emilia-Romagna & ENI-AGIP (1998), Boccaletti *et al*. (2004, 2011), Abu Zeid *et al*. (2014) and Ferrara province - RER (2007) revealed that the Quaternary succession is highly deformed and confirmed that the transitions between marine-continental sediments are the result of important tectonic phases followed by periods of strong subsidence. Therefore, the strong variable thickness of the Quaternary sequence from several hundreds to few tens of meters in correspondence of the growing anticlines; *i.e*. Mirandola, Casaglia, Argenta reflects the influence of the complex evolution of the blind thrusts belonging to the Ferrara Arc.

Previous geophysical studies conducted by numerous authors (*e.g*. Priolo *et al*., 2012; Paolucci *et al*., 2015) focused the attention on mapping the fundamental resonance frequencies and the corresponding shear-wave velocity profiles in the area affected by the Emilia 2012 seismic sequence by independently interpret the HVSR curves (in the first case) or using a simplified power law to describe Vs variation with depth in the latter case. This way, they were able to establish a link between the two main resonance peaks to known subsurface geological contacts. However, no information on possible lateral variations could be deduced from such interpretation.

With this premise, we carried out a geophysical survey along a profile, ca. 27-km long and oriented SSW-NNE, almost perpendicular to the regional trend of the buried structures belonging

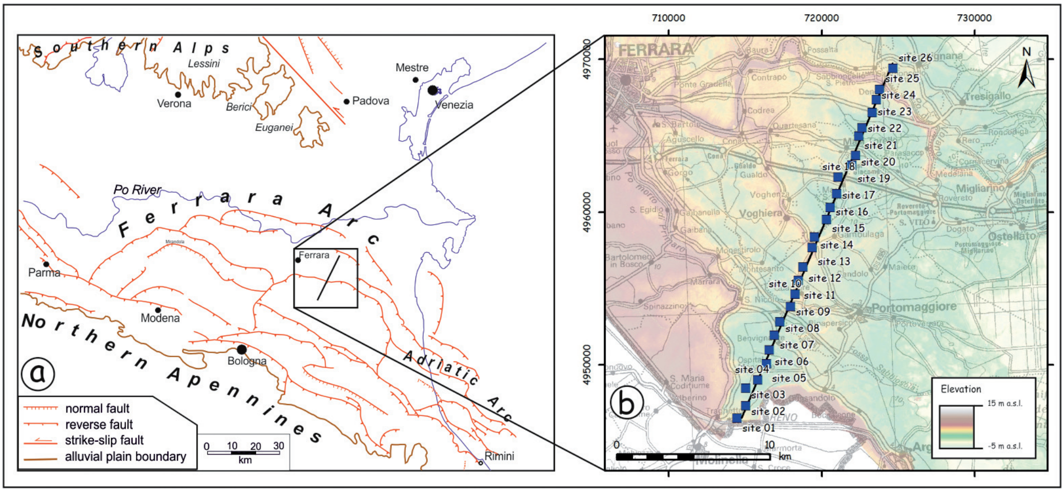


Fig. 1 – a) Simplified tectonic map of the blind northern Apennines showing the studied area [black boxes ESE of Ferrara: modified from CNR-PFG (1991)]. b) Location of the measured sites (blue dots) along investigated profile (black line).

to the central sector of the Ferrara Arc (Fig. 1a), which is one of the three arcs consisting of blind, north-verging thrusts and folds that represent the external northern Apennines front (Pieri and Groppi, 1981; Bigi *et al.*, 1982; Boccaletti *et al.*, 2004). The investigated profile runs in the middle of the elongated area investigated by the detailed gravimetric survey, described in the companion paper (see Palmieri *et al.*, 2015), between Traghetto (near Molinella) and Formignana (Fig. 1b).

Because the density variations of the Late Quaternary deposits are negligible, even performing a much denser grid of gravity measurements, the resolution of this approach, as described in the above mentioned companion paper, would not be sufficient to detect and reconstruct the surfaces and geometries of bodies in the shallow subsurface. In addition, the geometry of the sedimentary bodies, accumulated in the alluvial plain, is generally characterized by sharp lateral variations and hence the interfaces commonly lack planar geometry showing curvatures with wavelength varying between one to ten hundred meters and several meters wide. Accordingly, as far as the expected deformation structures (*i.e.* fault-propagation folds) in the youngest and hence shallowest deposits could have comparable dimensions, the gravimetric survey was integrated by geophysical measurements sensitive to more variable properties in the shallowest subsurface than density.

Therefore, our investigations based on seismic techniques, exploited the ambient seismic noise. In particular, we applied the ESAC (Aki, 1957, 1964; Asten and Henstridge, 1984; Ohori *et al.*, 2002) strategy to obtain several 1D shear wave velocity profiles, providing quantitative shear velocity models down to 120-150 m depth, and HVSR technique (Nakamura, 1989) to infer the fundamental resonance frequency and an estimate of the depth of major impedance contrast(s) at each site. Afterwards, the local 1D Vs profiles and HVSR curves were assembled in order to reconstruct two independent pseudo-2D sections. In what follow we shall show that it is possible to obtain reliable pseudo-2D sections from surface seismic noise data so emphasizing the occurrence of lateral shear wave velocity and spectral ratio amplitude variations. Further, a characterization beyond the nominal depth of 30m results in very useful information for site characterization especially for the quantitative evaluation of the local site specific seismic response (Abu Zeid *et al.*, 2012).

**Data acquisition.** Along the investigated profile, we carried out 26 ESAC arrays associated with single station recordings at the centre of the array, roughly one kilometre spaced. The coordinates of the investigated sites are listed in Tab. 1.

Tab. 1 - Coordinates (WGS84 – UTM, zone 32N) of the seismic noise measurements.

| site | type of measurement | latitude (UTM 32N) | longitude (UTM 32N) | site | type of measurement | latitude (UTM 32N) | longitude (UTM 32N) |
|---|---|---|---|---|---|---|---|
| 01 | array | 4946530 | 714459 | 14 | array | 4958360 | 719532 |
| 01 | single station | 4946550 | 714380 | 14 | single station | 4958390 | 719530 |
| 02 | array | 4947330 | 715029 | 15 | array | 4959510 | 720312 |
| 02 | single station | 4947320 | 715028 | 15 | single station | 4959540 | 720302 |
| 03 | array | 4948470 | 715036 | 16 | array | 4960300 | 720546 |
| 03 | single station | 4948450 | 715037 | 16 | single station | 4960290 | 720563 |
| 04 | array | 4949020 | 715811 | 17 | array | 4961180 | 720964 |
| 04 | single station | 4949020 | 715802 | 17 | single station | 4961190 | 720981 |
| 05 | array | 4950090 | 716382 | 18 | array | 4962270 | 721064 |
| 05 | single station | 4950110 | 716382 | 18 | single station | 4962290 | 721059 |
| 06 | array | 4950990 | 716572 | 19 | array | 4963050 | 721965 |
| 06 | single station | 4950990 | 716573 | 19 | single station | 4963050 | 721951 |
| 07 | array | 4951940 | 716901 | 20 | array | 4963680 | 722199 |
| 07 | single station | 4951930 | 716899 | 20 | single station | 4963670 | 722225 |
| 08 | array | 4952830 | 717258 | 21 | array | 4964950 | 722408 |
| 08 | single station | 4952840 | 717285 | 21 | single station | 4964950 | 722387 |
| 09 | array | 4953800 | 717964 | 22 | array | 4965510 | 722620 |
| 09 | single station | 4953790 | 717965 | 22 | single station | 4965530 | 722599 |
| 10 | array | 4954610 | 718249 | 23 | array | 4966490 | 723283 |
| 10 | single station | 4954610 | 718264 | 23 | single station | 4966480 | 723278 |
| 11 | array | 4955510 | 718460 | 24 | array | 4967340 | 723543 |
| 11 | single station | 4955530 | 718455 | 24 | single station | 4967330 | 723553 |
| 12 | array | 4956410 | 718774 | 25 | array | 4968020 | 723757 |
| 12 | single station | 4956430 | 718772 | 25 | single station | 4968010 | 723763 |
| 13 | array | 4957680 | 719364 | 26 | array | 4969380 | 724651 |
| 13 | single station | 4957670 | 719364 | 26 | single station | 4969390 | 724638 |

The ESAC (Extended Spatial Auto-Correlation; Aki, 1957, 1964; Asten and Henstridge, 1984, Ohori *et al.*, 2002) consists of collecting the ambient seismic noise by means of an array (seismic antenna) employing vertical geophones, laid out in an L, T or X geometry, allowing for different length of the segments in order to fit the available space at the measurement site, especially when in urbanareas. Data are fourier transformed and combined keeping into account the shape of the antenna to obtain the dispersion pattern of the Rayleigh waves. Then, an inversion process allows estimating the local vertical sequence of shear wave velocity (Vs), assuming an 1-D subsurface model. In the present survey, L-shaped arrays, composed of 24 geophones, 8 m spaced, were laid out at each site. We used 3-components 4.5 Hz proper frequency geophones. Seismic noise was recorded separately both for the vertical and horizontal components, obtaining time series of 15 minutes long sampled at 500 Hz. The inversion of the dispersion curves afterwards allowed for the 1-D shear wave velocity estimation using a set of constant thickness layers. Phase velocity data inversion was accomplished using a

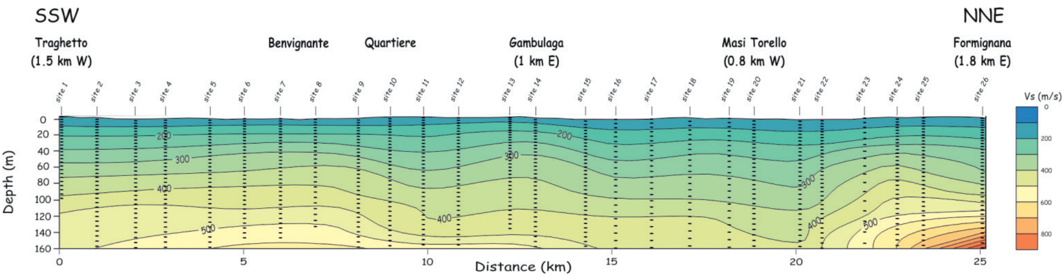


Fig. 2 – Pseudo-2D shear-wave velocity section reconstructed by the interpolation of several 1D shear-wave models obtained from the inversion of the ESAC seismic noise data.

"minimum roughness regularization" strategy, so to obtain smooth transitions with depth but still maintaining the capability of capturing the major impedance contrasts.

The HVSR (Horizontal-to-Vertical Spectral Ratio) technique, first proposed in 1970 by Nogoshi and Igarashi, based on the initial study of Kanai and Tanaka (1961), and today popular thanks to Nakamura (1989), is a "passive" method, which uses three-component recordings of ambient seismic noise to evaluate the site fundamental resonance frequency(ies), by estimating the horizontal-to-vertical ratio of the spectral amplitudes of motion. The measurements of the seismic noise were performed using a 3-component short-period seismometer (fc = 2 Hz) for time intervals variable between 30 and 50 minutes. The final HVSR curves as a function of frequency are given by the average of the H/V ratio computed for each window (window size = 60 s). The curves were computed by averaging the horizontal spectra with the quadratic average and dividing it for the vertical spectrum. Such spectra were smoothed following the filter proposed by Konno and Omachi (1986) using a constant b value of 40. Moreover, seismic noise source directionality was evaluated for all the measurements.

**Results: pseudo-2D sections.** The discrete information of all 1D models was interpolated with a minimum curvature algorithm in order to obtain the pseudo-2D velocity section. The resulting Vs profile is shown in Fig. 2. Although 1D models locally reached higher depths, the section we show reports the distribution of Vs down to an average depth of about 160 m b.g.l. (considering that the elevation of the sites ranges between 0 and 4.5 m a.s.l.). The shear wave velocity ranges between 100-150 m/s, just below ground surface, and locally reaches 600 m/s at the maximum investigation depths. The vertical gradient of Vs is stronger between sites 03-13 and between sites 21-26, while in the southernmost and central portions of the profile, between sites 01-02 and 14-20 the gradient is weaker and the Vs at 160 m b.s.l. is ca. 400-450 m/s. If we compare the Vs profile with the Structural Model of Italy (Bigi *et al.*, 1992) we observe that the strongest Vs gradients are located above the sets of thrust faults respectively pertaining to the Argenta and Ferrara anticlines; conversely, the sites where the gradient is weaker are located above a tectonically "depressed" area bounded by a reverse fault to the north.

The corresponding frequency section, obtained using the HVSRprofile routine (Herak *et al.*, 2010), which performs a side-by-side assembly of the observed HVSR-spectra, is based on the 26 single station measurements of seismic noise, elaborated following the HVSR method. Considering the characteristics of the seismometer and the influence of weather-climate conditions for frequencies below 0.5 Hz (SESAME, 2004), the analysis was limited to the frequency band between 0.5 and 5 Hz. The HVSR amplitudes, depending on the impedance contrast at the discontinuity surface, are color-coded and these are greater in the southern portion of the profile with respect to the northern one. The fundamental frequency varies along the profile from a minimum of 0.55 Hz up to a maximum of 1.6 Hz (Fig. 3a).

Assuming the Vs pattern and the fundamental resonance frequency variations to be determined by lateral lithological variations, especially in terms of differential compaction (i.e. age) of the sediments, the two pseudo-2D sections (Figs. 2, 3a) allow hypothesizing the

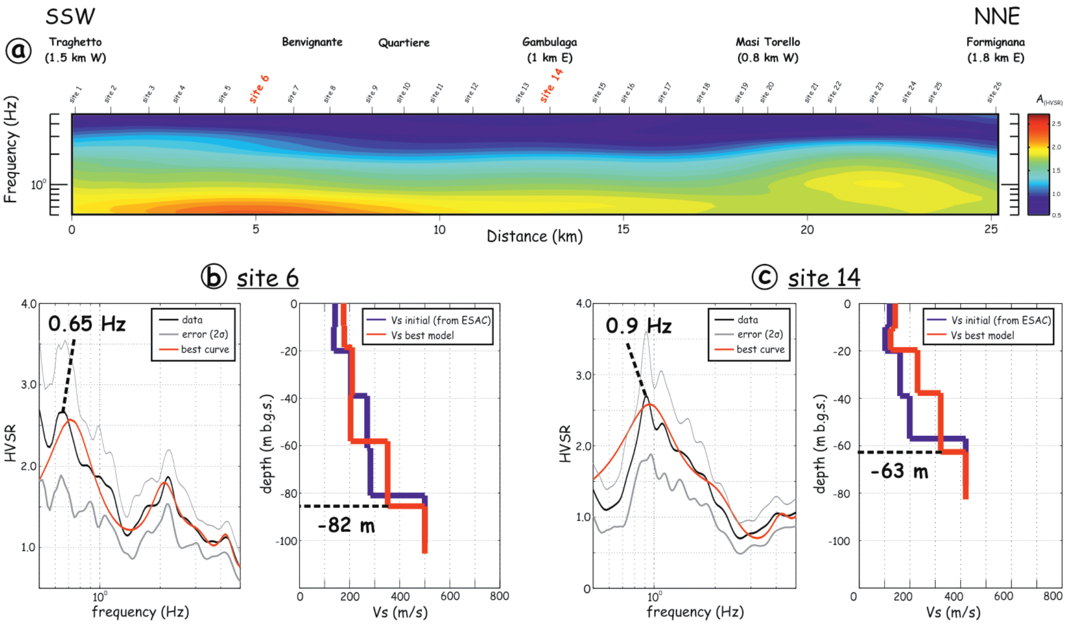


Fig. 3 – a) Smoothed HVSR profile obtained by gridding each average HVSR curve, between 0.5 and 5 Hz. Relative amplitudes are color-coded (see colorbar). The HVSR spectra of each measurement, which were grouped together according to a comparable fundamental resonance frequency, are also shown. b) Result of the HVSR curve inversion of site n. 6 with the "OpenHVSR" routine. On the left graph are shown the observed HVSR spectra (black line) and the best curve obtained after the inversion procedure (red line). On the left diagram are shown the Vs starting model from ESAC survey (blue line) and the final Vs profile relative to the best HVSR curve (red line). c) Result of the HVSR curve inversion of site n. 14.

occurrence of buried anticline structures in correspondence to the "condensed" stratigraphy and their recent tectonic evolution. This is further confirmed by a preliminary inversion of some ad-hoc selected HVSR curves, performed using the open source "OpenHVSR" routine, developed by our research group to specifically invert large HVSR datasets; which shall be freely available soon. In Figs. 3b and 3c the obtained results of two HVSR curves are shown. The smooth Vs subsurface model obtained from the ESAC was used as starting model for the HVSR inversion. This allowed to start from a model already in the basin attraction of the HVSR inversion global minima. We were so able to optimize the local Vs profiles to both minimize the ESAC and the HVSR objective functions even if the two inversion routines are based on different assumptions.

Despite these limitations,, the resultant depth of the major impedance contrast is consistent with those of the other geophysical tests and available information about the subsurface stratigraphy. The comparison with the available stratigraphic data (RER & ENI-AGIP, 1998; Ferrara province – RER, 2007; Martelli *et al.*, 2014) indicates a good correspondence with the known main stratigraphic unconformities. In particular, the seismic pseudo-bedrock here detected could correspond to the contact between two Middle Pleistocene sedimentary cycles, both belonging to higher rank sedimentary cycle represented by the Upper Emiliano-Romagnolo Synthem (AES).

**Conclusions and future works.** The reconstructed pseudo-2D sections document the possibility to highlight the recent tectonic activity of buried structures underlying the eastern sector of the Po Plain by means of low-cost geophysical surveys (not expensive equipment nor large teams). The seismic passive methods allowed collecting a massive dataset in a short period of time, which in turn, allowed retrieving a large number of local 1D shear wave velocity profiles that were capable of exploring the subsurface down to ca. 150-200 m depth. Further, the fundamental resonance frequencies and the depth to the major impedance contrast of the investigated sites were obtained. Accordingly, it is possible to carry out a sufficient number of such measurements in order to derive reliable pseudo-2D sections, several kilometers-long, so emphasizing the possible occurrence of lateral shear wave velocity (and amplitude) variations, which will likely reflect the stratigraphic changes.

Although we did not observe in the reconstructed Vs pseudo-2D section the velocity values that should be expected for a strict definition of the position of the seismic bedrock (i.e. Vs≥ 800 m/s), it is however possible to recognize a pseudo-bedrock located roughly at 100-150 m depth and characterized by Vs values between 400 and 500 m/s. As a benefit result, the subsurface characterization beyond the traditional 30 m represents a very useful information toward a better urban planning and to a more realistic evaluation of the local site response, especially in view of anticipating new laws that may in the future prescribe to extend this kind of investigations to higher depths.

The comparison between the results described and discussed above with those of the companion paper (see Palmieri *et al.,* 2015), suggests that the shallow stratigraphic features documented in this work can be directly associated with the deep ongoing tectonic activity of the blind thrusts throughout the Quaternary.

**Aknowledgements.** This study has benefited from funding provided by the Italian Presidenza del Consiglio dei Ministri - Dipartimento di Protezione Civile (DPC). This paper does not necessarily represent the official opinion and policies of the DPC.

**References**

Abu Zeid, N., Bignardi, S., Caputo, R., Mantovani, A., Tarabusi, G., Santarato, G.; 2014: *Shear-wave velocity profiles across the Ferrara arc: a contribution for assessing the recent activity of blind tectonic structures*. Proceedings of the 33th National Convention National Group Solid Earth Geophysics. ISBN 978-88-940442-2-5.

Abu Zeid, N., S. Bignardi, S., Caputo, R., Santarato, G., Stefani., M.; 2012: *Electrical Resistivity Tomography investigation on co-seismic liquefaction and fracturing at San Carlo, Ferrara Province, Italy*. Annals of Geophysics. Vol. 55; p. 713-716, ISSN: 2037-416X, DOI: 10.4401/ag-6149.

AGIP MINERARIA; 1959: *Campi gassiferi padani*. Atti Convegno Giacimenti Gassiferi dell'Europa Occidentale. Acc. Naz. Lincei, 2, pp. 45-497.

Aki, K.; 1957: *Space and time spectra of stationary stochastic waves, with special reference to microtremors*, Bull. Earthquake Res. Inst. 35, 415–456.

Aki, K.; 1964: *A note on the use of microseisms in determining the shallow structures of the earth's crust*, Geophysics 29, 665–666.

Amorosi, A.; 2008: *Delineating aquifer geometry within a sequence stratigraphic framework: evidence from the Quaternary of the Po River Basin, Northern Italy*. In: Amorosi, A., Haq, B.U., Sabato, L. (Eds.), Advances in Application of Sequence Stratigraphy in Italy, vol. 1. GeoActa Special Publication, pp. 1–14.

Amorosi A. and Colalongo M.L.; 2005: *The linkage between alluvial and coeval nearshore marine successions: evidence from the Late Quaternary record of the Po River Plain, Italy*. In: Blum, M.D., Marriott, S.B., Leclair, S.F. (Eds.), Fluvial Sedimentology VII, vol. 35. Special Publication of the International Association of Sedimentologists, pp. 257–275.

AQUATER; 1976: *Elaborazione dei dati geofisici relativi alla Dorsale Ferrarese*. Rapporto inedito per ENEL.

AQUATER; 1978: *Interpretazione dei dati geofisici delle strutture plioceniche e Quaternarie della Pianura Padana e Veneta*. Rapporto inedito per ENEL.

AQUATER-ENEL; 1981: *Elementi di neotettonica del territorio italiano*. Volume speciale, Roma.

Asten, M. W., and Henstridge J. D. (1984): *Array estimators and the use of microseisms for reconnaissance of sedimentary basins*, Geophysics 49, 1828–1837.

Bigi G., Cosentino D., Parotto M., Sartori R., and Scandone P.; 1992: *Structural Model of Italy, scale 1:500.000*. Prog. Fin. Geodinamica, Quad. "La RicercaScientifica", C.N.R., 114 (3), Roma.

Boccaletti M., Bonini M., Corti M., Gasperini G.P., Martelli L., Piccardi L., Severi P., Vannucci G.; 2004: *Carta sismotettonica della Regione Emilia-Romagna scala 1:250000*. Note illustrative, A cura di M. Boccaletti e L. Martelli. S.EL.C.A, Firenze, 2004.

Boccaletti M., Corti G. and Martelli, L.; 2011: *Recent and active tectonics of the external zone of the Northern Apennines (Italy)*. Int. J. Earth Sci. (Geologische Rundschau), 100:1331-1348.

Ferrara province – RER; 2007: *Risorse idriche sotterranee della Provincia di Ferrara*. Provincia di Ferrara, Servizio

Politiche della Sostenibilità e Cooperazione Internazionale; Regione Emilia-Romagna, Servizio Geologico, Sismico e dei Suoli; Università degli Studi di Ferrara, Dipartimento di Scienze della Terra, DB Map, Firenze, Italy, 80 pp.

Herak M., Allegretti I., Herak D., Kuk K., Kuk V., Maric, K., Markusic, S. and Stipcevic, J.; 2010: *HVSR of ambient noise in Ston (Croatia): comparison with theoretical spectra and with the damage distribution after the 1996 Ston-Slano earthquake*, B. Earthq. Eng., 8, 483–499.

Holbrook J. and Schumm S.A.; 1999: *Geomorphic and sedimentary response of rivers to tectonic deformation: a brief review and critique of a tool for recognizing subtle epeirogenic deformation in modern and ancient settings*, Tectonophysics, 305, 287-306.

ISPRA; 2009: *Carta Geologica d'Italia, Foglio 204 Portomaggiore*. Coord. Scientifico: Calabrese et al., Regione Emilia-Romagna. ISPRA, Servizio Geologico d'Italia – Regione Emilia-Romagna, Servizio geologico, sismico e dei suoli. SystemCart, Roma.

Kanai K. and Tanaka T.; 1961: *On microtremors*, VIII Bull. Earthq. Res. Inst. 39.

Martelli L., Severi P., Biavati G., Rosselli S., Camassi R., Ercolani E., Marcellini A., Tento A., Gerosa D., Albarello D., Guerrini F., Lunedei E., Pileggi D., Pergalani F., Compagnoni M., Fioravante V., Giretti D.; 2014: *Analysis of the local seismic hazard for the stability testsof the main bank of the Po river (Northern Italy)*. Boll. Geofis. Teor. Appl., 55, 119-134.

Nakamura Y.; 1989: *A Method for Dynamic Characteristics Estimation of Subsurface using Microtremor on the Ground Surface*, Quarterly Report of Railway Technical Research Institute (RTRI), Vol. 30, No.1.

Nogoshi M. and Igarashi T.; 1970: *On the propagation characteristics of microtremors*. J. Seism. Soc. Japan 23, 264-280.

Ohori M., Nobata A., Wakamatsu K.; 2002: *A Comparison of ESAC and FK Methods of Estimating Phase Velocity Using Arbitrarily Shaped Microtremor Arrays*. BSSA, 92, 2323–2332.

Okada Y.; 1985: *Surface deformation due to shear and tensile faults in a half-space*. Bull. Seism. Soc. Am., 75, 1135-1154.

Okada, H., K. Matsushima and E. Hidaka; 1987: *Comparison of spatial autocorrelation method and frequency wavenumber spectral method of estimating the phase velocity of Rayleigh waves in long-period microtremors*, Geophys. B. Hokkaido Univ. 49, 53-62 (in Japanese with English abstract).

Pieri M. & Groppi G.; 1975: *The structure of the Pliocene-Quaternary sequence in the subsurface of the Po and Veneto Plains, the pedeapenninic Basin and the Adriatic Sea*. Quad. Ric. Scient., 90, pp. 409-415.

Pieri M. & Groppi G.; 1981: *Subsurface geological structure of the Po Plain, Italy*. CNR, Prog. Final. Geodinamica, pubbl. n. 414, Napoli.

Priolo E., M. Romanelli, C. Barnaba, M. Mucciarelli, G. Laurenzano, L. Dall'Olio, N. Abu-Zeid, R. Caputo, G. Santarato, L.Vignola,C. Lizza and P. Di Bartolomeo; 2012: *The Ferrara Thrust Earthquakes of May-June 2012 – Preliminary Site Response Analysis at the Sites of the OGS Temporary Network*. Annals of Geophysics, 55 (4), 7 pp.

RER & ENI-AGIP; 1998: *Riserve idriche sotterranee della Regione Emila-Romagna*. A cura di G. DI DIO. S.EL. CA. (Firenze).

Ricci Lucchi F.; 1986: *Oligocene to Recent foreland basins of northern Apennines*. In: PH. Allen and P. Homewood (Eds.), Foreland Basins, IAS Special Publication No. 8, 105-139.

Site Effects Assessment using Ambient Excitations (SESAME) European project, 2004; Deliverable D23.12: *Guidelines for the implementation of the H/V spectral ratio technique on ambient vibrations: measurements, processing and interpretation*; deliverable D13.08, Final report WP08, *Nature of noise wavefield*.

Schumm S.A., Dumont J.F and Holbrook J.M.; 2000: *Active Tectonics and Alluvial Rivers* (Cambridge University Press), pp. 290.

## MAIN TECTONIC IMPLICATIONS OF THE ONGOING KINEMATIC PATTERN (GPS) IN THE ITALIAN REGION

**E. Mantovani[1], N. Cenni[2], M.Viti[1], D. Babbucci[1], C.Tamburelli[1]**

[1] *Dipartimento di Scienze Fisiche, della Terra e dell'Ambiente, Università di Siena, Italy*

[2] *Dipartimento di Fisica ed Astronomia, Università di Bologna, Italy*

**Introduction.** The geodynamic context in the Mediterranean region is still object of debate. Some authors (e.g., Mantovani *et al.*, 2006, 2007, 2009; Viti *et al.*, 2006, 2011) suggest that the convergence of the confining plates (Africa, Eurasia and the Anatolian-Aegean system)

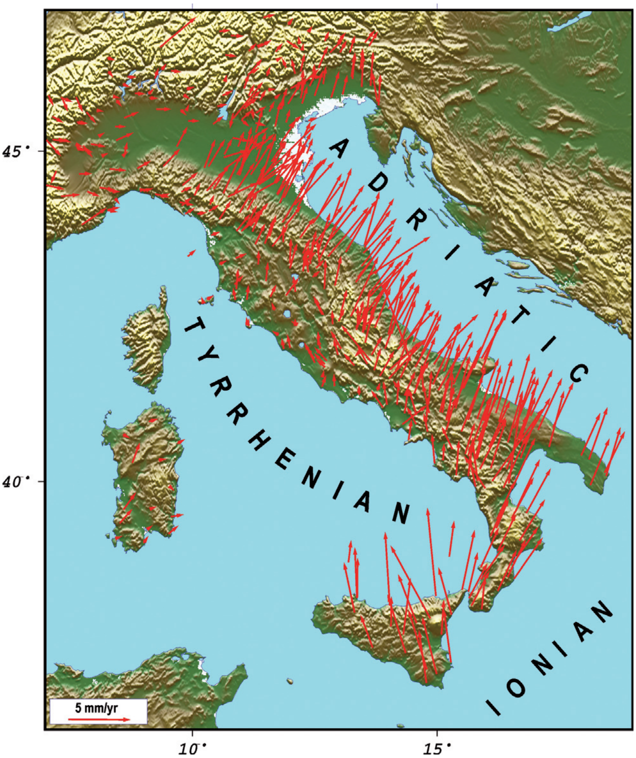


Fig. 1 – Horizontal velocity vectors of the GPS sites considered in this work, with respect to a fixed Eurasian frame [Euler pole at 54.23°N, 98.83°W, ω = 0.257°/Myr; Altamimi *et al.* (2012)].

may plausibly explain the spatio-temporal distribution of major Neogenic deformations observed in the study area, whereas other authors (e.g., Malinverno and Ryan, 1986**;** Faccenna *et al.*, 2007) argue that such driving mechanism cannot account for the generation of back arc basins and invoke the contribution of slab roll-back. The spreading of opinions about the geodynamic setting in the Mediterranean region is also due to the fact that the kinematics of the main confining plates (Africa and Eurasia) is not uniquely recognized yet. Uncertainty mainly concerns the trend of the Nubia (sensu De Mets *et al.*, 2010)-Eurasia convergence and the configuration and kinematics of the Adriatic plate. Global kinematic models based on the analysis of long-term evidence [late Pliocene-Quaternary, DeMets *et al.* (2010)] suggest that at Mediterranean latitudes Nubia moves roughly NW to NNW ward with respect to Eurasia. Global models inferred from short-term space geodesy data (Argus *et al.*, 2010) provide a Nubia-Eurasia relative motion with an even larger westward component. However, as argued by Mantovani *et al.* (2007), the motion trends mentioned above can hardly be reconciled with several major features of the Plio-Quaternary tectonic setting in the whole Mediterranean region, which rather suggests a NNE ward orientation of such plate convergence. In this work, we make an attempt at gaining insights into the above problem by considering the possible tectonic implications of the present velocity field in the Italian area derived by the analysis of geodetic observations carried out by a fairly dense network of continuous GPS stations (Fig. 1). Details about the network and the acquisition and analysis of GPS data are given by Cenni *et al.* (2012, 2013).

**Southern Adria kinematics and Nubia-Eurasia relative motion.** The geodetic velocity field shown in Fig. 1 clearly indicates that the Apulia zone (south-eastern Italy), certainly belonging to the southern Adriatic domain (e.g., Fantoni and Franciosi, 2010), is moving roughly NE ward, with a rate of about 4-5 mm/year. This evidence is fairly robust since it is coherently indicated by a relatively high number (more than 20) of GPS velocity vectors. Since no clear active tectonic discontinuity is actually recognized between southern Adria and Nubia (e.g., Babbucci *et al.*, 2004), one can reasonably expect a coherent kinematics of these two domains. However, this condition is not fulfilled if the Nubia-Eurasia relative motion is taken from the global kinematic models (Argus *et al.*, 2010, De Mets *et al.*, 2010), which provide a roughly NW to NNW ward motion of the Nubian domain in the Mediterranean area (Mantovani *et al.*, 2007).

To tentatively overcome this major problem, a number of authors have hypothesized the presence of an active tectonic decoupling between Adria and Nubia [see Babbucci *et al.* (2004),

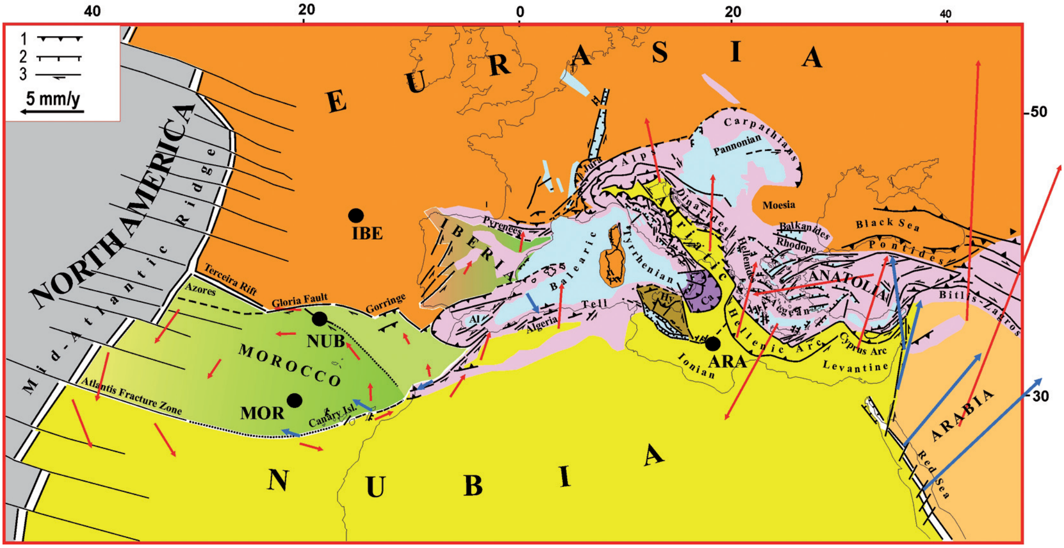


Fig. 2 – Plate configuration and long-term (Quaternary) kinematic pattern in the Mediterranean region provided by Mantovani *et al.* (2007). Black dots identify the location of the proposed Euler poles of the Arabia (ARA), Iberia (IBE), Morocco (MOR) and Nubia (NUB) plates with respect to Eurasia. Red arrows indicate the motions of the above plates with respect to Eurasia predicted by the respective Euler poles and the motion of the Anatolian-Aegean system. Blue arrows along plate borders show the relative motion of the Morocco and Arabia plates with respect to Nubia. CA=Calabrian wedge (violet), Hy=Hyblean wedge (brown), see Mantovani *et al.* (2009) and Viti *et al.* (2011) for the proposed kinematic pattern. The velocity field shown in the Anatolian-Aegean system is compatible with geological evidence (see Mantovani *et al.*, 2007a; Viti *et al.*, 2011). Main orogenic belts are pink. 1,2,3) Compressional, extensional and transcurrent features.

Argnani (2006) and Mantovani *et al.* (2007) for a detailed discussion and the more recent works of D'Agostino *et al.* (2008) and Weber *et al.* (2010)]. However, the considerable spreading of the decoupling zones so far proposed, concerning location (from the central Adriatic Sea to eastern Sicily), trend (various) and tectonic nature (from compressional to extensional), clearly underlines the ambiguity of the available evidence. The most significant evidence in support of an insignificant present relative motion between Nubia and Adria is given by the low level of seismicity in the presumed decoupling zones and the lack of a clear fault system cutting through the Adria domain.

In our opinion, the above arguments cast serious doubts about the reliability of the Nubia-Eurasia relative motion provided by global kinematic models, suggesting the need of looking for an alternative less problematic solution. In this regard, it is worth considering that the Apulia kinematics indicated by GPS data (Fig. 1) is fairly compatible with the motion trend and rate of Nubia predicted by the long-term kinematic model proposed by Mantovani *et al.* (2007), as shown in Fig. 2. Since such model can also account for the Quaternary deformation pattern in the whole Mediterranean region and for the north Atlantic kinematic constraints, it seems to be the most reliable solution so far proposed.

This opinion is not shared by Argus *et al.* (2010), who cast doubts about the reliability of the Mantovani *et al.* (2007) kinematic model. In particular, the above authors do not recognize the Iberia and Morocco independent microplates. As concerns Iberia, Argus *et al.* (2010) postulate that no significant relative motion between that domain and Eurasia is taking place at the Pyrenean collision zone, in particular the 1.5 mm/yr convergence rate implied by the Mantovani *et al.* (2007) model. However, it is difficult to believe that such small relative motion can be ruled out for a boundary zone where significant seismic activity takes place, and

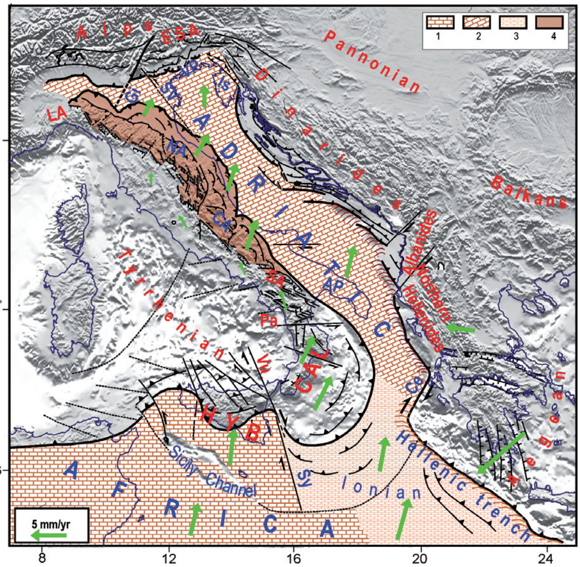


Fig. 3 – Tectonic setting and long term kinematics in the central Mediterranean area, compatible with the post-early Pleistocene deformation pattern (Viti *et al.*, 2006, 2011; Mantovani *et al.*, 2007a, 2009): 1-2) African and Adriatic continental domains, 3) oceanic Ionian domain, 4) outer sector of the Apennine belt carried by Adriatic plate (Adria). Green arrows indicate the long-term kinematic pattern (middle Pleistocene to Present) with respect to Eurasia. AP=Apulia, CAL=Calabrian wedge, Ce=Cephalonia fault system, ESA=eastern Southern Alps, Gi=Giudicarie, HYB=Hyblean wedge, Is=Istria, LA=Ligurian Alps, NA, CA, SA =northern, central and southern Apennines, Pa=Palinuro fault system, SV=Schio-Vicenza fault system, Sy=Siracusa fault system, VP=Venetian Plain, Vu=Vulcano fault system.

several compressional and traspressional active faults have been identified (e.g., Lacan and Ortuno, 2012). In our opinion, the fact that both the boundary zones between Iberia and Eurasia are affected by significant seismicity cannot easily be reconciled with a null relative motion between such plates.

As concerns the Morocco microplate, Argus *et al.* (2010) point out a discrepancy between the predictions of the Morocco-Nubia pole provided by Mantovani *et al.* (2007) and the geodetic velocities at Maspalomas (Canary Islands). However, it must be considered that such site lies along an active tectonic boundary zone (as recognized by Argus *et al.*, 2010) and that consequently the real meaning of such observation cannot easily be recognized. Argus *et al.* (2010) also suggest discrepancies between the predictions of the Mantovani *et al.* (2007) Morocco-Eurasia pole and the geodetic velocities in the Ponta Delgada (Azores) and Rabat sites (lying inside the presumed Morocco microplate). However, the entities of such discrepancies are compatible with the possible uncertainty of geodetic data.

**Adria plate?** The GPS velocity field shown in Fig. 1 provides very significant information on the present kinematics of two zones certainly belonging to the Adria continental domain (Fig. 3), one is the Apulia, as discussed in the previous point, and the other is the Venetian plain and Istria, i.e. the northernmost sector of the Adria foreland which underthrusts the eastern southern Alps (e.g., Fantoni and Franciosi, 2010). This evidence is very significant since it is coherently indicated by a relativel high number (more than 20 for both zones) of subparallel velocity vectors.

If Adria were assumed as a rigid independent plate, the two geodetic constraints mentioned above would imply an Adria-Eurasia rotation pole roughly located in the western Alps. This result, also supported by the analysis of earthquake slip vectors in peri-Adriatic zones (e.g., Anderson and Jackson, 1987; Weber *et al.*, 2010) would mean that Adria does not move in close connection with Nubia, whatever Nubia-Eurasia pole is considered among the ones so far proposed. However, such conclusion can hardly be reconciled with the lack of a clear active tectonic decoupling zone between the present Adria domain and Nubia (Babbucci *et al.*, 2004; Argnani, 2006; Mantovani *et al.*, 2006). Thus, we rather suppose that the present velocity field in the Adria domain results from a transient non rigid behaviour of the Adria domain. This effect may be due to the peculiar distribution of seismic decouplings and related post seismic relaxation effects that have occurred in the periAdriatic boundary zones during the last tens of years. For the choice of such time interval we have taken into account the evidence and arguments presented by Mantovani *et al*. (2015a, 2015b) and Viti *et al*. (2015), which suggest that major seismicity in the peri-Adriatic zones tends to undergo a progressive northward migration through the eastern (Dinarides) and western (Apennine) boundary zones, up to reach the northern front of the Adria plate (eastern Southern Alps). The analysis of the post 1400 seismic history has allowed the recognition of a number of migrating sequences, each lasting about 200 years. The last presumably complete sequence has probably developed until about 1930. Since then, major peri-Adriatic shocks have mainly occurred in the southern peri-Adriatic boundaries (southern and central Apennines and southern Dinarides, Albanides), while only few shocks have affected the Adriatic boundary zones located more to the north (northern Apennines, northern Dinarides and eastern southern Alps). Considering this seismicity pattern and the post-seismic relaxation effects that such earthquakes have triggered in the Adria domain, one could suppose that at present the southern part of Adria is affected by higher mobility with respect to the northern sector, which is still constrained by high resistance at its boundaries (Mantovani *et al*., 2015a, 2015b; Viti *et al*., 2015). This hypothesis would suggest that Adria is not actually behaving as a rigid structure. For instance, the lower motion rate of the northern Adria (indicated by GPS data, 2-3 mm/yr) with respect to that expected from an Adria Euler pole coincident with the one of Nubia (Fig. 2) could be accommodated by internal deformation of the Adria continental domain, for instance an upward longitudinal flexure.

**Apennine belt, Calabrian Arc and Sicily.** In the Apennine belt, the GPS velocity field points out a considerable variation of velocity from the outer to the inner sectors (Fig. 1). This feature is compatible with the kinematic pattern of the Apennine belt deduced by the analysis of long-term evidence (Mantovani *et al*., 2006, 2009, 2015c; Viti *et al*., 2006, 2011; Cenni *et al*., 2012). The outer mobile portion of the Apennine belt (Fig. 3) is constituted by the Molise-Sannio wedge in the southern Apennines, the eastern sector of the Lazio-Abruzzi carbonate platform in the central Apennines, and the Romagna-Marche-Umbria and Toscana-Emilia wedges in the northern Apennines (Mantovani *et al*., 2009, 2015c; Viti *et al*., 2015b).

The proposed geodynamic interpretation (Viti *et al*., 2006, 2011, 2015b; Mantovani *et al*., 2009, 2015c) suggests that some mobility also characterizes the inner sector of the Apennines, even though at lower rates with respect to the outer Apennine sectors and with a roughly north to NNW-ward orientation (Fig. 3). This long-term pattern is compatible with the short-term kinematic field delineated by GPS data.

Other investigations on the present kinematic pattern in the Apennine belt, carried out by the analysis of geodetic data, are reported in literature. Notwithstanding that some of the resulting velocity fields (e.g., Bennett *et al*., 2012; Devoti *et al*., 2011) are similar to the one shown in Fig. 1, the proposed tectonic interpretations are drastically different from the one described above (Fig. 3), since they invoke the gravitational sinking of the Adriatic subducted lithosphere beneath the Apennine belt as the main driving mechanism of the observed surface kinematics. However, such interpretation involves some major problems, as argued in the following. First of all, it must be considered that the real development of the presumed slab roll-back and consequent trench retreat along the Apennine belt is very uncertain. Most authors (e.g., Spakman and Wortel, 2004) suggest that the evidence of subducted lithosphere beneath the Apennine belt is lacking in large sectors of the Adriatic trench zone, in particular below the central Apennines. Thus the proposed process cannot account for a basic feature of the GPS velocity field (Fig. 1), i.e. the fact that the Apennine belt moves almost uniformly roughly NE ward from the southern Apennines to the northernmost Apennines. Moreover, the NE-ward rollback of the Adriatic plate would induce a similar motion in the adjacent upper plate (e.g., Schellart and Moresi, 2013), whereas the GPS velocity vectors along the Tyrrhenian coast are north to NW-oriented. Nocquet (2012) also noted the discrepancy between the kinematics of the outer and inner sectors of the Apennines. The results of seismic surveys (CROP, Finetti *et al*., 2005) and tomography (Scafidi and Solarino, 2012) show that subducted lithosphere beneath the northern and central Apennines only reaches some tens of km. Thus the proposed slab pull mechanism cannot account for a basic feature of the GPS velocity field (Fig. 1), i.e. the fact that the Apennine belt moves almost uniformly roughly NE-ward from the southern Apennines to the northernmost Apennines.

Another major problem of the slab roll-back mechanism is explaining some major features of the GPS velocity field in Calabria and Sicily, i.e. the belt sectors where the presence of a well developed slab is documented by the distribution of deep seismicity. In particular one should explain why in the first zone the vectors are parallel to the main axis of the belt (Fig. 1 and e.g., D'Agostino *et al*., 2011), and in Sicily the vectors are oriented roughly northward, towards the Tyrrhenian basin, i.e. about opposite to what happen in the northern Apennines. In summary, it seems very difficult to understand why the invoked slab pull mechanism induces very different or even opposite effects in the various sectors of the trench zone.

The geodynamic interpretation proposed by Mantovani *et al*. (2009) and Viti *et al*. (2011) for the central Mediterranean region provides that the compressional regime induced by the convergence of the confining plates (Nubia, Eurasia and Anatolia-Aegean system) causes the outward escape of the Calabrian and Hyblean wedges with respect to the Apennine-Maghrebian belt, as sketched in Fig. 3. It is worth noting that such long-term kinematic pattern, involving a roughly ENE ward motion of the Calabrian Arc and a roughly northward motion of the Hyblean wedge, is very similar to the short-term one derived by geodetic data (Fig. 1).

**Conclusions.** The present kinematic pattern of the Italian region, tentatively inferred from continuous GPS observations in a relatively high number of sites, provides significant insights into the geodynamic/tectonic setting in the central Mediterranean area. A significant number of data in the Apulian zone clearly indicate that the southern Adriatic domain moves roughly NE-ward. This evidence creates a problem if the Nubia-Eurasia relative motion is taken from global kinematic models, since it implies a significant relative motion between Adria and Nubia, in contrast with the fact that no clear decoupling zone can be recognized between such plates.

It is difficult to believe that the expected relative motion between the southern Adria domain (moving roughly NE-ward) and the adjacent Nubia domain (moving about NNW-ward, following the NUVEL 1 model) only causes significant seismotectonic activity in the Gargano zone, a small sector of the southern Adriatic platform (e.g., Argnani, 2006). This major difficulty may imply that the Nubia-Eurasia rotation pole derived by global kinematic models is not reliable. This possibility is also suggested by the fact that the trend of the Nubia-Eurasia relative motion provided by the above models (NNW- to WNW-ward) cannot account for other major Quaternary tectonic features in the whole Mediterranean area, which rather suggest a NNE-ward trend of the Nubia-Eurasia relative motion (Mantovani *et al*., 2007). To explain why the Nubia-Eurasia pole provided by global kinematic models may be not reliable, Mantovani *et al*. (2007) argue that the plate configuration adopted by such investigation is oversimplified, since it involves a two plates model (Nubia and Eurasia), notwithstanding that the distribution of seismic and tectonic features in the Mediterranean regions strongly suggests the presence of two microplates (Morocco and Iberia, Fig. 1), not moving in close connection with the Nubia and Eurasia main plates. To overcome the above difficulties, Mantovani *et al*. (2007) have proposed an alternative kinematic model (Fig. 1), which provides that Nubia moves roughly NNE-ward in the central Mediterranean region. This hypothesis does not involve significant difficulties, since it may account for the motion of the southern Adria domain derived by GPS and other data, it is compatible with the Mediterranean long-term evidence mentioned by Mantovani *et al*. ( 2007) and can also be reconciled, within errors, with the north Atlantic kinematic constraints, if the proposed four plates configuration is taken into account (Mantovani *et al*., 2007).

The GPS velocity field (Fig. 1) clearly defines the kinematics of two Adriatic zones, one located in the southern part (Apulia) and the other located in the northernmost Adria domain (Venetian plain). If such kinematic constraints are interpreted as related to a rigid structure, the resulting Adria-Eurasia rotation pole would be located in the western Alps, implying an independent motion between Nubia and Adria, whatever Nubia-Eurasia Euler pole is adopted among the ones so far proposed. Since this result can hardly be reconciled with the lack of a decoupling zone between Nubia and Adria, we suppose that such evidence might result from a transient non-rigid behavior of the Adria lithosphere. This hypothesis is supported by the fact that in the last tens of years (since 1930) most major peri-Adriatic decoupling earthquakes have mostly occurred in the southern boundary zones (northern Hellenides, Albanides, southern Dinarides, southern and central Apennines). Considering the effects of post seismic relaxation induced by such shocks, the above seismicity distribution may imply that Adria is affected by a transient internal deformation, for instance accommodated by longitudinal upward flexure.

It is then argued that the GPS velocity field is compatible with the kinematic pattern of the Apennine belt, Calabria and Sicily proposed by Mantovani *et al*. (2009) and Viti *et al*., (2011), whereas it can hardly be reconciled with the kinematics expected from the alternative geodynamic interpretation proposed by a number of authors, invoking the contribution of slab roll-back in the Apennine trench zone.

**References**


Altamimi Z., Métivier L., Collilieux X.; 2012: *ITRF2008 plate motion model*. J. Geophys. Res., **117**, B07402.

Anderson H., Jackson J.; 1987: *Active tectonics of the Adriatic region*. Geophys. J.R. Astron. Soc., **91**, 937-983.

Argnani A.; 2006: *Some issues regarding the central Mediterranean neotectonics*. Boll. Geof. Teor. Appl., **47**, 13-37.

Argus D.F., Gordon R.G., Heflin M.B., Ma C., Eanes R.J., Willis P., Peltier W. R., Owen S.E.; 2010: *The angular velocities of the plates and the velocity of Earth's centre from space geodesy*. Geophys. J. Int., **180**, 913-960.

Babbucci D., Tamburelli C., Viti M.,Mantovani E., Albarello D., D'Onza F., Cenni N., Mugnaioli E.; 2004: *Relative motion of the Adriatic with respect to the confining plates: seismological and geodetic constraints*. Geophys. J. Int., **159**, 765-775.

Bennett R. A. *et al*.; 2012: *Syn-convergent extension observed using the RETREAT GPS network, northern Apennines, Italy*. J. Geophys. Res., **117**, B04408.

Cenni N., Mantovani E., Baldi P., Viti M.; 2012: *Present kinematics of Central and Northern Italy from continuous GPS measurements*. J. Geodynamics, **58**, 62-72.

Cenni N., Viti M., Baldi P., Mantovani E., Bacchetti M.,Vannucchi A.; 2013: *Present vertical movements in central and northern Italy from GPS data: possible role of natural and anthropogenic causes*. J. Geodynamics, **71**, 74-85.

D'Agostino N., Avallone A., Cheloni D., D'Anastasio E., Mantenuto S., Selvaggi G.; 2008: *Active tectonics of the Adriatic region from GPS and earthquake slip vectors*. J. Geophys. Res., **113**, B12413.

D'Agostino N., D'Anastasio E., Gervasi A., Guerra I., Nedimovic M.R., Seeber L., Steckler M.; 2011: *Forearc extension and slow rollback of the Calabrian Arc from GPS measurements*. Geophys. Res. Lett., **38**, L17304.

DeMets C., Gordon R.G., Argus D.F.; 2010: *Geologically current plate motions*. Geophys. J. Int., **181**, 1-80.

Devoti R., Esposito A., Pietrantonio G., Pisani A.R., Riguzzi F.; 2011: *Evidence of large scale deformation patterns from GPS data in the Italian subduction boundary*. Earth Planet. Sci. Lett., **311**, 230-241.

Faccenna C., Funiciello F., Civetta L., D'Antonio M., Moroni M., Piromallo C.; 2007: *Slab disruption, mantle circulation, and the opening of the Tyrrhenian basins*. In: Beccaluva L., Bianchini G., Wilson M. (Eds.), Cenozoic Volcanism in the Mediterranean Area. Geol. Soc. Am. Spec. Paper **418**, 153-169.

Fantoni R., Franciosi R.; 2010: *Tectono-sedimentary setting of the Po Plain and Adriatic foreland*. Rend. Fis. Acc. Lincei, **21** (Suppl.1), S197-S209.

Finetti I.R., Boccaletti M., Bonini M., Del Ben A., Pipan M., Prizzon A., Sani F.; 2005: *Lithospheric tectono-stratigraphic setting of the Ligurian sea-Northern Apennines-Adriatic foreland from integrated CROP seismic data*. In: Finetti I.R (Ed.), Deep Seismic Exploration of the Central Mediterranean and Italy, CROP PROJECT. Elsevier, Amsterdam, pp. 119-158 (Chapter 8).

Lacan P., Ortuno M.; 2012: *Active tectonics of Pyrenees: a review*, J. Iberian Geol., **38**, 9-30.

Malinverno A., Ryan W.B.F.; 1986: *Extension in the Tyrrhenian Sea and shortening in the Apennines as result of arc migration driven by sinking of the lithosphere*. Tectonics, **5**, 227-245.

Mantovani E., Viti M., Babbucci D., Tamburelli C., Albarello D.; 2006: *Geodynamic connection between the indentation of Arabia and the Neogene tectonic evolution of the Central-Eastern Mediterranean Region*. In: "Post-collisional tectonics and magmatism in the eastern Mediterranean region", Dilek, Y. and Pavlides, S. (Eds.), Geol. Soc. Am., Special Volume **409**, 15-41.

Mantovani E., Viti M., Babbucci D., Albarello D.; 2007: *Nubia-Eurasia kinematics: an alternative interpretation from Mediterranean and North Atlantic evidence*. Ann. Geophysics, **50**, 311-336.

Mantovani E., Babbucci D., Tamburelli C., Viti M.; 2009: *A review on the driving mechanism of the Tyrrhenian-Apennines system: jmplications for the present seismotectonic setting in the Central-Northern Apennines*. Tectonophysics, **476**, 22-40.

Mantovani E., Viti M., Babbucci D., Tamburelli C., Cenni N., Baglione M., D'Intinosante V.; 2015a: *Recognition of periAdriatic seismic zones most prone to next major earthquakes: insights from a deterministic approach*. In: D'Amico S. (Ed.), Earthquakes and Their Impact on Society. Springer Natural Hazard Series, Springer, in press.
Mantovani E., Viti M., Cenni N., Babbucci D., Tamburelli C., Baglione M., D'Intinosante V.; 2015b: *Seismotectonics and present seismic hazard in the Tuscany-Romagna-Marche-Umbria Apennines (Italy)*. J. Geodynamics, **89**, 1-14.
Mantovani E., Viti M., Babbucci D., Tamburelli C., Cenni N., Baglione M., D'Intinosante V.; 2015c: *Present tectonic setting and spatio-temporal distribution of seismicity in the Apennine belt*. Int. J. Geosciences, **6**, 429-454.
Nocquet J.-M.; 2012: *Present-day kinematics of the Mediterranean: A comprehensive overview of GPS results*. Tectonophysics, **579**, 220-242.
Scafidi D., Solarino S.; 2012: *Can local earthquake tomography settle the matter about subduction in the Northern and Central Apennines? Response from a new high resolution P velocity and Vp/Vs ratio 3-D model*. Tectonophysics, **554-557**, 63-73.
Schellart W.P., Moresi L.; 2013: *A new driving mechanism for backarc extension and backarc shortening through slab sinking induced toroidal and poloidal mantle flow: Results from dynamic subduction models with an overriding plate*. J. Geophys. Res. Solid Earth, **118**, 3221-3248.
Spakman W., Wortel R.; 2004: *A tomographic view on Western Mediterranean Geodynamics*. In: Cavazza W., Roure F., Spakman W., Stampfli G.M., Ziegler P. (Eds.), The TRANSMED Atlas, The Mediterranean Region from Crust to Mantle, pp. 31-52.
Viti M., Mantovani E., Babbucci D., Tamburelli C.; 2006: *Quaternary geodynamics and deformation pattern in the Southern Apennines: implications for seismic activity*. Boll. Soc. Geol. It., **125**, 273-291.
Viti M., Mantovani E., Babbucci D., Tamburelli C.; 2011: *Plate kinematics and geodynamics in the Central Mediterranean*. J. Geodynamics, **51**, 190-204.
Viti M., Mantovani E., Babbucci D., Tamburelli C., Cenni N., Baglione M., D'Intinosante V.; 2015: *Belt-parallel shortening in the Northern Apennines and seismotectonic implications*. Int. J. Geosciences, **6**, 938-961.
Weber J., Vrabec M., Pavlovčič-Prešeren P., Dixon T., Jiang Y., Stopar B.; 2010: *GPS-derived motion of the Adriatic microplate from Istria Peninsula and Po Plain sites, and geodynamic implications*. Tectonophysics, **483**, 214-222.

## A GEOPHYSICAL TRANSECT ACROSS THE CENTRAL SECTOR OF THE FERRARA ARC: DETAILED GRAVIMETRIC SURVEY – PART I

**F. Palmieri[1], A. Mantovani[2], G. Santarato[2]**
*[1] OGS (Istituto Nazionale di Oceanografia e di Geofisica Sperimentale) Trieste, Italy*
*[2] Dipartimento di Fisica e Scienze della Terra, Università degli Studi di Ferrara, Italy*

**Introduction.** The investigated area for this study is the eastern sector of the Po Plain that represents the foredeep basin of both Southern Alps and northern Apennines. We focused our attention on the Ferrara Arc (Fig. 1a), which is one of the major arcs, consisting of blind, north-verging thrusts and folds, which represent the external northern Apennines front (Pieri and Groppi, 1981; Bigi *et al.*, 1982; Boccaletti *et al.*, 2004). The recent tectonic activity of this area is well documented by the occurrence of moderate earthquakes, such as the 1570 Ferrara, and 1624 Argenta earthquakes (Guidoboni *et al.*, 2007; Rovida *et al.*, 2011) and recently in May 2012, when two moderate (Mw = 6.1 and 5.9; e.g. Pondrelli *et al.*, 2012) earthquakes affected the western Ferrara province.

The bending of the topographic surface and the consequent uplift of the broader epicentral area are among the major coseismic effects due to the reactivation of reverse blind faults as, for example, in the case of the northern Apennines underlying the Po Plain: in fact, as a consequence of the fault geometry and kinematics, the rock volume above the co-seismic rupture tip is characterised by a typical fault-propagation folding process (Okada, 1985). Depending on the seismotectonic parameters of the underlying seismogenic source, the uplifted area has an

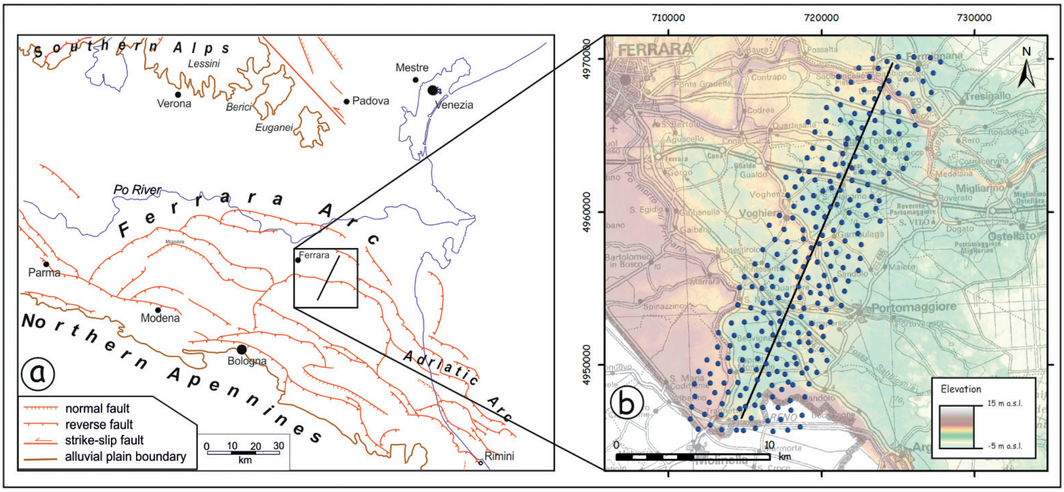


Fig. 1 – a) Simplified tectonic map of the buried northern Apennines showing the studied area (black boxes ESE of Ferrara. Modified from CNR-PFG, 1991). b) Location of the measured sites (blue dots) along investigated profile (black line).

elliptical shape that is characterized, in correspondence of the epicentral area, by a maximum vertical displacement of some tens of centimeters. The application of satellite interferometry (DinSAR technique) and high-precision levelling (Bignami *et al.*, 2012; Salvi *et al.*, 2012; Caputo *et al.*, 2015) to the Emilia seismic sequence clearly documented the occurrence of this phenomenon; in particular, the main shocks of May 20 and 29 produced two uplifted areas, characterized by a maximum vertical displacement of about 25 cm, partly overlapping and with a cumulative length of about 50 km in an E-W direction.

The recurrence of similar "areal morphogenic earthquakes" (Caputo, 2005) and the "competition" with the high subsidence and depositional rates that characterize the Po Plain, have progressively modified the geomorphology and stratigraphy of the region. In these conditions, the hydrographic network has proven to be particularly sensitive to vertical deformations, so even small altimetric and gradient changes led to river avulsions and diversions, highlighted by the presence of several drainage anomalies (Burrato *et al.*, 2003, 2012). Consequently, the alluvial plain is actually crossed by numerous abandoned river channels, some of which are still well preserved (Castiglioni *et al.*, 1999). Obviously, the presence of active tectonic structures responsible for the local uplifts and even for the complex interactions with the hydrographic network has influenced not only the distribution of the sediments on the surface, but also in the subsoil (down to some tens of meters) producing important stratigraphic variations and therefore also changes in the geophysical properties of the materials. Therefore, determining the uplift spatial distribution is crucial for reconstructing the recent tectonic evolution of the region as well as for understanding where active faults are located, and what is their possible seismogenic potential.

With this premise, we planned a geophysical survey across some major tectonic structures affecting the subsoil of the eastern Po Plain, that possibly represent the seismogenic volumes of the above mentioned historical earthquakes. Our investigation consisted in a gravity survey carried out along a transect (Fig. 1b), ca. 170 km$^2$ and oriented SSW-NNE, i.e. almost perpendicular to the regional trend of the buried structures belonging to the central sector of the Ferrara Arc. Along a profile centered around the studied transect, in order to investigate the shallow subsurface (say, down to ca. 150-200 m), several passive seismic measurements of ambient noise were also performed, whose results are described and discussed in a companion paper (see Mantovani *et al.*, 2015).

**Method and data acquisition.** Gravity prospecting is a geophysical method used to infer the subsurface density distribution measuring changes, of the order of a few parts per million or lower, in the Earth's gravitational field caused by densities' lateral variations.

A gravity survey was carried out on a rectangular area (6 x 28 km) that runs between Traghetto (near Molinella) and Formignana, in the eastern Ferrara Province (Fig. 1b); according to local topography and roads' pattern, the average spacing between contiguous measurement points was roughly 800 m. To carry out the gravity survey a LaCoste&Romberg mod. D, equipped with a ZLS feedback, whose range is about 10 mGal, was used and a whole of 274 stations, as much as homogeneously distributed, were acquired.

Since the gravity meters measure gravity differences from place to place, a First Order Gravity Net (FOGN) has been established in the surveyed area; and to define the gravity datum, 2 stations belonging to FOGN have been linked to an eccentric point of the absolute station situated at the Radio Astronomical Station of Medicina (Bo) (Cerruti *et al.*, 1992). The FOGN gravity data have been adjusted by means of the least square method after removing the instrumental drift whose systematic variations, which are common for all measured stations, have been modelled by means of a third order polynomial curve. The rms of the FOGN gravity station values has been ±0.0025 mGal. Starting from FOGN's stations, 24 gravity loops have been organized according to a sequence data acquisition allowing the instrumental drift checking and loops's closure error detection. The loops' gravity data have been adjusted in two steps: firstly, the instrumental drift has been linearly distributed, in function of the time, among the loop's stations, then the error closure has been distributed in function of the number of ties of the loop. The instrumental drift spans between -0.004 and +0.003 mGal/h and the closure errors between -0.003 and +0.005 mGal.

The elevation and position of the measuring points were estimated from the CTR of the Regione Emilia Romagna at scale 1:5000; the estimated altimetric and planimetric errors were ±0.15 m and ±5.00 m, respectively.

The observed gravity values, $g_{obs}$, are then compared with the theoretical values $g_{th}$, computed on the a homogeneous earth at the ellipsoid surface at the coordinates of the measuring point, corrected also for the height, Faye (CF) and Bouguer (CB) corrections, and terrain effects (CT).

Therefore, the so called Bouguer anomaly ($g_{geol}$) could be written as:

$$g_{geol} = g_{obs} - (g_{th} - CF + CB) + CT.$$

It means that the Bouguer anomaly is the difference between the gravity acceleration measured, on the true Earth, and the theoretical gravity acceleration at the same point computed on a homogeneous Earth, whose density could change vertically but not horizontally. Therefore, the pattern of the Bouguer anomalies reflect horizontal variations of densities inside the Earth.

In the data processing, the theoretical gravity values ($g_{th}$) were computed according to the GRS80 ellipsoid formula (Moritz, 1980); the Faye correction (CF), according to the GRS80 ellipsoid and considering also the second order term of the height (Hinze *et al.*, 2005); the Bouguer correction (CB) considering also the Earth's curvature, *i.e*. Bouguer slab and Bullard B term, which reduces the infinite Bouguer slab to that of a spherical cap, (LaFehr, 1991a, 1991b). The terrain effects (CT) were computed in two different steps: from 0.001 up to 0.010 km by means of the sloping wedge technique (Olivier *et al.*, 1981; Barrows *et al.*, 1991), due to the mostly flat surveyed area this technique was applied only in three points; from 0.010 to 15,000 km by means of an algorithm based on vertical right parallelepiped (Banerjee *et al.*, 1977), in particular from 0.010 to 1,000 km it was utilized the Digital Elevation Model of the Regione Emilia-Romagna, opportunely resampled with a grid resolution of 0.005 km, instead of the original 0.010 km; and from 1,000 to 15,000 km the SRTM database resampled with a grid resolution of 0.050 km, instead of the original 3"x3", roughly 0.090x0.065 km. Starting from 10 km it was also considered the Earth's curvature; it is worth notice that the spherical approach in CT calculation introduces negative contribution due the masses located above the

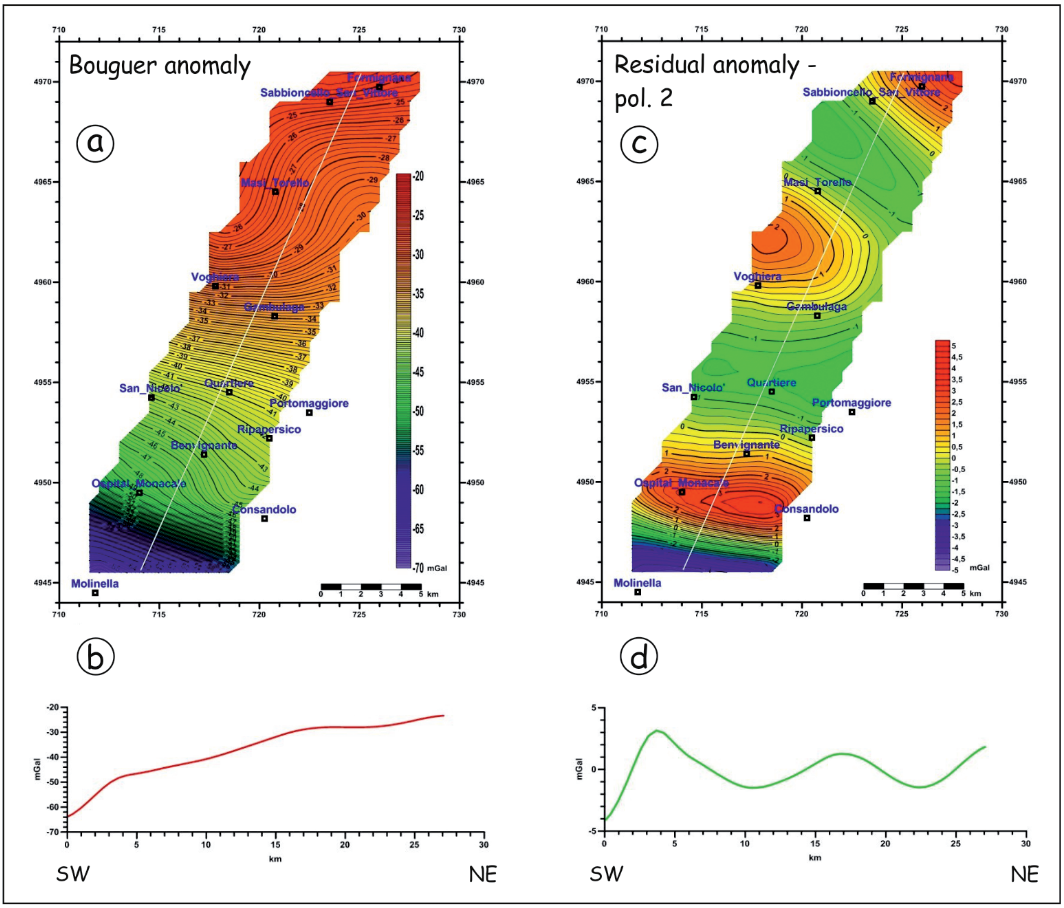


Fig. 2 – a) Bouguer anomaly over the transect and b) along the investigated profile. c) Residual anomaly over the transect and d) along the investigated profile.

spherical plate, but that are below the top of planar Bouguer plate. The estimated density value for CB and CT corrections was 2.00 g/cm$^3$, bearing in mind that the elevations range from -2.30 to 14.20 m asl and the shallow subsurface is composed of loose, fine sediments. The cumulative error of the gravity anomalies is equal to the square root of the estimated errors of the individual components involved in the calculations above briefly described; the estimated error is of the order of ±0.035 mGal.

As well known, the observed Bouguer anomaly is the summation of the gravity effects related to deep anomalous bodies with shallower ones: the different effects can be recognized by the different curvatures, weaker for deeper bodies, steeper for shallow ones.

A lot of strategies were introduced to separate the contributions of the deeper sources from the shallower ones. Among them, the upward continuation, the calculation of the horizontal and vertical gradients and the least-square residual anomaly separation were applied to the map reported in Fig. 2a.

The upward continuation smooths the effects of the higher frequencies to enhance the lowers: an approach based on the equivalent source technique (Dampney, 1969; Xia *et al.*, 1993) was used to carry out this analysis. The heights of the upward continuation spanned from -1 to -5 km: the results show that the overall anomaly pattern that increases the height, is mainly due to the deepening of the basal detachment of the Apennines accretionary wedge.

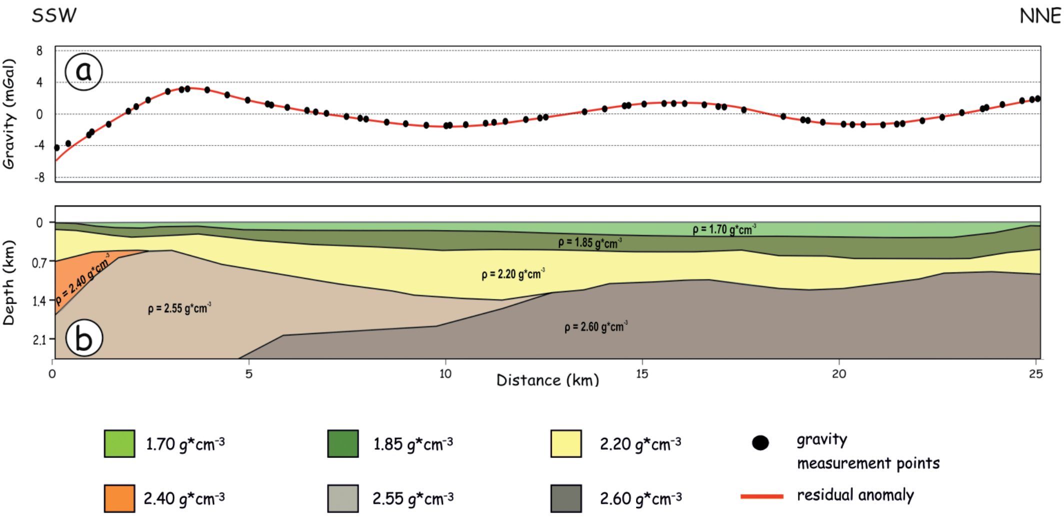


Fig. 3 – a) Observed residual anomaly along the investigated profile (blue dots) and modelled (red line). b) Model of the density distribution in the subsurface, up to ca. 2 km, obtained by the interpretation of the observed residual anomaly.

The horizontal gravity gradient map, whose purpose is to delineate the location of lateral discontinuities corresponding to the maxima gravity gradient, shows a strong horizontal gradient (roughly +5 mGal km-1) whose maxima is in the area between Ospital Monacale/Consandolo and Molinella, whose geological meaning is briefly explained below. The vertical gravity gradient map, whose aim is to sharpen anomalies, roughly shows the same features of the least-square residual anomaly separation that will be described below.

To enhance the shallowest bodies whose presence affects the data, a residual map has been obtained by means of least-square residual anomaly separation where the regional field has been fitted by means of a second-order surface (Agocs, 1951).

**Gravity anomalies and data modelling.** In Fig. 2a, the negative Bouguer anomalies span between -66 and -23 mGal, steeply decreasing northwards from a minimum near Molinella to the central part (Voghiera), then the anomaly pattern rotates towards NW. The profile shown in Fig. 2b represents the Bouguer anomaly along white trace in map, which corresponds to the same profile investigated in the companion paper (see Mantovani *et al*., 2015).

The residual anomaly map, i.e. the difference between the Bouguer anomaly map and the best fit surface, is shown in Fig. 2c, where it is possible to observe a sequence of minima and maxima (see also the profile in Fig. 2d). From SSW to NNE, a strong maximum is located below the villages of Ospital Monacale and Consandolo (+3.4 mGal), while two less strong maxima appear between Voghiera and Masi Torello (+2.1 mGal) and below Formignana (+2.9 mGal) The minima are located to the north of Molinella (-4.0 mGal), between Quartiere and Gambulaga (-1.5 mGal) and between Masi Torello and Sabbioncello San Vittore (-1.5 mGal).

Both Bouguer and residual anomaly profiles, shown in the Figs. 2b and 2d were modelled in order to reconstruct the density distribution in the subsurface, but here we shown only the reconstructued density model distribution (Fig. 3b) based on the residual anomaly (Fig. 3a). The Talwani's *et al*. (1959) method, further developed by Won *et al*. (1987) was used and a "trial-and-error" approach was applied, bearing in mind the subsurface structure known by available geological information, like seismic reflection profiles and wells for hydrocarbon exploration (Boccaletti *et al*., 2004; Fantoni and Franciosi, 2008, 2010). In particular, we correlate the southern residual positive anomaly of the gravity field to the Argenta anticline, the northern one to the Ferrara anticline and the anomaly in the middle of the investigated profile to a secondary structure, here referred as the Monestirolo structure.

**Conclusions and future works.** A gravity survey, for a total of 274 stations whose gravity datum has been referred to an eccentric point of the absolute station of Medicina (Bo), has been carried out along a transect (ca. 170 km$^2$) in the eastern sector Ferrara province, between Traghetto (near Molinella) and Formignana. The gravity data have been corrected according to standard procedures and the error of the Bouguer gravity anomalies is resulted of the order of ±0.035 mGal. In order to separate the several sources of anomalies different methods have been used: upward continuation, vertical and horizontal gradients, and polynomial surface fitting. The Bouguer and residual anomalies, located along the profile defined by the extreme ESAC stations, have been modelled in 2D.

The reconstructed density model distribution documented in this research is in good agreement with the occurrence, in the eastern sector of the Po Plain subsurface, of well known major fault-related folds and associated blind thrusts (i.e. Argenta and Ferrara anticlines, and Monestirolo structure). In addition, the described and discussed results suggest a good accordance with the shallow stratigraphic features documented in the companion paper (see Mantovani *et al.*, 2015), which can be related with the deep ongoing tectonic activity of the blind thrusts throughout the Quaternary.

**Aknowledgements.** This study has benefited from funding provided by the Italian Presidenza del Consiglio dei Ministri - Dipartimento di Protezione Civile (DPC). This paper does not necessarily represent DPC official opinion and policies.

**References**

Agocs B.; 1951: *Least squares residual anomaly separation*, Geophysics. 16 (4), 686-696.
Banerjee B., Das Gupta S.P.; 1977: *Gravitational attraction of a rectangular parallelepiped*. Geophysics, 42(5), 1053-1055.
Barrows L.J. and Fett J.D.; 1991: *A sloping wedge technique for calculating gravity terrain*. Geophysics, 56 (7), 1061-1063.
Bigi G., Cosentino D., Parotto M., Sartori R., and Scandone P.; 1992: *Structural Model of Italy, scale 1:500.000*. Prog. Fin. Geodinamica, Quad. "La RicercaScientifica", C.N.R., 114 (3), Roma.
Bignami C., Burrato P., Cannelli V., Chini M., Falcucci E., Ferretti A., Gori S., Kyriakopoulos C., Melini D., Moro M., Novali F., Saroli M., Stramondo S., Valensise G. and Vannoli P.; 2012: *Coseismic deformation pattern of the Emilia 2012 seismic sequence imaged by Radarsat-1 interferometry*. Annals of Geophys., 55(4), 788-795, doi: 10.4401/ag-6157.
Boccaletti M., Bonini M., Corti G., Gasperini P., Martelli L., Piccardi L., Severi P., Vannucci G.; 2004: *Note illustrative alla Carta Sismotettonica della Regione Emilia-Romagna*. Servizio Geologico Sismico dei Suoli
Burrato P., Ciucci F. and Valensise G.; 2003: *An inventory of river anomalies in the Po Plain, northern Italy*: evidence for active blind thrust faulting. Annals of Geophys., 46 (5), 865-882.
Burrato P., Vannoli P., Fracassi U., Basili R. and Valensise G.; 2012: *Is blind faulting truly invisible? Tectonic-controlled drainage evolution in the epicentral area of the May 2012, Emilia-Romagna earthquake sequence (northern Italy)*. Annals of Geophys., 55(4), 525-531.
Caputo R.; 2005: *Ground effects of large morphogenic earthquakes*. J. Geodyn., 40(2-3), 113-118.
Caputo R., Pellegrinelli A., Bignami C., Bondesan A., Mantovani A., Stramondo S. and Russo P.; 2015: *High-precision levelling, DInSAR and geomorphological effects in the Emilia 2012 epicentral area*. Geomorphology, 235(2015), 106-117.
Castiglioni G.B., Biancotti A., Bondesan M., Cortemiglia G. C., Elmi C., Favero V., Gasperi G., Marchetti G., Orombelli G., Pellegrini G. B. and Tellini C.; 1999: *Geomorphologic map of the Po Plain, Italy, at a scale of 1:250 000*. Earth Surface Processes and Landforms, 24, 1115-1120.
Cerutti G. and De Maria P.; 1992: *Misura assoluta dell'accelerazione di gravità a Medicina (Bo)*. Rapporto Tecnico Interno, R355, IMGC Torino.
CNR-PFG (Progetto Finalizzato Geodinamica): *Synthetic structural-kinematic map of Italy, Structural model of Italy, Sheet n. 5*. S.El.Ca., Florence, 1991
Dampney C.N.G.; 1969: *The equivalent source technique*. Geophysics, 34(1), 39-53
Fantoni R. and Franciosi R.; 2008: *8 geological sections crossing Po Plain and Adriatic foreland*. Rendiconti online Soc. Geol. Italiana, 3(1), 367–368.
Fantoni R. and Franciosi R.; 2010: *Tectono-sedimentary setting of the Po Plain and Adriatic foreland*. Rend. Fis. Acc. Lincei, 21 (Suppl.1), S197-S209.
Guidoboni E., Ferrari G., Mariotti D., Comastri A., Tarabusi G. and Valensise G.; 2007: *CFTI14Med, Catalogue*

*of Strong Earthquakes in Italy (461 B.C.-1997) and Mediterranean Area (760 B.C.-1500)*. INGV-SGA. http://storing.ingv.it/cfti14med.
Hinze W.J., Aiken C., Brozena J., Coakley B. and Dater D.; 2005: *New standards for reducing gravity data: The North America gravity database*. Geophysics, 70 (4), J25-J32.
Hinze W.J., Von Frese R.R.B. and Saad A.H.; 2013: *Gravity and Magnetic Exploration*. Cambridge University Press
La Fehr T.R.; 1991a: *Standardization in gravity reduction*. Geophysics, 56 (8), 1170-1178.
La Fehr T.R.; 1991b: *An exact solution for the gravity curvature (Bullard B) correction*. Geophysics, 56 (8), 1179-1184.
Moritz H.; 1980: *Geodetic Reference System 1980*. Bulletin Géodésique, 54 (4), 395–405.
Okada Y.; 1985: *Surface deformation due to shear and tensile faults in a half-space*. Bull. Seism. Soc. Am., 75, 1135-1154.
Olivier R.J. and Simard R.J.; 1981: *Improvement of the conic prism model for terrain correction in rugged topography*. Geophysics, 46 (7), 1054-1056.
Pieri M. and Groppi G.; 1981: *Subsurface geological structure of the Po Plain, Italy*. Consiglio Nazionale delle Ricerche, Progetto finalizzato Geodinamica, sottoprogetto Modello Strutturale, pubbl. N° 414, Roma, 13 pp.
Pondrelli S., Salimbeni S., Perfetti P. and Danecek P.; 2012: *Quick regional centroid moment tensor solutions for the Emilia 2012 (northern Italy) seismic sequence*. Ann. Geophys. 55 (4), 615-621.
Rovida A., Camassi R., Gasperini P. and Stucchi M.; 2011: *CPTI11, the 2011 version of the Parametric Catalogue of Italian Earthquakes*. Milano, Bologna (http://emidius.mi.ingv.it/CPTI11).
Salvi S., Tolomei C., Merryman Boncori J.P., Pezzo G., Atzori S., Antonioli A., Trasatti E., Giuliani R., Zoffoli S. and Coletta A.; 2012: *Activation of the SIGRIS monitoring system for ground deformation mapping during the Emilia 2012 seismic sequence, using COSMO-SkyMed InSAR data*. Annals of Geophys., 55(4), 796-802, doi: 10.4401/ag-6181.
Talwani M., Worzel J.L. and Landisman M.; 1959: *Rapid gravity computations for two-dimensional bodies with application to the Mendocino submarine fracture*. Journal of Geophysical Research, 64 (1), 49-59.
Won I. J. and Bevis M. D.; 1987: *Computing the gravitational and magnetic anomalies due to a polygon: Algorithms and Fortran subroutines*. Geophysics, 52 (2), 232-238.
Xia J., Sprowl D.R. and Adkins-Heljeson D.; 1993: *Correction of topographic distorsions in potential data: a fast and accurate approach*. Geophysics, 58 (4), 515-523.

## RECENT/PRESENT DEFORMATION PATTERN IN THE NORTHERN APENNINES

**M. Viti[1], E. Mantovani[1], D. Babbucci[1], C. Tamburelli[1], N. Cenni[2], M. Baglione[3], V. D'Intinosante[3]**
*[1] Dipartimento di Scienze Fisiche, della Terra e dell'Ambiente, Università di Siena, Italy*
*[2] Dipartimento di Fisica ed Astronomia, Università di Bologna, Italy*
*[3] Settore Sismica, Regione Toscana, Firenze, Italy*

**Introduction.** In previous works (Mantovani *et al.*, 2006, 2009, 2015a, 2015b; Viti *et al.*, 2006, 2011; Cenni *et al.*, 2012) we have discussed the geodynamic context that may generate seismic activity in the axial and outer sectors of the Apennine belt. The proposed interpretation provides that such activity is mostly produced by the relative motion between the outer sector of the belt, that stressed by the Adriatic plate is undergoing lateral escape and uplift, and the inner less mobile zones. The escaping material only includes the sedimentary cover, decoupled from its crustal basement at seismogenic depths (of the order of 6-10 km) by mechanically weak lithological horizons as the late Triassic Burano formation (e.g., Mirabella *et al.*, 2008).

The outer, more mobile belt is constituted by the Molise-Sannio (MS) wedge in the southern Apennines, the eastern sector of the Lazio-Abruzzi carbonate platform (ELA) in the central Apennines, and the Romagna-Marche-Umbria (RMU) and Toscana-Emilia (TE) wedges in the northern Apennines. The oblique divergence between the mobile Apennine wedges and the inner, less mobile belt has been accommodated by extensional and sinistral transtensional deformation, mainly concentrated in the axial zones, where a series of continental intramontane basins has developed in the Quaternary. This context has also involved compressional deformation at the outer front of the extruding wedges, where they overthrust the Adriatic domain.

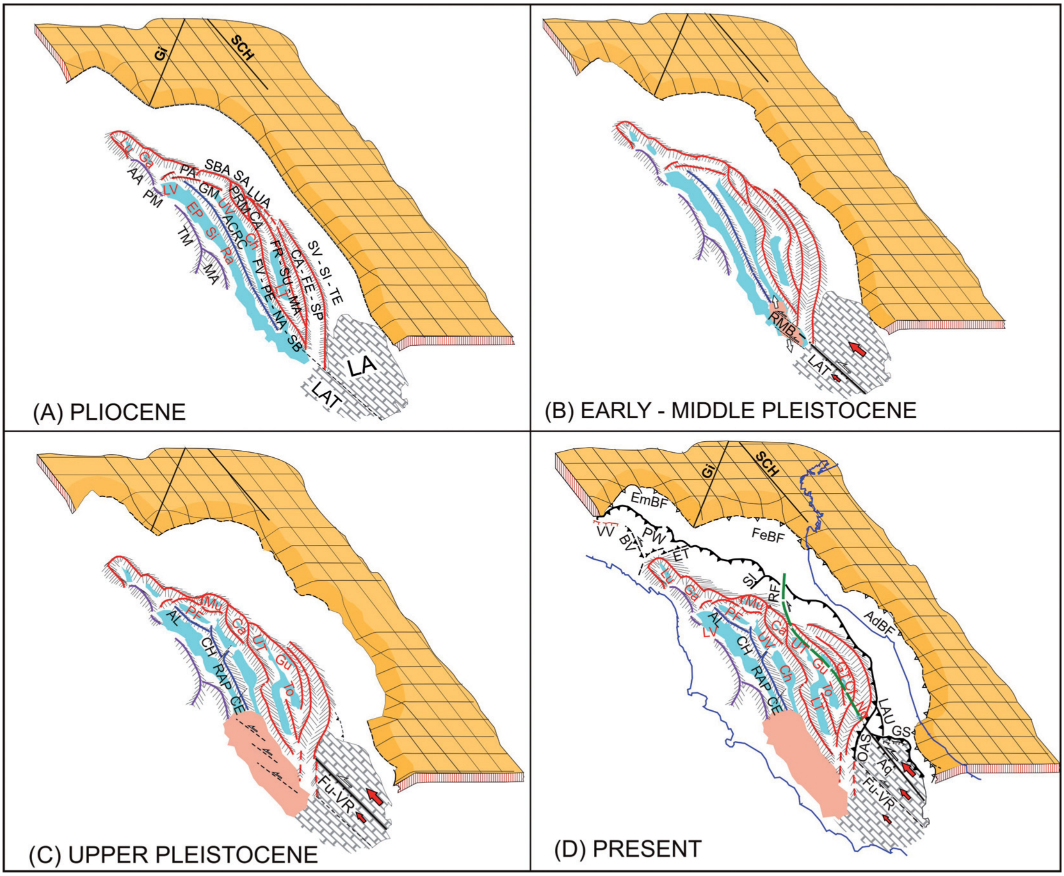


Fig. 1 – Tentative reconstruction of the main morphological elements (ridges and basins) in the northern Apennines since the Pliocene (after Viti *et al.*, 2015). A) Pliocene. The red lines identify the main ridges in the RMU and TE wedges: CA=Catenaia Alps, CA-FE-SP=Catria-Fema-Spoleto, FR-SU-MA=Frontano-Subasio-Martani, FV-PE-NA-SB=Favalto-Peglia-Narni-Sabini, GM=Giovi-Morello, LUA=Luna Alps, PA=Pistoia Apennines, PRM=Pratomagno, SA=Serra Alps, SBA=San Benedetto Alps, SV-SI-TE=S.Vicino-Sibillini-Terminillo. The blue line indicates the Albano-Chianti-Rapolano-Cetona (ACRC) ridge. The violet lines indicate the metamorphic ridge (taken as the inner limit of our reconstruction): AA=Apuane Alps, MA=Montalcino-Amiata, PM=Pisano Mt., TM=Toscana metamorphic belt. The blue zones identify the main basins: Ch=Chiana, EP=Elsa-Pesa, Ga=Garfagnana, LT=Lower Tiber, Lu=Lunigiana, LV=Lower Valdarno, Ra=Radicofani, Si=Siena, UV=Upper Valdarno. LA=Lazio-Abruzzi platform, LAT=Latina fault system. B) Early-Middle Pleistocene. RMB=Roman Magmatic Body. C) Upper Pleistocene. New basins: Ca=Casentino, Gu=Gubbio, Mu=Mugello, PF=Pistoia-Firenze, To=Topino, UT=Upper Tiber. Segments of the previous ACRC ridge: AL=Albano, CE=Cetona, CH=Chianti, RAP=Rapolano. Fu-VR=Fucino-Val Roveto fault system. D) Present. Aq=L'Aquila fault system, GS=Gran Sasso arc, LAU=Laga units. See text for explanations.

In the short-term (tens to hundreds of years), the above kinematic/tectonic context mainly develops during and just after major decoupling earthquakes. When a strong shock occurs at the inner extensional boundary of the MS wedge that block accelerates, increasing its belt-parallel push on the ELA. This indentation may cause the seismic activaction of the L'Aquila or Fucino sinistral transtensional fault systems, located at the western edge of the ELA. The sudden acceleration of ELA stresses in turn the RMU and TE wedges in the northern Apennines, favouring further seismotectonic activity.

The proposed tectonic context is compatible with the spatio-temporal distribution of major earthquakes that occurred during the main seismic crises developed in that belt since 1300 (Mantovani *et al.*, 2010, 2012). A possible explanation for the timing of the major earthquakes is provided by the numerical modeling of post-seismic relaxation induced by major shocks (Viti *et al.*, 2012, 2013).

The fact that a significant mobility, even though slower with respect to the outer belt, also affects the inner sector of the Apennine belt, is related with the motion of the African plate, transmitted by the Calabrian wedge and southern Apennines (e.g., Viti *et al.*, 2006; Mantovani *et al.*, 2009, 2015a, 2015b). In particular, belt-parallel shortening has controlled, since the Late Pliocene, the recent-present evolution of the inner sector of the northern Apennines and may account for seismic activity in the central-western Tuscany (Viti *et al.*, 2015).

In this note, we discuss the recent/present development of the outer and inner sectors of the northern Apennines by adopting the belt-parallel shortening as main driving mechanism (section 2 and 3 respectively). Furthermore, we show that the implications of such interpretation are compatible with the short-term kinematic pattern obtained from space geodetic (GPS) measurements (section 4).

**Belt-parallel shortening in the outer sector of the northern Apennines.** As argued earlier, the belt-parallel push of the Molise-Sannio wedge is transmitted to the northern Apennines by the eastern sector of the Lazio-Abruzzi platform (LA). However, major evidence suggests that the sector of LA indenting the northern Apennines has become narrower and narrower over time, as tentatively sketched in Fig. 1 (see Viti *et al.*, 2015 and references therein).

In the late Pliocene (Fig. 1a), no major longitudinal decoupling fault system was active in LA, so the push of the southern Apennines was transmitted by a large part of that platform. At that time, the northern Apennines were mainly constituted by a system of almost parallel ridges and basins, formed in the late Miocene and early-middle Pliocene extensional tectonic phases.

In the early-middle Pleistocene (Fig. 1b), the activation of the Latina fault system allowed the mobile LA sector (ELA) to decouple from its inner part and accelerate roughly NNW ward. Since then, the indentation of such wedge caused outward escape and oroclinal bending of main ridges in the northern Apennines. This effect was particularly intense in the zones lying just north of the indenter (i.e., Olevano-Antrodoco, Sabini Mts. and Narni). The oblique divergence between the outward escaping wedges and the inner more stable structures induced transtensional deformation in the zone presently covered by the Roman volcanic products. The plausibility of this hypothesis is supported by the fact that such kind of strain regime, often accompanied by the generation of pull-apart troughs, produce sub-vertical fractures that represent preferential pathways for melt ascent through the upper crust (e.g., Gundmundsson, 2001; Acocella and Funiciello, 2001).

In the upper Pleistocene (Fig. 1c), belt-parallel decoupling inside LA became more and more efficient in the Val Roveto and Fucino fault systems, while the Latina fault system was less and less active. The new configuration of the ELA indenter caused stronger and stronger bending and outward escape of orogenic material in the outer part of the RMU units, also reaching the northern ridges (Catenaia, Luna, Pratomagno and San Benedetto in Fig. 1c). In some zones, the divergence between adjacent ridges, which were undergoing different lateral bending, caused the generation of transtensional troughs. Such mechanism may have formed the Casentino and Upper Tiber troughs, as effect of oroclinal bending in the Romagna-Umbria Apennines. Similarly, oroclinal bending in the Toscana Apennines (Fig. 1c) may have formed the Firenze-Pistoia and Mugello troughs and accelerated the development of the Lunigiana and Garfagnana basins. The fact that oroclinal bending has not affected the westernmost edge of the belt (Ligurian Apennines), can be explained by the absence of late Triassic evaporites at the base of that sector (e.g., Ciarapica and Passeri, 2005; Bosellini, 2004).

During the last evolutionary phase (Fig. 1d), the Gran Sasso Arc started developing as an effect of the belt-parallel push of the northeastern sector of the Molise-Sannio wedge. In the inner side of the Gran Sasso Arc (experiencing a transtensional regime), the L'Aquila fault system developed. Since the late Pleistocene (Fig. 1d), decoupling in the LA platform has continued to develop at the Fucino fault, but the most efficient and frequent seismic decoupling has involved the L'Aquila fault system. This decoupling and the consequent acceleration of the Gran Sasso wedge, has induced shear stress in the RMU units, causing the formation of a major fault system (Norcia-Colfiorito-Gualdo Tadino-Gubbio), which has been the source of major earthquakes.

The roughly belt-parallel compression exerted by the RMU wedge causes shortening in the Padanian side of the Toscana-Emilia Apennines. One possible effect of this process is recognized in the Sillaro front (Fig. 1d), where the Umbria-Marche turbiditic units, outcropping in the Romagna Apennines, underthrust the Emilia Apennines, still covered by the Ligurian units.

Another major consequence of belt-parallel shortening in the Emilian Apennines may be the roughly NNWward lateral escape of the Piacenza wedge (Fig. 1d). The decoupling between this wedge and the Ligurian Apennines is accommodated by sinistral transpressional motion at the Bedonia-Varzi fault system and by roughly N-S divergent motion at the Villarvernia-Varzi (VV) fault, both characterized by significant seismic activity (Viti *et al.*, 2015 and references therein). The kinematics proposed for the Piacenza wedge is compatible with the configuration of the Emilia folds, presumably formed by the roughly northward displacement of this indenter. The decoupling of the Piacenza wedge from the eastern portion of the Emilia Apennines could be accommodated by transpressional deformation at the Enza-Taro fault system, evidenced by various tectonic features (Viti *et al.*, 2015). It is worth noting that the Enza-Taro fault may be the surface projection of a discontinuity (Giudicarie) that affects the Adria domain (Fig. 1d).

**Belt-parallel shortening in the inner side of the northern Apennines.** Considering the available evidence (Viti *et al.*, 2015 and references therein), we argue that the late Quaternary tectonic activity in this sector of the northern Apennines has been driven by belt-parallel compression, induced by the push of the inner sectors of the southern and central Apennines (Fig. 1). The effects of the proposed kinematic/dynamic context have probably been emphasized by the peculiar mechanical properties of the crust in the Roman magmatic body, that, being pervaded by magmatic intrusions, is presumably characterized by higher rigidity with respect to the surrounding orogenic structures and can thus more efficiently transmit the roughly northward push of the central and southern Apennines.

In particular, we argue that since the upper Pleistocene the Albano-Chianti-Rapolano-Cetona ridge has undergone significant belt-parallel shortening, which was mostly accommodated by uplift and some lateral shifts (Fig. 1c). In particular, the sinistral lateral displacement and uplift of the Rapolano ridge along the Ambra fault system, may have generated the relief now located between the Upper Valdarno and Chiana basins. The compressional interaction between the Chianti ridge and the Northern RMU wedge may have enhanced the relief that now separates the Pistoia-Firenze basin from the Upper Valdarno basin.

The above hypothesis is consistent with the following observed features (Fig. 2):

- Uplifted Pleistocene deposits have been recognized in the segments of the above ridge and in the adjacent basins, such as the Elsa-Pesa, Siena, Radicofani and Upper Valdarno. This phenomenon has also been recognized at the easternmost margin of the Firenze basin.
- During the late Pleistocene, the Arno river has undergone a drastic deviation, turning from a roughly southward path to the present one. This event could be an effect of the dextral displacement and uplift that the Rapolano ridge (Fig. 2) has undergone to accommodate the supposed longitudinal shortening. This hypothesis is also compatible with the location of the 1558 earthquake (M=5.8) that probably activated the sinistral Rapale fault in the Ambra valley.
- The Cetona and Rapolano ridges are dissected by SW-NE sinistral transversal fault systems, such as the Sentino and Sarteano ones, where pull-apart mechanisms are recognized.
- Some Quaternary NE-SW trending sinistral transtensional fault systems are recognized in the basins located along the inner side of the Albano-Chianti, Rapolano and Cetona ridges, i.e. the Elsa-Pesa and Siena-Radicofani. For instance, the Poggibonsi lineament separates the Elsa-Pesa from the Siena basin. More to the south, the sinistral Arbia fault could represent the westward prosecution, through the Siena Basin, of the Ambra fault.

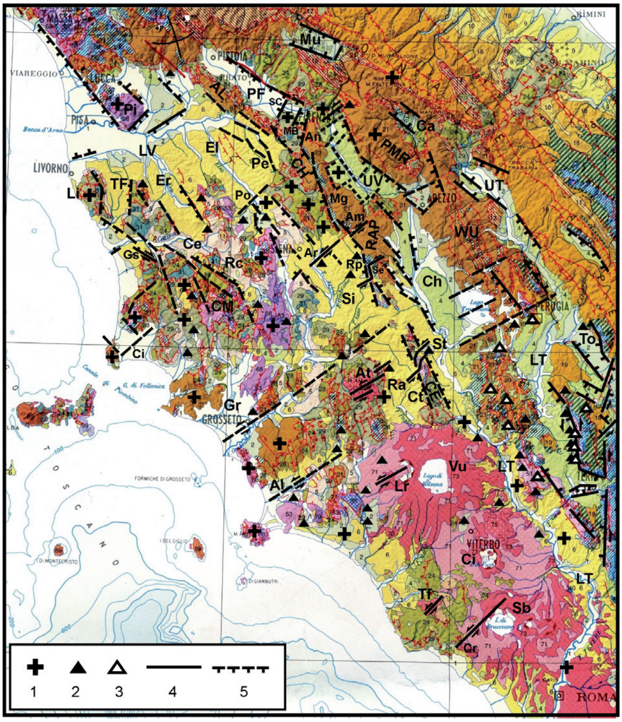


Fig. 2 – Main tectonic features recognized in the inner side of the northern Apennines (after Viti *et al*., 2015). 1) Quaternary uplift 2) Deposits of travertines and calcareous tufa 3) Quaternary Umbrian volcanism 4) Faults where late Quaternary activity is likely 5) Inferred or buried faults with uncertain late Quaternary activity. Northern Lazio volcanoes (Roman magmatic body): Ci=Cimini, Sb = Sabatini, Vu = Vulsini. Main ridges: AL = Albano, CE = Cetona, CH = Chianti, CM = Colline Metallifere, Li = Livorno Mts., Pi = Pisano Mt., PRM = Pratomagno, RAP = Rapolano, WU = Western Umbria. Neogene basins: Al = Albegna, Ca = Casentino, Ce = Cecina, Ci = Cornia, Ch = Chiana, El = Elsa, Er = Era, Gr = Grosseto, LT = Lower Tiber, LV = Lower Valdarno, Mu = Mugello, Pe = Pesa, PF = Pistoia-Firenze, Rc = Radicondoli; Ra = Radicofani, Si = Siena, TF = Tora-Fine, To = Topino, UV = Upper Valdarno, UT = Upper Tiber. Fault systems: An = Antella, Am = Ambra (Rapale), Ar = Arbia, At = Amiata, Cr = Ceriti, Ct = Cetona, Gs = Guardistallo, Lr = Latera, MB = Maiano-Bagno a Ripoli, Mg = Montegrossi, Po = Poggibonsi, Rp = Rapolano, Sc = Scandicci-Castello, Se = Sentino, St = Sarteano, Tf = Tolfa.

- The longitudinal compression exerted by the Rapolano ridge, being mostly applied to the eastern sector of the Chianti ridge could be responsible for the generation of a longitudinal decoupling faults located inside that ridge, such as the SSE-NNW Montegrossi fault system (Fig. 2). The above fault may allow a sinistral sliding between the eastern and western parts of the Chianti ridge.
- More to the north, the relative northward displacement of the Chianti ridge with respect to the adjacent less mobile structures (Albano ridge and Firenze-Pistoia basin) may be accommodated by a system of S-N to SW-NE faults, such as the Antella, Maiano-Bagno a Ripoli and Scandicci-Castello ones, which are probably related with the most intense historical earthquakes (1148 I=VII, M=5.2; 1453 I=VII-VIII, M=5.3; 1895 I=VIII, M=5.4; 1959 I=VII, M=4.8) that occurred in the Firenze area**.**
- The recent seismic swarms occurred in the Elsa-Pesa and western Chianti zones (from December, 2014 until January, 2015) may have been generated by the system of SSE-NNW to S-N faults in the Elsa-Pesa basin, which might constitute the northward prolongation of the faults located in the western side of the Chianti ridge (Fig. 2). This hypothesis is compatible with the fault plane solutions of six moderate shallow earthquakes occurred during the above swarms, which coherently indicate a strike-slip strain regime, with P and T axes directed NW-SE and NE-SW respectively (data available at www.ingv.it). These faults are probably related with the 1812 intense earthquake (I=VII-VIII, M= 5.2).

The proposed tectonic setting in the interaction zone between the Chianti ridge and the RMU wedge implies that the fault systems located in the Firenze area and the ones lying in the western Chianti and Elsa-Pesa zones both favour the decoupling of the Chianti ridge from the less mobile structures (Albano ridge and Pistoia-Firenze basin) lying to the west of that ridge. This means that the seismic activation of one of those fault systems may increase tectonic load (and earthquake probability) in the other zone. Such tectonic connection could explain why the seismic phases in those two zones show an interesting time correlation. This correspondence

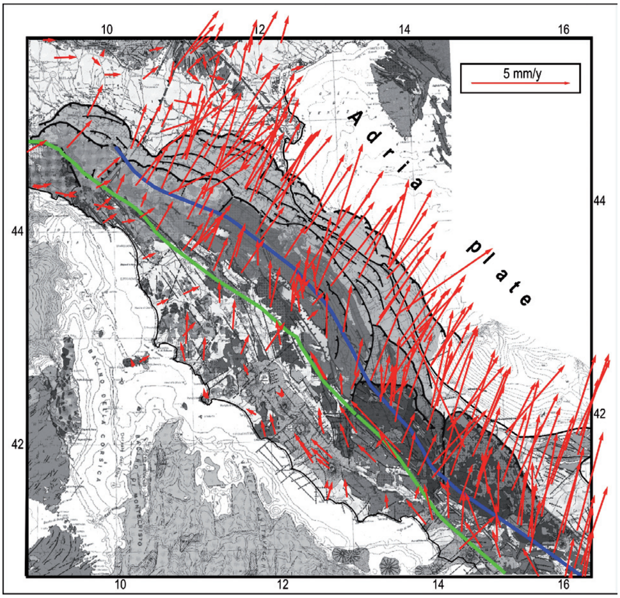


Fig. 3 – Tentative recognition of the boundaries (green and blue lines) between roughly homogeneous kinematic domains in the central and northern Apennines, based on the space geodetic (GPS) velocity field. Velocity vectors are referred to a fixed Eurasian frame (after Viti *et al*., 2015).

holds in particular for the seismic period that roughly started in 1887 in the Firenze zone, but also involves other shorter phases in those zones (Viti *et al*., 2015).

The fact that the Upper Valdarno and Chiana basins are almost aseismic, while seismic activity in the inner belt mainly occurs within a relatively S-N narrow zone, corresponding to the Elsa-Pesa-Siena-Radicofani basins, might imply that the oroclinal bending of the Chianti-Rapolano-Cetona ridge tends to create a compressional regime at its outer margin (upper Valdarno and Chiana basins) and an extensional/transtensional regime at its inner boundary (Elsa-Pesa-Siena-Radicofani basins).

Other considerations about the evidence of belt-parallel compression in the western part of Toscana and northern Lazio are reported by Viti *et al*. (2015).

**Velocity field in the Apennine belt by GPS data.** The GPS observations obtained from several networks in the study area (involving 450 continuous stations operating over the period 2001-2014) have been considered in order to define the present horizontal velocity field in the central and northern Apennines. The methodology adopted for data processing is described by Cenni *et al*. (2012, 2013).

The resulting velocity field with respect to an Eurasian frame is mapped in Fig. 3. This pattern confirms the major features of the long-term kinematics tentatively deduced by Quaternary deformations, in particular the fact that the outer part of the Apennine belt moves faster and with a greater eastward component, with respect to the inner belt.

The relatively high density of GPS sites in the central and northern Apennines has allowed us to tentatively recognize roughly homogeneous kinematic domains (Fig. 3). The highest velocities (3-5 mm/yr) and a prevailing NE-ward orientation of vectors characterize the outermost belt (east of the blue line in Fig. 3), including the buried thrusts and folds under the Po valley, while the lowest velocities (<1.5 mm/yr), with NW-ward to northward orientation, are observed in the innermost belt (west of the green line in Fig. 3). These two sectors are separated by an axial zone, characterized by intermediate velocity values and average orientation similar to the one that occurs in the outer belt. In the Padanian zone lying north of the buried folds the amplitude of the velocity vectors decreases significantly.

**Conclusions.** It is argued that the complex tectonic pattern presently recognized in the Northern Apennines has mainly been determined by belt-parallel shortening, which has developed at higher rates in the outer sector of the belt (RMU and TE wedges). Most major seismic sources (Norcia-Colfiorito-Gualdo Tadino-Gubbio-Upper Tiber, Mugello, Garfagnana and Lunigiana) are located in the zones where adjacent ridges have undergone different oroclinal bendings, inducing transtensional deformation. The fact that the effects of the above shortening processes have progressively involved more and more outer sectors of the northern Apennines is closely connected with the activation of more and more eastern decoupling fault systems (Latina, Val Roveto, Fucino and L'Aquila) in the Lazio-Abruzzi indenter (Fig. 1). The recent (late Pleistocene) development of the L'Aquila fault, in the inner side of the Gran Sasso arc, has favoured the formation of a major discontinuity in the northern Apennines (Norcia-Colfiorito-Gualdo Tadino-Gubbio), whose seismic activations allow the transtensional decoupling of the outermost sector of the RMU wedge from the inner belt (Fig. 1d). Sometimes, this decoupling extends northward, through the Upper Tiber and Romagna-Forlì fault systems.

Belt-parallel compression has also stressed the inner side of the northern Apennines, even though at a lower rate. Such process has caused longitudinal shortening and uplift of the ridge and basin systems that had formed during the upper Miocene and early Pliocene. The most evident effects of this deformation can be recognized in the Albano-Chianti-Rapolano-Cetona ridge and surrounding basins. The proposed tectonic context could explain why the Upper Valdarno and Chiana basins, lying along the outer boundary of that ridge, are almost aseismic, whereas the Elsa, Pesa, Siena and Radicofani basins, lying at the inner side of the same ridge, are affected by moderate seismic activity. The interaction between the Chianti-Rapolano-Cetona ridge and the northern part of the RMU wedge has generated seismogenic fault systems in the Firenze area. The correlation tentatively recognized between the time patterns of seismic activity in that zone and in western Chianti could be related with the fact that the activations of those fault systems both favour the decoupling of the Chianti ridge from the surrounding structures.

Finally, the long-term kinematic pattern deduced by the Quaternary deformation is compatible with the present velocity field indicated by space geodetic measurements. In particular, the above observations, being provided by a fairly dense network of continuous GPS sites, allow us to propose a good definition of the Apennine sectors which are characterized by different kinematic regimes.

**References**


Acocella V., Funiciello R.; 2006: *Transverse systems along the extensional Tyrrhenian margin of Central Italy and their influence on volcanism*. Tectonics, **25**, TC2003.

Bosellini A.: 2004: *The Western passive margin of Adria and its carbonate platforms*. Special volume of the Italian Geological Society for the 32nd International Geological Congress, Florence, Italy, 79-92.

Cenni N., Mantovani E., Baldi P., Viti M.; 2012: *Present kinematics of Central and Northern Italy from continuous GPS measurements*. J. Geodynamics, **58**, 62-72.

Cenni N., Viti M., Baldi P., Mantovani E., Bacchetti M.,Vannucchi A.; 2013: *Present vertical movements in central and northern Italy from GPS data: possible role of natural and anthropogenic causes*. J. Geodynamics, **71**, 74-85.

Ciarapica G., Passeri L.; 2005: *Late Triassic and Early Jurassic sedimentary evolution of the Northern Apennines: an overview*. Boll. Soc. Geol. It., **124**, 189-201.

Gudmundsson A.; 2001: *Fluid overpressure and flow in fault zones: field measurements and models*. Tectonophysics, **336**, 183-197.

Mantovani E., Viti M., Babbucci D., Tamburelli C., Albarello D.; 2006: *Geodynamic connection between the indentation of Arabia and the Neogene tectonic evolution of the Central-Eastern Mediterranean Region*. In: "Post-collisional tectonics and magmatism in the eastern Mediterranean region", Dilek, Y. and Pavlides, S. (Eds.), Geol. Soc. Am., Special Volume **409**, 15-41.

Mantovani E., Babbucci D., Tamburelli C., Viti M.; 2009: *A review on the driving mechanism of the Tyrrhenian-Apennines system: jmplications for the present seismotectonic setting in the Central-Northern Apennines*. Tectonophysics, **476**, 22-40.

Mantovani E., Viti M., Babbucci D., Albarello D., Cenni N., Vannucchi A.; 2010: *Long-term earthquake triggering in the Southern and Northern Apennines*. J. Seismology, **14**, 53-65.

Mantovani E., Viti M., Babbucci D., Cenni N., Tamburelli C., Vannucchi A.; 2012: *Middle term prediction of earthquakes in Italy: some remarks on empirical and deterministic approaches*. Boll. Geofis. Teor. Appl., **53**, 89-111.

Mantovani E., Viti M., Cenni N., Babbucci D., Tamburelli C., Baglione M., D'Intinosante V.; 2015a: *Seismotectonics and present seismic hazard in the Tuscany-Romagna-Marche-Umbria Apennines (Italy)*. J. Geodynamics, **89**, 1-14.

Mantovani E., Viti M., Babbucci D., Tamburelli C., Cenni N., Baglione M., D'Intinosante V.; 2015b: *Present tectonic setting and spatio-temporal distribution of seismicity in the Apennine belt*. Int. J. Geosciences, **6**, 429-454.

Mirabella F., Barchi M., Lupattelli A., Stucchi E., Ciaccio M.G.; 2008: *Insights on the seismogenic layer thickness from the upper crust structure of the Umbria-Marche Apennines (central Italy)*. Tectonics, **27**, TC1010, doi:10.1029/2007TC002134.

Viti M., Mantovani E., Babbucci D., Tamburelli C.; 2006: *Quaternary geodynamics and deformation pattern in the Southern Apennines: implications for seismic activity*. Boll. Soc. Geol. It., **125**, 273-291.

Viti M., Mantovani E., Babbucci D., Tamburelli C.; 2011: *Plate kinematics and geodynamics in the Central Mediterranean*. J. Geodynamics, **51**, 190-204.

Viti M., Mantovani E., Cenni N., Vannucchi A.; 2012: *Post-seismic relaxation: an example of earthquake triggering in the Apennine Belt (1915-1920)*. J. Geodynamics, **61**, 57-67.

Viti M., Mantovani E., Cenni N., Vannucchi A.; 2013: *Interaction of seismic sources in the Apennine belt*. Phys. Chem. Earth, **63**, 25-35.

Viti M., Mantovani E., Babbucci D., Tamburelli C., Cenni N., Baglione M., D'Intinosante V.; 2015: *Belt-parallel shortening in the Northern Apennines and seismotectonic implications*. Int. J. Geosciences, **6**, 938-961.

# sessione 1.3

## Vulcani e campi geotermici

**Convenor: F. Bianco e R. Petrini**

# PRELIMINARY MICROTREMOR SURVEY RESULTS IN SALINELLE MUD VOLCANOES: PATERNÒ, ITALY

**F. Panzera[1], S. Sicali[2], G. Lombardo[1], S. Imposa[1]**
[1] *Dip. di Scienze Biologiche, Geologiche e Ambientali – Sez. di Scienze della Terra, Università di Catania, Italy*
[2] *Istituto Nazionale di Geofisica e Vulcanologia – Osservatorio Etneo, Catania, Italy*

**Introduction.** The gas emissions observed at Etna, are linked to the persistent emission of a huge volcanic plume, in the summit craters during both quiescent and eruptive magma degassing, and others gas manifestations such as mud volcanoes and soil degassing which occur in peripheral sectors of the volcano (Allard *et al.*, 1991; Caracausi *et al.*, 2003; Aiuppa *et al.*, 2007). The *Salinelle* of Paternò are mud volcanoes located in the lower southern western flank of Mt. Etna, that it is one of the largest basaltic active volcano in Europe (Fig. 1a). The *Salinelle* are characterized by emissions of muddy and frequently salty water which sometime create specific pseudo-volcanic structures known as mud volcanoes. Their formation is due to the presence, in the subsoil, of over-pressured gases that escape upward through permeable rocks and structural and/or lithologic discontinuities, carrying to the surface a mixture of water, mud, hydrocarbon fluids and lithoid fragments that is emitted as a flowing liquid (Aiuppa *et al.*, 2004).

The water emitted at mud volcanoes frequently contains salty solutions that precipitate forming deposits. For this reason, in certain areas of Italy they are named *Salinelle*. Such phenomena have been observed and studied in different parts of the world and in different

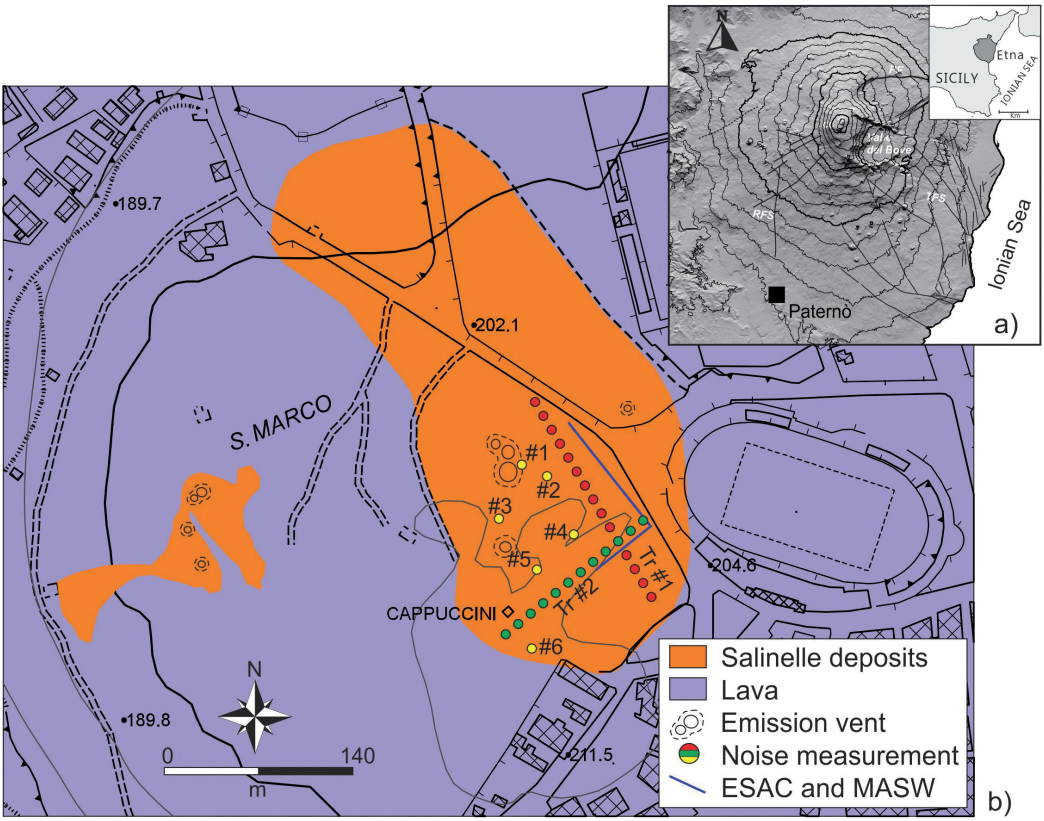


Fig. 1 – a) Simplified geological map of Mt. Etna showing the main structural features (RFS = Ragalna fault system, TFS = Timpe fault system, PF = Pernicana fault). b) Simplified geo-lithologic map of the *Salinelle* area.

areas of Italy (Dimitrov, 2002; Carveni *et al*., 2012; Adrian *et al*., 2015). In Sicily, in addition to Paternò (Catania), mud volcanoes can be observed in the areas of Agrigento and Caltanissetta, where they are also known with the name *Macalube* (Carveni *et al*., 2001; Etiope *et al*., 2002; Cangemi and Madonia, 2014). The results of some studies conducted on mud volcanoes represent the basis for the geothermal energy utilization, which presence is inferred by the composition of the gas ascending from depth (Mburu, 2014).

The present study through microtremor survey aims to provide useful information to increase the knowledge on the geo-thermal activity concerning the *Salinelle* of Paternò (Catania, Italy), whose activity is also well recognizable at a macroscopic level. Different studies throughout the world were performed to monitor the activity of mud volcanoes in terms of gas outflow (Albarello *et al*., 2012) and to study the presence of spectral anomalies in the passive seismic wavefield over different hydrocarbon reservoirs by using passive seismic surveys (Dangel *et al*., 2003; Holzner *et al*., 2005).

**The *Salinelle* mud volcanoes features.** Etna volcano edifice overlies the sedimentary basement made of flysch and clayey deposits that belong to the limestone of the Maghrebian-Appenninic chain (Lentini, 1982). The whole volcanic sequence can be considered as a highly porous medium, with a permeability coefficient that varies as a function of both the lithology and the volcano-tectonic structures. In particular, the volcanic sequence is characterized by alternating porous and fractured highly permeable lava layers and scarcely permeable pyroclastics. Then, the limit between lava and clay represents the base of the main aquifers of Etna. An exception is represented by the aquifer feeding the *Salinelle* mud volcanoes (Aiuppa *et al*., 2007). In this area the emitted waters are characterized by an abundant free gaseous phase and show typical features of waters linked to hydrocarbon reservoirs. Geothermometric estimates carried out on both the liquid and the gaseous phases emitted at the *Salinelle*, gave temperatures, at depth, that range 100-150°C (Chiodini *et al*., 1996). The fluids emitted generally consist of hydrocarbons (mainly $CH_4$) and hypersaline water (Giammanco *et al*., 1998; Amici *et al*., 2013). The mud and water mixtures are highly variable, and in some cases mud is the only fluid erupted with gas that builds cones up to a few meters high having a base diameter that can reach ten meters (Amici *et al*., 2013). These findings seem to suggest the presence of hydrocarbon reservoirs trapped in the shallow sedimentary rocks and characterized by the presence of thermal water enriched and heated by gas coming from magma of the Etna conduits.

The *Salinelle*, therefore, represent a very interesting geological-natural area, located at the NW boundary of Paternò, covering around 30,000 m$^2$ (Savasta, 1905). The main activities take place in two sites of Paternò area: *Salinelle del Fiume* and *Salinelle dei Cappuccini*. We focused our investigations in the latter site, in an area located close to the public football stadium (Fig. 1b), which is characterized by the most active vents. For practical reasons, we will refer to the general name *Salinelle* to indicate the study area. How thermal water reaches the surface is not fully clear, but some authors believe that at the *Salinelle* the mud rises through an old lava conduit (Carveni *et al*., 2001). To support this hypothesis there are data concerning a mechanical drilling performed during 1958 for hydrocarbons research (Carveni *et al*., 2001). A thick vacuolar lava rich in pyrite up to 400 m was found, in contrast with the average thin thickness of the surrounding lava in the area.

The temperature of the muddy waters varies from 10 and 20°C (Giammanco *et al*., 2007), but during some paroxysmal phases (1866, 1879 and 1954) the temperatures reach values between 46 and 49°C (Etiope *et al*., 2002). In the latter case, columns of muddy water as high as 1.5 m (Cumin, 1954) were observed. Silvestri (1867, 1879) reports of intense eruptive events occurred in early 1866 and late 1878. This phenomena included fountains of muddy water up to 3 m high and water temperature increases up to 46°C, that the author associated with local seismic events that occurred some days/weeks prior to the gas eruptions. In addition, previous studies revealed a strong correlation between specific earthquakes in eastern Sicily, the paroxysmal phases of *Salinelle* and significant variation of the concentration of the main gases emitted.

In particular, anomalous changes in the emission of Helium, typical geochemical precursor of earthquakes, and methane have been observed during the earthquake of Carlentini of December 13, 1990 (D'Alessandro *et al.*, 1993). However, some authors assert that the overall heat flux from Etna region has shown to be significantly and strongly controlled by the regional structural framework (Minett and Scott, 1985).

**Method.** A quick estimate of the surface geology effects on seismic motion is provided by the horizontal to vertical noise spectral ratio technique (HVNR). This technique firstly introduced by Nogoshi and Igarashi (1971), was put into practice by Nakamura (1989) and became in recent years widely used since it provides a reliable estimate of the fundamental frequency of soft soil deposits. The good agreement observed between results obtained using earthquake records and ambient noise has pointed out that microtremors are a valid tool to investigate ground motion polarization properties (Rigano *et al.*, 2008; Di Giulio *et al.*, 2009; Panzera *et al.*, 2013; Panzera *et al.*, 2014).

Ambient noise recordings were performed randomly in the area where the main activity of Salinelle is located (yellow points in Fig. 1b) and along two profile Tr#1 and Tr#2 (red and green points in Fig. 1b). A total number of thirty-two recording sites were usedto investigate the main features of the area. Time series of 30 minutes length were recorded through a long period velocimeter, using a sampling rate of 256 Hz and processed through the HVNR technique. According to common assumptions (Bard, 1998; Parolai *et al.*, 2001), the shortest window length of the signal has to be selected in a way that at least 10 cycles of the lowest frequency analyzed are included. Then, time windows of 100 s were considered and the most stationary part of the signal was selected excluding transients associated to very close sources. In this way the Fourier spectra were calculated in the frequency range 0.05-20.0 Hz and smoothed using a proportional 20% triangular window. Finally the resulting HVNR were computed estimating the logarithmic average of the spectral ratio obtained for each time window, selecting only the most stationary and excluding transients associated to very close sources. The experimental spectral ratios were also calculated after rotating the horizontal components of motion by steps of 10 degrees starting from 0° (north) to 180° (south) in order to investigate about the possible presence of directional effects. Examples of the results obtained are plotted in figure 2 using contour plots of amplitude, as a function of frequency (x-axis) and direction of motion (y-axis).

However, in presence of lateral and vertical heterogeneities or velocity inversion, the HVNR can be "non-informative" due to the occurrence of amplification on the vertical component of motion (Panzera *et al.*, 2015). Thus in this study we also computed a direct estimate of the polarization angle, for noise data by using the method proposed by Jurkevics (1988). This technique is very efficient in overcoming the bias linked to the denominator behavior that could occur in the HVNR's technique. Polarization analysis makes full use of the three component vector field to characterize the particle motion and it is based on the evaluation of eigenvectors and eigenvalues of the covariance matrix obtained by three-component seismograms. Signals at each site were band-pass filtered using the whole recordings and considering a moving window of 10 s with 20% overlap, therefore obtaining the strike of maximum polarization for each moving time windows.

The dynamic site properties and, in particular, the shear wave velocity of Salinelle deposits were investigated through non-invasive techniques such as the Multichannel Analysis of Surface Waves (MASW: Park *et al.*, 1999) and Extended Spatial AutoCorrelation (ESAC: Okada, 2003). The combined use of different techniques allowed us to compare and check the obtained results going also all over the limitations of each methodology.

A "L" array configuration was used for the ESAC measurements, recording 20 minutes of noise (blue lines in Fig. 1b). The array was settled using a 26-channel seismograph and 4.5 Hz geophones. The length was 60 m in NE direction and 70 m in NW direction. Time windows of 20 s were considered to calculate dispersion curves of the fundamental mode and the average of the dispersion curves was computed, excluding those not showing a clear dispersion or in which

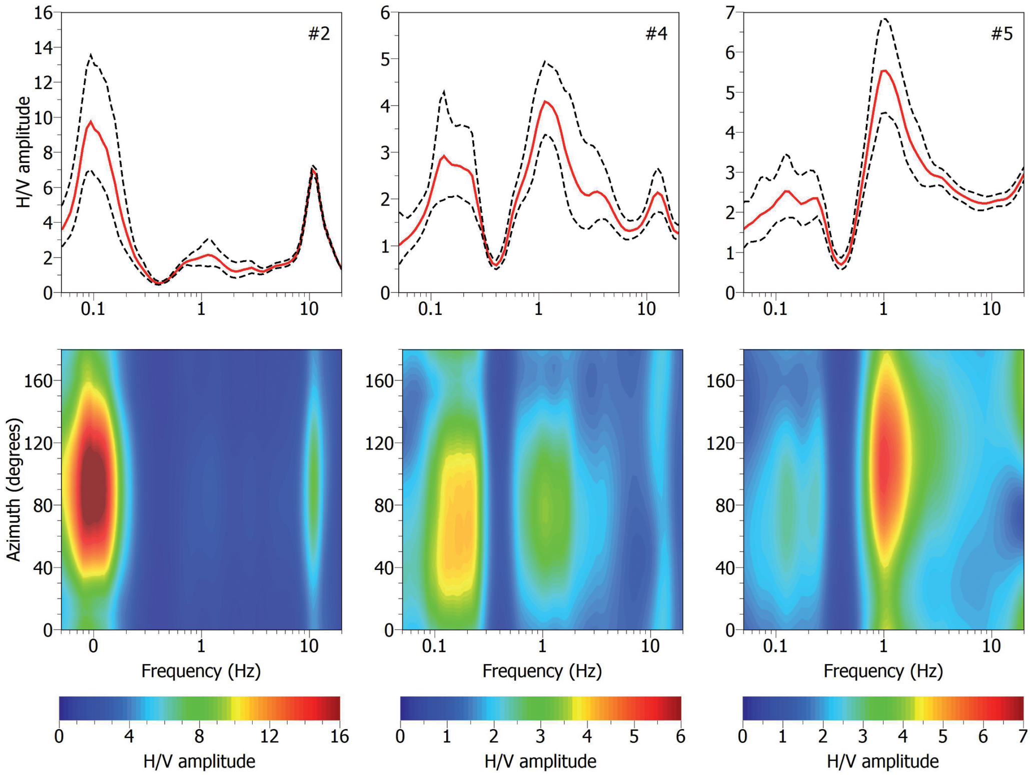


Fig. 2 – Examples of HVNR and directional resonance diagrams observed in the *Salinelle* area.

higher modes were dominant. The MASW tests were performed using the two branches of the array separately. Tests were made using a hammer source of 8 kg, with a fixed offset distance of 10 m, recording five shots to reduce the possible interference with other sources in the vicinity, with a registration length of 3 s and sample rate of 512 Hz.

In present study, the Rayleigh wave dispersion curves, obtained from the experimental setup, were inverted using the DINVER software (www.geopsy.org) which provide a set of dispersion curve models compatible with the observed dispersion curve. Inversion of the experimental dispersion curve needs a rough definition of the free parameters. This can be obtained using information coming either from a preliminary geological survey or from borehole data. If, as in our case, this information is not available, the values of parameters can be directly deduced from the fundamental mode of the Rayleigh wave dispersion curves (Albarello and Gargani, 2010). To invert the dispersion curve, a set of 1 to 8 uniform layers with homogeneous properties was considered, taking into account five parameters: shear waves velocity ($V_S$), thickness, compressional waves velocity ($V_P$), Poisson's ratio and density ($\varrho$).

**Results and discussions.** Present study was focused on the part of the *Salinelle* area in which main activity is concentrated, as shown by the mud flow deposits. A dense microtremor measurement survey was carried out, selecting the recording sites in order to obtain detailed information on subsoil structure. For this reason, many of the measurements were performed on a linear deployment.

The HVNR results set into evidence three different frequency ranges that appear interesting to get information on the subsoil structure. A low frequency peak at about 0.1 Hz was identified both on the Tr#1 and Tr#2, but with different amplitude (black arrows in Fig. 3a). Although, along the Tr#1 these peaks cannot be judged as particularly significant, we are incline to consider reliable such amplitude increase. In particular, we believe that these peaks could be interpreted as related to the presence of a discontinuity located at depth, linked to the clay overlaying the limestone. According to Aiuppa *et al*. (2004) this discontinuity could be the natural location of a hydrocarbon reservoir from which the mud rises through an old lava conduit (Carveni *et al*., 2001). Another signature of the presence of this reservoir can be extracted by inspecting the HVNRs, that show a strong HVNR de-amplification at about 0.4 Hz (grey arrows in Fig. 3a). Summarizing, low-frequency surficial waves (particularly Rayleigh waves), propagate through the subsoil with strength which varies in time. Then, as suggested by Lambert *et al*. (2007), when Rayleigh waves interact with the reservoir the resulting radiation pattern consists essentially in P-waves, along the vertical direction, and S-waves in the horizontal one. The observed low frequency peak and the de-amplification in the HVNRs could be interpreted as linked to the body waves generated at depth by the reservoir. At frequency values greater than 1.0 Hz the HVNRs show peaks variable both in frequency and in amplitude which could be related to the presence of the volcanic sequence characterized by blocks, free to oscillate and fractures filled by mud. The frequency peaks at values higher than 6.0-7.0 Hz could be interpreted as related to the *Salinelle* deposits whereas, at frequencies higher than 10.0 Hz the effects linked to noise generated by the gas emission can be observed (Fig. 3a).

We also investigated the existence of directional effects in the site response by rotating the horizontal components of the spectral ratios obtained at each measurement site (see examples in Fig. 2). Clear directional effects, with an angle of about 50°-80° N, in the frequency range 0.1-0.2 Hz, were detected. Conversely, different resonant frequencies and directions, that could be ascribed to the vibration of smaller blocks, can be observed at frequencies greater than 1.0 Hz. Furthermore, the rose diagrams of the noise polarization strikes, in the frequency range 0.1-0.5 Hz, are plotted (example in Fig. 3b). Rose diagrams are circular histograms in which instantaneous polarization azimuth measurements are plotted as sectors of circles with a common origin (class width 10°). In literature exists several studies (Panzera *et al.,* 2014 and references therein) discussing the role played by oriented fractures on seismic wavefield. In particular, in this kind of anisotropic medium the faster shear-waves became parallel to possible dikes, fissures and tensional cracks. On the contrary, the amplification of ground motion takes place orthogonally with the azimuth of the main fracture field (Panzera *et al.,* 2014 and references therein). As consequence the ENE-WSW polarization orientations observed in most of the sites could explained with the presence of a fracture field NNW-SSE oriented.

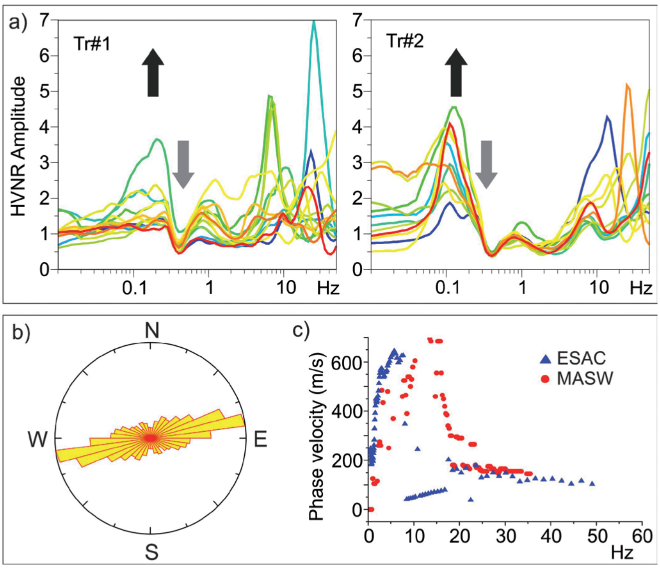


Fig. 3 – a) HVNR computed at each site along the Tr#1 and Tr#2 profiles. Black and grey arrows point out the low frequency peak and the spectral ratio de-amplification, respectively. b) Equal-area polar diagrams of the polarization azimuth obtained by filtering the noise in the frequency band 0.1-0.5 Hz. c) Dispersion curves obtained by ESAC and MASW tests.

Inspection of the dispersion curves acquired through ESAC and MASW prospections (Fig. 3c), shows that only slight differences in the quality of the obtained phase velocity – frequency plots, are present. The comparison of the two methodology clearly shows the prevailing of the contribution of high frequencies (>15.0 Hz) components in the definition of the MASW dispersion curves whereas, the phase velocity - frequency curves obtained through the ESAC approach, appear better defined at lower frequency (>5.0 Hz). Sediments outcropping at *Salinelle* according to the results of the dispersion curve inversion have a shear wave velocity in the range 100-200 m/s and a thickness of about 8-10 m.

**Concluding remarks.** The results obtained in the *Salinelle* area can be summarized as follow:

- the HVNRs put into evidence the presence of a hydrocarbon reservoir highlighted by the presence of a low frequency peak around 0.1 Hz followed by a de-amplification;
- the low frequency peak is strongly directional, with strike oriented ENE-WSW, suggesting the existence of a NNW-SSE oriented fracture system;
- the high variability in frequency and direction above 1.0 Hz could be linked to the vibration of small blocks or fractures. At frequencies higher than 10.0 Hz, evidences of a thin *Salinelle* deposit and noise generated by the gas emission is present;
- ESAC and MASW prospections allowed us to determine the possible thickness and shear wave velocity of the *Salinelle* deposits.

**References**


Adrian J., Langenbach H., Tezkan B., Gurk M., Novruzov A. G. and Mammadov A. L.; 2015: Exploration of the Near-surface Structure of Mud Volcanoes using Electromagnetic Techniques: A Case Study from Perekishkul, Azerbaijan. J. Environ. Eng. Geophys., 20, 153-164, 10.2113/JEEG20.2.153.

Aiuppa A., Allard P., D'Alessandro W., Giammanco S., Parello F. and Valenza M.; 2004: Magmatic gas leakage at Mount Etna (Sicily, Italy): relationships with the volcano-tectonic structures, the hydrological pattern and the eruptive activity. In: Bonaccorso, A., Calvari, S., Coltelli, M., Del Negro, C., Falsaperla, S. (Eds.), Mt. Etna: Volcano Laboratory. American Geophysical Union, Washington, DC, 129–145, doi:10.1029/143GM09.

Aiuppa A., Moretti R., Federico C., Giudice G., Gurrieri S., Liuzzo M., Papale P., Shinohara H. and Valenza M.; 2007: Hiroshi. Forecasting Etna eruptions by real-time observation of volcanic gas composition. Geology, 35, 1115-1118, doi: 10.1130/G24149A.1.

Albarello D. and Gargani F.; 2010: Providing NEHRP soil classification from the direct interpretation of effective Rayleigh waves dispersion curves. Bull. Seismol. Soc. Am., 100, 3284–3294, doi: 10.1785/0120100052.

Albarello D., Palo M. and Martinelli G.; 2012: Monitoring methane emission of mud volcanoes by seismic tremor measurements: a pilot study. Nat. Hazards Earth Syst. Sci., 12, 3617–3629, doi:10.5194/nhess-12-3617-2012.

Allard P., Carbonnelle J., Dajlevic D., Le Bronec J., Morel P., Robe M. C., Maurenas J. M., Faivre-Pierret R., Martin D., Sabroux J.C. and Zettwoog P.; 1991: Eruptive and diffuse emissions of CO2 from Mount Etna. Nature, 351, 387-391.

Amici S., Turci M., Giulietti F., Giammanco S., Buongiorno M. F., La Spina A. and Spampinato L.; 2013: Volcanic environments monitoring by drones mud volcano case study. International Archives of the Photogrammetry, Remote Sensing and Spatial Information Sciences, Volume XL-1/W2, 2013 UAV-G2013, 4-6, Rostock, germane, doi: 10.5194/isprsarchives-XL-1-W2-5-2013.

Bard P. Y.; 1998: Microtremor measurements: a tool for site effect estimation? Proceeding of the Second International Symposium on the Effects of Surface Geology on Seismic Motion. Yokohama, Japan, pp. 1251–1279.

Cangemi M. and Madonia P.; 2014: Mud volcanoes in onshore Sicily: a short overview. In: Wiese, F.; Reich, M. & Arp, G. (eds.): "Spongy, slimy, cosy & more…". Commemorative volume in celebration of the 60th birthday of Joachim Reitner. Göttingen Contributions to Geosciences 77: 123–127. http://dx.doi.org/10.3249/webdoc-3923.

Caracausi A., Italiano F., Nuccio P. M., Paonita A. and Rizzo A.; 2003: Evidence of deep magma degassing and ascent by geochemistry of peripheral gas emissions at Mt. Etna (Italy): assessment of the magmatic reservoir pressure. J Geophys Res 108 (B10): 2463 doi: 10.1029/2002JB002095.

Carveni P., Benfatto S. and Sturiale G.; 2001: Aspetti geologici e geomorfologici dei vulcani di fango del basso versante sud-occidentale etneo ed ipotesi sulla loro genesi. Il Quaternario, 14 (2), 117-130.

Carveni P., Barone F., Benfatto S., Imposa S. and Mele G.; 2012: Mud volcano fields in the Mt. Etna area (eastern Sicily). In: C. Giusti (Ed.), Geomorphosites 2009: raising the profile of geomorphological heritage through iconography, inventory and promotion, Paris Sorbonne Université, Paris, 54-60.

Chiodini G., D'Alessandro W. and Parello F.; 1996: Geochemistry of gases and waters discharged by the mud volcanoes at Paternò, Mt. Etna (Italy). Bull. Volcanol., 58, 51–58.

Cristofolini R.; 1967: La successione dell'attività vulcanica sulle pendici sud-occidentali dell'Etna. Atti dell'Accademia Gioenia di Scienze Naturali, Catania, VI, 18, 283-294.
Cumin G.; 1954: Le Salinelle di Paternò e la loro attuale attività. Bollettino dell'Accademia Gioenia di Scienze Naturali, Catania, IV, 2 (9), 515-528.
D'Alessandro W., De Domenico R., Parello F. and Valenza M.; 1993: Geochemical anomalies in the gaseous phase of the mud Volcanoes of Paternò, Sicily. Proc. Scient. Meet. Seism. Protec., Venice, 12-13 July 1993, 171-175.
Dangel S., Schaepman M. E., Stoll E. P., Carniel R., Barzandji O., Rode E.-D. and Singer J. M.; 2003: Phenomenology of tremor-like signals observed over hydrocarbon reservoirs. J. Volcanol. Geotherm. Res., 128, 135–158.
Di Giulio G., Cara F., Rovelli A., Lombardo G. and Rigano R.; 2009: Evidences for strong directional resonances in intensely deformed zones of the Pernicana fault, Mount Etna, Italy. J. Geophys. Res., 114, doi:10.1029/2009JB006393.
Dimitrov L.I.; 2002: Mud volcanoes—the most important pathway for degassing deeply buried sediments. Earth-Science Reviews, 59 (1–4), 49–76, doi:10.1016/S0012-8252(02)00069-7.
Etiope G., Caracausi A., Favara R., Italiano F. and Baciu C.; 2002: Methane emission from the mud volcanoes of Sicily (Italy) Authors. Geoph. Res. Lett., doi: 10.1029/2001GL014340.
Giammanco S., Inguaggiato S. and Valenza M.; 1998: Soil and fumarole gases of Mount Etna: geochemistry and relations with volcanic activity. J. Volcanol. Geoth. Res., 81, 297–310.
Giammanco S., Parello F., Gambardella B., Schifano R., Pizzullo S. and Galante G.; 2007: Focused and diffuse effluxes of CO2 from mud volcanoes and mofettes south of Mt. Etna (Italy). J. Volcanol. Geotherm. Res., 165, 46–63.
Holzner R., Eschle P., Zürcher H., Lambert M., Graf R., Dangel S., and Meier P. F.; 2005: Applying microtremor analysis to identify hydrocarbon reservoirs: First Break, 23, 41–46.
Jurkevics A.; 1988: Polarization analysis of three components array data. Bull. Seism. Soc. Am., 78, 1725–1743.
Lambert M., Schmalholz S. M., Podladchikov Y. Y. and Saenger E. H.; 2007: Low frequency anomalies in spectral ratios of single station microtremor measurements: Observations across an oil and gas field in Austria: 77th Annual International Meeting, SEG, Expanded Abstracts, 1352–1356.
Lentini F.; 1982: The geology of the Mt. Etna basement. Mem. Soc. Geol. It., v.23, 7-25.
Mburu M.; 2014: Geothermal energy utilization. Presented at Short Course IX on Exploration for Geothermal Resources, organized by UNU-GTP, GDC and KenGen, at Lake Bogoria and Lake Naivasha, Kenya, Nov. 2-23, 2014.
Minett S. T. and Scott S. C.; 1985: Theoretical considerations of heat flux on Mount Etna, Sicily. J. Volcanol. Geotherm. Res., 25, 53-67.
Nakamura Y.; 1989: A method for dynamic characteristics estimation of subsurface using microtremor on the ground surface. Quaterly Report of the Railway Technical Research Institue 30 (1), 25-30.
Nogoshi M. and Igarashi T.; 1971: On the amplitude characteristics of microtremor (part 2) (in Japanese with english abstract). Journal of seismological Society of Japan, 24, 26-40.
Okada H.; 2003: The microtremor survey method. Geophysical Monograph Series, SEG, 129 pp.
Panzera F., Lombardo G. and Muzzetta I.; 2013: Evaluation of buildings dynamical properties through in-situ experimental techniques and 1D modelling: the example of Catania, Italy. Phys. Chem. Earth doi: 10.1016/j.pce.2013.04.008.
Panzera F., Pischiutta M., Lombardo G., Monaco C. and Rovelli A.; 2014: Wavefield polarization in fault zones of the western flank of Mt. Etna: observations and fracture orientation modeling. Pure Appl. Geophys. DOI 10.1007/s00024-014-0831-x.
Panzera F., Lombardo G., Monaco C. and Di Stefano A.; 2015. Seismic site effects observed on sediments and basaltic lavas outcropping in a test site of Catania, Italy(Link). Natural Hazards, doi: 10.1007/s11069-015-1822-7.
Park C. B., Miller R. D. and Xia J. H.; 1999. Multichannel analysis of surface waves. Geophysics, 64, 800-808.
Parolai S., Bormann P. and Milkereit C.; 2001: Assessment of the natural frequency of the sedimentary cover in the Cologne area (Germany) using noise measurements. Journal of Earthquake Engineering, 5, 4, 541-564.
Rigano R., Cara F., Lombardo G. and Rovelli A.; 2008: Evidence for ground motion polarization on fault zones of Mount Etna volcano. J. Geophys. Res., 113, B10306, doi:10.1029/2007JB005574.
Savasta G.; 1905: Memorie storiche della città di Paternò - Catania, Galati.
Silvestri O.; 1867: I fenomeni vulcanici presentati dall'Etna nel 1863-64-65-66 considerati in rapporto alla grande eruzione del 1865. Mem. Acc. Gioenia Sc. Nat., 3 (1), 53-319.
Silvestri O.; 1879: Eruzione di fango presso l'Etna. Boll. Vulc. It., 6 (1-3), 28-31.

# EVALUATION OF THE EFFECTS INDUCED ON GROUNDWATER'S THERMAL STATE AFTER RE-INJECTION OF ALTERED TEMPERATURE WATER: THE CASE STUDY OF HEAT TRANSPORT SIMULATION IN THE SHALLOW AQUIFER OF TURIN CITY (NW ITALY)

**D. Barbero[1,2], D.A. De Luca[1], M.G. Forno[1], M. Lasagna[1], A.Tissoni[2], M. Zagami[2]**
[1] *Department of Earth Sciences, Turin University, Italy*
[2] *Freelance Geologist*

**Introduction.** A case study of heat transport modeling in the shallow aquifer of the Turin City (NW Italy) with finite-difference computer code is here reported. A detailed geological characterization of the subsoil and the estimation of hydrogeological and thermal features of the shallow aquifer are essential tools in support of heat transport simulations for the design of open-loop system. This modeling has the purpose of evaluate the thermal plume propagation connected to the re-injection of altered thermal water in the aquifer with temperature higher or lower than the average annual value.

This research focuses on the following problems: a) to study the effects induced by the discharge of water in the shallow aquifer at temperature higher than the annual average value and the consequent rise of temperature induced downstream of the same. In this case, the thermal modeling of the shallow aquifer allows to estimate the alteration on the thermal groundwater state in order to predict phenomena of "*groundwater's thermal pollution*" with associated environmental problems; b) to study the effects related to the injection in the aquifer of water at lower temperature than the annual average value. The discharge of water at lower temperature causes a decrease of the water calorific power with a consequent loss of efficiency of the geothermal plant.

From the practical point of view, the methodology here proposed can be applied in the preliminary stages of a geothermal system design, where it is convenient to assess the optimal distance between extraction and injection wells in order to avoid "*thermal feedback phenomena*" and, more generally, assessing the environmental impact related to the extension of the thermal anomaly in the subsurface.

**Morphological and geological setting of the Turin city.** The Turin city is located in a narrow strip of the north western Po Plain, between the Alps and Turin Hill (Fig. 1A). In particular, it is placed in a marginal position, at the edge with the Turin Hill, where the current course of the Po River is located that separates a plain sector from a hill one.

The plain area (altitude ranging from 200 – 350 m a.s.l.) shows a weak inclination towards east and NE (about 1‰).

In detail, the morphology is slightly articulated by the presence of small embankments and depressions connected with ancient trends of Po River, characterized by small areal extension, height of few meters and mostly discontinuous areal development (Forno and Lucchesi, 2012). Nevertheless, the morphology of the plain is affected by a generalized anthropic reshaping that causes the modification of numerous natural forms and the creation of new anthropic forms.

The plain does not have the typical structure of a subsiding plain, instead, it presents a sector with important recent uplift, connected to the Padane Thrust Front (TFP), that influences the geometry of the sedimentary bodies and created important variations of the hydrographic network during the Pleistocene up to the recent settling of the Po River to the north of the hill (Forno, 1982; Forno and Lucchesi, 2012).

The shallow subsoil of Turin consists of Pleistocene fluvial and outwash sediments linked to Alpine watercourses forming wide fans, cut by the erosional scarps linked to the present course of the Po River and partly filled by its Holocene fluvial sediments. The distribution area of the deposits linked to Po River is restricted to the narrow band at the edge of the river bed. Overall, the fluvial and outwash deposits show a shallow thickness, comprised between 10 m, on the edge with the Turin Hills, up to 80 m towards the Alpine chain. These sediments are organized

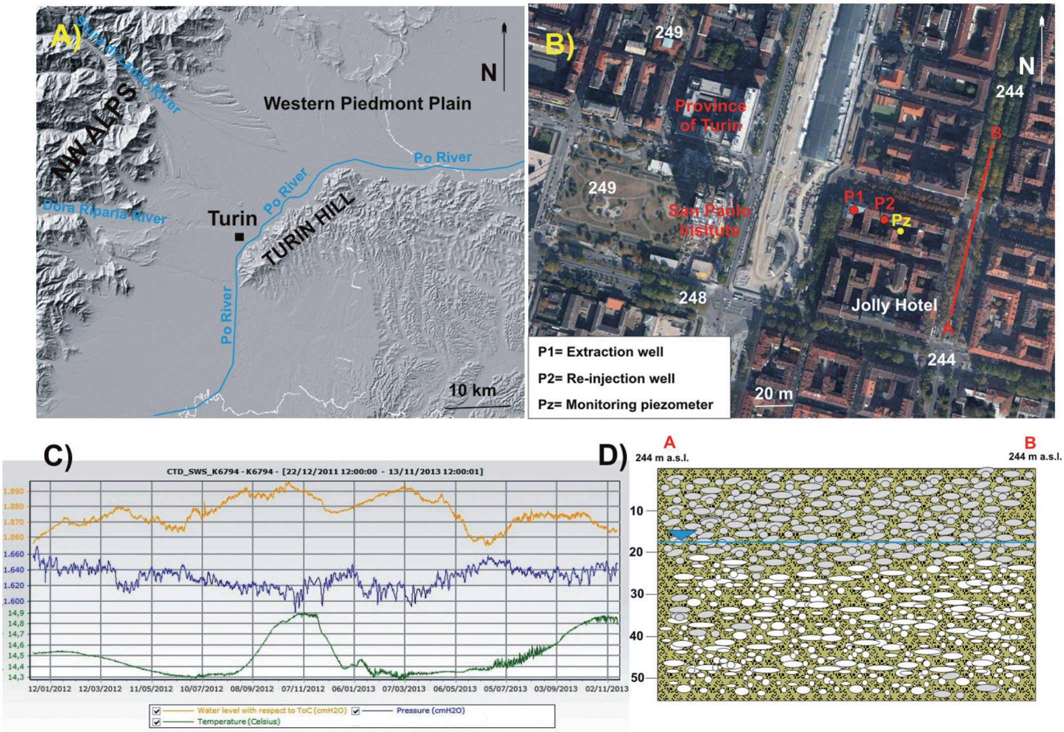


Fig. 1 – Sketch of north-western Piedmont Region (A); satellite view of the study area (B); monitoring parameters: static level and temperature of the aquifer (C); simplified stratigraphic cross section of the subsoil (D).

in different sedimentary bodies separated by erosional surfaces with areal range development, representing the main elements of the succession (Bonsignore *et al.*, 1969; Dela Pierre *et al.*, 2007). This sedimentary succession rests on the "villafranchian succession", comprising deltaic deposits (Lower Complex) and fluvial deposits (Upper Complex), referred to Piacenzian and Calabrian respectively, separated by an unconformity (Cascina Viarengo Surface) (Carraro Ed., 1996; Forno *et al.*, 2015), and deep marine clay deposits (Lugagnano Clay) with littoral sandy deposits (Asti Sand) referred to Zanclean (Festa *et al.*, 2009).

**Hydrogeological setting of the Turin city.** This study focuses on the shallow aquifer hosted within the fluvial deposits. The shallow aquifer is mainly supplied by direct rainfall and rivers at the outlet of the valleys in the plain. This aquifer has a thickness generally ranging between 20 and 50 m; in spite of the variable thickness of the aquifer, it has a high productivity and has a regional importance. The water table generally follows the topographic surface. The bottom of the shallow aquifer is generally well marked by a textural variability of the deposits. The local presence of thick and relatively continuous layers of silt or clay-rich deposits allows a clear separation between the shallow aquifer and deep aquifers, hosted mainly in marine and permeable horizons of the villafranchian succession (Canavese *et al.*, 2004; Bove *et al.*, 2005; De Luca and Ossella, 2012; Irace *et al.*, 2009).

**Technical characteristics of the geothermal open-loop system.** The project, object of this research, corresponds to an open-loop system constituted by two wells (P1 and P2 in Fig. 1B), extraction well and re-injection well, for heating-cooling and hot water health. The wells are placed at a distance of 20 m. Both wells were drilled up to 45 m depth from ground level and together intercept a shallow aquifer. The reintroduction of thermal water therefore, occurs in the same aquifer from which it was extracted for the operation of the open-loop system.

The wells have been realized in rotation with reverse circulation of fluid. The wells, with a diameter ∅ = 800 mm, are 45 m deep. The blank casing and the bridge screens, butt welded, have diameters ∅ = 406 mm.

Extraction well has bridge Johnson screens placed between 16.00 - 40.00 m from ground level; while the injection well has bridge Johnson screens placed between 10.00 - 40.00 m from ground level. The gravel packing (siliceous gravel) was put between 10.00 – 40.00 m from ground level.

A monitoring piezometer (Pz in Fig. 1B), with diameter ∅ = 127 mm and depth of 30 m, was realized downstream from the well of restitution at a distance of 12 m. The piezometer was equipped with a multiparametric probe ("Schlumberger water service"), placed at a depth of 25 m from ground level, with the aim of monitoring the variability of water table and the temperature of the water. Measurements collected concern the following parameters: static level and temperature of water (Fig. 1C).

**Geological and geotechnical features of the subsoil.** By the stratigraphy drawn up during the drilling of the wells and the piezometer, the subsurface can be so exemplified:

- 0.00-21.00 m: gravel and pebbles with very dense sandy-silty matrix, interbedded by cemented gray layers (conglomerate);
- 21.00-45.00 m: gravel with moderately compacted brown silty sand and subordinates pebbles.

In Fig. 1D is shown a simplified stratigraphic cross section of the subsoil.

The granular soil is characterized by a high angle of friction (expressed in terms of effective stress), and then by a high shear strength resistance. These geotechnical features are indicative of a load-bearing capacity of the soil where the high value cannot be reduced in any way as a result of any changes of the water table.

**Hydrogeological and thermodynamic features of the aquifer.** The hydraulic and hydrogeological features of the aquifer are essential tools for the simulations of thermal motion.

The aquifer is unconfined and the natural movement of the groundwater is towards NW-SE. The *static level of the water table* $l_s$ is equal to 18.50 m from ground level (value measured in November 2011).

The *hydraulic gradient i* is equal to 0.00476; the *horizontal hydraulic conductivity* $k_{x,y}$ is equal to $4.3 \cdot 10^{-3}$ m/s; the *vertical hydraulic conductivity* $k_z$ has been assumed equal to 1/10 $k_{x,y}$ m/s; the *radius of influence R* estimated and adopted in the simulations is 100 m.

The *specific storage* $S_s$ has been assumed equal to 0.0001 (1/m) and the *specific yield* $S_y$ has been assumed equal to 0.2.

The hydrogeological characteristics of the aquifer were deducted by performing a *pumping test* (step-drawdown test). The pumping test was carried out in 4 steps, with the duration of 45 minutes each. The test allowed to obtain the *critical discharge* $Q_c$ = 42 l/s according to the Dupuit equation. In particular, for a discharge of Q = 12 l/s corresponds a lowering of 0.17 m; for Q = 20 l/s corresponds a lowering of 0.30 m, for Q = 30 l/s corresponds a lowering of 0.50 m and, finally, for Q = 55 l/s corresponds a lowering of 1.60 m.

The *transmissivity* $T = 2.38 \cdot 10^{-2}$ m²/s was calculated using the equation $T = 0.183 \cdot Q_c/s$, where *s* is the lowering of the groundwater during the time interval considered. The *permeability K* $= 9.31 \cdot 10^{-4}$ m/s of the aquifer was obtained by dividing the transmissivity for the thickness of the aquifer.

The *specific discharge* was calculated with the expression $q_s$= Q/s, where s is the lowering of the water in the well and Q is the discharge. For Q =20 l/s and s = 30 cm, we obtained $q_s$ = 60 l/s·m.

The *specific lowering* s* = s/Q is equal to 15 m/m³/s for a discharge of Q = 20 l/s and a lowering of water s = 30 cm. In conclusion, at the maximum discharge operating of 12 l/s, the loss of linear load imposed by the hydrodynamic parameters of the aquifer (consequent to the laminar flow of the same) is to be considered negligible.

As SEAWAT simulates the temperature as a solute dissolved in the aquifer, is necessary to estimate the hydro-dispersive parameters: the *effective porosity* $n_e$ has been assumed equal to 0.20, *horizontal dispersivity* $\alpha_L$ has been assumed equal to 10 (m), the ratio between *horizontal and vertical dispersivity* ($\alpha_l$) and $\alpha_v$ was set equal to 0.1, while the ratio between the *vertical dispersivity* ($\alpha_v$) and $\alpha_L$ was set equal to 0.01 for each simulation.

The thermodynamic parameters required for the calculation are: the *dry bluk density* $\varrho_b$, the *molecular diffusion coefficient* $K_d$, assimilable to the *heat diffusion coefficient,* and then the *thermal diffusivity* $\alpha$. Based on the literature, for the shallow aquifer under consideration, were assumed the following parameters: $\varrho_b$ was set equal to 2000 kg/m$^3$, $K_d$ was set equal to $10^{-7}$ l/mg and $\alpha$ was set equal to 0.20 m$^2$/die.

Sensitivity analysis of the thermodynamic parameters carried in similar contexts (Piccinini *et al.*, 2012) have shown that as the heat transfer is a process mainly advective-diffusive, the progressive increase of two orders of magnitude of $\alpha$ not induce significant changes in temperature, instead an increase of $n_e$ over 60% leads to a decrease of 0.5°C for the temperature while, a variation of $K_d$ of an order of magnitude changes the velocity of rebalances of the system at the end of the activity. In conclusion, the most significant parameters for dimensioning the distance between the extraction and re-injection wells are $K_d$ and $n_e$, while, $\alpha$ may be considered negligible.

**Materials and methods.** *Thermal characteristics of the aquifer.* Through the introduction of a sensor installed inside the piezometer, at 25 meters of depth from ground level, the temperature data of the aquifer have been recorded. Starting from December 2011, temperature data are collected periodically, three times a day every eight hours (4:00,12:00 and 20:00) (Fig. 1C). The monitoring is still ongoing.

The analysis of data temperature collected during the monitoring period December 2011-December 2014, shows that the temperature ranges around a mean value of 14.6 °C. The recorded temperature are contained within the value 0.60 °C.

This average temperature value is in agreement with recent studies on temperature distribution in the subsoil finalized to check the “homoeothermic surface” with its relative temperature value, within the Quaternary fluvial deposits hosting a shallow aquifer. The study conducted in Turin city and its hinterland (Barbero *et al.*, 2015) and in the surrounding plain sector (Barbero *et al.*, 2014) show an average temperature value of $\langle T \rangle = (14.56 \pm 0.40)$ °C and $\langle T \rangle = 14.00 \pm 0.60$°C respectively.

*SEAWAT code*. Simulations of flow and heat transport have been performed in order to evaluate the environmental thermal impact within the aquifer product by the re-injection of water used for heat exchange cycle.

The simulations were performed using SEAWAT, a three-dimensional finite-difference computer code developed by the US Geological Survey for the modeling of the flow of variable density in saturated porous media. This code combines the capabilities of two existing codes: MODFLOW and MT3DMS, useful for the simulation of water flow of variable density and solute transport multi-species and heat respectively. SEAWAT (Version 4) is able to simulate the transport of heat and consider the variations in the density of the fluid as a function of the concentration of solute and temperature (Thorne *et al.*, 2006).

For the purpose of geothermal modeling, it’s necessary to determine both hydraulic and thermal parameters of the aquifer. The values of hydraulic conductivity and storage were obtained by pumping tests, described in the preceding paragraph instead, other parameters of difficult experimental testing as conductivity, heat capacity, effective porosity and dispersivity were taken from literature.

The hydrogeological and thermal parameters, have been implemented in SEAWAT for the realization, in the short and in long period, of some scenarios regarding the expansion of thermal bubble.

From the practical point of view, the results of the simulations in the short period can be used to optimize the distance between the extraction and re-injection wells during the preliminary stage of design, while in the long period are useful to assess the interference of the geothermal plant in question with other geothermal wells located in the area (i.e. Jolly Hotel and Province of Turin Institute) and other wells in the phase of realization (San Paolo Institute) in order to avoid thermal anomalies. Error design can in fact lead to "*thermal feedback phenomena*": this phenomenon occurs when the distance between the wells (extraction and injection wells) is relative short; in this case, a recall of the thermal plume by the well of extraction it is observed, with a consequent pumping of groundwater with temperatures close to those discharged, compromising the efficiency the geothermal plant (Cultrera, 2012; Piccinini *et al.*, 2012; Galgaro and Cultrera, 2013). Another phenomenon, known in literature, and partially related to the previous one, is "*thermal breakthrough*" (Banks, 2009; Piccinini *et al.*, 2012; Galgaro and Cultrera, 2013): it consists in the slow diffusion of the thermal plume upstream.

**Governing equation.** Heat transport and solute transport contain many similarities (Anderson, 2005). Their mathematical representation is similar when the terms describing heat transport are formulated in equivalent solute expressions. SEAWAT leverages these similarities by using MT3DMS to simulate heat transport.

The heat transport equation, manipulated by Thorne *et al.* (2006), highlights the similarity with the solute transport. In Eq. 1 tensors and vectors shown in bold.

$$\left(1 + \frac{(1-\theta)}{\theta}\frac{\rho_s}{\rho}\frac{c_{Psolid}}{c_{Pfluid}}\right)\frac{\partial(\theta T)}{\partial t} = \nabla \cdot \left[\theta\left(\frac{k_{Tbulk}}{\theta \rho c_{Pfluid}} + \boldsymbol{\alpha}\frac{\boldsymbol{q}}{\theta}\right)\cdot \nabla T\right] - \nabla \cdot (\boldsymbol{q}T) - q_s' T_s \qquad (1)$$

where: $q$ (m/s) is specific discharge; $\alpha$ (m) is the dispersivity tensor; $\theta$ (-) is the volumetric water content; $q'_s$ ($s^{-1}$) is a source or sink of fluid with density $\varrho_s$; $\varrho_s$ (kg/m$^3$) is the density of the solid (mass of the solid divided by the volume of the solid); $\varrho$ (kg/m$^3$) is the density of the fluid; $c_{Psolid}$ (J/kg·°C) is the specific heat capacity of the solid; $c_{Pfluid}$ (J/kg·°C) is the specific heat capacity of the fluid; $k_{Tbulk}$ (W/m·°C) is the bulk thermal conductivity of the aquifer material; $T$ (°C) is the temperature of the fluid; $T_s$ (°C) is the source temperature; t is time (s). $\varrho_b$, $\varrho_s$, and $\theta$ are related by: $\varrho_b = \varrho_s (1 - \theta)$.

Variations in temperature inside a saturated porous medium may give rise to vertical convective motions, which determine the upward movement of the water masses hottest and lighter and the downward movement of the masses more cold and heavy. These motions, can influence the water flow of the system.

The form of the equation of density-dependent flow is solved by SEAWAT Eq. 2 (Langevin *et al.*, 2007; Langevin *et al.*, 2010) and allows to consider the variations of density and viscosity as a function of temperature.

$$\nabla \cdot \left[\rho \frac{\mu_0}{\mu} K_0 \left(\nabla h_0 + \frac{\rho - \rho_0}{\rho_0}\nabla z\right)\right] = \rho S_{S,0}\frac{\partial h_0}{\partial t} + \theta \frac{\partial \rho}{\partial t} - \rho_S' q_S' \qquad (2)$$

where: $\mu$ (kg/m·s) is the fluid dynamic viscosity; $\mu_0$ (kg/m·s) is the reference fluid dynamic viscosity (reference fluid is generally freshwater at temperature $T$ = 25 °C); $K_0$ (m/s) is the hydraulic conductivity tensor of material saturated with the reference fluid; $h_0$ (m) is the hydraulic head (m) measured in terms of the reference fluid of a specified concentration and temperature; $z$ (m) is the cartesian coordinate; $S_{s,0}$ (1/m) is the specific storage, defined as the volume of water released from storage per unit volume per unit decline of $h_0$; $q'_s$ (1/s) is a source or sink of fluid with density $\varrho_s$.

**Computational domain.** The flow model was initially implemented with MODFLOW, along with SEAWAT code for the simulation of the heat transport. The domain of the model was discretized by a 1000 x 1000 m uniform grid mesh, with square cells of 10 m$^2$. In the area of distribution of the wells, the cell sizes have been reduced until obtaining cells of 1 m$^2$.

The subsurface was simplified into three layers:

1st layer: unsaturated zone located between the ground surface and the water table;

2nd layer: shallow aquifer;

3rd layer: impermeable soil beneath the aquifer.

**Boundary conditions.** Boundary conditions are used to define the water exchanges, mass or heat occurring at the interface between the volume modeled and the outside.

The hydraulic (piezometric) gradient was set through boundary conditions of type 1 (Dirichlet): this condition allows to assign the hydraulic load (m) to cells/nodes of the domain (command "*Constant and General Head in MODFLOW*").

The extraction and reinjection wells were simulated with conditions of 2nd type (Neumann) through which it's possible to assign a hydraulic flow (m/s) to cells/nodes of the domain (command "*Well in MODFLOW*").

As regards the thermal features of the model, the thermal regime of the aquifer has been reproduced with a condition of constant temperature (command "*Constant concentration* in SEAWAT"). This condition was set to upstream to the direction of groundwater flow. The constant value assigned at the temperature is equal to the undisturbed average temperature of the aquifer.

The model no examines phenomena of recharge of the aquifer and loss through evapotranspiration.

**Results.** After defining the hydrogeological conceptual model and heat transfer model of the area, several simulations were carried out with the aim to evaluate the effects on the thermal state of groundwater related to the propagation of thermal bubble.

As a reference value of undisturbed temperature we assumed the annual average recorded in the piezometer by multiparametric probe and equal to 14°C.

Two scenarios were simulated: the first concerns the thermal effects related to the use of extraction and re-injection wells (P1 and P2 in Fig. 1B); the second scenario considers the effects caused by the operation of the wells of Province of Turin Institute and the wells of the San Paolo Institute placed upstream of one's considered in the first scenario.

*First scenario*. It was hypothesized a cycle of operation so structured: In winter (October to March): $Q_{peak}$ = 10 l/s; extraction temperature water: 14°C; discharge temperature water: 10°C; $\Delta T$= 4°C.

In summer (April to September): $Q_{peak}$ =10 l/s; extraction temperature water: 14°C; discharge temperature water: 9°C; $\Delta T$= 5°C.

The two cycles are spaced from one month for stopping of the system.

In Fig. 2 it is shown the extension of the thermal bubble respectively at the end of the first summer cycle (Fig. 2A), after one year (Fig. 2B) and after two years (Fig. 2C) of operation of the plant.

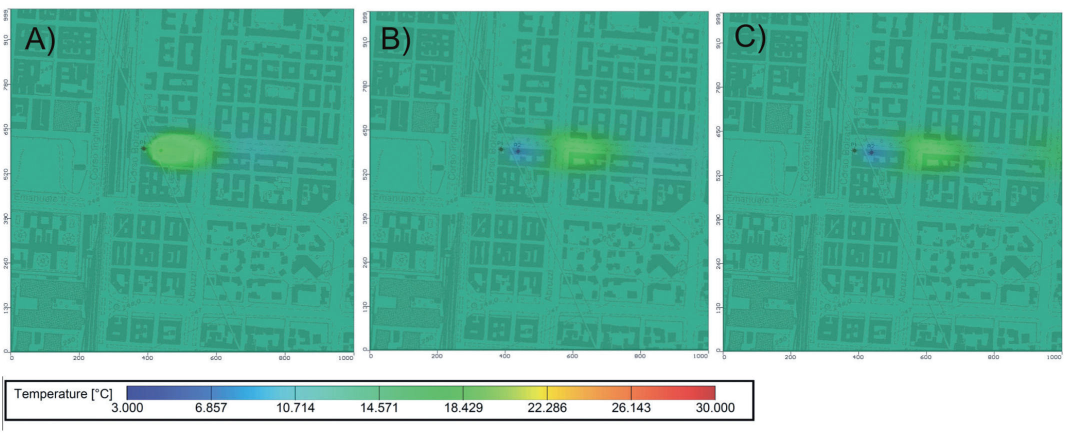


Fig. 2 – Simulations of thermal bubble extension at the end of the first summer cycle (A), after one year (B) and after two years (C) of operation of the plant.

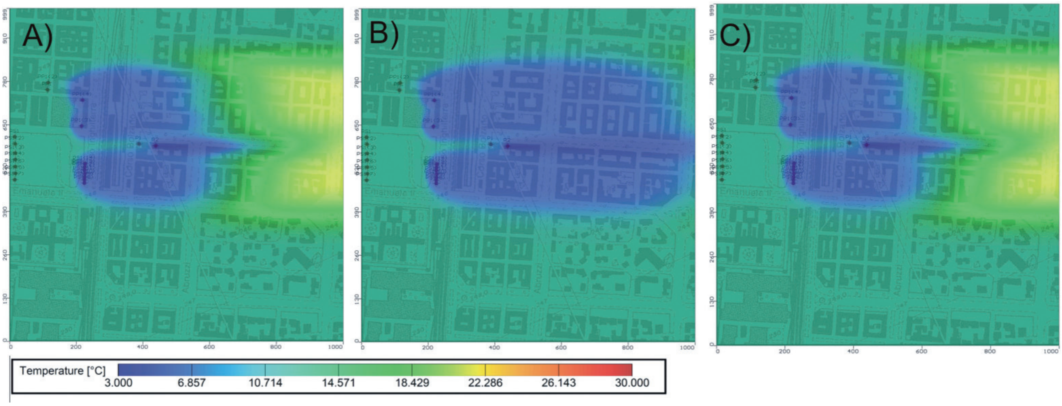


Fig. 3 – Simulations of thermal bubble extension after one year (A), after 16 months (B) and after two years (C) of operation of the plant.

The simulations show that the thermal impact a few hundred meters downstream of the discharge is practically negligible. The extension of the thermal plume upstream (i.e. "*thermal breakthrough*"), it is clearly more limited for hydraulic reasons. Finally, it is observed that the distance between the extraction and re-injection wells is sufficient to prevent the temperature increase of the groundwater in correspondence of the extraction well: this means absence of the phenomenon of "*thermal feedback*".

*Second scenario*. It was hypothesized a cycle of operation so structured: In winter (October to March): $Q_{peak}$ = 15 l/s; extraction temperature water: 8°C; discharge temperature water: 3°C; $\Delta T$= 5°C.

In summer (April to September): $Q_{peak}$= 15 l/s; extraction temperature water: 22°C; discharge temperature water: 27°C; $\Delta T$= 5°C.

The two cycles are spaced from one month for stopping of the system.

This hypothesis, highly conservative, assumes that the thermal plume, produced by the wells of Province of Turin Institute and San Paolo Institute, located upstream, are able to determine, in correspondence of the extraction well, a temperature of groundwater during the winter cycle equal to 8°C and during the summer cycle equal to 22°C.

The simulations (Fig. 3) show the extension of the thermal after one year (Fig. 3A), after 16 months (Fig. 3B) and after two years (Fig. 3C) of operation of the plant.

The thermal situation created by the operations San Paolo Institute and Province of Turin Institute wells, does not significantly change the operation of the wells P1 and P2. The simulations show a thermal bubble with increase or decrease of temperature in the aquifer of reduced size.

**Conclusions.** The study highlights the utility of using finite-difference computer codes in support of water flow and heat transport simulations. The modeling of groundwater flow with MODFLOW and heat transport with SEAWAT code, allow to evaluate the propagation of thermal bubble and therefore the correct design of the geothermal plant (e.g optimize the distance of extraction and re-injection wells) for estimating the effects on the thermal state of groundwater. Therefore, long period simulations are useful to evaluate the environmental effects inducted by the extension of the thermal plume.

The monitoring of groundwater temperature and other parameters (static level and electric conductivity of the aquifer), still ongoing, allows the future validation of the model as well as the protection of groundwater resources from groundwater's thermal pollution.

In conclusion, scenarios above proposed have shown a remarkable aptitude of the aquifer in the mitigation of thermal anomalies, as evidenced by the temperature values recorded in the monitoring piezometer and compatible with the average annual value of the temperature in the subsurface.

## References

Anderson M.P.; 2005: Heat as a ground water tracer. Ground Water, 43 (6), 951–968.

Banks D.; 2009: Thermogeological assessment of open-loop welldoublet schemes: a review and synthesis of analytical approaches. Hydrogeology Journal, 17, 1149–1155.

Barbero D., De Luca D.A., Forno M.G., Lasagna M., Magnea L.; 2014: A statistical approach to the study of thermal data of shallow aquifer in Piedmont region (NW ITALY). Abstract book DAMES 2014: 4th International Conference on Data analysis and modeling in Earth sciences, Milano 6-8 ottobre 2014.

Barbero D., Bucci A., De Luca D.A., Forno M.G., Gisolo A., Lasagna M., Magnea L; 2015: Temperature distribution and homoeothermic surface depth in the shallow aquifer of Turin and its hinterland (NW Italy). Abstract Book of the 42nd IAH Congress – AQUA 2015: Hydrogeology: back the future. Rome 13-18 September 2015.

Bonsignore G., Bortolami G.C., Elter G., Montrasio A., Petrucci F., Ragni U., Sacchi R., Zanella E.; 1969: Note illustrative della Carta Geologica d’Italia alla scala 1:100.000, Fogli 56 e 57 “Torino e Vercelli”, IIa ed., Serv. Geol. It., Roma.

Bove A., Destefanis E., De Luca A.D., Masciocco L., Ossella L. and Tunossi M.; 2005: Assetto geoidrologico della regione Piemonte. (Cd Rom). Idrogeologia della Pianura Piemontese, Regione Piemonte.

Canavese P. A., De Luca A.D. and Masciocco L.; 2004: La rete di monitoraggio delle acque sotterranee delle aree di pianura della Regione Piemonte: quadro idrogeologico. PRISMAS: Il monitoraggio delle acque sotterranee nella Regione Piemonte, Regione Piemonte, II.

Carraro F. (Ed.); 1996: Revisione del Villafranchiano nell’area-tipo di Villafranca d’Asti. Il Quaternario (It. Journ. Quatern. Sc.), 9 (1), 5–119.

Cultrera M.; 2012: Geotermia-Corto circuito termico nei sistemi di geoscambio a circuito aperto. Acque Sotterranee - Italian Journal of Groundwater, 3/130, 85-56.

De Luca D.A., Ossella L., 2012: Assetto idrogeologico della Città di Torino e del suo hinterland. 1, 10- 15, Atti del simposio: “Geologia Urbana di Torino”. Torino, 19 ottobre 2012.

Dela Pierre F., Piana F., Fioraso G., Boano P., Bicchi E., Forno M. G., Violanti D., Clari P., Polino R., Balestro G. and D’atri A.; 2003: Foglio 157 “Trino” della Carta Geologica d’Italia alla scala 1: 50.000. APAT, Dipartimento Difesa del Suolo, Roma.

Festa A., Dela Pierre F., Irace A., Piana F., Fioraso G., Lucchesi S., Boano P., Forno M. G., Bicchi E., Violanti D., TrenkWalder S., Ossella L., Bellardone G., Campus S., Tamberlani F.; 2009: Note illustrative del Foglio 156 “Torino Est”della Carta Geologica d’Italia alla scala 1:50.000. APAT, Agenzia per la Protezione dell’Ambiente e per i Servizi Tecnici. Dipartimento Difesa del Suolo, Roma, 1-143.

Forno M.G.; 1982: Studio geologico dell’Altopiano di Poirino (Torino). Geogr. Fis. Dinam. Quat., 5, 129-162.

Forno M.G., Lucchesi S.; 2012: La successione pliocenico-quaternaria su cui è edificata la Città di Torino e il suo significato per l’utilizzo del territorio. 1,3–9, Atti del simposio: “Geologia Urbana di Torino”. Torino, 19 ottobre 2012.

Forno M. G., Gattiglio M., Comina C., Barbero D., Bertini A., Doglione A., Irace A., Gianotti F., Martinetto E., Mottura A., Sala B.; 2015: Stratigraphic and tectonic notes on the Villafranca d’Asti succession in type-area and Castelnuovo Don Bosco sector (Asti reliefs, Piedmont). Alpine and Mediterranean Quaternary, 28(1), 5-27.

Galgaro A., Cultera M.; 2013 Thermal short circuit on groundwater heat pump. Applied Thermal Engineering 57(s 1–2), 107–115.

Langevin C.D., Thorne D.T. Jr., Dausman A.M., Sukop M.C., Guo W.; 2007: SEAWAT Version 4: a computer program for simulation of multi-species solute and heat transport. U.S. Geological Survey Techniques and Methods, book 6, cap.A22, Reston, Virginia: USGS.

Langevin C.D., Dausman A.M., Sukop C.; 2010: Solute and heat transport model of the Henry and Hilleke laboratory experiment. Ground Water, 48, 5, 757-770.

Irace A., Clemente P., Natalicchio M., Ossella L., Trenkwalder S., De Luca D.A., Mosca P., Piana F., Polino R., Violanti D.; 2009: Geologia e idrostratigrafia profonda della Pianura Padana occidentale. La Nuova Lito Firenze, 110 pp.

Piccinini L., Vincenzi V., Pontin A., Tonet F.; 2012: Modello di trasporto di calore per il dimensionamento di un sistema di geoscambio a circuito aperto. Acque Sotterranee - Italian Journal of Groundwater, 3/130, 41-53.

Thorne D., Langevin C.D., Sukop M.C.; 2006: Addition of simultaneous heat and solute transport and variable fluid viscosity to SEAWAT. Computer and Geosciences, 32, 1758-1768.

# FEASIBILITY OF HIGH-FREQUENCY MICRO-GASCHROMATOGRAPHY SOIL GAS MONITORING REVEALED AT LA SOLFATARA (CAMPI FLEGREI, ITALY)

**S. Sicola[1], M.L. Carapezza[2], M. Ranaldi[1], F. Sortino[3], L. Tarchini[1]**
[1] *Dipartimento di Scienze, Università Roma Tre, Roma, Italy*
[2] *Istituto Nazionale di Geofisica e Vulcanologia, Sez. di Roma, Italy*
[3] *Istituto Nazionale di Geofisica e Vulcanologia, Sez. di Palermo, Italy*

Solfatara crater is a tuff cone located in the central part of Campi Flegrei caldera (Campania, Southern Italy) (Fig. 1). The most recent unrests (1970-1972; 1982-1984) were centered in the caldera inner part, exactly below Solfatara zone (Barberi *et al.,* 1984; 1989; Orsi *et al*., 1996). After the last bradyseismic event (1982-1984) upwards ground movement slightly decreased, but since 2000 a new increase was recorded, likely linked with new magmatic fluids input into the hydrothermal system, which caused both fluid-pressure increment in the system and chemical-physical macroscopic changes in fumarolic activity (Chiodini *et al*., 2008, 2010; 2012). Moreover, Orsi *et al*. (2004) include Solfatara crater in the most prone area for new vent opening.

In our work we studied soil gas reactions in near-surface soil, aiming at assessing the feasibility of a novel geochemical monitoring methodology. We performed two $CO_2$ and $H_2S$ soil diffuse degassing surveys with the accumulation chamber and soil concentration measurements of $CO_2$, $H_2$, $H_2S$, $CH_4$, $O_2$, $N_2$, He at 0.5 m depth over a target area of 50 points. Soil gas samples were also collected at different depths (0.3, 0.5, 0.8, 1 m) at 7 points out of the previous 50. The presented study permitted to highlight the main gas reactions taking place in near-surface soil, and showed up the feasibility of a new monitoring technique, high-frequency micro-gaschromatography, which could be settled in more easily accessible sites and under less aggressive environmental conditions than those found close to Solfatara fumaroles.

**Diffuse soil degassing assessment.** During February and April 2014, soil flux surveys were performed at Solfatara with an accumulation chamber equipped with a Li-820 infrared detector (0-2 vol. %) for $CO_2$ and with TOX-05 detector for $H_2S$ (0-20 ppm) (Carapezza *et al*., 2011). Measurements were acquired over a fixed grid of 50 points 5 m spaced. Both maps were processed using ordinary kriging in ArcGis.

*$CO_2$ flux survey.* The decadal monitoring of $CO_2$, in active and quiescent volcanoes, and at Campi Flegrei as well, plays an important role in volcanic surveillance. Besides fumarolic degassing, widespread gas diffusion from soil is affected by the presence of faults and fracture systems. $CO_2$ anomalies-trend therefore outlines the presence of faults and fractures, which represent the most prone way for magmatic/hydrothermal fluids to reach the surface (Granieri *et al*., 2010). Soil $CO_2$ flux map shows that the main faults within Solfatara crater have a NW-SE direction and an associated NE-SW trend, and that the principal $CO_2$ anomalies are located in the inner area and in the zone of high-temperature fumaroles (e.g. Bocca Nuova T= 160 °C) in agreement with those indicated by Todesco *et al*. (2003), Chiodini *et al*. (2010) and Granieri *et al*. (2010).

We estimated the total diffuse $CO_2$ soil flux rate to 101.2 tonnes/day. A value very similar to the one estimated by Tassi *et al*. (2013), 79 tons/day, during the nearest in time published survey.

*$H_2S$ flux survey.* According to Giggenbach (1980), $H_2S$ fugacity in hydrothermal environments is controlled by pyrite coexisting with an unspecified aluminium-silicate. $H_2S$ dominates in low-temperature fumaroles and solfataras, where discharges arise from deep hydrothermal systems (Giggenbach, 1980). Since decades, fumarolic gas emissions were sampled and analyzed in order to monitor the hydrothermal system activity, and $H_2S$ concentration in Solfatara fumaroles spanned 0.5 to 1.5 vol.% (Caliro, *et al*., 2007; Chiodini *et al*., 2008; Tassi *et al*., 2013).

In this work we surveyed the $H_2S$ diffuse soil flux for the first time at Solfatara, using the same technique for $CO_2$ (Fig. 1). The $H_2S$ flux map (minima from green to yellow colors;

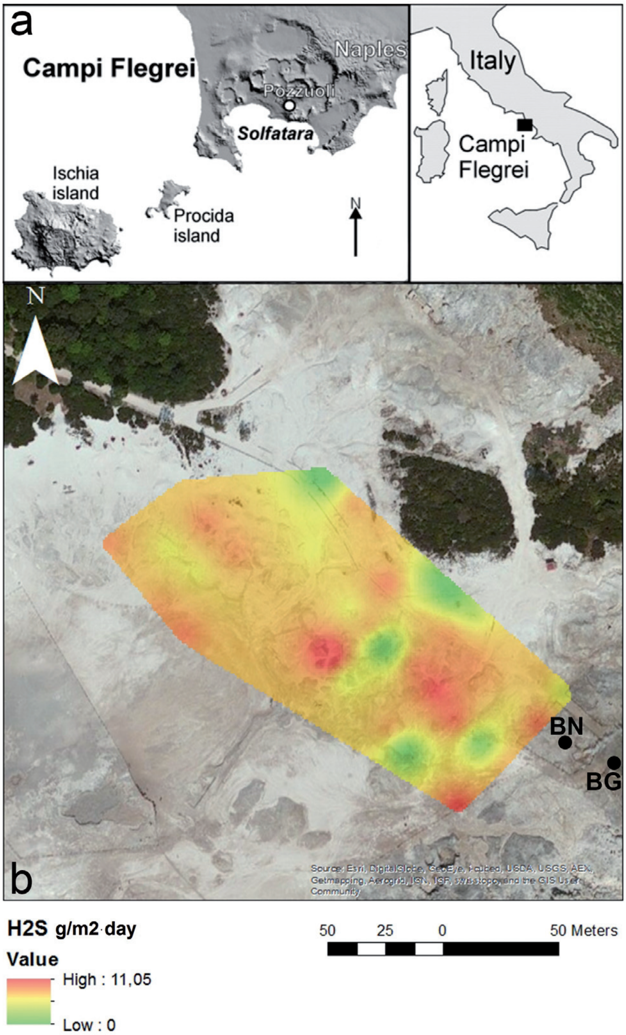


Fig. 1 – a) Hillshade DEM of Campi Flegrei caldera and location of Solfatara crater (mod. after Caliro *et al.* 2007). b) $H_2S$ soil flux map at Solfatara of this work.

maxima from yellow to red colors) shows large variability at small spatial scale. Zones with high values are evidenced not only in the SE sector near Bocca Grande and Bocca Nuova fumarolic vents (BG and BN), but also in the central and western investigated sector. Short-scale variations are commonly associated to micro-fracturing systems of the soil that occur even in apparently homogeneous ground. Also, the spatial variation of the flux is enhanced by the contiguous presence of hydrothermally altered and sealed terrain, low-permeability or less fractured zones (Granieri *et al.,* 2010). But short-scale variations can also depend on fluid interacting with very shallow soil levels, as we will discuss further.

The total soil flux estimated for this first $H_2S$ survey sums up to 0.4 tonnes/day from an area of 0.2 km$^2$.

**In-soil gas assessment.** Soil gas were sampled and T were measured at 0.5 m depth over the same 50 point grid of soil flux surveys. Furthermore, we sampled soil gas at different depths (0.3, 0.5, 0.8, 1 m) at seven sites chosen amongst the previous 50, in order to identify processes governing gas reactions at very shallow levels. Dry gas concentrations were measured with Agilent 490 Micro GC Analyzer.

Data acquired at 0.5 m depth over the fixed grid, point out that $CO_2$ is the predominant species, with percentages spanning 73 to 99 vol. % depending on air contamination, while $H_2$, $CH_4$ and $H_2S$ soil concentrations often are even higher than in H-T fumaroles (up to the 50 % more). $H_2$ spans 2 to 2900 ppm, and it shows a clear positive correlation with soil temperature. $H_2S$ maxima and minima are anticorrelated with those of the other gases. The latter species ($CO_2$, $CH_4$, $H_2$, He) do not show a perfect match in maxima and minima distribution (Fig. 2): as uprising gases, a mixture of magmatic fluids flashing hydrothermal liquid to vapour (Caliro *et al.*, 2007), interact with air-saturated waters in shallow low T (< 100 °C) levels, and diffuse through rock volumes of different permeability, explaining the differences in the observed soil gas concentrations. Nevertheless, also other phenomena need to be involved in generating short-scale variations in soil gases: in fact, $H_2$, $CH_4$ and $H_2S$ are enriched in some samples compared to fumarolic composition.

We, therefore, sampled soil gases at different depths in 7 of the previous 50 points, in order to investigate very shallow phenomena governing gas reactions. Figs. 3a and 3b clearly show

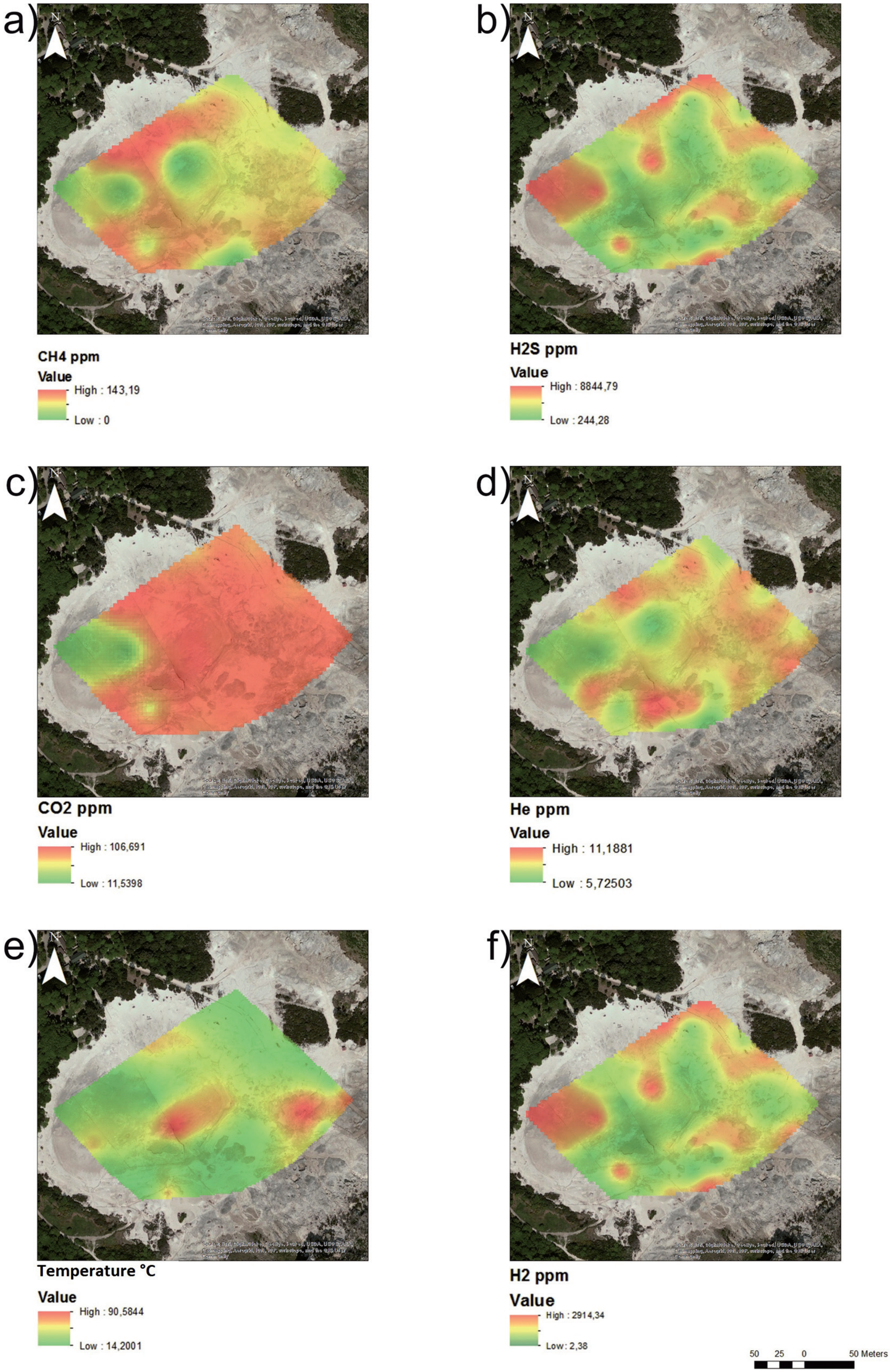


Fig. 2 – Solfatara area concentration maps of: a) $CH_4$; b) $H_2S$; c) $CO_2$; d) He; e) temperature; f) $H_2$.

that $CH_4$ and $H_2S$ concentrations are way higher is some soil samples than in fumaroles, and that [$H_2$] is always positively correlated with T. Furthermore, sampling data show that a decrease of $H_2$ matches an increase of $H_2S$ and $CH_4$ due to T increasing with depth (Figs. 3a and 3b).

On these evidences something has to be hypothesized causing either preferential enrichment of $CH_4$, $H_2S$ or variations in gases equilibrium processes. One possible explanation is the preferential $CO_2$ removal in surface acid muddy water pools. Another could be that near surface gases condense with neutral pH causing $CO_2$ dissolution, and thus enrichment in other species. If this cannot be excluded, the quick re-equilibrium of some reactions involving the analysed chemical species seems more noteworthy. We consider, then, two possible reaction for $CH_4$ and $H_2S$ genesis and enrichment:

$$CO_2+4H_2= CH_4 +2H_2O \quad (1)$$

Molar ratios in Eq. 1 justify the observed quick [$H_2$] decrease and the less significant ($CH_4$) increase with decreasing depth. The linear relation in Fig. 3a shows that reaction 1 occurs quickly and at shallow depth during gas arise, because we observed significative $H_2$ and $CH_4$ variations at different depths in the first meter of the soil.

To justify $H_2S$ enrichment, gas equilibria in sulphur species cannot be considered because $H_2S$ is the only gas species in the Solfatara volcanic/hydrothermal gas (Chiodini *et al*., 2001). As previously described, Giggenbach (1980) and Caliro *et al*. (2007) stated that $fH_2S$ in hydrothermal system is mainly controlled by pyrite coexisting with unspecified allumo-silicate. We can similarly speculate $H_2S$ enrichment in the shallow Solfatara soil by hydrolysis with sulphide minerals:

$$MeS_2+H_2 + (H_2O) = MeO + 2H_2S \quad (2)$$

All our soil samples show temperature values lower than 100°C and inverse relationship with $H_2S$ concentrations; this could reflect a variation in thermodynamic conditions compared to the hot fumarolic fluids. In our vertical profile sampling, an increase in $H_2S$ is very marked and this evidence suggests that the process happens close the surface. Reaction 2 can be related with emission temperatures, gas flow, soil humidity (condensate) and $fH_2$. In fact, when there are high flow/temperature conditions, Eq. 2 can be slowed or even inhibited by a "carrier effect" of the fumarolic gas which likely prevents gas-rock interaction of $H_2$ or doesn't allow changes in redox conditions.

As we have previously showed, variations in $fH_2$ modifies equilibria in Solfatara gas species. Soil (CO), analyzed only in vertical samplings, is affected by reactions in near surface levels too. In Fig. 3d (CO) is plotted as a function of temperature. Samples at T close to 90/100 °C show a CO concentration enrichment, relatively to fumarolic composition (up to 9 ppm against 3.2 ppm in Bocca Grande fumarole). Following Giggenbach (1987), we can linearly combine redox reactions (1) and (3):

$$CO_2 + H_2 = CO + H_2O \quad (3)$$

To obtain Eq. 4 which explains [CO] increase in the soil:

$$3CO_2+CH_4 =4CO+2H_2O \quad (4)$$

The previously discussed ($CH_4$) increase, framed in a re-equilibration system of all gas species described by Eqs. 1, 2 and 4, leads to a contemporaneous increase in (CO). The observed CO decrease in some soil samples at T< 80 °C is likely related to dilution into the soil with air, resulting also in a T decrease.

**Conclusions.** Previous authors proposed a conceptual geochemical model for Solfatara system, which describes the mixing process between the magmatic component and the hydrothermal one at depth, ruling out the emitted fluid composition and variations into the crater.

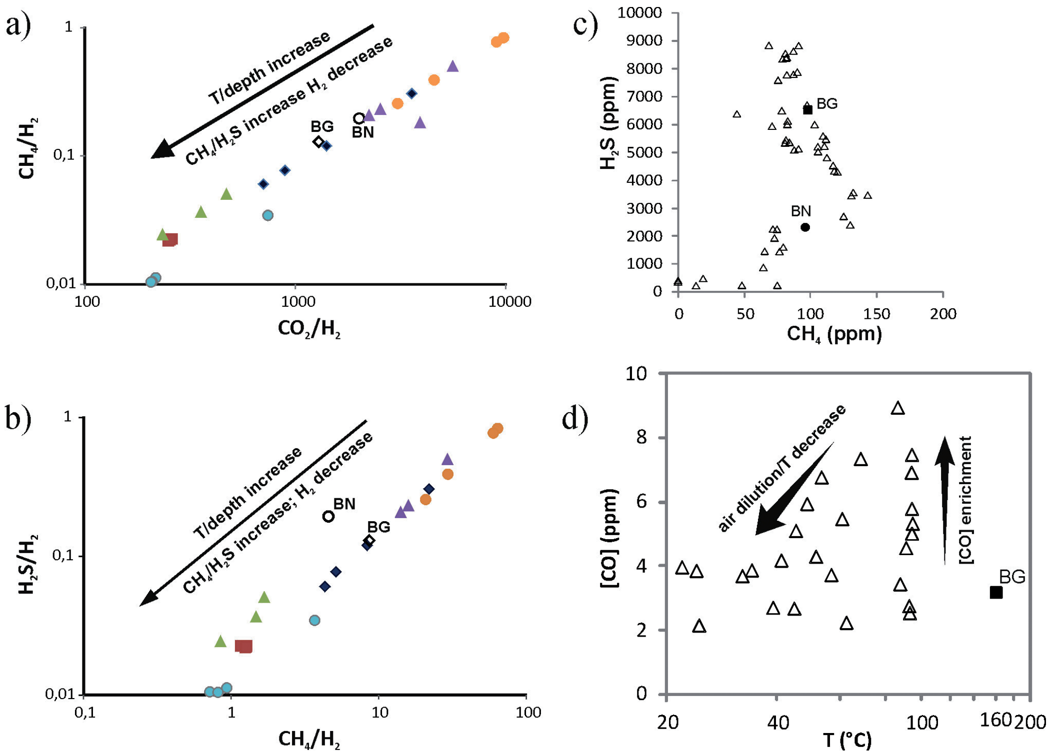


Fig. 3 – Binary plot of: a) $CH_4/H_2$ vs $CO_2/H_2$; b) $H_2S/H_2$ vs $CH_4/H_2$; both plots are relative to the 7 points transect at different depths (0.3, 0.5,0.8, 1 m) compared with fumaroles values (BG; BN) c) Scatter plot of $CH_4$ vs $H_2S$ at 0.5 m depth of the 50 points grid inside Solfatara crater. d) Variation of soil (CO) as a function of soil temperature.

Our data is in agreement with this model and we can conclude that, as an enhanced magmatic input causes higher fluid emissions and consequently chemical and physical changes, a chemical variation occurs also in the soil gases (in particular $H_2$, $CO_2$, $H_2S$, CO and $CH_4$) and a temperature rise in the whole area. The observed $H_2$/T positive correlation in our work shows us a very shallow system (actually very first meters below ground surface) of multi-equilibrium reactions described by Eqs. 1, 2 and 4, in which near-surface $fH_2$ variations justify enrichment in CO, $CH_4$ and $H_2S$.

Results of our study shows up the feasibility of a new approach in monitoring Solfatara gas emissions: the high frequency micro-gaschromatography (Sortino *et al.*, Interpretations on rise up of volcanic fluids through high-frequency gas analysis by micro gas-cromatograph, oral presentation at GNGTS Meeting, Trieste 2015), a newly experimented setup of classical gaschromatography, which could be installed at Solfatara in more easily accessible sites and under less aggressive environmental conditions than the fumarolic sites.

**References**

Barberi F., Corrado G., Innocenti F., Luongo G., (1984). *Phlegraean Fields 1982-1984: Brief Chronicle of a Volcano Emegency in a Densely Populated Area*. Bull. Volcanol., Vol 47-2. 175-185.

Barberi F., Navarro J.M., Rosi M., Santacroce R., Sbrana A., (1988). *Explosive interaction of magma with ground water: insight from xenoliths and geothermal drillings*. Rendiconti della società italiana di Mineralogia e Petrologia, 1988, Vol. 43, pp. 901-926.

Caliro S., Chiodini G., Moretti R., Avino R., Granieri D., Russo M., Fiebig J. (2007) *The origin of the fumaroles of La Solfatara (Campi Flegrei, South Italy)*. Geochimica et Cosmochimica Acta 71 (2007) 3040–3055

Carapezza M.L,, Barberi F., Ranaldi M., Ricci T., Tarchini L.,. Barrancos J., Fischer C., Perez N., Weber K. , Di Piazza A., Gattuso A. (2011). *Diffuse $CO_2$ soil degassing and $CO_2$ and $H_2S$ concentrations in air and related hazards at Vulcano Island (Aeolian arc, Italy)*. Journal of Volcanology and Geothermal Research 207 (2011) 130–144

Chiodini, G., Caliro S.,.Cardellini C., Avino R., Granieri D., Schmidt A., (2008). *Carbon isotopic composition of soil $CO_2$ flux, a powerful method to discriminate different sources feeding soil $CO_2$ degassing in volcanic-hydrothermal areas*, Earth Planet. Sci. Lett., 274(3–4), 372–379, doi:10.1016/j.epsl.2008.07.051.
Chiodini G., Caliro S., Cardellini C., Granieri D., Avino R., Baldini A., Donnini M., Minopoli C., (2010). *Long term variations of the Campi Flegrei (Italy) volcanic system as revealed by the monitoring of hydrothermal activity*. J Geophys Res vol. 115, ISSN: 0148-0227, doi: 10.1029/2008JB006258
Chiodini G., Caliro S., De Martino P., Avino R., Gherardi F. (2012). *Early signals of new volcanic unrest at Campi Flegrei caldera? Insights from geochemical data and physical simulations*. Geology, published online on 23 July 2012 as doi:10.1130/G33251.1
Giggenbach, W.F., (1980). *Geothermal gas equilibria*. Geochim. Cosmochim. Acta, 44, 2021- 2032.
Giggenbach, W.F., (1987). *Redox conditions governing the chemistry of fumarolic gas discharges from White Island, New Zealand*. Appl. Geochem, 2, 143-161.
Giggenbach, W.F., (1991). *Chemical techniques in geothermal exploration. In: D'Amore, F. (coordinator), Application of geochemistry in geothermal reservoir development*. UNITAR/UNDP publication, Rome, 119-142.
Granieri D., Avino R., Chiodini G. (2010). *Carbon dioxide diffuse emission from the soil: ten years of observations at Vesuvio and Campi Flegrei (Pozzuoli), and linkages with volcanic activity*. Bull Volcanol (2010) 72:103–118 DOI 10.1007/s00445-009-0304-8.
Orsi G., de Vita S., Di Vito M., (1996). *The restless, resurgent Campi Flegrei nested caldera (Italy): constraints on its evolution and configuration*. J. Volcanol. Geotherm. Res.,74, pp. 179-214.
Orsi, G., Di Vito, M.A., Isaia, R., (2004). *Volcanic hazard assessment at the restless Campi Flegrei caldera*. Bull. Volcanol. 66, 514–530.
Tassi F., Nisi B., Cardellini C., Capecchiacci F., Donnini M., Vaselli O., Avino R., Chiodini G. (2013). *Diffuse soil emission of hydrothermal gases ($CO_2$, $CH_4$, and $C_6H_6$) at Solfatara crater (Campi Flegrei, southern Italy)*. Applied Geochemistry 35 (2013) 142–153.
Tassi F., Venturi S., Cabassi J., Capecchiacci F., Nisi B., Vaselli O. (2015). *Volatile organic compounds (VOCs) in soil gases from Solfatara crater(Campi Flegrei, southern Italy): Geogenic source(s) vs. biogeochemicalprocesse*. Applied Geochemistry 56 (2015) 37-49.
Todesco M., Chiodini G., Macedonio G. (2003). *Monitoring and modelling hydrothermal fluid emission at La Solfatara (Phlegrean Fields, Italy). An interdisciplinary approach to the study of diffuse degas*sing. Journal of Volcanology and Geothermal Research, 125,1-2, 57-79.

## INSIGHTS INTO THE SEISMICITY AND ERUPTIONS OF PANTELLERIA ISLAND AND ITS SURROUNDINGS (SICILY CHANNEL, ITALY)

**S. Spampinato[1], A. Ursino[1], M.S. Barbano[2], C. Pirrotta[2], S. Rapisarda[1], G. Larocca[1], P.R. Platania[1,3]**
[1] *Istituto Nazionale di Geofisica e Vulcanologia – Osservatorio Etneo, Sezione di Catania, Italy*
[2] *Dipartimento di Scienze Biologiche, Geologiche e Ambientali, Catania, Italy*
[3] *now at Istituto Nazionale di Astrofisica – Istituto di Radioastronomia, Sezione di Noto, Italy*

**Introduction.** The Istituto Nazionale di Geofisica e Vulcanologia – Osservatorio Etneo (INGV-OE) manages a permanent local seismic network in Eastern Sicily, with the aim of monitoring the main tectonic areas (Iblei, Peloritani) and active Sicilian volcanoes (Etna, Vulcano, Stromboli). This network enables locating low magnitude earthquakes and detecting low energy signals that are typical of active volcanic areas (e.g. volcanic tremor, explosion quakes, LP events).

Apart from Mt. Etna and the Aeolian islands, another area characterized by active volcanism is the Sicily Channel, with the volcanic edifices of Pantelleria and Linosa islands. The emergence (and subsequent disappearance after about two months) in 1831 of the Ferdinandea island, as well as the Foerstner island in 1891 (about 4 km north of Pantelleria), is the most reliable and recent evidence of volcanism in the Sicily Channel, which is undersea for the most part (Fig. 1).

Since there are only a few onshore areas in the Sicily Channel, it is therefore difficult to instrumentally detect its seismicity with traditional onshore networks, with the exception of locating the foci of high-energy earthquakes, which often have poor azimuthal constraints. Ocean Bottom Seismometers (OBS) are not widely used owing to the high costs of the instruments and

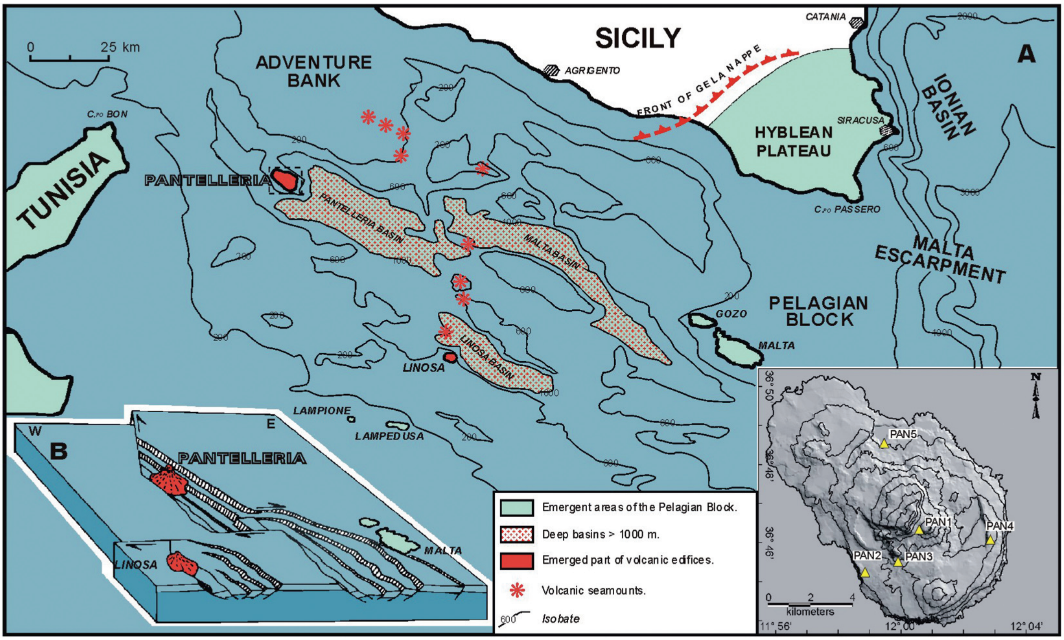


Fig. 1 – General framework (A) and structural pattern (B) of the Sicily Channel (modified after Lanzafame *et al*., 1994; Reuther and Eisbacher, 1985). The inset in the lower right corner shows the map of Pantelleria island; the yellow triangles show the stations of the mobile seismic network running at Pantelleria island from June 2006 to February 2007.

their running. Consequently, seismological knowledge of the Sicily Channel, and Pantelleria Island in particular, is still lacking in detail. Moreover, there is no permanent local network on the island, which could provide useful data, particularly on the microseismicity.

Between 2006 and 2007, we installed a temporary seismic network on the island of Pantelleria, with the aim of improving the knowledge on the local seismicity, and checking for any similarities with other volcanic areas, such as microseismic events that are typical of a hydrothermal environment (e.g. Fossa of Vulcano; Alparone *et al*., 2010).

In this paper, we compare the instrumental and historical seismicity, and provide a review on the historical eruptions in the Sicily Channel. Finally, we show the results of the experiment with the mobile seismic network deployed at Pantelleria.

**Geological framework.** Pantelleria is located in the Sicily Channel, a relatively shallow seaway (average depth 350 m), connecting the African continent to Sicily (Fig. 1). The Sicily Channel is affected by extensional tectonic processes, and characterized by three main tectonic depressions (the Pantelleria, Linosa and Malta troughs), which are the expression of a continental rift, extending in a NW-SE direction. The tectonic depressions of the Sicily Channel have been interpreted as large and discrete pull-apart basins involving deep crustal levels that developed in front of the Africa-Europe collisional belt within a large dextral wrench zone (Cello *et al*., 1985; Reuther and Eisbacher, 1985; Finetti and Del Ben, 2005).

The Sicily Channel is also a region of important volcanic phenomena. Regional magnetic anomalies clearly indicate an alignment of volcanic bodies on the seafloor NW and SE of Pantelleria as far as 37 km from the island, following a linear trend compatible with the main direction of the rift (Lodolo *et al*., 2012 and references therein). According to Argnani (1990), the basins are due to normal faulting, and strike-slip motion is found in a N-S trending “separation zone”, located between the troughs of Pantelleria, Linosa and Malta. This zone separates elements with different structural features and age (Argnani, 1990) and an effusive, tholeiitic and alkaline type of volcanism has developed inside the area. The two volcanic islands of Pantelleria and Linosa, and a large number of seamounts, many of which are poorly known (Fig. 1), testify to the volcanic activity. The main volcanic centres are aligned along N-S direction, from the Linosa Island to the Sicilian coast near Sciacca (Fig. 1). Historical eruptions were mainly underwater, of which there is only slight evidence for some of them (Calanchi *et al*., 1989), and the volcanism is still active.

The Pantelleria Rift forms the deepest part of the Straits and its floor consists of continental crust. The island of Pantelleria, with a NW–SE striking long axis of about 14 km and an orthogonal short axis of about 9 km, is the emerged portion of a volcanic structure, situated along the tectonic trench, which extends in a NW-SE direction for nearly 135 km. The recent eruption of the Foerstner volcano in 1891, along with the presence of thermal springs and fumaroles on the island, are evidence of a still active magmatic system at Pantelleria.

**Historical eruptions in the Sicily Channel.** Except for the last 1891 Pantelleria and the 1831 Ferdinandea island eruptions, historical data report little evidence of previous eruptions in the Sicily Channel. We carried out an historical research on some volcanological and seismological compilations, as well as regional and Italian libraries, looking for first-hand sources (diaries, chronicles, official records, travellers' reports, newspapers) and retrieving original documents written between 1600 and 1900. These documents have been critically analysed and interpreted to reconstruct the seismic and eruptive activity of the Sicily Channel.

The first earliest information from historical accounts about eruptions in the Sicily Channel dates back to 1632 (Perrey, 1848). The volcanic activity was probably located in the Banco Graham, in the same area where the 1701 eruption (Fuchs, 1881) and the well-known 1831 eruption occurred. A probable submarine eruption took place in 1818 (Imbornone, 1817). Lastly, the 1845 and 1846 eruptions were also observed offshore (Perrey, 1846). On the other hand, the 1863 eruption reported by Fucks (1881) and then by Mercalli (1883) is a fake event. The eruptions of 1818 and 1831 where preceded, accompanied and followed by seismic swarms. Most of the shocks were strongly felt in Sciacca and in southwestern Sicilian coast.

Regarding Pantelleria island, no eruption has occurred during the last 3000 years (Civetta *et al*., 1984), while a shallow submarine eruption occurred in 1891, about 4 km NW from the Pantelleria coast. This event was preceded by vigorous seismicity (Baratta, 1892) and increasing fumarolic activity on the island. Significant uplift (up to 0.8 m) occurred at the NE coast of Pantelleria in May-June 1890 (0.55 m) and in 1891 (0.30 m) (Riccò, 1891) preceded by some shocks. The eruption began on October 17, emitting steam and throwing up large scoria (up to 1 m in diameter) to heights of 20 m. The activity culminated on the second day and then rapidly declined, ending completely on October 25.

**Sicily Channel seismicity.** Although there are several studies on the ground deformation, gravimetry, petrography and structural geology of the island of Pantelleria (e.g. Mattia *et al*., 2007, Catalano *et al*., 2009, Lodolo et. al; 2012, and references therein), very little information about the seismic features of the Sicily Channel, and particularly Pantelleria island, is available.

In western Sicily, the only destructive known earthquakes are related to the seismic sequence of 1968 (Belice valley). Historical data show that most of the earthquakes are located along the Sicilian southern coast. According to Rigano *et al*. (1998), the seismic activity close to Sciacca (south-western Sicily), manifested by low-energy sequences and lasting for several months (1652, 1724, 1727, 1817, 1831), is located offshore. Sciacca was often the only site where the earthquakes were felt and for this reason, the location of the events is problematic. Many of these swarms could be related with volcanic activity, even if there is only evidence for the 1831 and 1891 earthquakes (Marzolla, 1831; Gemellaro, 1831; Washington, 1909) and probably for the 1816-17 sequence. Moreover, the historical information, which was gathered along the coasts and islands of the Sicily Channel, may be biased if the actual seismogenic sources are offshore. In some cases, the seismic activity was concomitant with submarine volcanic activity in the Sicily Channel, as for example in 1831 when the Ferdinandea Island was formed in the sea between Pantelleria and Sciacca (Gemmellaro, 1831; Mercalli, 1883). Evidence of more ancient earthquakes, which damaged the town of Selinunte, located on the coast about 25 km west of Sciacca, are provided by archaeological investigations, which suggest the occurrence of two shocks dated around 400-200 B.C. and 400-1200 A.D. (Guidoboni *et al.*, 2002; Bottari *et al.*, 2009), but the seismogenic sources are unknown.

The knowledge of the seismicity of Pantelleria, and also in nearby areas of the Sicily Channel, e.g. the Maltese Islands (Galea, 2007), has suffered both from poor accuracy of earthquake locations due to inadequate network coverage (especially before the 1980s) and the difficulty in detecting low magnitude shocks. Instrumental data recorded in the past are insufficient to provide a realistic framework of the seismicity of Pantelleria area and Sicily Channel. In these areas, the set-up of permanent stations dates back to 1980s, when a 1-component short period (1s) sensor was installed at Pantelleria. In August 2010, this analog station was replaced by a digital one (PTMD), equipped with a three-component broadband seismometer, installed in the central part of the island and managed by INGV-OE. However, analytical location of low magnitude earthquakes, and/or typical low energy seismic signals often recorded at active volcanic areas, has been overlooked to date. This is mainly because of the lack of a permanent local seismic network at Pantelleria. According to literature data, seismic activity in the Sicily Channel is characterized by shallow earthquakes (typically less than 25 km), and with magnitudes generally below 5.0 (typically between 2.0 and 4.0).

According to Agius and Galea (2011) most of seismicity, especially south of the Maltese islands, is either unreported or badly constrained. These authors refer to many earthquakes detected only by a digital broadband station running since 1995 on Malta Island, belonging to the MedNet network.

Besides, few earthquake fault plane solutions are available in order to characterize kinematic features of the Sicily Channel (e.g. Chiarabba *et al.*, 2005; Pondrelli *et al.*, 2002).

**The experiment with a mobile seismic network.** Between 2006 and 2007, a seismic experiment was carried out at Pantelleria, using five digital seismic stations equipped with 3-component broadband (20 s) sensors, belonging to the mobile network of INGV-OE. Unfortunately, the day after the installation the station PAN5 (Fig. 1) broke down and no substitution was available. The remaining four stations mainly monitored the central-southern sector of the island. Overall, the array recorded data from June 28, 2006 to February 23, 2007.

The mobile network recorded various types of seismic signals (i.e. teleseismic events, regional earthquakes, shocks in the Sicily Channel, and local events). Most of earthquakes were teleseismic, whereas the shocks that can be referred (see - http://iside.rm.ingv.it) to the Sicily Channel seismicity amount to sixteen. During the network operating period, only one earthquake (30/12/2006 – 00:02 UTC), with characteristics suggesting a source located very close to or on the island of Pantelleria, was detected. We could not perform any analytical location of this event, since it was recorded by PAN2 station alone, the other ones being out of order due to power supply failure. The analysis of the frequency content of the three components of the PAN2 records (Fig. 2) show a typical waveform of a low magnitude, local shallow volcano-tectonic earthquake.

To obtain some constraints on the epicentral area of the shock, we performed a single-station location, using a ray tracing method. Assuming a Vp equal to 5.2 km/s proposed by Chiarabba and Frepoli (1997), we located the earthquake at a distance of about 4 km offshore from the southwestern coast of Pantelleria. Moreover, the short S-P delay time (about 0.5 s) suggests a focal depth of few kilometres (< 5 km), We evaluated the magnitude Ml of the shock to be no greater than 1.0.

**Seismic data analysis.** To acquire information on the seismic characteristics of the Sicily Channel, and the island of Pantelleria in particular, we carried out a study of the instrumental seismicity by using earthquake catalogues (Castello *et al.*, 2006), reports, and instrumental

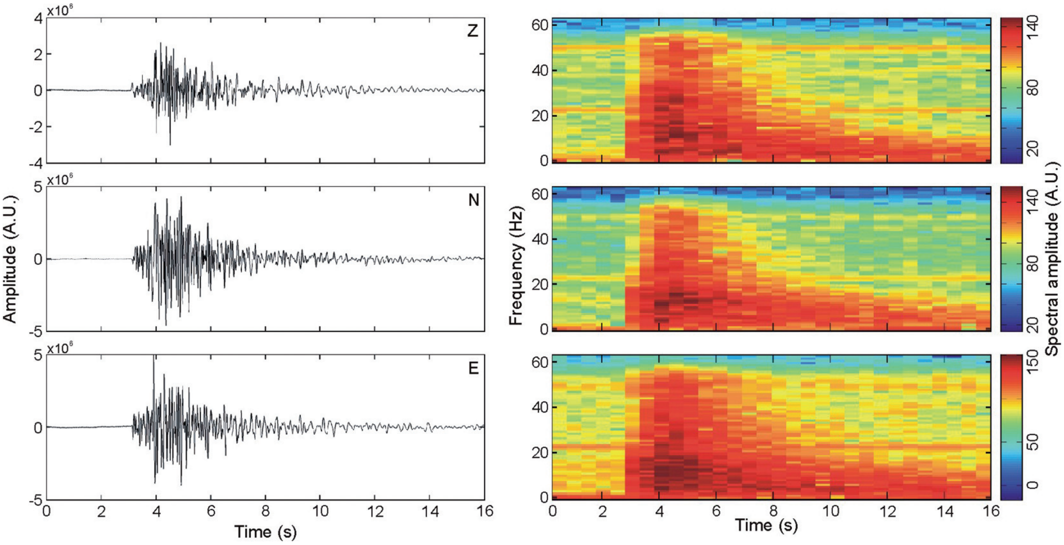

Fig. 2 – Waveform (left) of the local earthquake recorded by PAN2 station (30/12/2006 – 00:02 UTC) and relative spectrogram (right) obtained by 256-points FFT.

data recorded during the period 1981-2014 by the INGV permanent seismic network (http://iside.rm.ingv.it; http://bollettinosismico.rm.ingv.it/). We considered a roughly NW-SE oriented sector with coordinates of vertices: lat. 37.05 – long. 10.09, lat. 38.34 – long. 11.24, lat. 35.81 – long. 16.60, lat. 33.73 – long. 14.91. We compiled a catalogue of 575 earthquakes in the time span 1983-2014 (Fig. 3a), although it should be noted that often hypocentres, with large vertical and horizontal errors, are not well constrained because of the few recording stations and unsatisfactory azimuthal coverage of the network. Daily earthquake rate and the associated cumulative seismic strain release (Fig. 3b) was fairly low from 1983 to 2005, except for 1990 and 1992. From mid-2005 to 2013, an increase both in the daily rate of earthquakes and

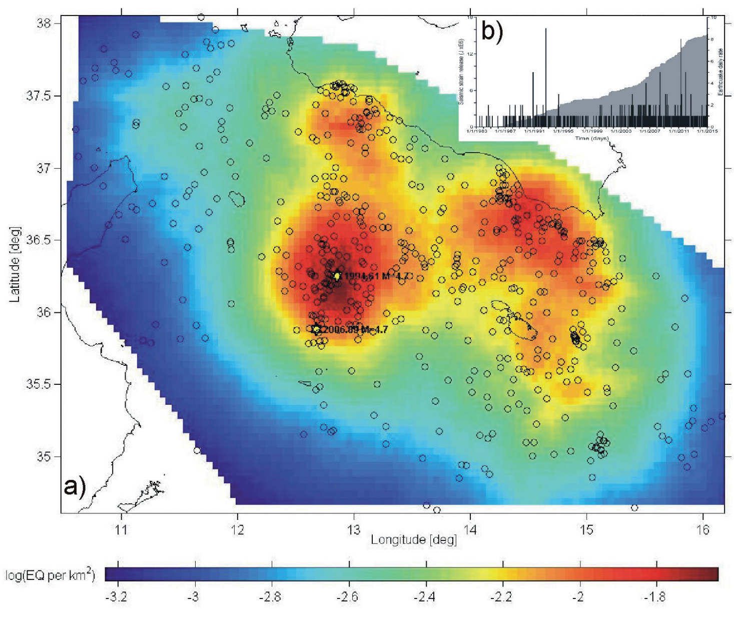

Fig. 3 – Earthquake density map during the period 1983-2014 using the algorithm ZMAP (Wiemer, 2001). The inset shows daily number of earthquakes and associated cumulative strain release in Sicily Channel between 1983 and 2014.

cumulative strain release occurred. This increase could, at least partially, be due to the increase in the number of seismic stations in southern Sicily, and therefore improvement in the detection capability of the Italian Seismic Network (Amato and Mele, 2008). It is worth highlighting that the seismicity shows a prevalent release characterized by isolated earthquakes rather than swarms. Most of earthquakes have magnitude ranging between 2.0 and 4.0 and located within 30 km of depth.

In general, the epicentres show a widespread distribution, even if an approximately N-S oriented clustering, between Linosa and Pantelleria islands, can be observed (Fig. 3a).

However, a comparison between historical and instrumental seismicity shows that the seismicity seems to move from the coast to offshore, confirming that the shocks located in Sciacca occurred offshore.

Zooming in on the Pantelleria area (Fig. 3a), the epicentral map of earthquakes indicates a very low level of seismicity, particularly if compared to other tectonic and volcanic areas of eastern Sicily (i.e. Mt. Etna). Moreover, the distribution of epicentres is scattered widely around the island, with few foci close to or on the island itself. This pattern concurs with the results of the analysis performed on the continuous seismic data recorded by PTMD station. We have scrutinized the seismograms of this station for the period 2010-2014, in order to highlight signals attributable to local earthquakes. Only six seismic signals of this kind have been recognized. Since these signals were recorded by only one station, it was not possible to obtain any analytical location.

**Discussion and conclusion.** Only few detailed studies deal with seismicity and historical eruptions of the Sicily Channel. For this reason, the aim of this study is to highlight the main features of the instrumental and historical seismicity of the Sicily Channel and provide an overview of the historical eruptions affecting this geodynamic sector.

South-western Sicily is characterised by seismogenic zones having different seismotectonic behaviour. Onshore, the strongest earthquakes are located in the Belice Valley, where six events with magnitudes ranging from 5.2 to 6.1 occurred in 1968. This intense seismic sequence seemed almost unexpected from a historical seismicity viewpoint, since no other strong earthquakes are reported in the catalogue for the previous period (Rovida *et al.*, 2011).

Most of the historical earthquakes seem to be located in the southern coast of Sicily. The seismicity is characterised by low magnitude seismic swarms affecting mostly the area of Sciacca. Earthquake magnitudes did not exceed 5.1, and they were probably located in the near offshore. The swarm-like features and vague references to submarine degassing phenomena suggest relationships with the volcanic activity in the Sicily Channel, even if there is evidence only for the 1831 and 1891 earthquakes and probably for the 1816-17 event. Moreover, the historical information, which was gathered along the coasts and islands of the Sicily Channel, may be biased if the actual seismogenic sources are offshore.

The instrumental seismicity recorded by the INGV seismic network during the period 1983-2014 in the Sicily Channel and during the experiment carried out in the Pantelleria island show that the earthquakes are shallow, few and isolated events rather than swarms. They are characterised by low magnitudes (M~4.0) and are more densely located along the “separation zone” trending N-S, located between the troughs of Pantelleria, Linosa and Malta. These results are in good agreement with those obtained by Calò and Parisi (2014) which performed a relocation of the earthquakes.

A comparison of data from the permanent network with the mobile one allows stating that the Pantelleria island and the Sicily Channel are characterized by a low rate of seismicity linked to tectonic release and that the current seismicity is not due to volcanic processes. Historical data indicate that seismic swarms and increasing fumarolic temperature preceded the eruptions, both in Pantelleria and in the Adventure Bank.

We cannot rule out *a priori* the existence at Pantelleria of seismic signals related to hydrothermal activity. We believe that the installation of a local permanent seismic network enables a better understanding of the seismic characteristics of the island and provides an important tool for volcanic risk assessment.

The eruption of 1891 near the Island of Pantelleria, and the presence of a magma chamber (Mattia *et al.*, 2007), would seem to point to its potentially high volcanic risk.

**References**


Agius M. R., Galea P.; 2011: A single-station automated earthquake location system at Wied Dalam Station Malta. Seismol. Res. Lett., 82(4), 545-559.

Alparone S., Cannata A., Gambino S., Gresta S., Milluzzo V., Montalto P.; 2010: Time-space variation of volcano-seismic events at La Fossa (Vulcano, Aeolian Islands, Italy): new insights into seismic sources in a hydrothermal system. Bull. Volcan., 72, 803-816.

Amato A., Mele F.; 2008: Performance of the INGV National Seismic Network from 1997 to 2007. Ann. Geophys., 51, 417–431.

Argnani A.; 1990: The strait of Sicily rift zone: foreland deformation related to the evolution of a back-arc basin. J. Geodyn., 12, 311–331.

Baratta M.; 1892: Gli odierni fenomeni endogeni di Pantelleria. Milano, Voghera tipografia F. Baratta, 8 pp.

Bottari C., Stiros S. C., Teramo A.; 2009: Archaeological evidence for destructive earthquakes in Sicily between 400 B.C. and A.D. 600. Geoarchaeology, 24, 2, 147-175.

Calanchi N., Colantoni P., Rossi P. L., Saitta M., Serri G.; 1989: The strait of Sicily rift system: physiography and petrochemistry of the submarine volcanic centre. Mar. Geol., 87, 55-83.

Calò M., Parisi L.; 2014: Evidences of a lithospheric fault zone in the Sicily Channel continental rift (southern Italy) from instrumental seismicity data. Geophys. J. Int., 199, 219–225.

Castello B., Selvaggi G., Chiarabba C. Amato A.; 2006: CSI Catalogo della sismicità italiana 1981-2002, versione 1.1. INGV-CNT, Roma, http://csi.rm.ingv.it/.

Catalano S., De Guidi G., Lanzafame G., Monaco C., Tortorici L.; 2009: Late Quaternary deformation on the island on Pantelleria: New constraints for the recent tectonic evolution of the Sicily Channel Rift (southern Italy). J. Geodyn., 48, 75–82.

Cello G., Crisci M., Marabini S., Tortorici L.; 1985: Transtensive tectonics in the Strait of Sicily: structural and volcanological evidence from the Island of Pantelleria. Tectonics, 4, 311–322.

Chiarabba C., Frepoli A., 1997: Minimum 1D velocity models in Central and Southern Italy: a contribution to better constrain hypocentral determinations. Ann. Geophys, XL (4), 937-954.

Chiarabba C., Jovane L., Di Stefano R.; 2005: A new view of Italian seismicity using 20 years of instrumental recordings. Tectonophysics, 395, 251– 268.

Civetta L., Cornette Y., Crisci G., Gillot P. Y., Orsi G., Requejo C. S.; 1984: Geology, geochronology and chemical evolution of the island of Pantelleria. Geol. Mag., 121, 541– 562.

Finetti I.R., Del Ben A.; 2005: Crustal tectono-stratigraphic setting of the Pelagian Foreland from new CROP seismic data, in: Crop Project: Deep Seismic Exploration of the Central Mediterranean and Italy I. R. Finetti (Editor), Atlases in Geoscience 1, Elsevier, 581–595.

Fuchs C.; 1881: Vulcani e Terremoti. Biblioteca scientifica internazionale, 27, Fratelli Dumolard (ed), Milano, 362 pp.

Galea P.; 2007: Seismic history of the Maltese islands and considerations on seismic risk, Ann. Geophys, 50 (6), 725-740.

Gemmellaro C.; 1831: Relazione dei fenomeni del nuovo vulcano sorto dal mare fra la costa di Sicilia e l'isola di Pantelleria nel mese di luglio 1831 letta nella gran sala della Regia Università degli Studi in Catania il dì 28 Agosto 1831. VIII, Catania.

Guidoboni E., Muggia A., Marconi C., Boschi E.; 2002: A case study in archaeoseismology. The collapses of the Selinunte temples (Southwestern Sicily): two earthquakes identified. Bull. Seism. Soc. Am., 92, 8, 2961-2982.

Imbornone F.; 1817: Relazione del tremuoto accaduto nelle città di Sciacca in Sicilia nella fine di dicembre 1717, e porzione del gennaio 1717, diretta al Console generale austriaco per la Sicilia a Palermo, barone Massimiliano Noyatzky, dal sig. Francesco Imbornone, agente consolare austriaco in quella citta. Biblioteca italiana: o sia giornale di letteratura, scienze et arti, 8, 350-352.

Lanzafame G., Rossi P. L., Tranne C. A., E. Lanti; 1994: Carta geologica dell'Isola di Linosa. Scala 1:5000. SELCA Firenze.

Lodolo E., Civile D., Zanolla C., Geletti R.; 2012: Magnetic signature of the Sicily Channel volcanism, Marine Geophys. Res., 33, 33–44.

Mattia M., Bonaccorso A., Guglielmino F.; 2007: Ground deformations in Pantelleria Island (Italy): insights into the dynamic of the current inter-eruptive period, J. Geophys. Res., 112, B11406.

Marzolla B.; 1831: Descrizione dell'Isola Ferdinandea al mezzogiorno della Sicilia. Zeitschrift fur Vulcanologie, Band V, Vulkanische Ereignisse und Bibliographie. 40-50, 8 tt.

Mercalli G.; 1883: Vulcani e fenomeni vulcanici in Italia. Milano, (rist. anast., Bologna 1981), 374 pp.
Perrey A.; 1846: Memoire des tremblements de terre ressentis pendant les années 1845 et 1846. Mémoires de l'Acadèmie des sciences, arts et belles-lettres de Dijon, années 1845-1846, partie des sciences, 393-479.
Perrey A.; 1848: Mémoire sur les tremblements de terre de la péninsule italique. Académie Royale de Belgique, Mémoires couronnées et mémoires des savants étrangers, 22, Bruxelles, 144 pp.
Pondrelli S., Morelli A., Ekstrom G., Mazza S., Boschi E., Dziewonski A.M.; 2002: European–Mediterranean regionalcentroid-moment tensors: 1997–2000. Phys. Earth Planet. Inter., 130, 71–101.
Reuther C. D., Eisbacher G. H.; 1985: Pantelleria rift-crustal extension in a convergent intraplate setting. Geol. Rund., 74, 585–597.
Riccò A.; 1891: Tremblements de terre, soulèlevement et eruption sous-marine à Pantelleria. Comptes rendues, 23 novembre; fasc. 21, p. 753.
Rigano R., Arena L., Barbano M.S., Antichi B., Azzaro R.; 1998: Sismicità e zonazione sismogenetica in Sicilia occidentale. 17° National meeting Gruppo Nazionale Geofisica della Terra Solida, abstracts, 161-162.
Rovida A., Camassi R., Gasperini P., Stucchi M. (ed); 2011: CPTI11, the 2011 version of the Parametric Catalogue of Italian Earthquakes, Milano, Bologna, http://emidius.mi.ingv.it/CPTI.
Washington H. S.; 1909: Submarine Eruptions 1831 and 1891 near Pantelleria, Am. J. Sci., IV, 27,131-150.
Wiemer S.; 2001: A software package to analyze seismicity: ZMAP. Seism. Res. Letters, 72 (3), 373-382.

## MAGMA DEGASSING, HEATING AND DEFORMATION AT CAMPI FLEGREI CALDERA

**G. Chiodini[1], F. Quareni[1], S. Caliro[2], C. Cardellini[3], A.R. Mangiacapra[2], Z. Petrillo[2]**
*[1] 1 INGV, Sezione di Bologna, Italy*
*[2] INGV, Sezione di Napoli, Italy*
*[3] Dipartimento di Fisica e Geologia, Università di Perugia, Italy*

**Introduction.** One of the most problematic issues of modern volcanology is the trigger mechanism of unrests at calderas (Newhall and Dzurisin, 1988; Lowenstern *et al*., 2006; Acocella *et al.,* 2015). Here we focus on Campi Flegrei caldera (CFc) which has recently given clear signs of potential re-awaking (Chiodini *et al*., 2012). In its history, CFc alternated phases of uplift followed by subsidence periods over a range of different timescales (Rosi *et al*., 1983; Di Vito *et al*., 1999; Orsi *et al*., 2004; Morhange *et al*., 2006). There are evidences of decades-long inflation prior to the last magmatic eruption, the AD 1538 Monte Nuovo eruption as described in Dvorak and Mastrolorenzo (1991). The Monte Nuovo eruption was followed by a general subsidence which lasted to the early 50s when inflation resumed and culminated into two major uplift, accompanied by an intense seismic activity ("bradyseism"), in 1969-1972 and in 1982-1984, with a total vertical displacement of 3.8±0.2m (Del Gaudio *et al*., 2010, and references therein). Since 1985, a slow subsiding phase, interrupted only by few minor uplifts, affected CFc until 2005 when a new inflation phase started, with an accelerating trend in the next following years. A maximum vertical displacement of about 31 cm has been attained in August 2015, according to the measurements referred in http://www.ov.ingv.it/ov/it/bollettini. This current inflation is accompanied by a weak seismicity, by a strong increase in the fumarolic activity, and by remarkable compositional variations of the fumaroles of Solfatara, the most active zone of CFc (Chiodini *et al*., 2012, 2015 and references therein). At Solfatara, thirty years of compositional data of the main fumarolic vent are made available for investigate the causes of the processes controlling the unrest. This long and detailed time series of geochemical data related to hydrothermal fluids released by a caldera is practically unique at global scale. Surprising correlations among the fluid compositions and the geophysical signals, as well as the results of physical numerical modelling, indicate that the ongoing unrest is controlled by repeated injections of magmatic fluids into the hydrothermal system of CFc. The process is

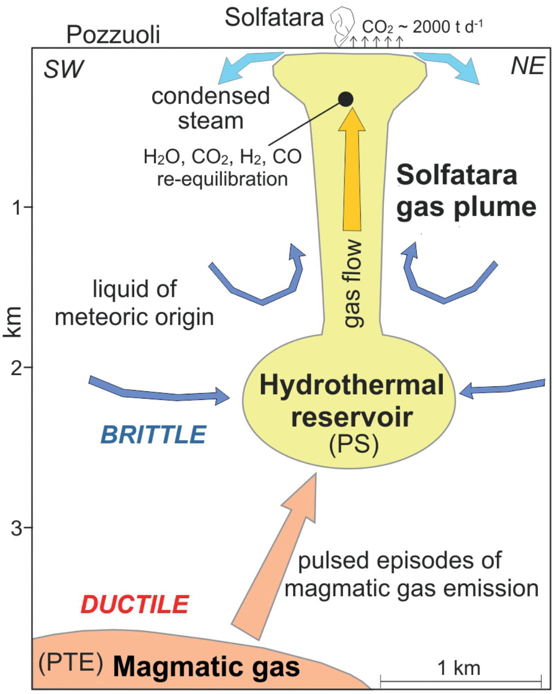


Fig. 1 – Conceptual model involving the release of magmatic fluids from the deeper part of the hydrothermal system (Magmatic gas, PTE) towards the shallower parts (Hydrothermal reservoir PS) below the Solfatara, where these mix with meteoric fluids (modified from Chiodini *et al.*, 2015). See the text for further explanations.

responsible of the heating of the system, which in turn shows the same accelerating trend of ground inflation, thus gaining the role of most likely candidate responsible of the current uplift.

**The hydrothermal system feeding Solfatara.** The total deeply derived $CO_2$ released from diffuse degassing processes at Solfatara and surrounding (~1.4 km$^2$) is estimated to be 1000 to 1500 t/d in the period 1998-2010 (Chiodini *et al.*, 2011). In addition, recent (2012-2015) measurements of the gas flux from the three main fumarolic vents, indicate a total $CO_2$ output ranging from 350 to 850 t/d (Aiuppa *et al.*, 2013). The total $CO_2$ flux of 1500-2000 t/d, i.e. the fumarole flux added to the diffuse emission, has to be considered as a minimum estimate of the total hydrothermal $CO_2$ output because the flux from the numerous minor fumarolic discharges is not taken into account, since it has never been measured.

The sketch of Fig. 1 shows the main features of the hydrothermal system feeding this large degassing process (Chiodini *et al.*, 2015). The system consists of a deep zone of magmatic gas accumulation and a shallower hydrothermal reservoir. The first is located at ~4 km depth (Vanorio *et al.*, 2005) and supplies fluid and heat to the overlying shallower part of the system: it has been hypothesized that it hosts a small batch of magma (De Siena *et al.*, 2010). In the upper part, the hydrothermal reservoir, magmatic fluids mix and vaporize liquid of meteoric origin, forming a gas plume in the subsoil of Solfatara. This scheme, which is derived from geochemical interpretations (e.g. Caliro *et al.,* 2007 and references therein), agrees with the most recent inversion of the ground deformation data observed in the 1982-2013 period (Amoruso *et al.*, 2014). The measured deformation would be in fact controlled by pressure changes in two sources: a pressurized triaxial ellipsoid (PTE) oriented NW - SE and centred at about 4 km depth in the subsoil of Pozzuoli, and a pressurized spheroid (PS) located at ~ 2 km depth below Solfatara crater. PTE and PS are coincident with the deeper magmatic gas and the shallower part of the hydrothermal system depicted in Fig. 1.

**Compositional changes of Solfatara fumaroles and the 2005-2013 ground deformation pattern.** At Solfatara fumaroles, the proportion of the magmatic component sharply increases during relatively short periods, which can be explained as the results of repeated episodes of magmatic fluid injections into the hydrothermal system (Chiodini *et al.*, 2012). Such episodes are characterized by the decrease of the methane content of the fumaroles due to the low $CH_4$ content of magmatic fluids and, possibly, the relatively high and transient oxidizing conditions during the process which prevent the formation of $CH_4$ in the hydrothermal environment (Chiodini, 2009). On the other hand, since the relative abundances of other gases of prevalent magmatic origin, such as $CO_2$ and He, may increase, ,the ratio of their contents with $CH_4$ content is a good indicator of the increased flux of the magmatic component. Allowing that,

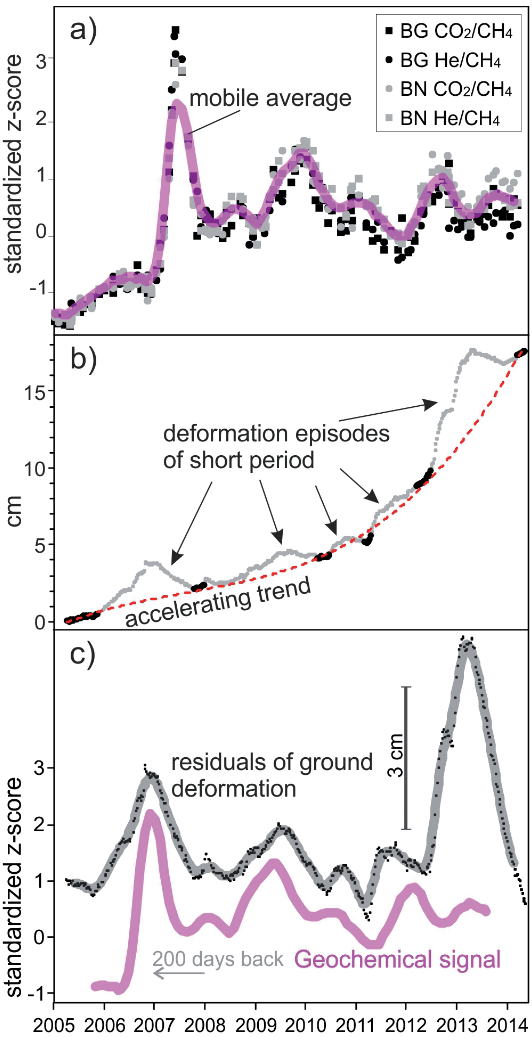


Fig. 2 – a) Measured CO2/CH4 and He/CH4 ratios at fumaroles BG and BN. In order to compare the different signals the measured data were normalized by dividing the difference between each value and the mean by the standard deviation (standardized z-score). The 4 month mobile average of all the data is assumed as the best representation of the geochemical signal; b) 2005-2014 baseline length variation between the ACAE and ARFE CGPS stations (De Martino *et al.*, 2014). The data used for the derivation of the 'accelerating trend' curve are reported as black dots (see the text for further explanations); c) the geochemical signal is compared with the 4 month mobile average of the ground displacement residual (redrawn from Chiodini *et al.*, 2015).

the six peaks, each lasting about one year, which affected the $CO_2/CH_4$ and $He/CH_4$ ratios of the main fumaroles BN and BG in 2007, 2008, 2009-10, 2011, 2012, 2013 (Fig. 2a) correspond to periods of discharge of fluids richer in the magmatic component at the Solfatara fumaroles.

Fig. 2b shows the deformation pattern of CFc during the same period, i.e. from 2005 to 2014. The whole CFc uplifted and expanded producing different total displacements, but following a similar accelerating process (continuous GPS data, CGPS, Fig. 2-4 in De Martino *et al.*, 2014). According to Chiodini *et al.* (2015), here we refer to the baseline variations between two CGPS stations of the INGV network [ACAE and ARAFE, see Chiodini *et al.* (2015) for further details]. The deformation curve (Fig. 2b) suggests the overlapping of a general trend of expansion with short periods of dilation (or uplifting) pulses, two of which were particularly important, in 2006-2007, and 2012-2013. Chiodini *et al.* (2015) fitted the CGPS measurements to a third-order polynomial equation considering only the points less affected by these pulses (i.e., the relative minima of the curve; Fig. 2b, black dots). The residuals of the observed data with respect to the curve (Fig. 2c) clearly repeat the same sequence of seven minima and six maxima, highlighted by the $CO_2/CH_4$ and $He/CH_4$ fumarolic ratios. The main difference is a time lag of about 200 days, with the geochemical signal following the ground deformation (Fig. 2c).

Excluding an improbable fortuity, this coincidence between two independent data sets can be interpreted as the consequence of pulsed inputs of magmatic fluids into the hydrothermal system feeding Solfatara fumaroles. The pressurization of the deeper part of the system (magmatic gas zone in Fig. 1), which likely anticipates the degassing event, and the pressure variations within the hydrothermal system during the injection episode cause the deformation. The delay of the geochemical signal represent the transient time of the magmatic fluids from the input zone to the fumarolic discharges. Only the last important deformation event (2012-2013) does not correspond to a geochemical peak of comparable intensity. It is worth to note that recently this deformation episode was attributed to magma intrusion at relatively shallow levels rather than to a fluid transfer process (D'Auria *et al.*, 2015).

Analyzing the entire data set of Solfatara fumarolic compositions, we infer that fourteen episodes of magmatic fluid injections affected the CFc from 1983 to 2014 enough to produce measurable geochemical anomalies. Their effects are investigated by physical numerical modelling.

**Modelling magmatic fluid injections into the CFc hydrothermal system.** Chiodini *et al.*, (2012) applied a physical numerical model [TOUGH2 by Pruess (1991), with an axisymmetric computational domain] to mimic the injection of batches of magmatic fluids into the hydrothermal system, feeding the fumarolic field of Solfatara. The results highlight the occurrence of the new unrest of CFc which apparently culminated in 2012-2013 with the above cited magma intrusion at relatively shallow levels. Repeated injections of hot fluids at the base of the hydrothermal system, i.e. beneath Solfatara crater, are imposed to the model, keeping a fixed $H_2O$-$CO_2$ ratio and adjusting the flux through a trial-and-error approach in order to reproduce the $H_2O$-$CO_2$ composition measured at the main Solfatara fumaroles. Twelve injections of variable intensity, each involving an amount of deep fluids of the order of the quantities involved in low-medium sized eruptions, well reproduce the compositional changes of the fumaroles in the 1983-2011 period (Chiodini *et al.*, 2012). The cumulative curve of injected fluids (for a total of ~ 25 Mt) clearly shows a change in the slope at the beginning of the 2000's which can be interpreted as the beginning of the new unrest phase at CFc, independently suggested by the inversion in the deformation pattern which, roughly at the same time, passed from a subsidence trend to the new uplift regime.

In the last years, new researches based on the fumarolic inert gas species suggested that the period studied in Chiodini *et al.* (2012) was likely affected by depressurization of the gas-magma separation process (Caliro *et al.*, 2014). This depressurization, which occurred from 1980's to 2011-2015, should have caused an important increase of the $H_2O/CO_2$ ratio of magmatic fluids because $H_2O$ is more soluble in magma than $CO_2$. This implies that the hypothesis of a fixed $H_2O$-$CO_2$ composition of Chiodini *et al.* (2012) cannot be taken as plausible. We present here the results of new modelling, which accounts for a progressive increase in the water content of the injected fluids.

Recently, several studies were aimed to improve the modeling of the hydrothermal system of CFc. They include, for example, the first definition of a 3-D domain with heterogeneous properties of the rocks derived from the density tomography of the caldera (Petrillo *et al.*, 2013), and the first application to CFc of MUFITS (Afanasyev *et al.*, 2015), a code which deals with high, magmatic temperatures of the fluids.

Here, however, we discuss the results of new modelling performed with TOUGH2 code (Pruess, 1991) and an axisymmetric computational domain, i.e. the same tools adopted in Chiodini *et al.* (2012), in order to compare these new results with the previous ones. TOUGH2 accounts for the coupled transport of heat and a multi-phase (gas and liquid) and multicomponent (water and carbon dioxide) fluid. The used computational domain, discretized in 850 cells of different volume, represents a 5 km diameter and 2 km height cylinder. Bottom and lateral boundaries are impermeable and adiabatic, while the top boundary has fixed atmospheric temperature and pressure. Values of the rock properties (porosity $\Phi = 0.2$; permeability $k = 10^{-14}$ m$^2$; density $\varrho = 2000$ kg/m$^3$; thermal capacity $C = 1000$ J/kg °C; thermal conductivity K = 2.8 W/m °C) are equal to those adopted in previous modelling (Chiodini *et al.*, 2012 and references therein).

The initial state is a steady state reached after 2000 years of injection of 3400 td$^{-1}$ of a gas mixture at 350°C with a relatively low $CO_2/H_2O$ molar ratio, and ideally represents the pure hydrothermal component discharged at Solfatara before the 1982-84 crisis. The transient solution is obtained with the pulsed injection into the hydrothermal system of large amounts of a gas mixture, with $H_2O$-$CO_2$ composition representing the magmatic fluid. The $CO_2/CH_4$ anomalies measured at Solfatara fumaroles provide the hint for the number and timing of each injection episode of magmatic fluids (14 in the 1983-2014 period), while the fumarolic $CO_2/H_2O$

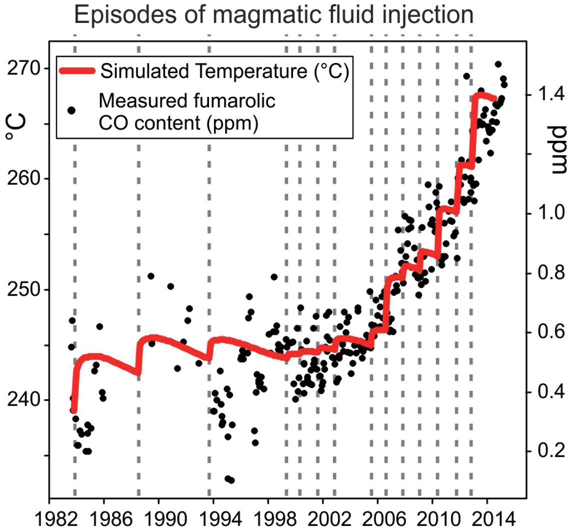


Fig. 3 – Evolution of the average temperature simulated for the deep central part of the computational domain compared with the measured carbon monoxide (CO) content of the fumaroles. The timing of the simulated magmatic fluid injections (dashed lines) were derived by the analysis of the $CO_2/CH_4$ and $He/CH_4$ fumarolic ratios (see the text for further explanations).

ratio constrains the total gas amount of each injection episode whit a trial-and-error procedure similar to that adopted in Chiodini *et al.* (2012).

While in Chiodini *et al.* (2012) approach the composition of the injected fluid was constant with time, in this study the $H_2O/CO_2$ ratio (by weight) of the injected magmatic fluids increases form the value of 0.67, in 1983, to 1.2, in 2012. This increase of the $H_2O/CO_2$ ratio agrees with the hypothesis of an open magmatic system, which depressurizes in time because of degassing. Practically, we depict one possible, but not unique, scenario previously proposed to explain the evolution of the fumarolic inert gas species compositions (see Fig. 8b in Chiodini *et al.*, 2015).

The results of the new model confirm the beginning of the new unrest phase in earlier 2000's, when the cumulative curve of injected fluids shows an inflection point as already noted by Chiodini *et al.* (2012). There are, however, two major differences with the previous simulations: 1) in order to reproduce the observed fumarolic compositions, the injected amounts of fluids have to be ~30% higher than in previous model; 2) the system is significantly heated during the process, a feature not observed in Chiodini *et al.* (2012). The increase of the $H_2O/CO_2$ ratio of the injected fluids with time causes, in fact, a remarkable increase of the total amount of steam injected into the system, and in turn of condensation and heating of the whole system.

Fig. 3 shows the evolution of the simulated average temperature in the deep central part of the domain, above the injection point (a cylinder of 1 km diameter and 1 km height). The resulting average temperature remains nearly constant from 1983 to 2005 (240-245 °C), while from 2006 to 2014 it increases from 245°C to 270°C.

The absolute temperature field is in some way controlled by the quite arbitrary choice of the function used to describe the $H_2O/CO_2$ increase of the magmatic component, which in turn constraints the total amount of injected steam. On the contrary, the time evolution of the temperature increase is much less affected by this choice, being mainly controlled by other constraints, such as the measured fumarolic $CO_2/CH_4$ ratio (frequency of the injections) and the $H_2O/CO_2$ ratio (intensity of the injections). It is worth to note that the reliability of the modelled evolution of the temperature finds confirmation on independent observations. The fumarolic content of carbon monoxide, which is the gas specie most sensitive to temperature variations (Chiodini and Marini, 1998), shows the same behavior (Fig. 3). In 2005-2006, concurrently with the beginning of the increase of the simulated temperature, the fumarole of Pisciarelli starts to increase its activity [increase of flow rate and discharge temperature: Chiodini *et al.* (2015)]. Finally, in 2005-2006 CFc starts to expand and uplift with an accelerating trend very similar to the temperature increase.

**Conclusion.** The almost unique, long time set of fumarolic compositions data at Solfatara highlight important changes in the hydrothermal system feeding the manifestation observed from 1983 to 2015 periods. In particular, during the ongoing unrest of CFc started in 2005, the occurrence of numerous episodes of injection of magmatic fluids into the hydrothermal system are recognized comparing geochemical and geophysical signals. The physical numerical modelling of such episodes, together with several other independent observations, indicates that the large amount of steam involved in the process is currently heating the hydrothermal system through condensation. This heating process, which for the first time is documented to occur with so many details during a caldera unrest, may be one of the main causes of the current deformation phase of CFc. The input of magmatic steam into geothermal systems is potentially a very efficient way both for heating and for deforming the rocks to such an extent that steam injection is used is used in oil industry for heavy oil exploitation (e.g. Dusseault and Collins, 2008; Dusseault, 2011).

**Acknowledgments.** This study has benefited from funding provided by the MEDiterranean SUpersite Volcanoes FP7 project (grant number 308665) and by the "Precursori d'eruzione" project (funded by DPC, Italian Presidenza del Consiglio dei Ministri – Dipartimento della Pro-tezione Civile). This paper does not necessarily represent DPC official opinion and policies.

## References

Acocella V., Di Lorenzo R., Newhall C., and Scandone R.; 2015: *An overview of recent (1988 to 2014) caldera unrest: Knowledge and perspectives*. Rev. Geophys., article in Press, doi: 10.1002/2015RG000492

Afanasyev A., Costa, A. and Chiodini G.; 2015; *Investigation of hydrothermal activity at Campi Flegrei caldera using 3D numerical simulations: Extension to high temperature processes*. J. Volcanol. Geotherm. Res., **299**, 68-77, doi:10.1016/j.jvolgeores.2015.04.004

Aiuppa A., G. Tamburello, R. Di Napoli, C. Cardellini, G. Chiodini, G. Giudice, F. Grassa and M. Pedone; 2013: *First observations of the fumarolic gas output from a restless caldera: Implications for the current period of unrest (2005–2013) at Campi Flegrei*. Geochem. Geophys. Geosys., doi:10.1002/ggge.20261.

Amoruso A., Crescentini L. and Sabbetta I.; 2014: *Paired deformation sources of the Campi Flegrei caldera (Italy) required by recent (1980-2010) deformation history*. J. Geophys Res. **119**, doi:10.1002/2013JB010392

Caliro S., Chiodini G. and Paonita A.; 2014: *Geochemical evidences of magma dynamics at Campi Flegrei (Italy)*. Geochim. Cosmochim. Acta **132** , 1-15

Caliro S., Chiodini G., Moretti R., Avino R., Granieri D., Russo M. and Fiebig, J.; 2007: *The origin of the fumaroles of La Solfatara (Campi Flegrei, South Italy)*. Geochim. Cosmochim. Acta, **71** (12), 3040-3055

Chiodini, G.; 2009: *$CO_2/CH_4$ ratio in fumaroles a powerful tool to detect magma degassing episodes at quiescent volcanoes*. Geophys. Res. Lett., **36**, L02302, doi:10.1029/2008GL036347.

Chiodini G. and Marini, L.; 1998: *Hydrothermal gas equilibria; the $H_2O$–$H_2$–$CO_2$–$CO$–$CH_4$ system*. Geochim. Cosmochim. Acta, **62**, 15, 2673–2687.

Chiodini G., Caliro S., Cardellini C., Granieri D., Avino R., Baldini A., Donnini M. and Minopoli C.; 2010: *Long-term variations of the Campi Flegrei, Italy, volcanic system as revealed by the monitoring of hydrothermal activity*. J. Geophys Res., **115,** 3, B03205

Chiodini G., Caliro S., De Martino P., Avino R. and Gherardi F.; 2012; *Early signals of new volcanic unrest at Campi Flegrei caldera? Insights from geochemical data and physical simulations*. Geology, **40**, 943–946.

Chiodini G., Vandemeulebrouck J., Caliro S., D'Auria L., De Martino P., Mangiacapra A. and Petrillo Z.; 2015: *Evidence of thermal driven processes triggering the 2005-2014 unrest at Campi Flegrei caldera*. Earth Planet. Sci. Lett. , **414**, 58–67.

Del Gaudio C., Aquino I., Ricciardi G. P., Ricco C. and Scandone R.; 2010: *Unrest episodes at Campi Flegrei: A reconstruction of vertical ground movements during 1905– 2009*. J. Volcanol. Geotherm. Res., **195**, 48–56, doi: 10.1016/j.jvolgeores.2010.05.014.

De Martino P., Tammaro U. and Obrizo F.; 2014: *GPS time series at Campi Flegrei caldera (2000-2013)*. Ann. Geophys., **57**, 2, 2014, S0213; doi: 10.4401/ag-6431

De Siena L., Del Pezzo E. and Bianco F.; 2010: *Seismic attenuation imaging of Campi Flegrei: Evidence of gas reservoirs, hydrothermal basins, and feeding systems*. J Geophys Res, **115**, 1–18.

Di Vito M. A., Isaia R., Orsi G., Southon J., De Vita S., D'Antonio M., Pappalardo L. and Piochi M.; 1999; *Volcanism and deformation since 12000 years at the Campi Flegrei caldera (Italy)*. J. Volcanol. Geotherm. Res., **91**, 221–246.

Dusseault M.B.; 2011: *Geomechanical Challenges in Petroleum Reservoir Exploitation*. KSCE Journal of Civil Engineering **15**, 4, 669-678, doi: 10.1007/s12205-011-0007-5.

Dusseault M.B. and Collins P.M.; 2008: *Geomechanics Effects in Thermal Processes*. CSEG Recorder, June 2008, 20-23.

Dvorak J. J. and Mastrolorenzo G.; 1991: *The mechanisms of recent vertical crustal movements in Campi Flegrei Caldera, southern Italy*. Spec. Pap. Geol. Soc. Am., **263**, 47

Lowenstern, J. B., Smith R. B. and Hill D. P.; 2006: *Monitoring super-volcanoes: Geophysical and geochemical signals at Yellowstone and other large caldera systems*. Philos. Trans. R. Soc. A, **364**, 2055–2072.

Morhange C., Marriner N., Laborel J., Micol T. and Oberlin C.; 2006: *Rapid sea-level movements and noneruptive crustal deformations in the Phlegrean Fields caldera, Italy.* Geology, **43**, 93–96.

Newhall C. G. and Dzurisin D.; 1988: *Historical unrest at large calderas of the world*. U.S. Geol. Surv. Bull., 1855, 1108.

Orsi G., Di Vito M. A. and Isaia R.; 2004: *Volcanic hazard assessment at the restless Campi Flegrei caldera*. Bull. Volcanol., **66**, 514–530.

Petrillo Z., Chiodini G., Mangiacapra A., Caliro S., Capuano P., Russo G., Cardellini C. and Avino R.; 2013: *Defining a 3D physical model for the hydrothermal circulation at Campi Flegrei caldera (Italy)*. J. Volcanol. Geotherm. Res.**264**,172–182

Pruess K.; 1991:*TOUGH2 - A General Purpose Numerical Simulator for Multiphase Fluid and Heat Flow.* L. B. L. Report. LBL, Berkeley, CA, p. 29400.

Rosi M., Sbrana A. and Principe C.; 1983: *The Phlegrean Fields: Structural evolution, volcanic history and eruptive mechanisms*. J. Volcanol. Geotherm. Res., **17**, 273–288.

Vanorio T., Virieux J., Capuano P. and Russo G.; 2005: *Threedimensional seismic tomography from P wave and S wave microearthquake travel times and rock physics characterization of the Campi Flegrei caldera*. J. Geophys. Res., **110**, B03201, doi:10.1029/2004JB003102.

# Indice degli autori

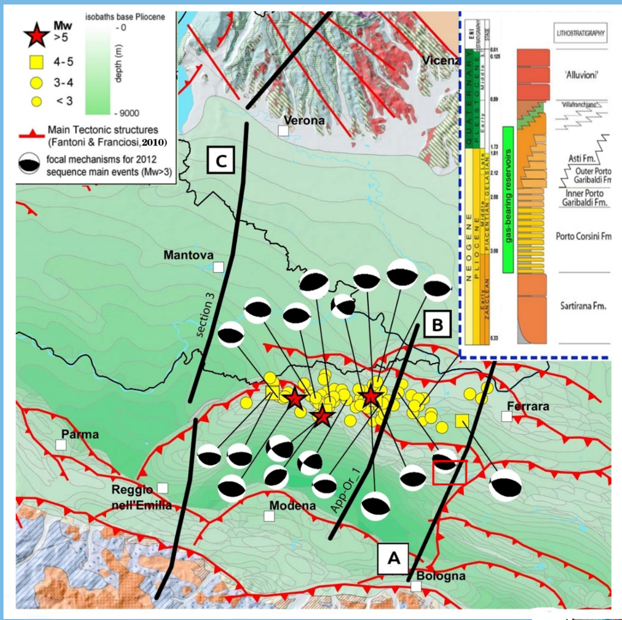


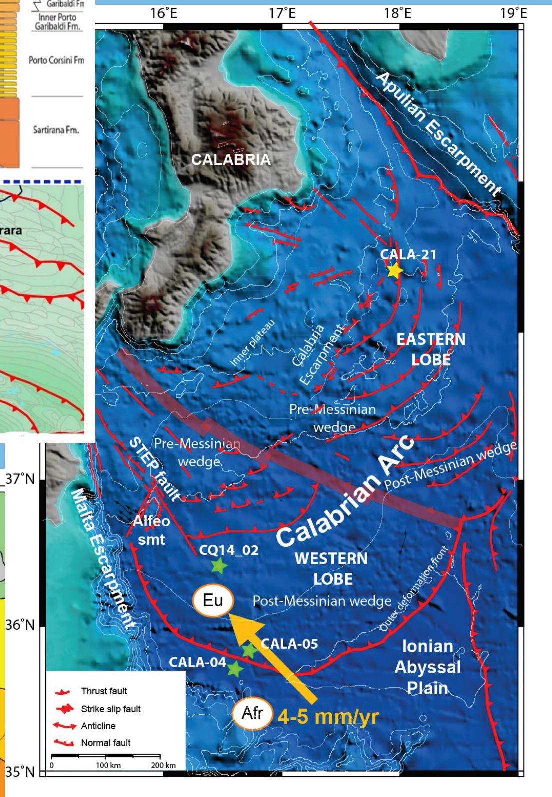


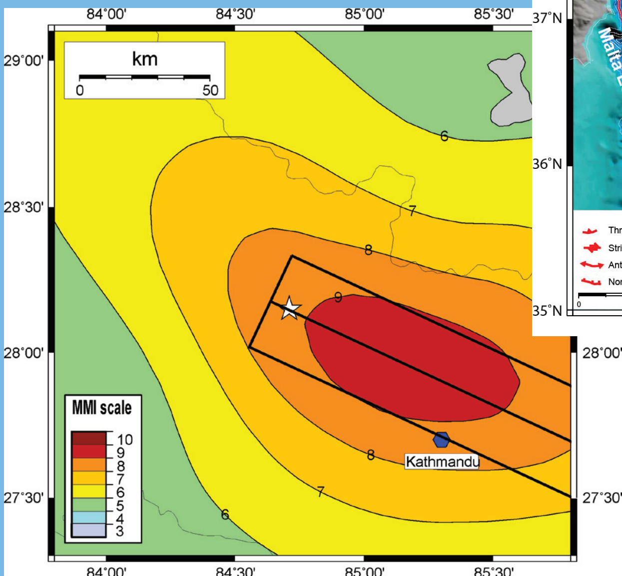


*con la sponsorizzazione di:*

EAGE
EUROPEAN ASSOCIATION OF GEOSCIENTISTS & ENGINEERS
SEG
SEZIONE ITALIANA

15° Convegno Nazionale

CODEVINTEC
Tecnologie per le Scienze della Terra

www.misuremeccaniche.it
strumenti e sensori
misure meccaniche

GNGTS

volume
ISBN 978-88-940442-5-6

raccolta
ISBN 978-88-940442-4-9